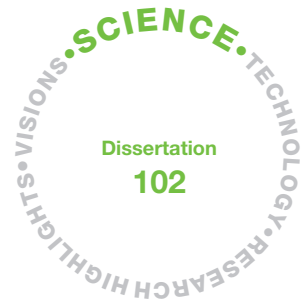# Biochemical modification and functionalization of nanocellulose surface

Suvi Arola

VTT

Biochemical modification and functionalization of nanocellulose surface

Suvi Arola

A doctoral dissertation completed for the degree of Doctor of Science (Technology) to be defended, with the permission of the Aalto University School of Science, at a public examination held in the lecture hall TU1 (Otaniementie 17, Espoo) of the school on 15th of August 2015 at 12 noon.

Abstract

Cellulose is an abundant biopolymer found in many different organisms ranging from microbes to plants and animals. The homopolymer, composed of repeating glucose units, forms mechanically strong nanosized fibrils and rods. In plants cellulose forms macroscopic fibers, which are incorporated in the cell walls. Recently, it has been shown that cellulose fibers can be disintegrated into the fibrils and rods by different chemical treatments. These materials are called nanocellulose. Nanocellulose is a promising material to replace fossil based materials because it is renewable, biodegradable and abundant. It holds great potential in many applications due to its superior mechanical properties and large surface area. For most applications modification of nanocellulose surface is needed due to its tendency to aggregate by hydrogen bonding to adjacent cellulose surfaces.

In this thesis we took a biochemical approach on nanocellulose surface modification to achieve modified and functional materials. The advantages of this approach are that the reactions are done in mild aqueous ambient conditions and the amount of functionalities of biomolecules is broad. Four different approaches were chosen. First, genetically engineered cellulose binding proteins, were used to introduce amphiphilic nature to nanocellulose in order to create surface self-assembled nanocellulose films and to stabilize emulsions. This method was shown to be a good method for bringing new function to nanocellulose. (Publication I) Second, covalent coupling of enzymes directly onto modified nanocellulose surfaces provided a route for protein immobilization in bulk. Nanocellulose derivatives were shown to be well suited platforms for easy preparation of bioactive films. More over the film properties could be tuned depending on the properties of the derivative. (Publication II) Third, by modifying the nanocellulose surface with specific enzymes we could study the role of hemicellulose in nanocellulose fibril surface interactions. We showed that hemicellulose has an important role in nanofibrillated cellulose networks, yet its effects were different in aqueous and dry matrixes. (Publication III) Fourth, by modifying the specific function of cellulose binding protein via genetic engineering we showed how the binding properties can be altered and thus the functionalization properties can be tuned, and that the cellulose binding protein properties are substrate dependent. We also showed that nanocellulose as a model substrate in binding studies is a valuable tool for gaining new insight in protein binding behavior. (Publication IV)

In conclusion, we showed that biochemical methods are feasible in nanocellulose modification and functionalization to study intrinsic properties of nanocellulose and cellulose binding proteins but also for creating new functional materials.

Tiivistelmä

Selluloosa on laajalti luonnossa esiintyvä biopolymeeri, jota tuottavat kasvien ja mikrobien lisäksi jotkin eläinkunnan jäsenet. Tämä homopolymeeri, joka muodostuu toistuvista glukoosiyksiköistä, muodostaa mekaanisesti vahvoja nanokokoluokan fibrillejä ja tikkuja. Kasveissa selluloosa muodostaa mikro- ja makrokokoluokan kuituja, jotka ovat osana soluseinärakennetta. Hiljattain on pystytty näyttämään, että selluloosakuidut voidaan hajottaa fibrilleiksi ja tikuiksi erilaisin kemian menetelmin. Näitä materiaaleja kutsutaan nanoselluloosaksi. Nanoselluloosa on lupaava materiaali korvaamaan öljypohjaisia materiaaleja, koska se on uusiutuva, biohajoava ja helposti saatavilla oleva. Nanoselluloosa on myös potentiaalinen materiaali monilla eri teknologioiden aloilla suuren pinta-alansa ja ylivertaisten mekaanisten ominaisuuksiensa takia. Suurin osa sovelluksista vaatii nanoselluloosapinnan ominaisuuksien muokkaamista, koska nanoselluloosakuidut liittyvät helposti yhteen vetysidosten välityksellä.

Tässä väitöskirjassa on tutkittu biokemiallisten menetelmien soveltuvuutta nanoselluloosapintojen muokkaamisessa ja funktionalisoimisessa. Näiden menetelmien etuja ovat, että reaktiot tapahtuvat miedossa vedellisessä ympäristössä ja että biomolekyylien toiminnollisuuksien joukko on erittäin laaja. Valitsimme neljä erilaista lähestymistapaa. Ensinnä käytimme geneettisesti muokattuja selluloosaan sitoutuvia proteiineja tuomaan amfifiilisyyttä nanoselluloosan pinnalle. Näitä rakenteita käytettiin muodostamaan itsestään järjestäytyneitä pintoja nanoselluloosasta sekä stabiloimaan emulsioita. Tämän menetelmän näytettiin toimivan nanoselluloosan funktionalisoinnissa. (Osajulkaisu I) Toiseksi näytimme, että nanoselluloosan johdannaiset toimivat hyvin matriisina proteiinien suoralle kovalenttiselle kiinnittämiselle bulkissa. Nämä johdannaiset sopivat hyvin bioaktiivisten filmien valmistukseen. Lisäksi filmien ominaisuuksia voitiin muuttaa ja muokata nanoselluloosajohdannaisen ominaisuuksista riippuen. (Osajulkaisu II) Kolmanneksi tutkimme hemiselluloosan roolia nanoselluloosamatriisissa muokkaamalla nanoselluloosan pintaa spesifisillä entsyymeillä. Pystyimme näyttämään, että hemiselluloosalla on tärkeä rooli näissä verkostoissa, joskin se on erilainen kuivissa ja kosteissa systeemeissä. (Osajulkaisu III) Neljänneksi, muokkaamalla geneettisesti selluloosaan sitoutuvan proteiinin spesifiä toimintoa, näytimme, että pystymme vaikuttamaan sen sitoutumisominaisuuksiin ja näin mahdollisesti myös nanoselluloosamateriaalien toiminnollisuuteen. Näytimme myös, että selluloosaan sitoutuvan proteiinin toiminta on riippuvaista sen substraatista ja että nanoselluloosa on hyvä mallisubstraatti sitoutumiskokeissa, sillä se tuo uutta tietoa näiden proteiinien toiminnasta. (Osajulkaisu IV)

Yhteenvetona voi todeta, että erilaiset biokemialliset menetelmät soveltuvat nanoselluloosapinnan muokkaukseen ja funktionalisointiin, nanoselluloosan ja siihen sitoutuvien proteiinien luontaisten ominaisuuksien tutkimisessa, mutta myös uusien toiminnallisten materiaalien luomiseen.

Preface

The practical work of this Ph.D. thesis was carried out at VTT Technical Research Centre of Finland Ltd during the years 2010–2015. I warmly thank current and former technology managers Dr. Kirsi-Marja Oksman-Caldentey, Dr. Raija Lantto, and Dr. Niklas von Weymarn, and especially the Vice President R&D Professor Anu Kaukovirta-Norja for providing excellent working facilities and equipment. I express my gratitude to Professor Liisa Viikari, the director of the former BIOREGS – Biomass Refining Graduate School, who accepted me as a Ph.D. student and provided a top-notch scientific environment where to conduct my thesis. BIOREGS, Tekes – The Finnish Funding Agency for Innovation, Academy of Finland, Academy of Finland's Centre of Excellence HYBER, and Emil Aaltonen's foundation are acknowledged for funding the work.

I thank my pre-examiners Professor Kiyohiko Igarashi and Dr. Tanja Zimmermann for evaluating my thesis and for giving me valuable comments. I also want to thank my opponent, Professor Neel S. Joshi, for accepting this task and coming to Finland to examine my work.

I want to express my gratitude to Academy Professor Olli Ikkala who took me into his Molecular Materials group at the Department of Applied Physics in 2010 to do my Ph.D. work. My first thought was: "A molecular biologist in an applied physics group... What's going on?" But I quickly learned, that although the "walls were high, the sealing was open" in the MolMat group. And I enjoyed this privilege of freedom very much. I'm also very grateful for Professor Ikkala for his support throughout my studies and his enthusiasm and passion for science that feeds the great research done in his group.

I want to acknowledge Dr. Kvar Black for reading the thesis and correcting my English on such a short notice. Thank you Mr. B! I don't think anyone else would have done the job better than you!

I have had the privilege of working together with the BEST of the best supervisors, Professor Markus Linder. I cannot imagine a better teacher in science, academy, or life for that matter than him. During these years Markus has become more of a mentor and friend than a boss and supervisor for me. I have too many things to thank him for but to list a few I'll start by thanking Markus for initially taking me into

his Nanobiomaterials group at VTT to be a researcher. That was where it all started from! I'm forever thankful for Markus for giving me a chance to chase my dream, to become a Ph.D., and finding the absolute best way to do it; as an Ext at VTT. Markus, you have always had the time for me and the patience to listen and guide me to the right direction, yet, giving me the freedom to learn and be independent. Your enthusiasm and motivation for the science has been the best fuel for this Ph.D. work. I've always felt that I've had your 150% support throughout the whole time. (You even had tissues in your office for the times I wasn't doing so well in the lab, not to mention the very last weeks of the writhing process of this thesis! Okay, maybe the tissues weren't only for me, but still…) I'm grateful for the open and warm working environment that you've provided. It has had a great impact on the work and also made me feel that no matter what, you'll stand behind my back and take a catch if needed. Thanks to Markus, I'm also confident that I'm a better storyteller now than I was five years ago. I also know now that such terms like "quick and dirty" do not apply in science, at least the "quick" part of it. Yet, what is quick, remains to be defined and might vary depending on one's academic status. ☺ All this is only a tip of the iceberg and there are so many other things I would need to say here, but to keep it short… Markus, thank you for everything, really, everything! This thesis would not be as good as it is without your commitment and dedication!

Over the years I have had the pleasure of working with absolutely the best and most skilled experts. I want to thank all my co-authors (Prof. Päivi Laaksonen, Dr. Timo Laaksonen, Dr. Hanna Valo, Dr. Hendrik Hähl, Dr. Arja Paananen, Dr. Tekla Tammelin, Dr. Harri Setälä, Antti Tullila, Dr. Jani-Markus Malho, and Dr. Martina Lille) and colleagues for helping me in getting this work done. Without all of you this thesis would not exist! Especially, I want to thank Dr. Tekla Tammelin for helping me understand the surface chemistry of nanocellulose and for her expertise in this field. I enjoyed our collaboration and discussions very much! I thank Dr. Martina Lille for her excellence and knowledge in the field of rheology and specifically rheology of nanocellulose. I would have been lost many times during this work without you! I want to express my warmest thanks to all my former group members (Nanobiomaterials and Protein Discovery and Engineering) at VTT. You made me feel accepted and welcome, and coming to work every day was a great joy simply because you were there. I want to thank Dr. Riitta Partanen for being such a great team leader for the Nanobiomaterials group promoting the excellent team spirit we had. You were always open for discussion and I felt that you really cared for us. You also did a great job in bringing people from different disciplines together and making the team really well functioning.

In addition I express my deepest gratitude to Dr. Arja Paananen who initially introduced me to VTT and to most of the techniques I used in this thesis. I must say, it was quite tough on me learning so much during so little time but I also enjoyed it very much, thanks to you! You have not only been a great colleague and a great scientific support to me but also a great friend too! I really miss working together with you! I want to thank Professor Päivi Laaksonen for the great scientific input on my work. We've had a lot of fun working together and I'm grateful for all the help and guidance I received from you during this work. I really look up to you as a great

role model. I'm also very happy that we have become great friends and that our boys enjoy the time spent together as much as we do. ☺ I want to express my gratitude to Dr. Dilek Ercili-Cura for introducing me to the secrets (and pain) of surface shear rheology and teaching me how to use the AR-G2. The sometimes frustrating days at the rheometer were more fun with you than alone! I thank Dr. Géza Szilvay especially for helping me a lot in the genetic engineering part of this work. You have always been so very helpful in every possible way. I enjoyed our scientific discussions and also the not-so-scientific ones! I thank Arja Kiema for excellent assistance with the *Trichoderma* work and protein production. You and Géza took the work forward during my maternity leave, and I'm very grateful for that. I want to express my warmest and deepest gratitude to Riitta Suihkonen, our "mom" in the small lab, for being such a big help during the experimental work. But you have been more than just technical help, you are a great and dear friend to me! You were always there for me (in the ÄKTA room) to listen, laugh, gossip, cry, hug, and celebrate before, during and after work! I really miss our everyday chit-chat so much! I really miss you!

I left VTT at the end of the year 2014 and went on to Aalto Biomolecular Materials group (lead by Markus). And I have to say... What a group!! We have such great people doing such great science! All of you: Markus, Heli, Georg, Katja, Bartek, Bart, Chris, Wenwen, and Pezhman I want to thank you for making the group what it is! You make my day every day when I come to work. Especially I want to thank our office crew at D332a; Heli, Georg, Katja and Bartek. I've laughed so much with you during the past months and we have had so much fun that I couldn't imagine a better office! You kept me going and encouraged me during the writing process, you shared your joys and sorrows with me, and you always went for coffee with me even though you probably didn't have the time (I know I certainly always didn't, but it was definitely worth it). I will miss you guys dearly when I move out!

My friends, You truly are the best and I'm privileged to have you in my life! Johanna, I want to thank you for sharing the great joys and bumps on the way of becoming a Ph.D.! You have picked me up with your encouragements when I felt that nothing was working and I'll just quit! You have shared the celebrations of "today the stuff worked in the lab" because you really know that it might not be that great tomorrow! We've always had the best scientific discussions on what's really going on with nanocellulose since it isn't that trivial. But you have not only been a great peer support in science but also as a mom! That is priceless! Kaisa, we've known since undergrad times from Chem, and no one else was as crazy and as enthusiastic about chemistry as you! I think I have to blame you I survived as long as I did there. We've had so much fun over the years! Come on... who else would order a GT in a bar (with UV-lights on the dance floor) and make an experiment with salt!! I think we were labelled as geeks at that bar! ☺ Alise, my dear friend from Tampere. We studied together at IMT and shared more than just the passion for bio... the passion for shoes, purses and Miyazaki films! I'm so glad I met you then, you really made the endless hours of studying more fun! You also introduced me to Tampere and made the city feel like home for me! You really mean the world to me! Kim, although life has taken us sometimes far away from each other physically, I've

always felt that you've been very close to me. That, I guess, happens when you've known someone most of your life. We've known for 30 years! You enrich my life with beauty and spirituality that you radiate! You are so special to me! Maria, my dear, dear, Maria! I simply love you! There is no one else who makes me laugh like you, or cry like you! To you, I can reveal all my secrets and I know you won't judge me. You're positivity, kindness and great selflessness never seems to stop amaze me! The girls' gourmet club (Maria, Iida, Arnevi, Anna J., Anna K., Anmi, Katja), what would I do without you!? Food (good wines) is a great way (good excuse) to escape the ordinary life and have fun! I have no words to describe the gratitude I feel for having such great people in my life! Growing up with you has made an impact on me that can only be described with the most positive and fun adjectives! I love you all so much! Leandro, you were the one who encouraged me to pursue my dream of getting a Ph.D., and you did it with your own example! I'm so lucky that I got to know you! Thank you for sharing science and life with me! Sanja, where do I start!? Thank you for sharing the ups and downs of owning and loving dogs. Thank you for sharing the passion for animal welfare and nature! Thank you for sharing the passion for being an activist! ☺ Thank you for the countless hours in the middle of Espoo forests and endless discussions on how we would make the world a better place! Thank you for being a part of my life! Thank you for being exactly what you are! Anna-Maria and Pekka, I want to thank you both for your hospitality that you have shown for my family and me for the past years! You are also to blame for our Hugo. Without you, I'm certain that we would not have thought of getting a coated hairless dog. ☺ I want to thank Pekka for my first "real" job after I finished my undergraduate studies. Finnzymes was certainly a great place to work, like a big family! You, with your wise and firm but warm mentality, made the environment absolutely remarkable! Anna-Maria, thank you for introducing me to Peruvian hairless and their mysteries! But also you have introduced me to my second home, the back forests of Espoo and the great dog hobbies we have! That is priceless! Thank you for being such a great friend, and a great support in all aspects of life!

My family, the whole lot of you! I'm so lucky to have you all. I have two great sister-in-laws who full my life with laughter and joy. Thank you Milma and Varja for being a part of my life. In addition I want to thank Jaakko (Varja's husband) for making sure that Alari and I get to eat also other food than just mashed potatoes and meatballs! ☺ I want to thank my dear sister, Saija, for being in my ilfe. You are the best sister in the whole world. The completion of this thesis would have not been possible without the help and support from my parents and my in-laws. I want to express my warmest regards and deepest gratitude to my mother and father in-law, Hilkka and Kari. You have been more than kind to me always. You have taken me in to your home and family and supported us and me no matter what! Hilkka, you truly are a supper woman, being able to fix everything and anything, having the longest nerves I ever seen and being able to stay calm no matter what happens. I admire you for that! Kari, I want to thank you for countless kilometers that you have been driving for us, bringing forgotten items to work, picking up kids from hobbies, rushing to the supermarket just to get us something we thought we had but didn't… Even more, I want to thank you for being you, our pappa, a very dear and special

person for all of us, especially the kids. I want to thank my father (isi), Olli, and his wife, Jutta, for all the love and support. You have always trusted my judging and supported me on every quest I've gone for in my life! Isi, you have always been my hero, and continue to be. You have always been by my side and you have always defended me if needed. I love you so much! My mom (äiti), Outi, and her husband, Tom, I am forever grateful for your endless support in science and life. No matter what has come in front of me, I've always known where to get help and where to go! Your door has always been open for me. I'm grateful for the offerings of your kitchen when I was a student with little money and a fridge with merely a light in it. I want to thank Tom for being the best personal tutor in physical chemistry during my chemistry studies. I owe you for those top grades! Äiti, I want to thank you for giving me a personal view to what it is to be a researcher and showing me how wonderful it can be. I love you both so much!

My husband, Alari, I cannot begin to describe how much you mean to me. Saying "I love you" is simply not enough. Without your unquestioning support and love this thesis would not exists. You took care of the kids and the dogs while I was working, especially the last year of my Ph.D. must have been tough on you, not to mention the last three weeks or so when you were practically a single parent. And now, you've even agreed to move to the other side of the globe for me! Thank you for being my rock! I thank you for giving me "my everything", my family. Through Alari I have had the privilege of getting to know the sweetest 11-year old girl in the world, Nona! Whom I love very much. Nona has taught me to be an adult, and to let go of my silly fears and fixations. Nona, you are a very special girl! We have two very special personas in the family, Hugo and Irinka, my furry babies. They keep my feet to the ground and my head in the forest!

Finally, I want to dedicate this book to my son, the love of my life, Tuukka! You take me to adventures (usually involving a car drive) every day. The very moment I arrive home you make me forget all my worries and life is perfect. You have shown me what means unconditional love, you have taught me more than any school I ever gone to has, and you have put things into perspective for me. I really don't have to worry about small stuff anymore! I feel proud and privileged to be your mom.

Somewhere over the Atlantic, 10th June 2015
Suvi Arola

Academic dissertation

Supervising
professor   Professor Markus Linder
               Department of Biotechnology and Chemical Technology
               Aalto University, Finland

Thesis
advisors   Associate Professor Kiyohiko Igarashi
                Department of Biomaterials Sciences, Graduate School of Agricul-
                tural Sciences
                The University of Tokyo, Japan

                Head of Applied Wood Materials Laboratory Dr. Tanja Zimmermann
                Applied Wood Materials, EMPA, Switzerland

Opponent   Associate Professor Neel S. Joshi
                Wyss Institute, School of Engineering and Applied Sciences
                Harvard, Boston, MA, USA

List of publications

This thesis is based on the following original publications which are referred to in the text as I–IV. The publications are reproduced with kind permission from the publishers.

I   Suvi Varjonen, Päivi Laaksonen, Arja Paananen, Hanna Valo, Hendrik Hähl, Timo Laaksonen and Markus B. Linder. 2011. Self-assembly of cellulose nanofibrils by genetically engineered fusion proteins. Soft Matter, 7, 2402–2411.

II   Suvi Arola, Tekla Tammelin, Harri Setälä, Antti Tullila, and Markus B. Linder. 2012. Immobilization-stabilization of proteins on nanofibrillated cellulose derivatives and their bioactive film formation. Biomacromolecules. 13, 594–603.

III Suvi Arola, Jani-Markus Malho, Päivi Laaksonen, Martina Lille, and Markus B. Linder. 2013. The role of hemicellulose in nanofibrillated cellulose networks. Soft Matter. 9, 1319–1326.

IV   Suvi Arola and Markus B. Linder. Binding properties of single and double cellulose binding modules reveal differences between cellulose substrate. Manuscript submitted to Nature Chemical Biology.

Author's contributions

Publication I

NFC and CNC were gained from the Finnish Centre for Nanocellulosic Technologies. The proteins used in the study were produced and purified by research assistant. The ^{3}H-labbellig and the purification of the labelled HFBI-DCBM were planned and conducted by the author (previously S.V., now S.A.). The binding studies were planned, conducted and the results were interpreted by author. The Langmuir-trough experiments were planned by the author together with A.P. and conducted by the author. Results were interpreted by the author. The Langmuir-Schaefer films were prepared by the author. The AFM imaging was done by the author and teaching on the use of the equipment was received form A.P. The AFM images were handled by the author and results were interpreted by the author together with P.L. The surface dilatational rheology experiments on air-water interface were planned and conducted by the author. The results were interpreted by the author together with P.L. The interfacial dilatational rheology experiments on oil-water interface were planned, conducted, and the results were interpreted together by the author and P.L. The emulsion studies were planned, conducted and results were interpreted by P.L., author helped in conducting the experiments. The epifluorescence and confocal microscopy experiments were planned, conducted and results were interpreted by P.L., author helped in conducting the experiments. The drug nanoparticle TEM experiments were planned, conducted and otherwise handled by H.V. and T.L. Ellipsometry experiments were planned, conducted and otherwise handled by H.H. QCM-D experiments were planned, conducted and otherwise handled by A.P. The surface shear rheology experiments were planned and conducted by the author, and results were interpreted by the author with the aid of P.L. The manuscript was written mainly by M.B.L. and P.L. The author actively contributed in the writing process of the manuscript. M.B.L. supervised the research.

Publication II

The NFC materials used for the modifications and the TEMPO-NFC were received from the Finnish Centre for Nanocellulosic Technologies. Amine modification of NFC and the characterization of the material (XPS) were done by T.T. The epoxy modification of NFC and the characterization of the material (CP/MAS NMR and Kjeldahl method) were done by H.S. The anti-hydrocortisone antibody and the hydrocortisone-AP conjugate were provided by A.T. The author planned and performed the rest of the experiments and interpreted the all results. The author wrote the manuscript with valuable comments from T.T. under the supervision of M.B.L. The research was supervised by M.B.L.

Publication III

The NFC used in the work was received from the Finnish Centre for Nanocellulosic Technologies. The pI9 xylanase was received from Dr. Matti Siika-aho. The author planned, conducted and analyzed the results of total hydrolysis of NFC and pI9 hydrolysis of NFC. The author planned the small deformation rheological experiments and interpreted the results together with M.L. The author conducted the small deformation rheological experiments. The author planned the extensional experiments of the NFC films together with J-M.M. The author prepared the films used in the study. J-M.M. conducted the extensional experiments on the films. The author analyzed the data of the extensional experiments together with J-M.M. The author planned the cryo-TEM experiments and prepared the samples. The cryo-TEM imaging was done together with J-M.M. and the results were analyzed by the author. The author planned and conducted the AFM experiments and analyzed the results. The author planned and conducted DWS experiments. The author analyzed the DWS results together with P.L. The author wrote the manuscript under the supervision of M.B.L. The research was supervised by M.B.L.

Publication IV

The author planned the work and wrote the manuscript with the aid of M.B.L. The work was fully conducted by the author, except for protein production carried out by Dr. Michael Bayley, and protein purification and cleavage carried out by Riitta Suihkonen. The results were interpreted by the author with the aid of M.B.L. who also supervised the research.

Contents

List of symbols

A_f	Free amplitude
A_{sp}	Set point amplitude
AFM	Atomic force microscopy
AGU	Anhydroglucopyranose unit
Amine-NFC	Amine modified nanofibrillated cellulose
AP	Alkaline Phosphatase
a-w	Air-Water
B	Langmuir one-site binding isotherm
B'	Derivative of Langmuir one-site binding isotherm
BC	Bacterial cellulose
B_{max}	Maximum binding capacity
BMCC	Bacterial microcrystalline cellulose
°C	Degrees Celsius
$CaCl_2$	Chemical formula of calcium chloride
CBD	Cellulose binding domain
CBM-Cel6A	Cellulose binding module of cellobiohydralase II
CBM-Cel7A	Cellulose binding module of cellobiohydralase I
CBHI	Cellobiohydralase I
cbhI	Cellobiohydrolase I encoding gene
CBHII	Cellobiohydralase II
CBM	Cellulose binding module
CD	Catalytic Domain

Cel6A	Cellobiohydralase II
Cel7A	Cellobiohydralase I
cm^2	Cubic centimeter
CNC	Cellulose nanocrystals
cryo-TEM	Cryogenic transmission electron microscopy
δ	Phase angle (delta)
DCBM	Double cellulose binding module
DCBM-12	Double cellulose binding module with a linker of 12 amino acids
DCBM-24	Double cellulose binding module with a linker of 24 amino acids
DCBM-48	Double cellulose binding module with a linker of 48 amino acids
deg	Degree
DMSO	Dimethyl sulfoxide
DNA	Deoxyribonucleic acid
DP	Degree of polymerization
DVS	Dynamic vapor sorption
E	Young's modulus, tensile modulus
E'	Dilatational storage modulus
E''	Dilatational loss modulus
E*/|E|	Dilatational complex modulus
E. coli	*Echerichia coli*
ELISA	Enzyme-linked immunosorbent assay
Epoxy-NFC	Epoxy modified nanofibrillated cellulose
ESI	Emulsion stability index
g	Gram
γ	Strain (gamma)
G'	Shear storage modulus
G''	Shear loss modulus
G*	Shear complex modulus
ΔG	Gibb's free energy difference
GGC	Golden gate cloning

GPa	Giga Pascal (10^9 Pascals)
gpdA	Glyceraldehyde-3- phosphate dehydrogenase gene
^{3}H	Tritium
HCl	Chemical formula of hydrochloric acid
HCl-CNC	Hydrochloric acid hydrolyzed cellulose nanocrystals
HFBI	Hydrophobin HFBI
HFBI-DCBM	Hydrophobin HFBI double cellulose binding module fusion protein
HFBI-DCBM-12	Hydrophobin HFBI double cellulose binding module fusion protein with a linker of 12 amino acids between the binding modules
HFBI-DCBM-24	Hydrophobin HFBI double cellulose binding module fusion protein with a linker of 24 amino acids between the binding modules
HFBI-DCBM-48	Hydrophobin HFBI double cellulose binding module fusion protein with a linker of 48 amino acids between the binding modules
H_2O	Chemical formula of water
hph	Hygromycin resistance gene
H_2SO_4	Chemical formula of sulfuric acid
Hz	Hertz
K_a	Association constant
K_d	Dissociation constant
k_d	Affinity
kDa	Kilo Dalton (10^3 Daltons)
KH_2PO_4	Chemical formula of monopotassium phosphate
kPa	Kilo Pascal (= 10^3 Pascals)
K_r	Partitioning coefficient
L	Liter
LC	Liquid crystal
LB	Langmuir-Blodgett
LbL	Layer-by-layer
LS	Langmuir-Schaefer
m	Meter

MALDI-TOF MS Matrix-assisted laser desorption/ionization – time of flight mass spectrometry

MC   Methyl cellulose

MCC   Microcrystalline cellulose

µeq   microequivalent

MFC   Microfibrillated cellulose

µg   Microgram (10^{-6} grams)

$MgSO_4$ Chemical formula of magnesium phosphate

ml   milliliters (10^{-3} liters)

µm   Micrometer (10^{-6} meters)

mm   Millimeter (10^{-3} meters)

mM   millimolar (10^{-3} moles per liter)

mmol   Millimole (10^{-3} moles)

mN   Milli Newton (10^{-3} Newtons)

m/z   mass to charge ratio

NC   Nanocellulose

NFC   Nanofibrillated cellulose

$(NH_4)_2SO_4$ Chemical formula of ammonium sulfate

nm   Nanometer (10^{-9} meters)

NR   Natura rubber

ω   Frequency (omega)

OLED   Organic light emitting diode

o-w   Oil-Water

Pa   Pascal

p-NPP   Para-nitrophenyl phosphate

PCR   Polymer chain reaction

PD   Potato dextrose

PDS   Particle delivery system

PEI   Polyethylene imine

PIPPS   Piperazine-N,N'-bis(3-phosphanesulfonic acid)

pmol	Picomole (10^{-15} moles)
R	The universal gas constant
RH	Relative humidity
RP-HPLC	Reversed phase high performance liquid chromatography
RP-UPLC	Reversed phase ultra-high performance liquid chromatography
σ	Stress (sigma)
SDS	Sodium dodecyl sulfate
SFB	Succinimidyl-4-formylbenzoate
SIEBIMM	Strain-induced elastic buckling instability for mechanical measurements
SiO_2	Chemical formula of silicon dioxide
Sulfite-CNC	Sulfuric acid hydrolyzed cellulose nanocrystals
T	Temperature
TEMPO	2,2,6,6-tetramethylpiperidine-1-oxyl
TEMPO-NFC	2,2,6,6-tetramethylpiperidine-1-oxyl oxidized nanofibrillated cellulose
TEV	Tobacco eche virus
TFA	Trifluoro acetic acid
T. reesei	*Trichoderma reesei*
w/w	Weight per weight ratio
XPS	X-ray photoelectron spectroscopy
∞	Infinite
Ø	Diameter

1. Introduction

Cellulose is an interesting material due to its structural features, biodegradability, and renewability. It is also the most abundant polymer on Earth and thus easily available. For example, it can be found in all plants, some alga, and also bacteria. Figure 1 presents the molecular structure of cellulose polymer.[1] Cellulose is a homopolymer formed by D-anhydroglucopyranose units (AGU). The AGUs are linked together by a β-(1→4) glycosidic bond connecting the C-1 and C-4 atoms of adjacent molecules with a 180° rotation in respect to each other that form the repeating unit of cellulose chains, cellobiose. The length of a native cellulose chain (degree of polymerization, DP) varies depending on the origin and treatment. Each AGU has three hydroxyl groups on C-2, C-3, and C-6 position making cellulose a hydrophilic polymer. Terminal groups on cellulose chains are chemically different. On one end the C-1 OH is an aldehyde and has reducing power and it is therefore called the reducing end. On the other end the C-4 OH is an alcohol and thus it is called the non-reducing end.[2,3]
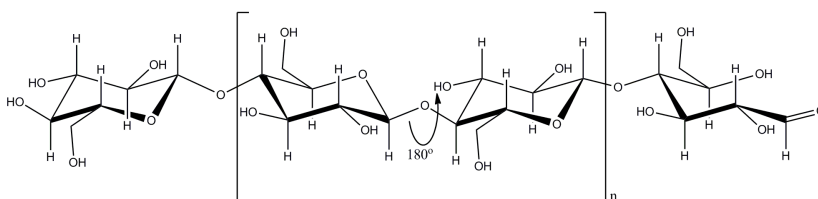
Figure 1. Molecular structure of cellulose chain showing the repeating unit, cellobiose, and the reducing (right) and non-reducing (left) end-groups. The AGUs are rotated by 180° with respect to each other.

Cellulose can exist in six different polymorphs; I, II, III$_I$, III$_{II}$, IV$_I$, and IV$_{II}$.[2,4] In nature cellulose is found in the cellulose I polymorph structure where the chains are packed parallel-up and edge-to-edge via extensive intra- and intermolecular hydrogen bonding to form sheet-like structures which form fibril structures.[4] Cellulose I exists in two crystalline forms, cellulose Iα and cellulose Iβ, which have different hydrogen bonding networks.[5–7] The two forms coexist in cellulosic materials but the ratio var-

ies depending on the source. Cellulose Iß is predominant in higher plants and cellulose Iα in bacteria and tunicate.[7] In the fibrils the crystalline parts are accompanied with less structured amorphous-like regions.[8] The ratio of crystalline-to-amorphous cellulose also varies depending on the source of cellulose. In wood, cellulose is found in the cell wall structures where it is hierarchically packed to form large fibers. These fibers are formed by the stacking of cellulose chains to nanosized elemental fibrils with crystalline and less ordered amorphous parts. These in turn pack into larger nanofibrils that further pack into micron sized and microscopic fibers (Figure 2). In wood cell wall hemicellulose, pectin, and lignin together with cellulose fibrils form a complex bio-composite that offers mechanical support to the tree and protects the tree against environmental factors such as changing climate and pathogens.[9,10]

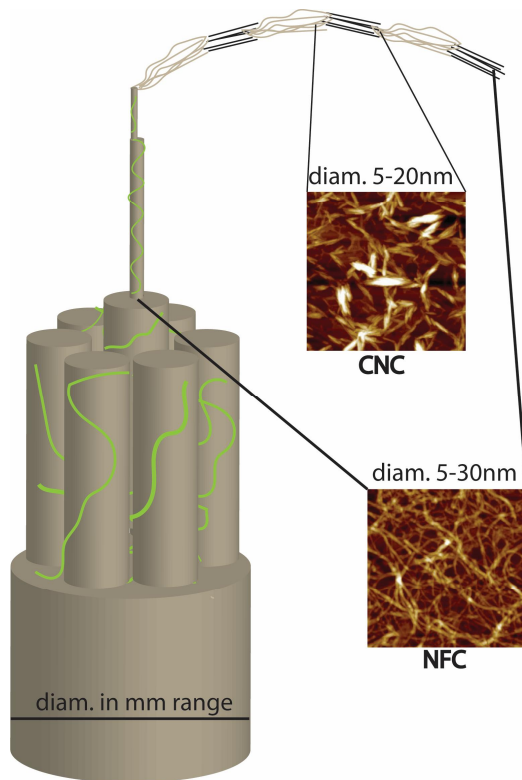**Figure 2.** A schematic illustration of the hierarchy in macroscopic cellulose fibers. Hemicellulose (shown in green) and lignin are incorporated in the structure between fibers and fibrils. AFM images showing cellulose nanocrystals (CNC) and nanofibrillated cellulose (NFC) point out at which level of hierarchy these materials originate form. The image is not in scale but is only representative.

1.1 Nanocellulose

Recently, methods combining chemical, mechanical and enzymatic treatments to disintegrate wood fibers to produce nanocellulose (NC) have been developed.[11–14] Depending on the treatment fibrils with a diameter of 5–30 nm and length in micrometers, or rod-like crystals with a diameter of 5–20 nm and length of tens to hundreds of nanometers to micrometers can be obtained. The fibril/crystal dimensions depend strongly on the treatment and the source but they are always nanosized in at least one dimensions.[3,15–17] The name first adopted for the fibril material from wood source was microfibrillated cellulose (MFC)[18], later the material has been referred to as nanofibrillated cellulose (NFC) or cellulose nanofibrils (CNF).[16,17] The nanosized crystals have previously been called cellulose nanowhiskers or simply whiskers but later a more informative term, cellulose nanocrystals (CNC) has been adopted.[19–21]

1.1.1 Nanofibrillated cellulose, NFC

Nanofibrillated cellulose (NFC, Figure 2) can be prepared from wood based pulp material by simultaneous enzymatic and mechanical treatment [22,23] or just mechanical treatment.[24] NFC materials have extraordinary properties due to their nanoscale dimensions. The long and entangled fibrils have high aspect ratio and large surface area exhibiting vast amounts of reactive hydroxyls groups on their surface. [22,25–27] They form an extensively percolating network with low weight percentages. In water NFC forms a gel, which strength is dependent on the fibril concentration. Upon drying NFC forms hierarchical nanoporous aerogels or strong films depending on the drying process.[22,28,29] The mechanical properties of NFC paper films have been reported to be better than ordinary paper and the reinforcing ability in composite materials has also been shown to be superior compared to pulp fibers.[30,31] This is caused by the larger surface area of fibrils exhibiting extensive hydrogen bonding compared to macroscopic fibers. Moreover these films have good gas barrier properties which can be of benefit in many coating and barrier technologies[32]. The aerogels have been shown to have very different properties compared to traditional aerogels due to the long and entangled fibrils forming a hierarchical nanoporous structure.[28] They open up new application areas for the use of aerogels in general. Due to its biocompatibility NFC is also a promising material for biotechnological and pharmaceutical applications.[15,33]

1.1.2 Cellulose nanocrystals, CNC

Cellulose nanocrystals (CNC, Figure 2) can be obtained from different sources by hydrolysis with a concentrated mineral acid.[12,20,21,34,35] The treatment hydrolyses the non-crystalline parts of cellulosic materials yielding a dispersion of rod-like crystalline cellulose sticks. These nanosized rods range in size depending on the source

they are obtained from and by the reaction conditions but usually are 5 to 20 nm in width and 0.1 to ~1 µm in length.[20,21,36] CNC has smaller aspect ratio than NFC and in solution does not form as strong gel as NFC due to the lack of extensive percolation of the network.[22,37] Yet the rods are mechanically extremely strong. Experimentally, the Young's modulus of a single crystal of cellulose I is ~134 GPa and the strength in the GPa range.[38] Due to the crystalline rod-like structure, CNC display other interesting properties such as liquid crystallinity.[39]

The mineral acid used in the hydrolysis of cellulose material determines whether the resulting CNC will carry charge on their surface or not.[20] By hydrochloric acid hydrolysis the surface of the crystals will be almost neutral and display almost solely hydroxyl groups. These CNC are usually referred to as HCl-CNC. In this form the CNC are poorly dispersed in water and other solvents due to their tendency to aggregate via strong hydrogen bonding.[13,40] The colloidal stability of HCl-CNC is affected by their concentration and aggregation is more pronounced in higher concentrations.[13] If the hydrolysis is performed with sulfuric acid the resulting CNC will hold sulfate groups on the surface and a net negative charge, referred to as sulfate-CNC. The sulfate-CNC are readily dispersed in water due to their charged surface. They form stable colloidal dispersions in water but can be aggregated with increasing ionic strength.[12,13,20,27] CNC can also be dispersed in some organic polar solvents, such as DMSO.[41]

1.2 Applications for nanocellulose materials

There is a growing need for sustainable and more environmentally friendly materials and products in the market to replace plastics and other unsustainable materials. For this cellulose as a material is well suited. Due to its large surface area and high aspect ratio leading to superior mechanical properties compared to macroscopic cellulose fibers and regenerated cellulose, NC could be used in applications where traditional cellulosic products would not be well suited, for example aerogels, composite reinforcement and flexible electronics.[28,42–49] The research done in the field of nanocellulosic materials is growing and new application areas are being explored by the growing knowledge on these very interesting materials. This chapter deals with the application areas where NC could potentially replace other materials, broaden the use of these applications, and show examples on how NC has been used in these fields.

1.2.1 Rheology modifiers

Rheology studies the flow and flexure of materials. In many applications it is very useful if the flow of matter can be altered during processing. Altered flow properties can for example allow broader applicability for existing materials. Gels with percolating networks can be used to modify the rheological properties of other materials when mixed together. The need to modify how matter stands applied force is often useful in such cases as in paint and lacquer applications, in cosmetic applications,

in polymer processing, and in food technology. In many applications it is useful if the rheological properties of the material can be tuned to fit certain needs for example in processing; e.g. to ease the spreading of paint to wall or melt processing or extrusion of a polymer, or simply adding strength to the material in wet state in different environmental conditions.[50–52] On the other hand the rheological properties of a material determine how it can be used in specific applications, such as hydrogels, reinforcing phase in composites, thin film applications or emulsion and foam stabilization.

NFC forms a strong gel in aqueous media in broad range of concentrations in contrast to CNC dispersions which form gels only in very high concentrations. Pääkkö et al. have studied NFC (prepared from soft wood sulfate pulp by mechanical and enzymatic means) rheological properties. They showed that these materials display typical ideal gel behavior, i.e. elasticity, that is the storage modulus, G', is much greater than the loss modulus, G'', and G' is independent of frequency in low solid content dispersions (0.125 % w/w) as well as in high (5.9 % w/w).[22] Shafiei-Sabet et al. on the other hand have shown that CNC with net negative charge behave like viscous fluids in low concentrations (< 10 % w/w), the behavior is then gradually changed to weak gels (~12 % w/w) and to stiff gels with G' (~10^2 Pa) > G''.[53] The strength of the gel or dispersion, i.e. G'-values, were dependent on the concentration in both cases. The modulus of NFC was noted to be 2-orders of magnitude higher for NFC dispersions compared to CNC dispersions, which showed that NFC forms a strongly percolated entangled network compared to CNC. The NFC dispersion showed shear thinning behavior, which is typical for such gels. For CNC dispersions, at lower concentrations (1–4 % w/w), different states during the shear thinning process were observed; a transition from isotropic to liquid crystal (LC) phase, the destruction of LC phase and the orientation of individual CNC rods along the shear force. For CNC at higher concentrations (> 4 % w/w), the transitions from alignment of LC to aligned LC phase to destruction of LC phase and formation of gel were seen. The higher shear viscosity of NFC compared to CNC is due to the entangled network that prevents the individual elements from flowing under increasing shear in contrast to CNC dispersions, where the elements are interconnected less extensively and can flow upon increased shear.

The presence of hemicellulose in the NFC material and its effect on the viscosity was also studied[22]. It was noted that the net negative charge of the material (44.2 µeq/g) was solely caused by the presence of hemicellulose. The viscosity of the dispersion was increased by the lowering of pH, i.e. the amount of negative charge in the material was reduced. This reduction of negative charge decreased the repulsion between the fibrils and allowed more interfibrillar interactions that lead to increase in viscosity. The opposite was seen upon increase of pH; more negative charge on fibrils caused more charge and more repulsion between fibrils, this in turn lead to less interfibrillar interactions and lower viscosity.[22] The same observation of effect of charge was seen with CNC when two preparations with lower and higher net negative charge were compared.[53] The flow properties of HCl-CNC and sulfate-CNC have been studied by Araki et al. [13]. In their study they conclude that both CNC show shear thinning properties yet HCl-CNC more strongly. The time dependent

viscosity measurements showed that the viscosity of sulfate-CNC dispersions was not dependent on time and was a stable colloid throughout the experiment. On the other hand the viscosity of HCl-CNC was time dependent; high concentrations (>5 gL^{-1}) showed thixotropic behavior (decrease in viscosity) and low concentrations (<3 gL^{-1}) anti-thixotropic behavior (a slight increase in viscosity was seen). The structurally very similar materials showed remarkably different flow properties and thus were concluded to be useful with different applications in respect to each other.

These investigations highlight the importance of the rheological properties of NFC and CNC in relation to many applications. The dependence of the viscosity and strength of the gel or dispersion on concentration and the shear thinning behavior can be especially interesting for many applications where ability to tune material properties and change behavior according to processing are desired, yet where it is important that gel properties and the entangled network structure are preserved. Also the fact that CNC undergo phase transitions during shearing process is relevant in many cases. Due to the different rheological behavior of CNC dispersions compared to NFC, i.e. lower viscosity, weaker dispersions/gels, and liquid crystallinity, the applications for them would be somewhat different. Although both materials show promise in strengthening composites and hydrogels.[54]

1.2.2 Composites

Composites are materials that combine two usually very different materials together in a way that the mechanical properties of the composite are better compared to the materials that it is made up of alone. Composites usually contain a softer continuous phase and a stiffer or harder reinforcing phase. The materials in composites do not dissolve into each other but are separate and can be distinguished from one another.[55–57]

Practically all natural materials are composites. These materials are in many perspectives superior in their properties compared to manmade ones. For example the mechanical properties of natural ceramics (e.g. bone, shell, and dentine) combine stiffness and toughness witch is very hard to achieve in synthetic analogs. Their moduli are lower than those of synthetic ones, but their tensile strengths are similar and their toughness is much greater. Natural polymers (e.g. cellulose, chitin, collagen, and silk) have much larger moduli and tensile strengths than engineered polymers, excluding Kevlar fibers, which have highly oriented molecular structure, as do natural polymer fibers, and covalent bonding.[58–60]

Natural composites illustrate very well the effect of structure within the composite to the overall mechanical properties of the material. An example is the differences in mechanical properties of tendons, ligaments, skin, cartilage and bone. They are all composed mainly of two components; collagen and elastin. The distinction of the materials and thus their very different properties lie in the fraction and architecture of each component.[58] All natural composites have hierarchical structure from nanoscale to macro scale to mesoscale. At the sub-nanoscale the self-assembly of atoms and molecules will drive the formation of nanoscale structures that in turn will

self-assemble and cause large well defined structures to form and these in turn induce the next scale structures to form. This is called the bottom-up method of building structures and this is the way materials and structures are built in nature.[57,59,61] The hierarchical assembly of natural composites adds fracture toughness and allows better energy dissipation within the material when outside force is applied.[57,61] Manmade composites are blends of two materials and their properties are mostly dictated by the manufacturing process.[55] Recently attempts to mimic nature's way of bottom-up approach have been taken into practice in making engineered composites.[56]

Two features are important when considering a composite material: 1) The interface between the two materials should interact with each other in order for the material to transfer applied stress and load during impact. 2) The reinforcing material should be well dispersed into the soft phase otherwise no reinforcement or only local reinforcement occurs which does not allow reinforcement throughout the whole material.

The strength of a composite can be studied by the relation between stress and strain. The stress is the applied force on an object divided by the area of where it is applied to, and the strain is the resulting deformation of the sample. Typically if the applied stress is small the material will undergo elastic deformation, i.e. it can recover to its original shape when stress is released. In this elastic region the strain is linearly proportional to the stress. When applied stress becomes higher the response of the material becomes non-linear but can still be elastic. Above a critical point (yield point) the response of the material becomes plastic and the material will not recover to its original shape after stress is released. The strain-to-failure will occur when the material ruptures. The tensile modulus, E, or Young's modulus is determined in the linear-elastic region of tensile tests and is the ratio of tensile stress and tensile strain (elongation).[58]

For composite materials both NFC and CNC could be interesting materials. NFC can be used as a percolating network of strong interconnected fibrils which is embedded in a softer polymeric matrix. In the same way, CNC can be used to reinforce a softer matrix material to strengthen the system. NFC can also been used as a soft, yet strong, connecting material together with tough and strong materials such as graphene to mimic nacre architecture.[19,25,48]

Abraham et al. present an example of a natural rubber latex (NR) – NFC –composite (NR/NFC-composite) where the NR matrix has been reinforced with NFC obtained from jute fibers by steam explosion.[62] The NR/NFC-composite was either cross-linked or not and the biodegradability, morphology, crystallinity and mechanical properties were studied. The biodegradability of NR/NFC-composites was confirmed and the more NFC the materials contained the better they were degraded. Cross-linking of the composite hindered the biodegradability, yet the cross-linked composites showed superior mechanical, thermal and barrier properties compared to non-cross-linked composites. They propose a mechanism for the cross-linking and show that due to the cross-linking reaction, the crystallinity of NFC is totally lost. So in the sense reinforcement of the composite does not come from crystalline cellulose but well dispersed amorphous cellulose fibrils or chains interacting with and

cross-linked to the NR-matrix. In the non-cross-linked NR/NFC-composite the crystallinity of NFC is preserved and the composites compared to non-cross-linked NR alone show higher Young's modulus and tensile strength, yet the ability of the composite to elongate is hindered compared to NR. This shows that NFC fibrils can reinforce the NR matrix.

Another example of NFC used as a reinforcing material is the work of Fernandes and co-workers where they used NFC to reinforce chitosan to prepare transparent, flexible, mechanically and thermo-mechanically better films compared to neat chitosan films.[63] The preparation was done by simple mixing of solution of chitosan (high or low molecular weight chitosan in acidic solution, or their water-soluble derivatives) with different amounts of NFC (maximum of 60% NFC in the film). The mechanical properties were improved drastically by the addition of NFC into the matrix (improvement of Young's modulus of up to 150% with the water-soluble high molecular weight chitosan and 320% with the water-soluble low molecular weight chitosan). The thermo-mechanical properties and the thermal stability of the composites were also better than those of the neat chitosan.

NFC can also be used as the "soft" or "continuous" phase of a composite and be reinforced with a harder material. An example of this is presented in the work of Aulin et al. where nanoclay particles are used to reinforce NFC matrix resulting in optically transparent, flexible biohybrid films with stiff and strong mechanical properties, and better oxygen barrier properties compared to the NFC alone.[44] In this work, interaction between the NFC matrix and nanoclay particles is enhanced by surface modification of NFC so that the fibrils carry a net negative charge.

Capadona et al. have shown in their work how CNC reinforced polymer matrix results in a stimuli-responsive composite material inspired by the sea cucumber dermis.[64] They showed that CNC from tunicate reinforce the polymer matrix and upon a stimuli (depending on the polymer used; for example chemical or thermal) the mechanical properties are changed. They show that the interaction of the chemical stimuli with the CNC in the matrix causes the disturbance of the percolating network of CNC and cause the lowering of mechanical properties. They show that these materials could be useful in biomedical applications serving as adaptive substrates for intracortical microelectrodes.

1.2.3 Porous scaffolds

Hydrogels and aerogels, both porous materials to the nanometre scale, are promising for making stimuli responsive materials, to embed and transfer functional moieties, for architectural scaffolds, for microelectronics, acoustics, and optics among other applications.[65–68]

1.2.3.1 Hydrogels

Hydrogels are hydrophilic polymeric networks that can retain large amounts of water and still maintain their three dimensional structure. The hydrogel network is either

chemically (covalent bonds) or physically (van der Waals, charge or hydrophobic interactions) cross-linked and it can be stimuli responsive (heat, light, chemical etc.) in adsorbing and desorbing water.[67] There are numerous examples on hydrogel usage in for example bio-medical applications such as tissue engineering, diagnostics, and drug delivery [69–73], in pharmaceutical and cosmetic applications [74], as adsorbent materials in diapers and other everyday items, and in fillers and paints.[67] Traditional hydrogels are not strong in their mechanical properties due to the large amount of water they hold, and thus do not allow applicability in areas where load bearing is needed.[67,68]

NFC forms hydrogels in low weight to volume ratio when it is produced. The gels are mechanically strong and the strength is dependent to their solid content. The NFC network is physically cross-linked by interfibrillar hydrogen bonding. The fact that NFC is fully biological and biodegradable also offers a possibility to replace polymer-based hydrogels in existing applications.[22]

NFC hydrogels offer a good platform for biotechnological applications such as tissue engineering and cell culture where hydrogels are often used, due to its three dimensional well hydrated porous scaffold with desirable and tunable structure, low toxicity and biocompatibility. This has been demonstrated by Bhattacharya and co-workers.[73] In their work they show that the hydrogel of native NFC from wood source serves as a three dimensional extracellular matrix mimic for liver cell growth and differentiation. No cytotoxicity was observed, and the rheological properties of NFC were noted to be beneficial for processing of the material into three dimensional cell cultures; specifically, it was injectable and allowed mixing of cells into the gel structure, yet provided the mechanical strength that was needed for the support of cell growth and differentiation.

CNC can be used to reinforce stimuli responsive hydrogels to give better mechanical properties compared to the hydrogel alone.[54] McKee et al. used mechanically strong CNC to reinforce thermo-responsive yet mechanically weak methylcellulose (MC) to yield an all-cellulose thermo-reversible and tunable nanocellulose-based hydrogel. The mechanical properties were improved by the growing concentration of CNC in the matrix while the MC concentration remained constant throughout the study. At low temperatures (20 °C) and low CNC concentrations the hydrogels behaved as viscous dispersions, upon increasing CNC concentration weak gels were obtained. At higher temperatures (60 °C) the hydrogels behaved as distinct gels. McKee and colleagues conclude that they show a facile and scalable method for preparation of fully cellulose containing nanocomposite hydrogels with a broad window of viscoelastic properties that can be tuned simply by choosing CNC concentration and temperature according to the need of the application.

1.2.3.2 Aerogels

Aerogels are ultra-light weight porous solid materials traditionally made of inorganic silicon dioxide.[65,66,75] They can also be manufactured from other materials such as

carbon, carbon nanotubes and graphene, or other organic materials, which can also be pyrolyzed to carbon.[76–81] The porosity of an aerogel is very high (usually over 75 %) and they are usually transparent and very brittle due to this reason.[75] To enhance silicon based aerogels mechanical properties organic-inorganic silicon based aerogels have also been prepared. Aerogels have an open-pore structure and they have large surface area due to their structure. The traditional SiO_2-based aerogels have a structure that resembles string of pearls (the particle size being ~4nm) joint together from here and there so that the voids in between the strings are in average ~30 nm (Figure 3). Aerogels are usually made from solvent swollen wet gels by supercritical drying process. The key in preparing the aerogel is that the percolating network of solid material is not lost (prevention of collapse and shrinkage of network is essential) during the drying process.[65,66,75]
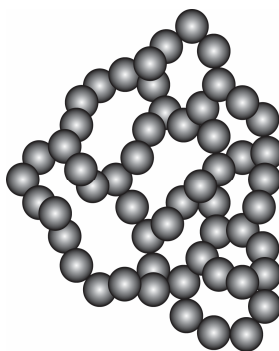

Figure 3. A schematic illustration of a traditional aerogel based on silicon. The particles are connected to each other like pearl neckless, structures are three dimensional and the voids are typically ~30 nm in size. Adapted from [75].

Aerogels have applications in many fields ranging from chemistry to material science to physics; they are used in Cerenkov detectors, they can be used as insulators, in passive solar energy usage, as catalytic substrates, in acoustics, and as filters to name a few.[75]

NFC forms a nanoporous hydrogel as it is prepared. This hydrogel can be used to prepare light weight flexible aerogels with very different properties compared to the SiO_2-based and carbon based aerogels.[28,47,49,82,83] Cellulose-based aerogels have been prepared previously but their emphasis has been on using regenerated cellulose derivatives (cellulose II) or cellulose-starch blends.[84–88] Cellulose II is mechanically weaker than the native cellulose I so NFC offers a feasible route for mechanically strong, biodegradable, bio-based platform for aerogels.

There is a growing number of examples on NFC aerogels used to prepare for example functional materials.[45,89–92] One of the first to show the preparation and applicability of NFC aerogels were Pääkkö and co-workers.[28] They showed that NFC hydrogels without chemical cross-linking can be used to prepare flexible and

mechanically durable aerogels in vacuum oven by freeze-drying. Due to the entanglement of the fibrils in the network no cross-linker was needed and the cross-linking of the aerogel was caused by physical intermolecular interactions (hydrogen bonding) of fibrils. In contrast to inorganic and organo-modified silica aerogels, NFC aerogels showed an order of magnitude higher strain and had maximum compression strength of ~200 kPa. These results highlight the fact that NFC aerogels are not brittle as traditional aerogels. Pääkkö et al. also show that these aerogels can be used to prepare conducting aerogels simply by immersing the aerogel to a solution of conducting polymer with surfactant. The polymer used in their work was polyaniline doped with dodecyl benzene sulfonic acid.

Jin et al. show how NFC aerogel can be used to create superhydrophobic and superoleophobic materials and show their applicability as cargo carriers on water and on oil.[49] The material was shown to be able to carry a load much larger than its own weight. They show that these materials mimic the water striders in their ability to form a layer of air between the solid material and water (a plastron layer). This was also shown to occur in oil. The material showed reduces viscous drag when it was in contact with oil, which originates from its ability to create the plastron layer. The material was also shown to selectively permeate gases by not fluids.

These examples show that NFC aerogels can be applied in very different ways than the traditional aerogels made of inorganic silica, paving the way towards green and bio-based aerogels.

1.2.4 Stabilization of surfaces and interfaces in foams and emulsions

In many foam and emulsion applications, especially in food, pharmaceutical, and cosmetic industries, the stabilization of surfaces and interfaces is a key issues for product development.[93,94] Another way to improve foam and emulsion stability is to modify the properties, for example viscosity, of the continuous face. Traditionally foams and emulsions can be formed and stabilized by the presence of amphiphilic molecules such as detergents. These molecules are considerably small in size and contain a longer hydrophobic moiety and a small hydrophilic moiety, such as sodium dodecyl sulfate (SDS), which is commonly used in everyday items like toothpaste. Detergents self-assemble to cover gas or oil droplets in water environment so that the hydrophobic side of the molecule is facing the gas/oil (i.e. the hydrophobic material) face and hydrophilic facing water, or the hydrophilic material (Figure 4A). They lower the surface or interfacial energy and thus allow the formation of foams and emulsions and keep the formed gas bubbles or oil droplets apart. Traditional detergents do not stabilize the foams and emulsions very well allowing the coalescence of oil droplets or gas bubbles during time.[93,94] In foams this is known as Oswald ripening where gas flows from smaller bubbles to larger bubbles causing the loss of foam structure.[94] More effective stabilization of surfaces and interfaces is gained by the use of polymers.[95] Once adsorbed to the surface or interface they are more efficient in keeping the interfaces apart. [93,95]
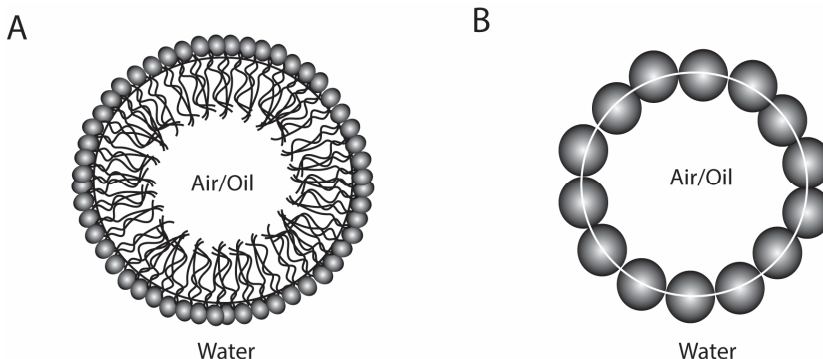
Figure 4. A schematic illustration of A) detergent, such as SDS, stabilized emulsion/foam, and B) a solid-stabilized emulsion (Pickering emulsion)/foam.

Along traditional emulsifiers and foaming agents, solid stabilizers of nanoscale size have been developed. These solid particles self-assemble on surfaces and interfaces and produce more stable foams and emulsions. Solid-stabilized emulsions are also called Pickering emulsions. The solid particles assemble on the interface due to their tendency of being partially wetted by water and partially by the hydrophobic matter (Figure 4B). The same principal drives them to gas-water interfaces.[96,97] These solid particles are also called Janus particles due to their two-phased nature.[98–100] Janus particles exist in nature as well, for example the protein amphiphile, hydrophobin, from fungi is well known to lower the surface tension of water by self-assembling onto the air-water surface and allowing the hyphae to penetrate through the surface. [101,102] They also readily assemble to any hydrophobic material, liquid or solid.[101,103–105]

Nanocellulose having nanoscale dimensions could be a useful bio-based solid colloidal material for the stabilization of emulsions and foams.[106–112] It is known that in the crystalline cellulose parts of cellulose I the cellulose chains are arranged in such a fashion that the different faces of the crystallites have different properties; two of them are more hydrophobic while the other two are clearly hydrophilic.[113,114] This is a useful feature in NC that could aid its assembly at interfaces and potentially be used as a stabilizer in emulsions and foams. Also the fact that NC is bio-based and bio-degradable adds interest in using them instead of polymers and non-biological solid particles especially in the fields of food, pharma, and medical technologies.

In literature many times the phrase "foam" is used instead of "aerogel", which the material actually is. I will here make a difference in that an aerogel is a material that has been prepared by the exchange of liquid to gas as described earlier. By foam is meant a structure where gas in one way or another has been trapped in a matrix containing liquid and possibly solid material. The foam can be dried after preparation to yield solid foam or dry foam.

In our work in Publication (I) we saw that both CNC and NFC assemble onto the oil droplet interfaces creating oil-in-water emulsions and that especially NFC had a significant effect on the emulsion stability. In addition to the assembly at the interface, NFC also changed the viscosity of the continuous phase (water) of the emulsions and thereby hindered the movement of the oil droplets within the matrix thus stabilizing the emulsion further compared to CNC.

Other examples of emulsion stabilization by NC materials are presented by Sèbe and colleagues[112], who used CNC, and Ougiya and colleagues[115], who used bacterial cellulose (BC). Cervin et al. have used NFC to stabilize foams[108].

In the first example, Sèbe et al. created Pickering emulsions of oil-in-water type with surface modified CNC. They had two different surface modifications and three different non-polar to slightly polar phases that were used to create the emulsions. The surface modifications were vinyl acetate and vinyl cinnamate, and they saw that the modification had an effect on the emulsion stability. They speculate that the vinyl cinnamate modified CNC emulsions could be useful in creating photo responsive emulsion systems. They also propose that the emulsion stabilization of such a system based on polymerizable monomers could be applied to polymerization in dispersion media.[112]

Ougiya et al. investigated BC compared to other more macroscopic cellulose materials (microcrystalline cellulose, MCC, microfibrillated cellulose, MFC), a natural polymer (xanthan gum), and a small surfactant (sorbitan monolaurate). They saw that BC stabilized the emulsions better than the rest of the cellulosic materials. This was due to its fine nanoscale size in comparison to the coarser MCC and MFC. It was also noted that the BC stabilized emulsions were stable against pH change, temperature change and NaCl concentration which neither the polymeric material nor the surfactant were. They saw that in addition to creating a mechanical barrier on the oil droplet surface, BC fibrils were observed in the continuous phase of the emulsion forming a scaffold for the oil droplets. This scaffold structure in their opinion contributed to the stability of the emulsion. This seems to be the same observation that we had with NFC stabilized emulsions, specifically that the fibrils in the continuous phase, in addition to the mechanical barrier on the droplet surface, serves to stabilize emulsions.[115]

Cervin et al. have shown that carboxymethyl modified NFC can be used together with a polymeric substance to stabilize foams and that these foams can be dried to solid foams without the collapse of the foam structure. The lifetime of the aqueous foams was significantly prolonged compared to foams that were not stabilized with NFC. The mechanical properties of the solid foams were measured and noted that the Young's modulus of compression was better than that of freeze-dried cellulose aerogels but lower than that of polystyrene foams. The structure of the aqueous foams was investigated by different microscopy methods. They saw that NFC assembled on the air bubble surfaces. They speculate that this assembly of the polymer coated NFC on the surface inhibits the diffusion of air from smaller bubble to larger bubbles and thus inhibits the coalescence of the bubbles and causes the stability of the foam.[108]

1.2.5 Thin films

Thin films are used in many different applications including electronics, coating and pharma technologies, biosensors, as well as employed to understand fundamental material interactions.[40,116–122] These films are often prepared on solid supports by spin-coating[123], solvent casting[124], chemical vapor deposition (CVD)[125,126], atomic layer deposition (ALD)[127] or prepared on a Langmuir trough by self-assembly of molecules onto air-water/oil-water interface and then lifted on solid supports by either Langmuir-Blodgett (LB) or Langmuir-Schafer (LS) -method[128–130]. Molecules with a self-assembling tendency can be adsorbed directly onto solid supports from bulk[101,104]. These different methods can be used to prepare thin films with monomolecular layers, or multiple layers of altering (or the same) materials referred to as layer-by-layer deposition (LbL)[131]. LbL allows a controlled architecture of alternating layers of different materials to be present in a film. Polymers, metals and nanomaterials are used for preparation of thin films for their desirable and tunable properties, which include conductivity, porosity, hydrophobicity, and plasmon resonance. Self-assembly is a feature that is, in most materials that form thin films, a key for the preparation and structure of the resulting film. Static self-assembly occurs when molecules assemble to reach a thermodynamic equilibrium or energetic minimum at certain conditions.[132]

CNC and NFC readily form thin films upon for example spin-coating, casting, LS-, and LB-techniques[32,133–135]. NFC thin films have been used as model films to study the interactions of native cellulose with several other molecules, such as hemicelluloses and cellulases[136,137]. NFC has also been used to prepare flexible, transparent organic light emitting diodes (OLED)[46]. The multilayers of NFC and polymeric materials have also been prepared and their mechanical and adhesive properties have been studied[138,139]. CNC has been used to create thin films with birefringence properties due to their rod-like structure[140]. These materials would offer an environmentally friendly approach for electronic and other thin film applications.

In Publication (II) of this thesis, we have investigated the use of NFC to create bioactive thin films that could be used in diagnostic applications but also in other applications where biomolecule immobilization is required, such as enzymatic pretreatment in paper making and other industrial scale processes that take advantage of enzyme reactions. In our work, we used NFC to take the immobilization chemistry from solid surface (2D) to bulk (3D), by attaching the biomolecules to NFC fibrils in aqueous dispersions. After the coupling the NFC ability to create films upon spin-coating was exploited in creating porous thin films with bioactivity. The benefit of NFC in this case was also the fact that multiple layers could be spin-coated and due to the porosity of the films bioactivity was seen throughout the whole film.

Cranston et al. used LbL deposition of NFC and polyethylenimin (PEI) to create thin films of different thicknesses of alternating NFC and PEI.[139] The elastic properties of the films were investigated by strain-induced elastic buckling instability for mechanical measurement (SIEBIMM) technique. This technique allows the determination of Young's modulus of thin films with thickness down to ~40 nm. In their

work Cranston and co-workers show that NFC thin films and SIEBIMM are useful tools to investigate how the properties of the thin films change with humidity and thickness, provide in-depth information on the fibril-fibril and fibril-polymer interactions and show that SIEBIMM is an applicable technique to large aspect ratio colloidal particles. They show that humidity causes a significant decrease in the mechanical properties and highlight that in order to achieve strong reinforcement by NFC extensive cellulose-cellulose interactions are needed and water adsorption has to be minimized. They predict that the technique will be useful to study different combinations of NFC (modified with anionic or cationic groups), lignin, and hemicelluloses to mimic and understand the interactions of thin lamellae in the fiber wall but can also be applied generally to determine moduli of films containing nanofibers, nanocrystals, dissolved cellulose, and other biomimetic thin films.

1.3 Modification of nanocellulose surface properties

The properties discussed above make NFC and CNC very promising materials for rheology modifiers, mechanical reinforcement, as templates for smart materials, in barrier technologies, flexible electronics, and many biotechnological and biomedical applications.

CNC prepared by HCl-hydrolysis has a very poor colloidal stability. This is due to lack of repulsive forces between the crystallites and thus the suspensions are very unstable. The use of H_2SO_4 in the hydrolysis adds enough negatively charged groups (sulfate) on the crystal surface to create repulsion between the individual rods and thus yields a more stable dispersions in aqueous media. If one wants to embed them in other materials such as hydrophobic polymers further surface modification is needed for sufficient interaction to take place between the two materials at the interface.

The same need for surface modification applies for NFC yet it is more stable in aqueous media after preparation than unmodified CNC. In NFC materials derived from wood source this is most probably due to the hemicelluloses present in the material acting as a colloidal stabilizer and preventing aggregation. NFC is also less crystalline and contains substantial amount of unordered amorphous parts in the fibrils that do not aggregate as strongly as crystalline regions. Nevertheless NFC is very sensitive to processing and tends to flocculate or aggregate upon different treatments such as solvent exchange, application of mechanical force etc. (III). Blending unmodified NFC or CNC together with other materials rarely works out due to the lack of interaction of the fibril surface with the other materials. In other words, the cellulose crystal and fibril surfaces are passive and do not readily interact with other materials.

To overcome these issues NFC and CNC surfaces need to be modified for their efficient use in most applications. The modification of NFC and CNC can be grouped to chemical and physical modifications as with any colloidal particles. Chemical modifications involve covalent bonding and the chemistries are usually done in solvent media. They can involve chemicals that are hazardous, such as azides or metal

catalyst, and the reaction conditions can be harsh, including extreme pH, high temperature, and inert gas environment. Physical modifications are generally done in less harsh conditions than chemical; they involve adsorption of molecules on to the surface via weaker chemical interactions than covalent bonding i.e. electrostatic interactions, hydrophobic interactions, or van der Waals interactions.

In the following sections the different modifications and their use in functionalization of NFC and CNC will be discussed.

1.3.1 Chemical covalent modification of nanocellulose surface

The different chemical modification of NFC and CNC can be divided roughly into three major groups; negatively charged, positively charged, and hydrophobic NC. The degree of modification will affect the materials properties. In the case of CNC the amount of negative groups on the surface will determine how well the individual rods are dispersed and in what concentrations they will behave as gels or liquid crystals.[37,53] In the case of NFC chemical modification can reduce the amount of hemicellulose and affect the colloidal stability (II, epoxy modified NFC) or it can alter the pH sensitivity of the material [141]. The idea in NFC and CNC modification is to sustain the strong cellulose I crystal structure and to modify only the very surface of the fibril or crystal. Thus, the modification conditions need to be kept mild enough in order not to swell and subsequently dissolve the cellulose.[15] Also flocculation needs to be avoided and a good dispersion of fibrils and crystals during modification is important so that the product is evenly modified.

1.3.1.1 Anionic functionalization

As described earlier, CNC can be produced in such a way that the surface of the product will hold a net negative charge. This is simply done by choosing the acid for the hydrolysis reaction accordingly; sulfuric acid will derivate the resulting CNC surface with sulfate groups and hydrochloric acid will not derivate the CNC surface.[13] The sulfate-CNCs can readily interact with positively charged molecules[142], can be dispersed in water and some polar solvents[41], and can be used for further modification or functionalization[143]. The HCl-CNC can also be modified after production either to contain sulfate groups (treated with sulfuric acid) or to contain carboxylic acid groups[144]. The latter method is mostly applied to NFC materials and will be described in the following paragraph[145].

To produce negatively charged NFC with a very fine and even size distribution, a method called TEMPO (2,2,6,6,-tetramethylpiperidine-1-oxyl) -catalyzed oxidation has been developed.[146] TEMPO-oxidation of cellulosic material is solely specific to the C-6 hydroxyl (primary alcohols). The specificity and well controlled conditions of the reaction allow the reaction to take place only on the primary alcohols exposed on the fibril surface. The modification leads to fibrils where every second AGU on the fibril surface carries a modified C-6 hydroxyl. Due to the specific nature and well controlled reaction conditions TEMPO-oxidation produces cellulose fibrils with a

very uniform diameter depending on the source they originate from.[147–149] The properties of TEMPO-oxidized NFC (TEMPO-NFC) are very different from the original non-modified NFC first due to the high density of negative charge on the fibril surface and second due to the fibril dimensions being smaller and more homogeneous.[145,147] The size of TEMPO-NFC fibrils and their fine dispersions in water allow fully transparent hydrogels with high viscosity in comparably small solid content and they form transparent films with high oxygen barrier properties upon drying[32,145]. The wettability of TEMPO-NFC is very different from that of neat NFC. A dry TEMPO-NFC film adsorbs water almost immediately but this can be reduced by surface hydrophobization commonly used in papermaking. Also the thermal degradation of TEMPO-NFC is altered and it is lower than that of unmodified fibrils. The thermal expansion on the other hand is very low, much lower than that of glass.[32] This feature together with the high transparency makes TEMPO-NFC a potential substrate for flexible electronics. The large surface area, high aspect ratio and high charge density offer an interesting starting material also for further modification and functionalization, which has been investigated for example in Publication II of this thesis by conjugation of enzymes to TEMPO-NFC.

1.3.1.2   Cationic functionalization

For interactions with negatively charge materials, such as kaolin clay[150] and oxidized graphene[151], for further modifications with functional groups, such as proteins (II), or to add strength and antibacterial properties to materials[152,153], cationic groups have been introduced on NFC surface. Different routes to prepare cationic NFC have been reported in literature[141,150,152–154]. These reactions rarely alter the rheological properties of NFC dispersions or the fibril morphology too dramatically, as compared to for example TEMPO-mediated oxidation, but rather introduce reactive groups on the fibril surface with lower degree of substitution.

In Publication (II) we show one route to alter the surface of NFC by introduction of amine groups in order to further modify NFC with bioactive moieties, i.e. enzymes. The synthesis was performed via silylation reaction originally tailored for dissolving pulp. The amount of amine groups in the modified NFC was calculated to be 1.24 mmol g^{-1} cellulose and the degree of surface substitution for the material was ~0.2. The surface substitution was possible to estimate since x-ray photoelectron spectroscopy (XPS) was used to analyze the surface silicon and nitrogen content. In contrast many times the total substitution level of the material is reported and then assumed that all reactive groups lie on the fibril surface. In the latter case the fibril dimensions will affect the surface substitution degree and vary accordingly.

1.3.1.3   Hydrophobic functionalization

Hydrophobicity of NFC and CNC materials is often desired for interactions with polymers that are hydrophobic. This is usually done by polymerization reactions either

from or onto fibril and crystal surface. There are numerous examples of these reactions and they are well reviewed.[15,155,156] In some cases hydrophobicity in combination with nanoscale hierarchical structure of the material can lead to super hydrophobicity of the resulting material[157]. Another reason for hydrophobizaton of NFC or CNC would be that some of these groups are easily reacted further. An example of such modification is the epoxy moiety. Epoxy groups are well known to react with amine groups and can be used to cross-link materials (epoxy glues) or for example covalently immobilize proteins onto solid supports[158–160].

In Publication (II) of this thesis we made and examined the use of epoxy modified NFC in protein conjugation and immobilization. The epoxy containing NFC was prepared through an allylation step described earlier by Huijbrechts et al. for starch. The amount of epoxy groups for the final NFC material was analysed to be 0.64 mmol g^{-1} per glucose and calculated to correspond to a degree of substitution of 0.061. This is a total degree of substitution and the surface substitution would be higher assuming all epoxy groups were on the fibril surface. This assumption is justified since the fibrillar structure of the NFC material was sustained and not destroyed by the reaction conditions. The surface substitution in this case is very hard to estimate due to the broad size distribution of the fibrils in the material.

1.3.2 Physical adsorption of molecules onto nanocellulose surface

For NFC and CNC containing charged groups on their surface the adsorption of other molecules can be performed using charge interactions. This can be used to decorate the fibrils or crystals with functional groups or to yield better interaction with another material in composites. CNC and NFC can also be readily modified by adsorption of other carbohydrate containing molecules such as hemicelluloses and branched polymers containing sugar moieties[137,161–163]. In nature there are also proteins that specifically adsorb to cellulose surface. These are called cellulose binding modules (CBM, or cellulose binding domains, CBD)[1], and they are produced by organisms that can degrade cellulose, for example some fungi and some bacteria.[164,165]

1.3.2.1 Adsorption of hemicelluloses to cellulose

It has been observed that other natural carbohydrate containing polymers, i.e. hemicelluloses, of different sizes interact with cellulose surface and adsorb readily[26,137,162,163,166–168]. The adsorption is dependent on their size and branching; the larger they are the more they adsorb and the more branched they are the less they adsorb. For example studies on xyloglucan adsorption have shown that polymers

---

[1] In the first publication (I) the term CBD was used. In this thesis and the fourth manuscript (IV) the term CBM is used.

smaller than 12 sugar units do not adsorb on cellulose surface. For xylan the critical length has been shown to be 15 units.[163,169]

NFC from wood source has always residual hemicelluloses; from soft wood source galactoglucomannan, and from hard wood source glucuronoxylan [170,171]. The hemicellulose in pulp has been shown to aid fibrillation the process[170]. The drying of pulp has also a negative effect on the fibrillation process; the fibrils coalesce irreversibly by the formation of strong hydrogen bonding and due to the contamination of the fiber surface, it is made passive or less reactive. It has been shown that the more hemicellulose is present in the pulp the less it suffers from the effects of drying.[170,172–174] In this regard, it can be considered that NFC from wood source has already a natural modification on the fibril surface by the physical adsorption of hemicellulose. This surface modification of NFC has an impact on the preparation and handling of the material but also on the mechanical properties of the products prepared from it. This was seen in the third publication of this thesis (III) where the role of xylan in hard wood NFC matrixes was studied by specifically removing xylan by xylanase enzyme. It acts as a colloidal stabilizer of the fibrils[22] but it also affects the chemical modification of NFC material. It is more reactive than cellulose and the conditions in the reactions solubilize hemicelluloses making it more accessible for the reagents than cellulose. Thus hemicelluloses usually lower the reaction yields. This was seen for example in the second publication of this thesis (II), when NFC was modified with epoxy functionalization.

1.3.2.2 Specific adsorption of cellulose binding module, CBM, on nanocellulose

In nature many organisms ranging from fungi to bacteria produce proteins or peptides that have the ability to bind specifically to crystalline cellulose. In the filamentous fungus, *Trichoderma reesei*, some of the cellulose degrading enzymes, cellulases, have a CBM, which are members of the family 1.[164]

The CBMs of the two major cellulases of *T. reesei*, cellobiohydrolase I (previously named CBHI, later Cel7A) and cellobiohydrolases II (previously named CBHII, later Cel6A) have been studied extensively.[2] Recent and past reviews offer a good overview on what their role for the cellulase action is proposed to be[164,175]. The enzymes have two functional domains; a core enzyme with the catalytic activity, referred to as catalytic domain (CD) and the CBM which is attached to the core enzyme by a relatively long linker that is O-glycosylated (Figure 5A).[176,177] The fungal family 1 CBM proteins are small peptides of ~3 kDa in size. The amino acids that are crucial for the binding have been identified. For the CBM-CEL7A there are three tyrosine residues (Y5, Y31, and Y32) on the binding face which are critical (Figure 5B) and for CBM-CEL6A there are two tyrosine residues (Y33 and Y34), and a tryptophan

---

[2] In Publication I the nomenclature CBHI and CBHII have been used instead of Cel7A and Cel6A. In this thesis and in Publication IV the nomenclature Cel7A and Cel6A has been used.

residue (W7) responsible for the binding.[178,179] By mutating these residues the binding properties of the CBMs are altered[180]. The affinity of the CBMs has been previously studied with substrates such as BMCC, tunicin, Avicel and chitin. It has been shown that the binding affinities differ on different substrates.[113,178,181] It has also been shown that when these two CBMs are linked together genetically, a boost in affinity is detected [182]. This is a common phenomenon seen with binding proteins [183].
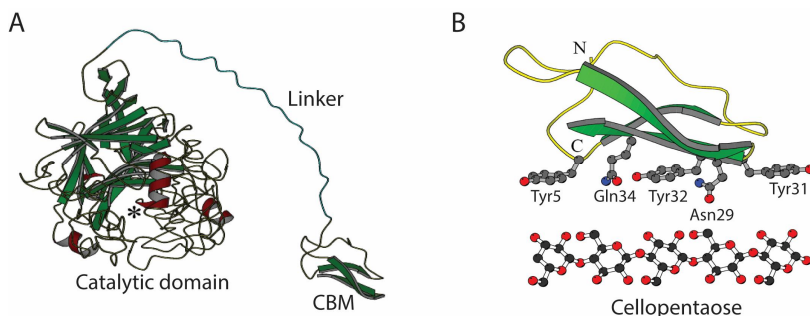

Figure 5. A) Structure of Cel7A cellulase showing the catalytic domain, the cellulose binding module and the linker between the two domains. (Image surtesy of Markus Linder.) B) The structure of CBM of Cel7A enzyme (CBM-Cel7A, adapted from the entry 1CBH in RCSB PDB), where the amino acids in the flat binding face are shown (Tyrosine (Tyr) 5, Tyr31, Tyr32, Glutamine (Gln) 34 and Asparagine (Asn) 29), and the structure of a five unit long cellulose chain, cellopentaose, aligned with the binding face of CBM-Cel7A.[184]

CBMs have been applied in biotechnology to bring function to cellulosic materials; cross-link cellulose with other materials such as starch, and to immobilize enzymes or proteins on paper[185–189]. In Publication (I) of this thesis we used a double cellulose binding module (DCBM) protein genetically fused to hydrophobin HFBI to stabilize surfaces and interfaces. In the fourth publication (IV) of this thesis we studied the role of the linker in the DCBM protein and its effect on the binding properties compared to the single CBMs. By altering the linker length it is possible to manipulate the protein binds onto NFC surface. This has been studied by Malho & Arola (manuscript under revision) and it has been shown that the linker length of the DCBM protein alone affects the film properties. Another example of the functionalization of NFC via HFBI-DCBM protein has been shown by Laaksonen et al. [190]. They used the ability of HFBI to exfoliate graphene [104] and combined it with DCBM ability to bind to NFC to create tough and strong nacre mimetic composites where the bifunctional protein connects the two materials at their interfaces.

   In Publication IV we also show that the CBMs have preferences in binding to different substrates. We showed that the DCBM exhibit a boost in affinity when binding to BMCC compared to individual CBMs, which has been seen before[182]. On NFC

though, the CBM-Cel7A had higher affinity than any of the other proteins. We speculated that CBM-Cel7A has another binding site on NFC that does not exist on BMCC and which is not seen by CBM-Cel6A or the DCBMs. In this regard, NFC can also prove to be a very useful tool for cellulase research and opens up new insight and possibilities for the mechanisms on how these enzymes act on different substrates. HCl-CNC should also be potential for the study of cellulose degrading enzymes as well as CBMs alone. The pure crystalline cellulose nature of CNC would be useful for solely studying the enzyme activity on cellulose and CBM binding without the other materials that are present in NFC or lignocelluloses; namely hemicelluloses and lignin but also amorphous cellulose.[13,191–193]

2. Aims of the present study

The overall aim of this work was to study how nanocellulose can be modified and functionalized through biochemical routes.

1. How can specific affinity be used to introduce novel function to nanocellulose surface? (I)

2. Can nanocellulose be used to stabilize interfaces? (I)

3. Can nanocellulose be used to immobilize biomolecules and what are the benefits compared to existing methods? (II)

4. What is the role of hemicellulose in NFC matrixes? (III)

5. How does structure of DCBM affect their adsorption properties onto nanocellulose and what are the benefits in using nanocellulose in binding studies as a substrate? (IV)
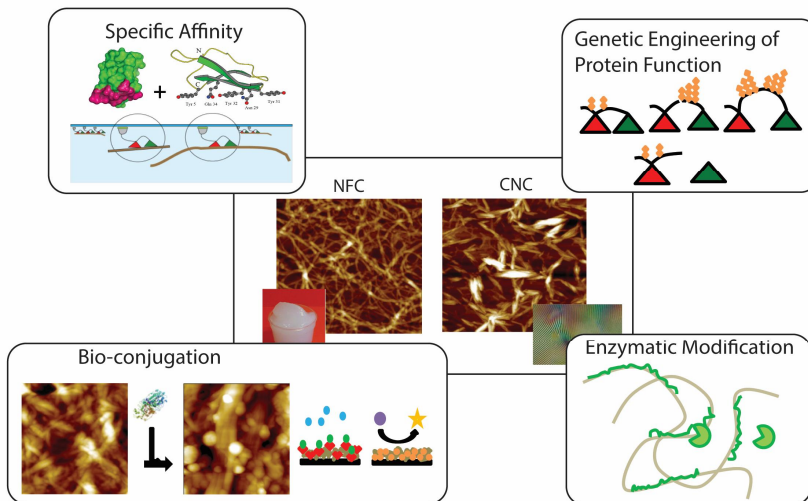

Figure 6. The different methods used in this study to accomplish biochemical modification and functionalization of nanocellulose.

3. Results and discussion

3.1 Using specific affinity of cellulose binding module (CBM) to introduce novel function to nanocellulose (Publication I)

In the first article we used a bi-functional recombinant protein, called the hydrophobin double cellulose binding module protein (HFBI-DCBM), to introduce amphiphilic function to nanocellulose surface. In HFBI-DCBM there are two CBM from the two major cellulases of the filamentous fungus *Trichoderma reesei*, Cel7A and Cel6A, and a class II hydrophobin, HFBI, of *T. reesei* (Figure 7).[194] The binding properties of the fusion protein to nanocellulose were studied using tritium labelled protein and the protein's ability to self-assemble at interfaces was studied in a Langmuir trough. The structure of the interfacial films that the HFBI-DCBM - nanocellulose complexes formed was studied by atomic force microscopy (AFM). The effect of nanocellulose on the strength of the interfacial film was studied by surface shear and dilatational rheology. The effect of nanocellulose on emulsion stability and structure was studied by different microscopy methods and by calculating the emulsion stability index.
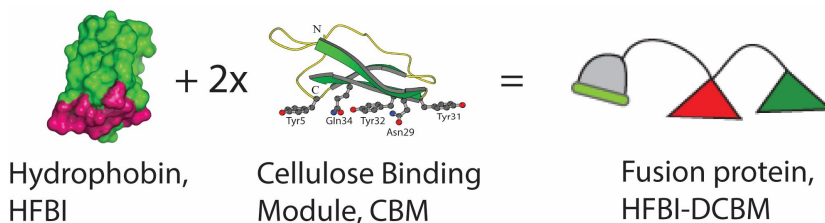

Hydrophobin, HFBI   Cellulose Binding Module, CBM   Fusion protein, HFBI-DCBM

Figure 7. A schematic illustration of the components of the fusion protein HFBI-DCBM. HFBI structure[195] (PDB entry 2FZ6) is presented with hydrophobic to hydrophilic surface coverage of amino acids showing hydrophilic residues in green and hydrophobic residues in pink (the hydrophobic patch). The stick model of CBM is that of Cel7A cellulase[184] (PDB entry 1CBH). The two different CBM in the fusion protein are presented in different colors, CBM-Cel6A is in red and CBM-Cel7A is in green.

The binding capacity for HFBI-DCBM on NFC was very similar to what has been previously observed for an individual DCBM-construct on bacterial cellulose. It has also been previously shown that affinity can be increased by placing two CBM in tandem compared to using single CBM.[182] This was why DCBM was chosen as the fusion partner for the HFBI protein.

The rate of release of HFBI-DCBM was investigated to understand how stable the modification on nanocellulose would be under changing conditions. The results showed that in two hours, only a small amount of HFBI-DCBM came off from NFC

surface due to dilution indicating that the desorption rate is very slow. The exchange rates of the single CBM have been studied previously and it has been shown that the binding of Cel7A-CBM is truly reversible on BMCC substrate in contrast to Cel6A-CBM that showed minimal exchange on BMCC during the time course of the experiment. In this study for the HFBI-DCBM a non-complete or very slow adsorption could thus be expected. This was seen as a good property since in materials uncontrolled release of the DCBM moiety of the fusion protein could cause problems.

The ability of HFBI-DCBM modified NFC and CNC to assemble at the air-water surface was studied in a Langmuir trough. The formed surface films were visualized by atomic force microscopy (AFM) (Figure 8), which were lifted on graphite by Langmuir-Schaefer -method (LS). The protein modified NFC and CNC readily assemble at the surface. In contrast no assembly of NFC or CNC was seen if protein was not used. These results showed that the protein does bring function to nanocellulose surface and that it can be used in the formation of nanocellulose interfacial films.
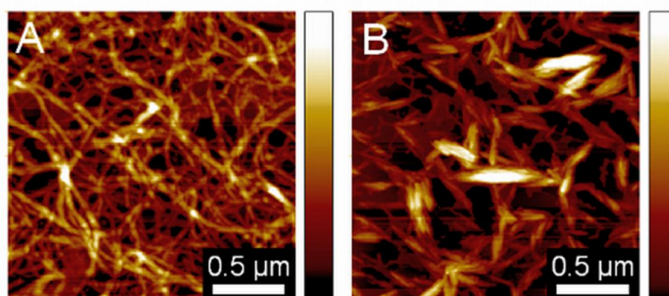

Figure 8. AFM images of Langmuir-Schaefer -films of A) a self-assembled film of NFC + HFBI-DCBM and B) a self-assembled film of CNC + HFBI-DCBM at the air-water surface. Scan size 2x2 µm, height 30 nm.

To study the effect of NFC in the surface self-assembled films, we performed surface shear rheology experiments at the air-water surface. The results of the HFBI-DCBM + NFC -films were compared to HFBI-DCBM and HFBI films. All the films showed a high elastic modulus, G', compared to the viscous modulus, G'', indicating that the films were very elastic. The highest value for G' was gained for HFBI film and it formed faster than the other films. The results showed also that NFC does not contribute to the strength of the film indicating that it is not incorporated in the film structure but rather under the protein film. This was also seen in the AFM images. NFC caused variation in the results suggesting an uneven distribution of the fibrils under the films.

Interfacial dilatational rheology experiments were used to study the NFC assembly with and without HFBI-DCBM at air-water surface and oil-water interface. Table

1 summarizes the dilatational rheology results. A low phase lag for all film types was observed implying a formation of an elastic film. Surface tension was significantly lowered by HFBI-DCBM on both air-water surface and oil-water interface, which indicates that the fusion protein adsorbs on both. The values gained for surface tension of HFBI-DCBM + NFC -films were comparable to those obtained for the protein only films indicating that the incorporation of NFC did not affect the proteins ability to self-assemble. The adsorption of NFC alone did not lower the surface tensions of either of the surfaces as much as the protein did which indicates that the protein has a stronger tendency to adsorb on the surfaces than NFC. NFC lowered the interfacial tension of the oil-water interface more than the surface tension of air-water surface, which indicates that NFC has a larger tendency to adsorb on oil-water interfaces. The dilatational moduli, E' and E'', for NFC at oil-water interface were also significantly larger than the ones for air-water surface indicating that NFC forms a stronger interfacial film on oil-water interface than at air-water surface. The values for dilatational elastic modulus (E') at air-water surface for pure protein were the highest indicating that HFBI-DCBM alone forms the strongest film with strongest intermolecular interactions. The lowest values were gained for pure NFC at air-water surface indicating insignificant self-assembly behavior but rather precipitation of fibrils unevenly. The mixed film of fusion protein and NFC gave intermediate values at air-water surface indicating some disturbance of the protein film structure by NFC. At the oil-water interface E'-values were generally much lower compared to the air-water surface, which indicates that the protein film structure or the interactions formed are different on the different interfaces/surfaces. The fusion protein alone gave the highest E'-values at oil-water interface. This behavior is comparable to the air-water surface. The behavior of fusion protein + NFC -films was different on oil-water interface compared to air-water surface giving the lowest E'-values at oil-water interface. This indicates that NFC disturbs the protein film structure more at oil-water interface than at air-water surface. The result was expected since NFC alone forms a stronger film at oil-water interface than at air-water surface.

Table 1. The surface and interfacial dilatational moduli of HFBI-DCBM, NFC, and their mixture -films at air-water surface and oil-water interface. |E| represents the complex modulus, E' is the elastic modulus and E'' the viscous modulus of the films.

	Surface tension (mN m^{-1})	|E| (mN m^{-1})	E' (mN m^{-1})	E'' (mN m^{-1})	Phase lag (deg)
HFBI-DCBM (a-w)	57	235	243	6	-1
HFBI-DCBM (o-w)	9	33	32	5	8
NFC (a-w)	63	8	8	0	1
NFC (o-w)	15	21	20	4	11
HFBI-DCBM + NFC (a-w)	53	146	145	16	6
HFBI-DCBM + NFC (o-w)	9	14	14	1	5

As was shown above the self-assembly of HFBI-DCBM and NFC lead to interfacial films at oil-water interface. Thus we investigated how the formation of such films could affect emulsion properties. Emulsions of water and hexadecane were prepared in the presence of HFBI-DCBM and/or NFC and the resulting emulsion structures were studied by microscopy. The emulsions were confirmed to be oil-in-water type by staining the oil face. In emulsions made by only HFBI-DCBM or both NFC + HFBI-DCBM the droplet size was much smaller than in those formed by NFC alone. In the emulsions where NFC was present it could be seen covering the oil droplets and when the amount of NFC was increased it filled the continuous phase forming a network where the oil droplets were trapped. Similar structures were observed for CNC with and without HFBI-DCBM.

The stability of the emulsions was studied by following the separation of the emulsion phase from the aqueous phase. The results were presented as emulsion stability indexes (ESI). ESI is calculated from the volume of separated water and the total amount of water in the system (equation (1) in Materials and Methods, Section

4.3). Emulsions with NFC or CNC were prepared with and without HFBI-DCBM and a control emulsion with only HFBI-DCBM was also prepared. NFC containing emulsions were more stable than those made with CNC. In general the stability of NFC-containing emulsions was dependent on the cellulose concentration. A further enhancement of the stability was achieved by the addition of HFBI-DCBM to the system. Full stability (100%) of emulsion was achieved in conditions where NFC concentration was ~1.25 g L^{-1} and HFBI-DCBM concentration was 1 g L^{-1}. With only NFC-containing emulsions at the studied concentration range (up to 2 g L^{-1}) the most stabile emulsion had a volume of 80%. HFBI-DCBM alone functioned quite well in stabilizing the emulsions with concentrations higher than 1 g L^{-1} but the equilibrium volumes above 80% could not be achieved. The ESI value for control emulsion made with 1 g L^{-1} HFBI and 1 g L^{-1} NFC was 54%. The only variable that showed a clear dependency on the ESI values was the amount of bound protein that could be calculated from the binding isotherm. This indicates that the best emulsion stability occurs when maximal binding capacity of HFBI-DCBM to NFC is achieved.

In contrast to previous studies where NC materials have been used in emulsion stabilization, here we introduced a specific function of self-assembly to nanocellulose via specific function of DCBM fusion protein, and created stronger surface and interfacial films of nanocellulose than could be achieved without the specific protein functions.[107,109,110,112] The study shows that emulsions can be stabilized further by the functionalization of nanocellulose compared to nanocellulose alone or the modifying protein alone.

3.2 Using NFC as a platform for protein conjugation and the bioactive film formation of the conjugates (Publication II)

Protein immobilization onto surfaces is widely used in many biotechnical applications ranging from the ability to reuse enzymes in industrial processes to diagnostic methods largely relying on antigen/anti-body immobilization[196–200]. The most significant drawbacks of protein immobilization methods are that surface chemistries are often very slow relying on diffusion, immobilization effectiveness is restricted by steric hindrance of immobilized molecules, protein unfolding on surfaces, and poor control of the orientation of the immobilized molecule all causing loss of the bioactivity. Surface chemistries are also problematic to scale up for large surface areas.[159,196,198,201–204]

In the second publication of this thesis we took advantage of NFC intrinsic properties of dispersing to aqueous solutions and to form nanoporous films from solutions to immobilize enzymes and to form bio-active surfaces from the conjugates (Figure 9). We used three different bio-conjugation methods in bulk depending on the NFC-derivative, used spin-coating technique[123] to form bio-active surfaces of enzyme-NFC conjugates, and tested how the structure of NFC-derivative affected the formation and activity of multiple layers, analyzed the bioactivity on the films with different number of spin-coated layers, and investigated the structure of the films by AFM.
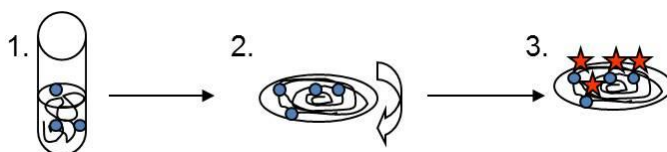
Figure 9. A schematic illustration of the bioconjugation process of a biomolecule to NFC. Step 1: Conjugation is done in solution. Step 2: Bioactive films are readily formed by spin-coating. Step 3: Bioactivity is detected.

The three different NFC-derivatives were; epoxy-modified (epoxy-NFC), amine-modified (amine-NFC), and carboxylic acid-modified (TEMPO-NFC). The amount of active groups on each derivative differed from one another. The degree of substitution (DS) for epoxy-NFC was 0.061, for amine-NFC 0.2 and for TEMPO-NFC 0.9. The DS-values gave an indication for us on how well the immobilization should work for each derivative. Alkaline phosphatase (AP) was chosen as an immobilization partner because it gives a colored reaction. The reaction yields and the success of the spin-coating of films were measured as the amount of bound AP per mass of NFC. Spin-coating was also used to create multiple layers of bioactive films to study the porosity of the NFC films and to add bioactivity onto the films.

The results showed that all the immobilization reactions were successful and that multiple layers of bioactive films could be formed by all conjugates adding activity onto the previous layer (Figure 10). AFM revealed that the structure of the bioactive films in general were very different from one another and were very much dependent on the starting material and the conjugation chemistries (Figure 11).
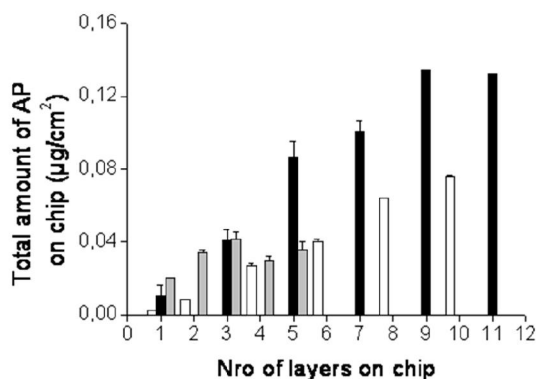

Figure 10. The amount of AP (µg) immobilized by each successive layer of the different NFC derivatives shown by the area of the chip (cm^2). White bars represent epoxy-NFC, grey bars represent amine-NFC, and black bars represent TEMPO-NFC.

The AFM images of all films formed by the non-conjugated NFC-derivatives and the AP-conjugated NFC-derivatives showed that the epoxy-NFC (Figure 11A) and the amine-NFC (Figure 11C) were more heterogeneous in fibril dimensions than TEMPO-NFC (Figure 11E). The epoxy-NFC formed the most coarse and unevenly distributed films. TEMPO-NFC formed the finest films and amine-NFC formed more tightly packed films than epoxy-NFC.

The structure of the AP functionalized epoxy-NFC film (Figure 11B) did not differ from the original non-functionalized film. The AP molecules were not seen in the images and were most likely immobilized as monomers or dimes (AP molecule is a dimer in its active form). In AP functionalized amine-NFC (Figure 11D) and TEMPO-NFC (Figure 11F) however, larger aggregates of height of ~70 nm were seen. This was most likely caused by immobilization of AP clusters rather than single AP dimers (5–6 nm). The clustering of AP molecules in the case of TEMPO- and amine-NFC is very likely due to the chemistries used in the immobilization. The clustering is not possible in the epoxy-NFC case.
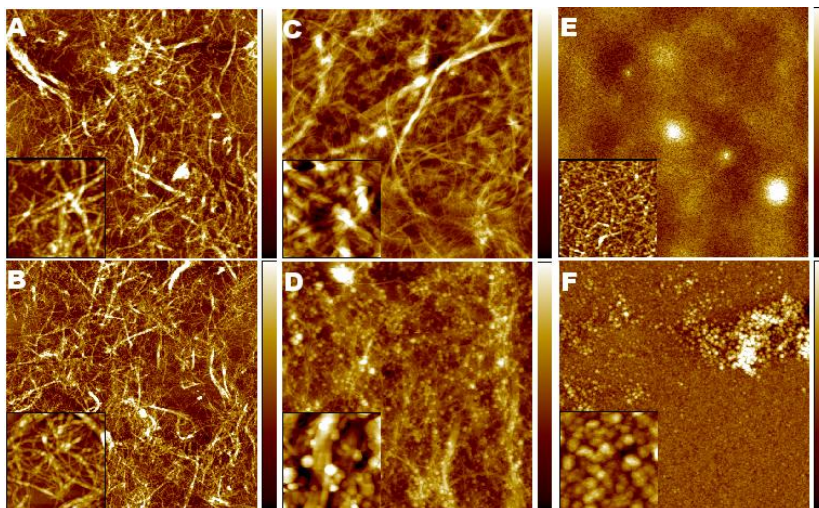

Figure 11. The AFM images of spin-coated layers of A) epoxy-NFC, B) AP functionalized epoxy-NFC, C) amine-NFC, D) AP functionalized amine-NFC, E) TEMPO-NFC, and F) AP functionalized TEMPO-NFC.

The film tightness, porosity and structure were also assessed by calculating the amount of AP (pmol) immobilized per amount of NFC (µg) in the films in each successive spin-coated layer (Figure 12). The data showed how the substrate for AP, a small molecule (*para*-nitrophenyl phosphate, *p*-NPP) is able to penetrate into the layers and react with AP. The data also showed that the most efficient of all the NFC derivatives was TEMPO-NFC; immobilizing the most AP compared to the amount of NFC spin-coated.

The amine-NFC formed the most tightly packed films, which caused the decrease in detection of AP per each spin-coated layer. From Figure 10 it was also evident that the amount of AP activity on the films could not be increased after four spin-coated layers for amine-NFC. In contrast, epoxy-NFC and TEMPO-NFC formed films that allowed the penetration of *p*-NPP and AP detection all the way through ten of more layers. Epoxy-NFC was shown to immobilize the least AP per NFC. Looking from the AFM image it seemed that the film structure was coarser than with the other derivatives allowing the penetration of *p*-NPP deeper into the multilayered film. With the TEMPO-NFC the swelling of the material is much better compared to non-modified or other chemically modified NFC. This is also a very good property for multilayering and protein immobilization allowing the formation of well hydrated loosely packed films with nanoporous structure. The hydrated environment is well suited for the proteins and the loose packing and porous structure allows diffusion of small molecules deep into the film structure.
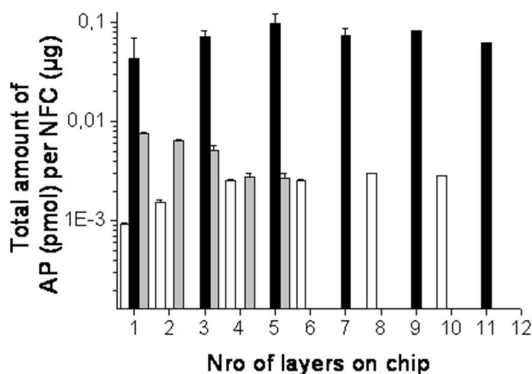

Figure 12. The amount of AP (pmol) immobilized by the different NFC derivatives (µg) per each spin-coated layer. White bars represent epoxy-NFC, grey bars represent amine-NFC, and black bars represent TEMPO-NFC.

There are two features which are thought to be very effective in protein immobilization and enzyme stability preservation; 1) multipoint covalent immobilization of proteins, and 2) carrier-bound cross-linked enzymatic aggregation [196]. In the case of epoxy-NFC the first criteria is met. In the case of amine- and TEMPO-NFC both criteria are met. This makes NFC a very good immobilization carrier for enzymes with the benefits of taking the immobilization chemistry from surface to bulk and being able to scale the process to large surfaces thanks to the ability of NFC to form films by simply casting.

3.3 Effect of xylan in NFC matrix

The formation of interacting nodes in percolating networks has been seen as the major explanation of the superior properties of NFC[22]. In the third publication (III) we address the question of how hemicellulose, a major component in NFC preparations from wood source, affects the NFC properties.

Depending on the origin and the processing history, NFC can contain almost 30% of hemicellulose (Publication III). In hardwood NFC, the main hemicellulose is glucuronoxylan[171]. As discussed earlier hemicelluloses aid the fibrillation process of pulp to MFC, which is most likely caused by the negative charges of hemicellulose that cause repulsion between fibrils[205,206]. To address the questions of how the hemicellulose is located in the fibril structure and how it affects NFC material properties in solution and in dry state, we used a specific enzyme, pI9 xylanase of *T. reesei*, to specifically remove xylan without affecting the cellulose structure[207]. We investigated the effect of xylan hydrolysis and mechanical mixing to the percolating gel network with rheology and to the film properties with extensional experiments. The morphology of fibrils was investigated by AFM and cryogenic transmission electron microscopy (cryo-TEM). To detect possible effects of xylanase treatment to cellulose structure we performed dynamic vapor sorption (DVS) studies.

The hydrolysis of NFC with only pI9 xylanase resulted in a release of 32-36% of the total xylan (~27 % of the material) as soluble saccharides from the material, corresponding to approximately 10% reduction of total mass. Physical agitation, i.e. mixing, did not affect the hydrolysis yield. These results indicated that xylan in hardwood NFC is only partly available for the enzyme.

AFM images and cryo-TEM images were obtained for all samples; NFC, xylanase treated NFC, mixed NFC, and xylanase treated mixed NFC. All in all the morphology and dimensions of the fibrils were not affected by the different treatments. Therefore from this data it is difficult to say how exactly xylan is associated with cellulose in the NFC matrix, whether it is as thin and evenly spread layer along the fibrils or only as loosely bound sparse patches.

DVS studies were done to verify that xylanase treatment did not result in the alteration of cellulose structure in NFC. It has been shown earlier that in relative humidity (RH) less than 75% the water vapor sorption capability of cellulosic materials is dictated by their crystallinity and above RH 75% by structural features such as their porosity[208]. All samples showed very similar water uptake profiles, thus xylanase treatment did not alter the crystallinity of NFC.

Small deformation stress sweep experiments were performed for all four samples. The elastic modulus (G'), viscous modulus (G''), phase angle (tanδ), and the critical stress at the onset of non-linear behavior were recorded. The systems were all elastic in nature. Xylanase treatment increased the elastic moduli and the critical stress value. However, mixing lowered the elastic moduli of both NFC samples in comparison to non-mixed NFC samples. The effect was more pronounced in the case of xylanase treated NFC. The effect of xylanase without mixing was interpreted as an increase in interactions between fibrils or as an increase in the number of

stronger cellulose-cellulose interactions (compared to xylan-cellulose), which resulted in a stronger percolating network. The mechanism of continuous mixing causing lowering of the elastic moduli was most likely related to less affective percolation throughout the gel due to the formation of flocs caused by the shear forces during mixing also seen previously[209]. Flocculation causes loss of global percolation in the gel and concentration of local interactions of fibrils. The xylanase treatment of mixed samples lead to an even larger decrease of elastic modulus, thus, the formation of flocs was apparently enhanced by xylanase treatment. These results indicated that xylan removal can be favorable to some extent but when shear forces are applied flocculation is greater and percolating network structure is lost more easily.

The elastic-to-viscous transition of the gels, i.e. the critical stress, studied by increasing the applied stress supported the findings from the above rheology experiments. The results followed the logic that mixing induces flocculation of fibrils causing loss of global interactions throughout the gel structure, which the xylanase treatment enhances, but if samples were at rest (no mixing), the xylanase removal made the gel network stronger.

NFC films of the differently treated samples were studied by extension experiments. Although the preparation protocol was identical different thicknesses were obtained for the different films and thus different densities. The reduction of thickness in the xylanase treated films was expected by the loss of mass due to hydrolysis. Also the mixing reduced the film thickness apparently by allowing a denser packing of the fibrils.

The measured parameters (Young's modulus i.e. stiffness, yield strength, ultimate tensile strength, and strain-to-failure) showed dependence to both mixing and xylanase treatment. In general, xylanase treatment decreased the values for mixed samples and increased the values for non-mixed samples, except in the case of strain to failure where xylanase treatment generally led to lower values. When NFC samples were not mixed during xylanase treatment, the films became stiffer and stronger. This was in line with the rheology data where gel strength was improved by the same treatment.

Opposite to rheology results, continuous mixing also resulted in stiffer and stronger films without xylanase treatment. Since the NFC samples not treated with xylanase were chemically identical, there must be other factors leading to improved properties. The thickness of the mixed NFC film compared to NFC without any treatments was lower. This indicates a better packing of fibrils in mixed samples, possibly caused by flocculation, and thus an increase in the interactions formed in the film. On the other hand, the xylanase treatment of mixed NFC samples further weakened the film properties indicating poorer interactions between the fibrils. The reduction in mass but not a markedly higher density implies also that the packing density of xylanase treated mixed NFC is poorer compared to NFC with only mixing and thus xylan seems to play a role in the packing of fibrils during drying. In all cases the strain-to-failure values were lower for xylanase treated NFC regardless of mixing. This showed that xylan has a role in fibril network extension in the plastic deformation region. Xylan mediated interactions between the fibrils apparently allow more creep and extension, while interactions between fibrils treated with xylanase

were stiffer but less flexible. Xylan, in this context, was beneficial and allowed better sliding of the fibrils against each other under tensile stress.

The results shown in Publication III support a major role of fibril network interactions in NFC properties, but also show that xylan as an additional component affects these interactions greatly and therefore the details of NFC performance in different applications. The results show also that xylan plays a key role in fibril stability in aqueous surroundings preventing for example fibril coalescence during mechanical mixing. In some cases the mechanical properties of materials can be enhanced by xylan removal, but considerations for the loss of stability of the fibrils and a better control of processing conditions may be needed.

3.4 Effect of linker length on DCBM binding properties and substrate dependency of CBM binding

As shown in Publication I, cellulose binding modules (CBM) can be used to functionalize NFC fibril surface. By genetic engineering and fusion protein technologies it is possible to introduce novel properties to NFC[190]. For application purposes it is important to know how the proteins function at the fibril surface.

It has been previously shown with CBM and DCBM (synthetic or produced in *E. coli*) on BMCC that the DCBM displays an increased affinity compared to CBM[182]. The role of the linker region in DCBM binding has not been studied previously. It has been speculated that the role of the linker between the catalytic domain and the CBM in the cellulase is to provide correct spacing of the two domains [210]. If the linker region is very rigid in structure and the CBM have specific binding sites on the substrate, the length of the linker can potentially play a very important role in the DCBM binding. In the fourth publication (IV) we addressed the question of how the linker region in the DCBM protein between the individual CBM affects the binding. We designed three different DCBM constructs where the linker length between the CBM was varied (Figure 13). DCBM-24 had the original linker of 24 amino acids that has been used by Linder et al. with one amino acid change of R to Q (13th amino acid of the linker)[182] to prevent the protein from trypsin cleavage. DCBM-12 had the first 12 amino acids of the original 24 amino acid linker, and DCBM-48 had a doubled 24 amino acid linker.

DCBM-12
RGPGGQACSSVWGQCGGQNWSGPTCCASGSTCVYSNDYYSQCLPGANPPGTTTTS
TQSHYGQCGGIGYSGPTVCASGTTCQVLNPYYSQCL

DCBM-24
RGPGGQACSSVWGQCGGQNWSGPTCCASGSTCVYSNDYYSQCLPGANPPGTTTTS
QPATTTGSSPGPTQSHYGQCGGIGYSGPTVCASGTTCQVLNPYYSQCL

DCBM-48
RGPGGQACSSVWGQCGGQNWSGPTCCASGSTCVYSNDYYSQCLPGANPPGTTTTS
QPATTTGSSPGPPGANPPGTTTTSQPATTTGSSPGPTQSHYGQCGGIGYSGPTVCASG
TTCQVLNPYYSQCL

Figure 13. Amino acid sequences of the three different DCBM. Linker regions are in black, CBM-Cel6A sequence is shown in red, CBM-Cel7A sequence is shown in green.

After expression, purification and proteolytic cleavage of the original HFBI-DCBM, we verified the identity of the single CBM cleaved with papain from HFBI-DCBM-12 with amino acid composition analysis and matrix assisted laser desorption ionization – time of flight mass spectrometry (MALDI-TOF MS). We also analyzed the extent of glycosylation of the linkers in DCBM cleaved by trypsin from HFBI-DCBM with MALDI-TOF. The results showed that the CBM-Cel7A and CBM-Cel6A were not glycosylated and that the digestion by papain leads to varying linker lengths attached on both sides of CBM-Cel6A, and CBM-Cel7A with no linker or only one or few amino acids of the linker. From MALDI-TOF it was also evident that DCBM-12 was not glycosylated but the other DCBM were heavily glycosylated; DCBM-24 by 14-25 and DCBM-48 by 34-50 glycan moieties. The glycosylation pattern is heterogeneous as expected for *T. reesei*.

For the binding studies, we labelled the five different proteins; DCBM-12, -24, -48, CBM-Cel7A, and CBM-Cel6A, with tritium (^{3}H) since this method is the most accurate and gives reliable results with a broad concentration range. We measured the binding isotherms of all proteins on BMCC and NFC. Figure 14 presents the start of the isotherms of all five proteins on BMCC and NFC. The Langmuir one site binding model was used to for fitting (Equation (2)) and relative partitioning coefficients (K_r) of the initial slopes for the binding isotherms were obtained (Equation (3)).

From the isotherms it was evident that the linker length affected the DCBM binding in the same way on both substrates; DCBM-24 having the highest affinity of the three, DCBM-12 having an affinity slightly lower than the DCBM-24 and DCBM-48 having the lowest affinity compared to the two other DCBM. These results clearly show that the linker length plays a role in the binding of the molecule. The most optimal linker length was the intermediate length with some glycosylation. The linker in DCBM-48 contained substantial amounts of glycan moieties and thus is most

likely to be more rigid in structure than the other two allowing less freedom for binding. Also the length is much longer than in the case of the others. The poorer binding of the DCBM-48 could be caused by geometrical issues or less favorable energetics connected with the binding event due to the rigid linker preventing optimal binding.

What was also evident from the binding isotherms was that on BMCC the doubling of the binding moiety causes an increase in affinity and the individual CBM both bind with lower affinity than the DCBM-24 and DCBM-12. This was in line with previous studies[182] and is a well-known phenomenon occurring with other binding events in nature[183]. A surprise in the results was seen with binding of the CBM with NFC. From the isotherms it can be seen that CBM-Cel7A binds with higher affinity to NFC compared to all the other proteins and that the doubling of the binding units does not increase the affinity but rather seems to hinder the binding of the one moiety (CBM-Cel7A) and/or increase the binding of the other moiety (CBM-Cel6A). This peculiar behavior could be explained by CBM-Cel7A having two distinct binding sites or two modes of binding on NFC, which are geometrically or energetically different from one another. By linking the CBM-Cel7A to CBM-Cel6A the other binding site or mode of CBM-Cel7A seems not to be available in the double form and thus the affinity is lower for the DCBM compared to CBM-Cel7A alone.
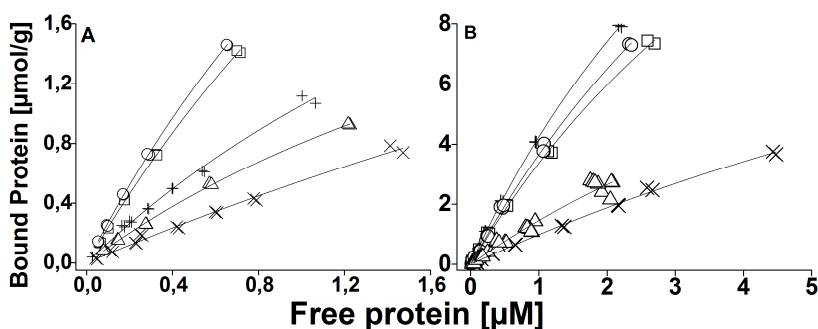

Figure 14. The initial slopes of the binding isotherms for the five different proteins on A) BMCC and B) NFC. (+) CBM-Cel7A, (x) CBM-Cel6A, (□) DCBM-12, (○) DCBM-24, (△) DCBM-48.

To be able to compare the binding energetics of the different proteins we can calculate Gibb's free energy of binding (ΔG, Equation (5)). For ΔG calculations reliable values for maximum binding capacity (B_{max}) are needed. To measure these, the binding studies were performed with higher concentrations of protein. The so called full binding isotherms for all the five proteins on both substrates are presented in Figure 15 as semi-logarithmic plots to illustrate how far or how close to the actual B_{max}-values the gained data were. From the full set of binding data it can be seen that CBM-Cel7A had the highest B_{max}-value of all the proteins on both substrates and clearly had a higher packing density on both substrates. It was also evident that

the maximum binding capacity for all other proteins except for DCBM-48 on both substrates was not reached. For DCBM-12 and -24 the B_{max}-values were very close to the actual B_{max}-values and could be used to calculate reliable ΔG-values. For the CBM the B_{max}-values are not accurate, thus the ΔG-values gained are merely directional.
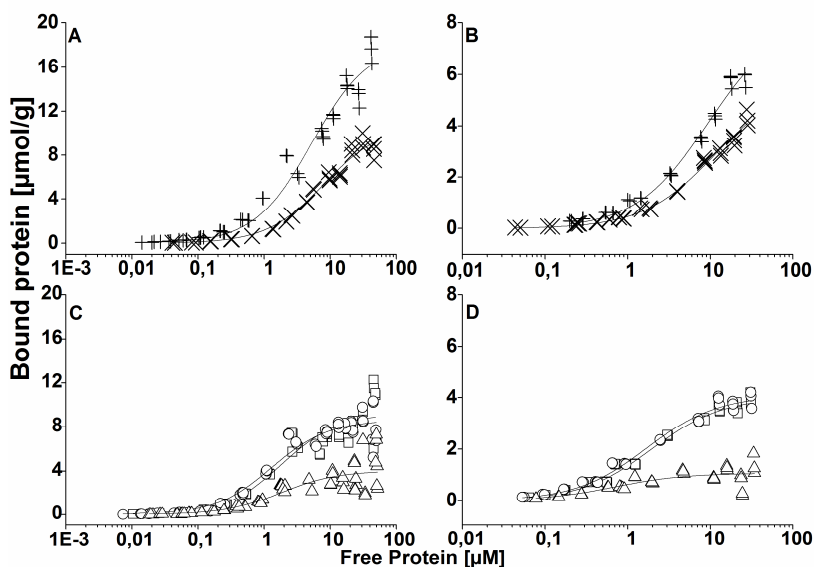

Figure 15. Semi-logarithmic plots of the CBMs on A) NFC and B) BMCC, and DCBMs on C) NFC and D) BMCC. (+) CBM-Cel7A, (x) CBM-Cel6A, (□) DCBM-12, (○) DCBM-24, (△) DCBM-48.

The B_{max}-values gained from the experimental data were accurate for the DCBM-48. For other proteins a theoretical minimum and maximum energies were calculated by using the accurate K_r-value gained from the initial slope of the beginning of the binding isotherm and using the B_{max} gained from the data in Figure 15 and by over estimating the B_{max}-value to see the effect on energy when the B_{max} is larger than measured data. The estimations were done by doubling and tripling the B_{max}-values gained from the full measured data. We refer to them as low, intermediate and high B_{max}-values. These values represent a range where the actual ΔG-values might lie and provide an estimate that can be used to compare the proteins to one another. This shows the importance of gaining accurate B_{max}-values for the calculations of the ΔG-values. The values gained from the initial slope for k_d and B_{max} are not accurate and thus not very good for estimating the ΔG-values for any binding event. On the other hand K_r-values gained from the same data are accurate due to their relative nature.

From Table 2 we can see that the energies of binding for the DCBM on both substrates are more favorable than those for the individual CBM. This shows that the coupling of the CBM together is energetically sensible. The energies of binding in the case of the CBM showed only slight differences in comparison between substrates or proteins. This suggests that the biding sites for CBM-Cel7A and CBM-Cel6A on both substrates are energetically equal and the difference for the binding affinity would come rather from geometry of the binding than from energetics of the binding. The binding energies of the different DCBM are also very close to each other and in their case also the difference in the binding properties must lie in the geometry rather than energy of the binding.

Table 2. Gibb's free energies (ΔG) for CBM and DCBM on BMCC and NFC with low, intermediate and high B_{max}-values.

	B_{max}	CBM-Cel7A	CBM-Cel6A	DCBM-12	DCBM-24	DCBM-48
NFC	low	-30,7	-28,2	-31,8	-32,1	
	inter	-29,0	-26,5	-30,1	-30,4	-31,7
	high	-28,0	-25,5	-29,1	-29,4	
BMCC	low	-29,6	-28,4	-32,7	-33,0	
	inter	-27,9	-26,7	-31,0	-31,3	-33,9
	high	-26,9	-25,7	-30,0	-30,3	

Since the peculiar binding properties of CBM-Cel7A could not be explained by the energetic differences of the binding sites, differences in substrate structure was interrogated: i) NFC has a nanosized fibril structure that could geometrically promote the affinity of CBM-Cel7A but not CBM-Cel6A, ii) NFC contains ~27 % xylan which could serve as another substrate for CBM-Cel7A but not CBM-Cel6A, iii) the crystal structure and the ration of crystalline to amorphous cellulose is different in NFC compared to BMCC and this could cause a difference in the binding of CBM. All or some of these could potentially affect the binding site geometry for the two proteins.

To test if the nanoscale structure of the NFC promoted the CBM-Cel7A binding we studied the protein binding on the pulp from which the NFC originates from. There were no differences compared to NFC binding noted. Thus, we concluded that the binding of CBM-Cel7A is not promoted by a nanoscale effect caused by NFC structure or processing.

Next, to test the effect of hemicellulose, we performed a binding experiment of CBM-Cel7A on NFC that was treated with pI9 xylanase, which has some 30 % less xylan compared to non-treated NFC. The hydrolysis was expected to reveal cellulose surface and promote CBM binding. To what extent, it was hard to assess. On the other hand, if CBM-Cel7A would bind to xylan, the effect of xylan removal on the binding would be smaller than if it bound only on cellulose surface. We saw that by enzymatically removing xylan from NFC we increased the binding of CBM-Cel7A by 20 %. This is a substantial increase and thus it does not sound plausible that

xylan in NFC would cause the higher affinity of the CBM-Cel7A compared to DCBM. If CBM-Cel7A would have an affinity towards xylan, the hydrolysis should lower the amount of bound CBM on xylan and at the same time increase the binding to cellulose. The difference in binding in this case would not be expected to be very large expecting that the surface are of fibrils are not changed dramatically by xylan hydrolysis. In Publication (III) we did not see any morphological or structural changes of fibrils associated with the xylan hydrolysis.

To assess whether the crystal structure affects the binding is harder. What we could do was to study the exchange rates of the different proteins on the different substrates. This was done by recording the time it took for the ^{3}H-labelled protein to exchange from the surface of the substrate to a non-labelled one at equilibrium. We performed the experiment to all five proteins on BMCC and NFC. The results are presented in Figure 16 and they show that both CBM exchange with a relatively fast time (<600 min) to 50 % from the original amount of bound ^{3}H-protein from BMCC. For CBM-Cel7A this has been shown previously but for CBM-Cel6A different results have been shown in different studies [113,181]. In our experiments the results suggest that both CBM exchange fully and the bindings were clearly reversible on BMCC. A different result was obtained with NFC; the individual CBM did not reach the 50 % exchange during the time course of the experiment and they showed only partial exchange suggesting that the exchange rate of the binding is much slower on NFC that BMCC.
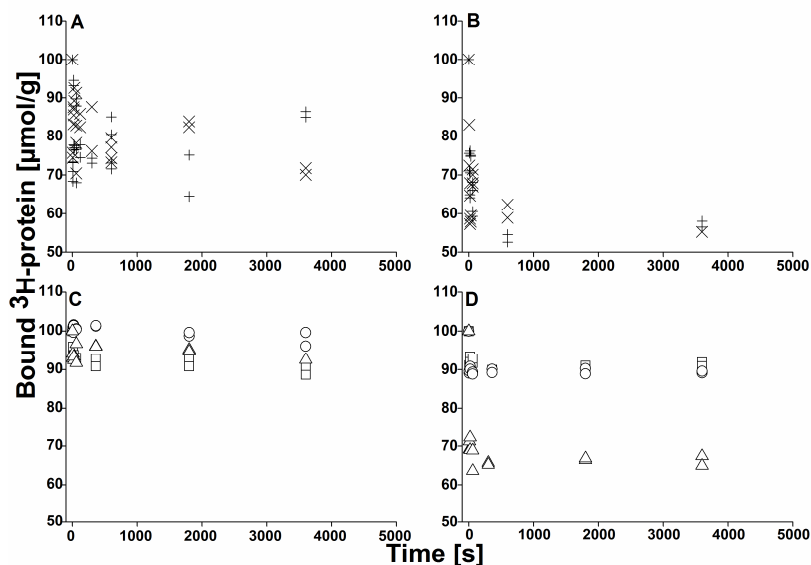

Figure 16. The exchange of ^{3}H-labelled protein to non-labelled protein. CBM on A) NFC and B) BMCC, and DCBM on C) NFC and D) BMCC. (+) CBM-Cel7A, (x) CBM-Cel6A, (□) DCBM-12, (○) DCBM-24, (△) DCBM-48.

For DCBM the exchange to 50% was not seen on either substrate suggesting that the exchange rate is greatly affected by linking of the CBM together. For BMCC; for DCBM-24 and DCBM-12 the first 10 % of the exchange was very fast and there after the exchange was very slow with no detectable changes during the experiment. For DCBM-48 the same fast exchange in the beginning until 30% was seen, but there after no detectable changes were seen. On NFC; the exchange of DCBM-24 was so slow that no changes were detected during the time course of the experiment. For DCBM-12 and DCBM-48 the exchange was fast for the first ~10% and then so slow that no changes occurred during the experimental time.

From the exchange experiments it can be concluded that the proteins experience NFC and BMCC as different substrates whether they are linked together or not. It also seems that linking dramatically affects the rate of exchange of the proteins on the surface making it slower. For the cellulases with CBM this has been previously shown and has been attributed as the cause of the CBM [211,212]. DCBM exchange with a different extent from NFC than BMCC but not fully on either. It seems that desorption of the DCBM from BMCC and CBM from NFC have one very fast component and another extremely slow component. The DCBM-24 desorption is all in all extremely slow. The DCBM-12 and DCBM-48 on the other hand still seem to have a fast component that can be measured in combination with a slow component. The linker length has a clear effect on desorption but it does not follow the same logic on the two substrates. On BMCC the extent of exchange is largest for the longest linker, DCBM-48. For the shortest, DCBM-12, and the intermediate, DCBM-24, extent of exchange is lower. For NFC the DCBM-24 exchange is not seen at all, and for the other two, DCBM-12 and DCBM-48, the exchange levels are similar.

4. Materials and methods

4.1 Nanocellulose

4.1.1 Nanofibrillated cellulose (NFC)

Never-dried bleached birch kraft pulp was fluidized with 1600 bar pressure 10 times to yield NFC. It was prepared by and gained from the Finnish Centre for Nanocellulosic Technologies. Total enzymatic hydrolysis of the material (Publication III) yielded a cellulose content of ~71 % and the hemicellulose content was ~27.3 %. The insoluble fraction of the material was ~1.7 %. The AFM images of the material (I, II, III) showed that the width of the fibrils is heterogeneious and varies between ~5 to 40 nm. The length of the fibrils in in micron scale.

4.1.2 Cellulose nanocrystals (CNC)

CNC used in Publication (I) of this thesis were prepared as described previously [13], using Whatman 541 ash-less filter paper (Whatman, UK) as the starting material. They were received from Dr. Eero Kontturi. The surface of HCl hydrolyzed CNC is not modified by the acid hydrolysis and they have the natural surface composition of cellulose crystallites. In the first publication (I) it was essential that the cellulose surfaces were not modified because that could affect the specific binding of the DCBM protein. The diameter of the single crystals was approximately 5 nm and length was ~100 to 300 nm as seen in AFM.

4.1.3 Bacterial microcrystalline cellulose

Bacterial microcrystalline cellulose (BMCC) or bacterial cellulose (BC) was obtained from Nata de Coco, by first grinding, then washing with water and sodium acetate buffer pH6, and then homogenizing with a mechanical stirrer. The end product had a solid content of which had a solid content of 2.55 gL^{-1}, and was used for the binding studies along with NFC. The diameter of the BC were shown to be 5-7 nm and bundled to larger ~20nm fibrils.[91] The length of BC is in micron scale. The crystallinity of BC is generally higher than that of wood derived cellulose materials. The BC used in our studies was shown to be mostly crystalline.[91]

4.2 Used proteins

4.2.1 HFBI-DCBM, DCBM, and CBM

The fusion protein HFBI-DCBM used in the first publication (I) of this thesis consisted of an N-terminal hydrophobin linked to two CBM in series (sequence in Figure 14)[194]. The class II hydrophobin HFBI was from *Trichoderma reesei* and the two CBM were those of Cel7A (first in the sequence) and Cel6A (second) cellulase also found in *T. reesei*. The different modules were connected by polypeptide linkers as reported earlier. The fusion protein was produced by recombinant means in *T. reesei* and purified by aqueous two phase extraction as described previously[194]. The protein was further purified by preparative reversed phase high performance liquid chromatography (RP-HPLC) using a water acetonitrile gradient with 0.1% trifluoro acetic acid (TFA).

The three different DCBM were all produced as HFBI-DCBM fusions in *T. reesei* to aid the purification. The proteins were purified as described by two phase extraction and RP-HPLC. The amino acid sequences of all HFBI-DCBM proteins are shown in Figure 17. Three modifications were made to the original HFBI-DCBM sequence. First, a tobacco etch virus (TEV) protease site (ENLYFQG) was introduced in the beginning of the linker between HFBI and CBM-Cel6A for a specific cleavage of the HFBI[213]. Second, the methionine residue (M) in the linker between HFBI and CBM-Cel6A was replaced by an arginine (R). This was done to introduce a trypsin cleavage site into the linker just in case if the TEV site would not function. Third, the arginine (R) in the linker between the two CBM was replaced by a glutamine (Q) to avoid trypsin cleavage.

Trypsin (sequencing grade modified trypsin, Promega) was used to gain the DCBM from the HFBI-DCBM (Figure 13) and papain (Promega) was used to gain CBM from HFBI-DCBM-12. The reactions were followed by reversed phase ultrahigh performance liquid chromatography (RP-UPLC) using a 2.1 x 100 mm, 1.7 μm, C4 Acquity BEH300 prST column and an Acquity I-Class system with a photodiode array detector (Waters, MA, USA) and a linear water acetonitrile gradient with 0.1% TFA. The preparative RP-HPLC was used to purify the DCBM and the CBM from the reaction mixtures.

HFBI-DCBM

SNGNGNVCPPGLFSNPQCCATQVLGLIGLDCKVPSQNVYDGTDFRNVCAKTGAQPLCCVAPVAGQALLCQTAVGA
PGASTSTGMGPGGQACSSVWGQCGGQNWSGPTCCASGSTCVYSNDYYSQCLPGANPPGTTTTSRPATTTGSSPG
PTQSHYGQCGGIGYSGPTVCASGTTCQVLNPYYSQCL

HFBI-DCBM-12

SNGNGNVCPPGLFSNPQCCATQVLGLIGLDCKVPSQNVYDGTDFRNVCAKTGAQPLCCVAPVAGQALLCQTAVGA
ENLYFQGPGASTSTGRGPGGQACSSVWGQCGGQNWSGPTCCASGSTCVYSNDYYSQCLPGANPPGTTTTSTQSH
YGQCGGIGYSGPTVCASGTTCQVLNPYYSQCL

HFBI-DCBM-24

SNGNGNVCPPGLFSNPQCCATQVLGLIGLDCKVPSQNVYDGTDFRNVCAKTGAQPLCCVAPVAGQALLCQTAVGA
ENLYFQGPGASTSTGRGPGGQACSSVWGQCGGQNWSGPTCCASGSTCVYSNDYYSQCLPGANPPGTTTTSQPAT
TTGSSPGPTQSHYGQCGGIGYSGPTVCASGTTCQVLNPYYSQCL

HFBI-DCBM-48

SNGNGNVCPPGLFSNPQCCATQVLGLIGLDCKVPSQNVYDGTDFRNVCAKTGAQPLCCVAPVAGQALLCQTAVGA
ENLYFQGPGASTSTGRGPGGQACSSVWGQCGGQNWSGPTCCASGSTCVYSNDYYSQCLPGANPPGTTTTSQPAT
TTGSSPGPPGANPPGTTTTSQPATTTGSSPGPTQSHYGQCGGIGYSGPTVCASGTTCQVLNPYYSQCL

Figure 17. The amino acid sequences of all HFBI-DCBM fusion protein. HFBI sequence is shown in blue, linker regions are shown in black, CBM-Cel6A is shown in red, and CBM-Cel7A is shown in green. The modified amino acids are shown in pink and added TEV site is shown in orange. The first sequence is that of HFBI-DCBM used in Publication I. The second, third and fourth are those of HFBI-DCBM-12, -24, and -48 respectively.

4.2.2 Alkaline phosphatase

Alkaline phosphatase (AP, E.C. 3.1.3.1.) is an esterase that catalyzes the hydrolysis of a bond between phosphor and oxygen in for example monoesters. It is routinely used as a fusion partner for example with antibodies or antigens in enzyme-linked immunosorbent assays (ELISA). When it hydrolyses a small molecule, *para*-nitrophenyl phosphate (*p*-NPP), the product of the reaction, *para*-nitrophenyl, adsorbs light strongly at A405 and can be quantified by a spectrophotometer. The amount of AP in a reaction can be gained by comparison to a standard curve of known amounts of AP.[214]

4.2.3 pI9 xylanase of *Trichoderma reesei*

The pI9 xylanase of *T. reesei* is one of the two major xylanases produced by the fungus. This enzyme has a specific activity towards xylan and does not hydrolyze cellulose or other polysaccharides. The pI9 xylanase has been shown to hydrolyze xylan to xylose and 2–7 unit xylo-oligomers.[207]

4.2.3.1 Xylans

Xylans are hemicelluloses composed of a β-1-4-linked unhydroxylopyranose unit backbone. Xylans are heteropolysaccharides that in addition to xylose can contain arabinose, methylglucuronic acid and acetic acid substituents. They are abundant in especially hardwood and annual plants.[137,171]

4.3 Emulsion stability index

The emulsion stability indexes were calculated as is presented in Equation (1).

$$ESI = \left[1 - \frac{V_{H_2O,separated}}{V_{H_2O,total}} \right] \times \textbf{100\%} \tag{1},$$

where $V_{H_2O,\,separated}$ is the volume of separated water from the emulsion phase and $V_{H_2O,\,total}$ is the total volume of the sample.

4.4 Langmuir trough

A Langmuir trough is an instrument used to create and study monolayers of materials at surfaces and interfaces. A surface is an interface between material and vacuum, and interfaces exist between two different liquids, two different solids or between a liquid and a solid, assuming they are not soluble. These surfaces and interfaces have a surface or an interfacial energy associated with them. The surface and interfacial energies can be measured as surface and interfacial tension or pressure.

Monolayers formed by, for example detergents, particles or proteins are of great importance in many industrial applications such as emulsion and foam technologies as discussed earlier. The details of the molecular interactions and the behavior of the molecules at the surface or interface can be studied in the Langmuir trough equipped with a pressure sensor (Figure 18) and a probe to measure surface tension, e.g. Wilhelmy plate or Du Noyü ring. A Langmuir film, i.e. a monolayer of molecules, can be formed by adsorption of material form the bulk. The change in surface pressure that is caused by the adsorption is measured by the pressure sensor. The monolayer that is formed on the surface or interface can be compressed by two barriers. From the pressure-area isotherm the average area of one molecule in the monolayer can be calculated if the amount of molecules at the surface and the total area they cover is known. It is also possible to gain the state (i.e. gas-, liquid-, solid-like) of the molecules in the monolayer from the isotherm.[215]

For many purposes such as microscopy imaging it is useful to be able to lift the monolayer onto a solid support from the trough. Depending on which side of the monolayer, hydrophilic or hydrophobic, is displayed on top of the support, two types of films can be created; Langmuir-Blodgett film (LB-film, Section 4.4.1) or Langmuir-Schaeffer film (LS-film, Section 4.4.2).
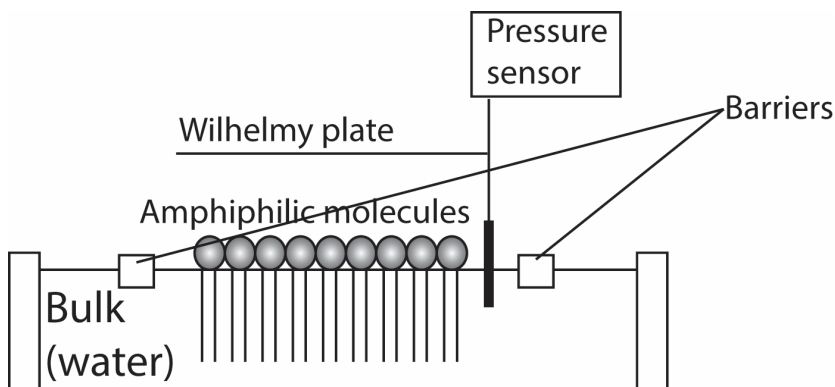
Figure 18. A schematic illustration of a Langmuir trough with compression barriers, a pressure sensor and a Wilhelmy plate.

4.4.1 Langmuir-Blodgett films

If the film is lifted from the bulk hydrophilic side phasing the support (Figure 19) the film is referred to as Langmuir-Blodgett film (LB-film). The film can be formed on the same support multiple times and in this way bilayers can be formed.[129,216]
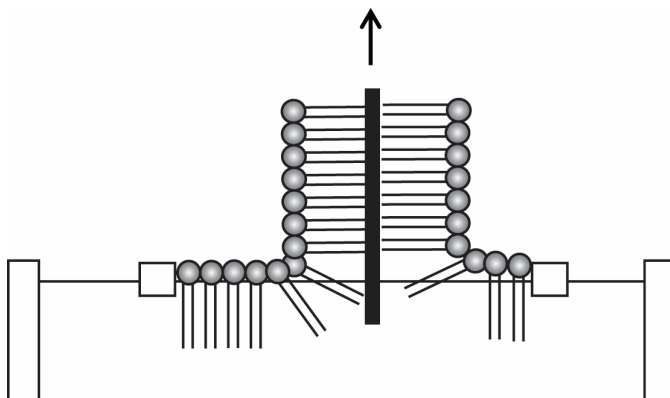

Figure 19. A schematic illustration of the preparation of LB-films.

4.4.2 Langmuir-Schaffer films

It the film is lifted with the hydrophobic side facing the solid support (Figure 20) the film is referred to as Langmuir-Schaeffer film (LS-film). This technique was used in the first publication of this thesis (I).[217]
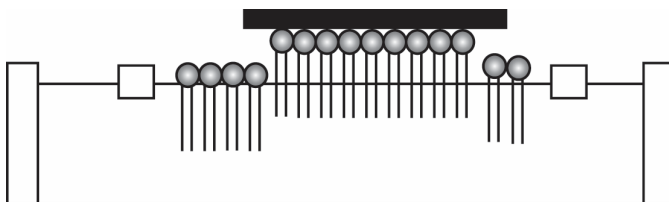
Figure 20. A schematic illustration of the preparation of LS-films.

4.5 Atomic force microscopy

Atomic force microscopy (AFM) is a powerful tool proven to be very useful in imaging, especially with regard to biological samples.[102,218–220] The biggest advantage of AFM in comparison to electron microscopy methods is that imaging can be done in ambient conditions and either in liquid media or in air. This makes it possible to image biomolecules in their natural environment. Another advantage is that no staining of the sample is needed but the sample needs to be attached on a solid support.

The principle of AFM is shown in Figure 21.[221] A laser is reflected on a cantilever's free end, which is carrying a tip. When the tip comes into contact with a sample surface the cantilever is bent due to the forces acting between the sample and the tip. The bending causes deflection in the laser beam and this is recorded by a photosensitive detector (photodiode). The sample is scanned by the tip line by line in XY-direction and a feedback loop between the photodiode and the Z-scanner provides the height information during scanning. The height of the sample is adjusted by the Z-scanner to keep the laser deflection constant. The Z-piezo movement is in the sub-nanometer range and sub-Ångstöm movement of the cantilever can be detected by the optics of the system.
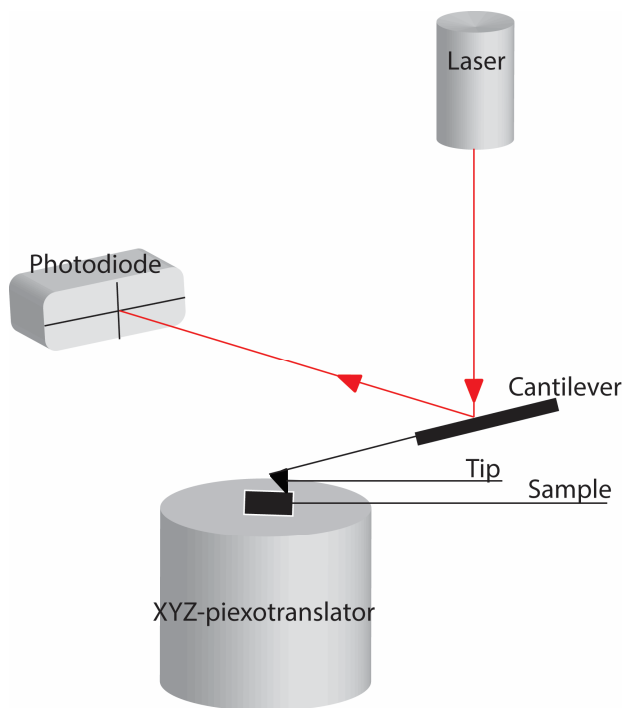
Figure 21. The basic principle of AFM imaging.

The tapping mode AFM is more useful for imaging biological sample due to less damaged caused by the more gentle contact of the tip to sample compared to above described contact mode. In this method the cantilever is oscillating near its resonant frequency very close to the surface of the sample and the tip is briefly touching the surface during each oscillation cycle. During scanning, damping of the free amplitude of the cantilever (A_f) is controlled by altering of the set point amplitude (A_{sp}). The A_f is a predetermined amplitude that is unique for each cantilever. The A_{sp} is the amplitude of the cantilever when it is in contact with the sample. The ratio of A_{sp} and A_f describes the force that is applied to the sample and it is called the damping ratio. The damping in the A_{sp} is kept constant during scanning and it is monitored by the feedback loop. The photodiode records changes in the received signal and they are corrected back to the predetermined set point value by the movement of the sample in Z-direction.

Tapping mode AFM (Nanoscope IIIa Multi Mode AFM, with E- and J-scanner, Digital Instruments/Veeco with NSCI5/AlBS cantilever, µMASCH, USA) was used in this thesis to image Langmuir-Schaeffer films of different proteins alone or in combination with nanocellulose (I), to image spin-coated films of NFC-derivatives and

films formed by NFC-derivatives conjugated with AP (II), and films prepared from NFC before and after xylanase treatment with or without mechanical shearing (III).

4.6 Rheology

Rheology is a study of flow and deformation of matter. Rheology describes the flow behavior of liquids and the deformation behavior of solids. Most materials lie in between two extreme ideal materials in their rheological behavior; the flow of ideal viscous fluids and the deformation of ideal elastic solids, thus making them viscoelastic liquids or viscoelastic solids comprising of both viscous and elastic portion. Viscoelastic solids behave differently in comparison to viscoelastic liquids depending on their rheology. Viscoelastic materials have a delayed response to the applied force and also when the force is removed.[51,222]

Small deformation time dependent oscillatory tests in shear rheology are used to examine interaction between molecules in all kinds of viscoelastic materials ranging from low-viscosity liquids to fairly rigid solids. These measurements are performed by deforming the sample by application of periodic oscillatory (sinusoidal) stress (σ) or strain (γ) at constant frequency (ω) and measuring the stress and strain respectively. When a sinusoidal shear force is applied the amplitude of the response and the delay in the phase angel (δ) will depend on the viscoelastic properties of the measured sample. In ideal elastic materials the stress and strain sinusoidal curves are in phase and the phase angle is 0°. In ideal viscous materials the stress and strain curves are out of phase and the phase shift angle is 90°. For viscoelastic materials the phase shift angle thus lies between 0° and 90°.

There are some parameters that are important for rheology; the complex shear modulus, G^*, which results from the sinusoidal shear process and consists of both the elastic and viscous response of the material. The shear storage modulus, G', that tells how solid-like the material is and how much the material stores energy during application of force, and the shear loss modulus, G'', which describes how liquid-like the material is and how much energy is lost during the application of force. The loss modulus or the tanδ (tangent delta) is calculated as G''/G'. This describes the ratio of viscous and elastic portion in the material. If tan$\delta = 0$, the material is fully elastic since $G' \gg G''$, on the other hand if tan$\delta = \infty$, the material is fully viscous since $G' \ll G''$. If the two components, viscous and elastic, are exactly equal tan$\delta = 1$.

In contrast to shear rheology, which is commonly used to study viscoelastic materials, the extensional rheology parameter that is gained from extension of flexure tests are referred to as E. In steady state measurements that are performed to solid materials to determine their strength yields the parameter E, i.e. tensile modulus, which is usually referred to as Young's modulus. The Young's modulus is determined in the linear-elastic region of tensile tests where the tensile stress and tensile strain or elongation shows a constant slope. The complex dilatational modulus, storage modulus and loss modulus are referred to as E^* or $|E|$, E', and E'' respectively

and describe the material during the application of periodical extensional or flexure force, i.e. small deformation oscillatory tests also referred to as dilatational rheology, to distinguish the difference between the type of applied forces.

In Publication III small deformation oscillatory shear tests using cylinder and cup geometry (CC 15, gap between bob and wall 0.5 mm), with the stress controlled rheometer (StressTech, Rheological Instruments Ab, Sweden) were performed to investigate the effect of xylan in the NFC gel matrix. Xylan hydrolysis was performed by pI9 xylanase enzyme and the effect to the gel strength was compared to non-hydrolyzed samples. The effect of xylan in NFC matrixes in dry state was investigated by steady state tensile measurements using a mini tensile tester (Deben, UK), on solid self-standing films prepared from the same samples.

4.6.1 Surface and interfacial rheology

Rheology in three dimensional systems is called bulk rheology but rheology can also be performed in two dimensions, i.e. at surfaces or at interfaces. The tests done apply small deformation to the sample and the parameters that are gained are the same as in bulk systems applying small deformation. The G-values refer to interfacial or surface shear moduli and E-values refer to dilatational interfacial or surface moduli. Deformation applied at the surface or interface layers provide indirect information on the molecular interaction between and within the adsorbed layer of molecules such as protein. When sinusoidal oscillation with pre-defined strain amplitude is applied the surface film is sheared analogously to the bulk system and the gained parameters are accordingly similar.[223,224] The shearing is done by placing a light weight Du Noüy ring geometry carefully onto the surface.

In dilatational rheology experiments the volume of the bubble/drop is changed and the response of the surface tension is determined from the shape of a bubble/drop by Gauss-Laplace equation that is transformed into a set of first-order differential equations, which are expressed by the geometrical parameters of the bubble/drop profile. As a result sinusoidally oscillating the bubble/drop and recording the changes in surface area with a high speed camera we are able to obtain the surface/interfacial tension as a function of time in parallel to the change in surface area. A Fourier analysis allows the extraction of pairs of parameters, such as |E| and phase angle, and E' and E".[223]

In Publication I of this thesis the surface/interfacial shear and dilatational rheology methods were used to investigate the strength and nature of the interfacial and surface films formed by HFBI-DCBM in combination with NFC and CNC and compared to HFBI-DCBM, NFC and CNC alone. The investigated interface was hexadecane-water and the surface was air-water.

Dilatational surface and interface rheology of the protein films with and without NFC and CNC as well as the NFC and CNC films were studied using an oscillating bubble or pendant drop, respectively. The air bubble in water and the water droplet in oil were formed and the surface/interfacial tension was followed until equilibrium

was reached using a contact angle measurement device (CAM 200, KSV Instruments Ltd., Finland). The equilibrated air bubble or water droplet was oscillated in a sinusoidal manner using a pulsating drop module (KSV PD 100, KSV Instruments Ltd., Finland). The change in surface area and tension of the bubble/droplet were determined from a set of oscillations (0.1 Hz) and then the measurement was repeated a few times. The rheological parameters were determined from the data with the instruments own software (OscDrop2008, KSV Instruments Ltd., Finland).

Small deformation shear oscillatory measurements were performed at air-water surface to protein films with and without NFC and CNC using the stress-controlled rheometer AR-G2 (TA-instruments, Crawley, West-Sussex, UK) equipped with Pt-Ir du Noüy ring (Ø 13 mm). The formation of the surface film was followed during time and frequency dependent experiments with constant strain were done after the film had equilibrated. The strain dependent experiments with constant frequency were done after the film had equilibrated.

4.7 Matrix assisted laser desorption-ionization – time of flight mass spectrometry

Matrix assisted laser desorption-ionization – time of flight mass spectrometry (MALDI-TOF MS) is a method used to analyze proteins and peptides from complex samples such as mixtures of different proteins/peptides or even tissue specimens.[225,226]

The basic principle of MALDI-TOF is that proteins or peptides, dried on a target with light-absorbing matrix molecules, are vaporized by short laser pulses hitting the sample. The proteins/peptides are ionized by the laser pulse, usually with single charge (z = 1) and accelerated in an electrical field with in a vacuum. Ions with low mass to charge ration (m/z) are accelerated to higher velocity and hit the detector earlier than those with high m/z. The time of flight depends solely on the mass of the specimen because the separation is done in vacuum. The accurate mass of the specimen is determined by calibration with a known standard.[227,228]

MALDI-TOF MS (Bruker autoflex II MALDI-TOF) was used in Publication II to analyze the extent of AP modification with SFB and in Publication IV to verify the size of individual CBM and the glycosylation of DCBM.

4.8 General overview of genetic engineering, transformation to *Trichoderma reesei* and expression of double cellulose binding modules

T. reesei codon optimized synthetic genes encoding HFBI, DCBM-12, DCBM-24, and DCBM-48 flanking with compatible BsaI-sites were ordered from GenScript USA Inc. (NJ, USA) in BsaI-free pUC57 plasmids. Golden Gate cloning (GGC), was used for assembling the *T. reesei* transformation cassettes from six pieces into a

destination plasmid, which was based on the pMK-RQ. GCC is a cloning method based on the activity of BsaI restriction enzyme and it can be used to assemble multiple DNA pieces in a single reaction.[229,230] The assembled parts were (in 5'-3' order) 1) *cbh1* promoter, 2) HFBI coding sequence with signal sequence for secretion, 3) DCBM (12, 24 or 48) coding sequence, 4) *cbh1* terminator, 5) *hph* hygromycin resistance marker gene under the *gpdA* promoter for strain selection, and 6) a 3' flank sequence that together with the *cbh1* promoter was used to recombine the gene into the *cbh1* locus in *T. reesei*.

The ligation products of GGC were transformed into *E. coli* XL1-Blue cells and plasmids containing transformants were selected on kanamycin plates and further selected by blue-white screening for insert-containing clones. Correct assembly of the cassette was verified by restriction enzyme analysis and the correct protein coding sequence was verified by DNA sequencing. The transformation cassettes were cut from the vectors using PmeI and purified by agarose gel electrophoresis followed by gel extraction using dialysis.

Biolistic PDS-1000/He Particle Delivery System or gold particle bombardment (Bio-Rad, CA, USA) was used for the transformation of *T. reesei* M122 spores according to the instruction manual of Bio-Rad laboratories. The particle bombardment is based on the gold particles (in this work Ø 0.6 µm) delivering the gene of interest (the transformation cassette discussed above) in to the host cell with the aid of helium pressure[231]. Gold particles without DNA are used as a control. After transformation the spores were plated on potato dextrose agar (PD) plates with top-agar containing necessary salts and hygromycin for selection and grown in 28 °C. For transformant selection colonies were picked and streaked on PD-Triton plates containing hygromycin, grown in 28 °C, and then re-streaked. Insert containing transformants were identified by direct PCR (Phire® Plant Direct PCR kit, Finnzymes, F-130) using suitable oligonucleotide primers. Correct recombination localization into the *cbh1* locus was verified by the absence of an amplicon using *cbh1* specific primers.

The proteins were produced in 50 ml shake flask cultures (*T. reesei* minimal media, 4% lactose , 2% spent grain extract, 100 mM PIPPS (Piperazine-N,N′-bis(3-propanesulfonic Acid)) pH 5.5, 2.4 mM $MgSO_4$, 4.1 mM $CaCl_2$, 28°C, 7 days) and protein producing strains were identified by western blotting using rabbit anti-HFBI antibodies. The strains were then cultivated in 7 L bioreactors (50 vol-% spent grain extract, 60 gL^{-1} lactose, 1 gL^{-1} yeast extract, 4 gL^{-1} KH_2PO_4, 2.8 gL^{-1} $(NH_4)_2SO_4$, 0.6 gL^{-1} $MgSO_4 \cdot 7H_2O$, 0.8 gL^{-1} $CaCl_2 \cdot 2H_2O$, 2 mlL^{-1} trace solution). The culture supernatants were separated from the biomass by filtration. Protein expression levels were analyzed by RP-UPLC and were 0.2 gL^{-1}, 0.4 gL^{-1}, and 3.0 gL^{-1} for HFBI-DCBM-12, -24, and -48, respectively. The proteins were purified RP-HPLC as described earlier followed by lyophilisation.

4.9 Calculation of binding constants and energies for DCBMs

For a given protein-substrate association, assuming Langmuir one site binding model applies and that the binding is reversible, binding is described by Equation (2).

$$B = \frac{[B_{max}] \times [Free]}{k_d \times [Free]} \qquad (2),$$

where B is the specific binding, $[B_{max}]$ is the maximum specific binding, [Free] is the concentration of free protein and k_d is the equilibrium binding constant that is analogous to the dissociation constant K_d. The k_d-values can be calculated if reliable B_{max}-values are obtained. For CBM this number is very hard to determine because most methods are limited in giving accurate results at the high concentration range, where small error in the free protein concentration results in large errors in the bound protein. By derivation of Equation (2) we can obtain Equation (3).

$$B'_{[Free] \to 0} = \frac{[B_{max}]}{k_d} = K_r \qquad (3),$$

where K_r is the relative partition coefficient that describes the relation of the maximal binding and the equilibrium binding constant when the free protein concentration approaches zero. This is the initial slope of the isotherm function. This initial slope can be gained for all the proteins that have been studied in the thesis, mainly the five proteins in Publication IV. The Gibb's free energy, ΔG, of a given binding can be expressed by Equation (4).

$$\Delta G = -RT ln K_a = RT ln K_d = RT ln k_d \qquad (4),$$

where R is the universal gas constant and T is the temperature in Kelvins. Now the k_d can be expressed as the ratio of the partitioning coefficient, K_r, and maximum binding capacity, B_{max}, (Equation 3) and inserted in equation (4) where we get Equation (5). [232]

$$RT ln \frac{B_{max}}{K_r} = RT \left(ln(B_{max}) - ln(K_r) \right) \qquad (5)$$

This is useful since the initial slope for all proteins can be obtained and from the full set of data we can obtain B_{max}-values that are for DCBM-48 very good, and for DCBM-12 and DCBM-24 quite close to the actual value. For the single CBM the values are quite far from the actual values. An estimation of how the binding energy is affected by the B_{max}-value can be gained by overestimation of B_{max}, by multiplying the gained B_{max} by two and three. By using those values, we can gain a range of

the free energy associated with the binding that shows the dependency of the energy to the maximum capacity. Figure 22 shows a graphical example of how this was done. In Publication IV we used this mathematical method to calculate the binding energies for DCBM-48 on NFC and BMCC, and to estimate the range of binding energies of the DCBM-12, DCBM-24, CBM-Cel7A and CBM- Cel6A.
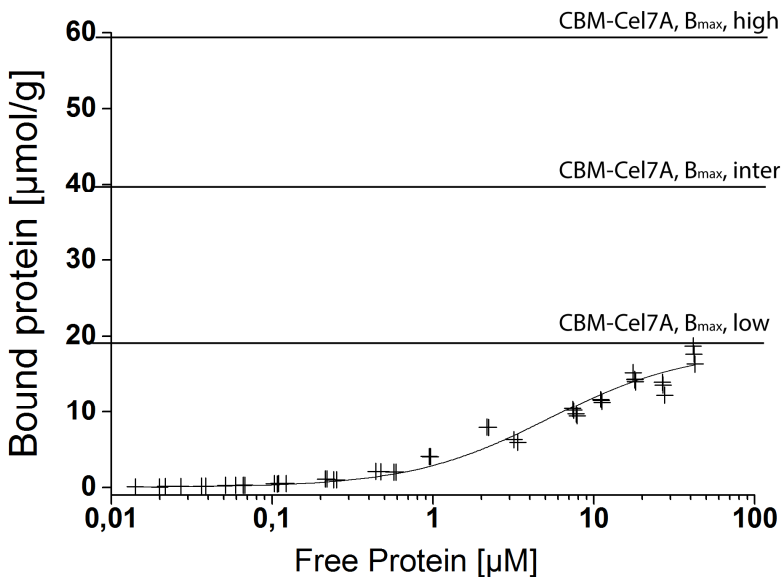

Figure 22. Graphical illustration of the B_{max}-values used to calculate the binding energies for the DCBM and CBM. The data is for CBM-Cel7A binding to NFC.

5. Conclusions and future prospective

Nanocellulose is a bio-based and renewable material with very interesting and promising properties. It has potential to be used in many high-tech applications where traditionally inorganic or fossil based materials are applied. The understanding of the materials properties and how it can be modified for different applications is a key question in nanocellulose research and application development.

In this work we took a biochemical approach in the modification and functionalization of nanocellulose surface. This approach was chosen for multiple reasons; firstly, biochemical reactions are performed in mild aqueous ambient conditions. Secondly, biology offers specific functions through proteins, which can be modified by genetic engineering to combine multiple proteins into one single recombinant protein. Genetic engineering can also be used to fine tune the protein properties or alter their function. Thirdly, enzymes can be used for very specific modification of materials, which is especially useful when it is important to preserve the original properties of the material. We show that biochemical methods are applicable to nanocellulose surface modification and functionalization and that these methods can be also used to gain new understanding of the materials properties.

By interaction and immobilization we showed that nanocellulose can be modified and functionalized by biochemical means giving new routes for use in surface and colloidal applications (Publications I & II). One critical limit, however, in applying these methods is the lack of understanding how nanocellulose as a substrate behaves. The aspects of this were shown by the role of hemicellulose in NFC matrix, and how the processing history affects the materials properties greatly (Publication III). Also the interaction studies of CBM and DCBM on NFC and BMCC show that NFC as a material is very different from BMCC (Publication IV). This shows that there is still a lot to be learned about cellulose as a substrate, even for the uses such as biofuels.

References

1.   Hon, D. N. S. Cellulose: a random walk along its historical path. *Cellulose* **1,** 1–25 (1994).

2.   Klemm, D., Heublein, B., Fink, H. P. & Bohn, A. Cellulose: Fascinating biopolymer and sustainable raw material. *Angew. Chemie - Int. Ed.* **44,** 3358–3393 (2005).

3.   Tingaut, P., Zimmermann, T. & Sèbe, G. Cellulose nanocrystals and microfibrillated cellulose as building blocks for the design of hierarchical functional materials. *Journal of Materials Chemistry* **22,** 20105 (2012).

4.   O'sullivan, A. Cellulose: the structure slowly unravels. *Cellulose* **4,** 173–207 (1997).

5.   Nishiyama, Y., Sugiyama, J., Chanzy, H. & Langan, P. Crystal structure and hydrogen bonding system in cellulose I(alpha) from synchrotron X-ray and neutron fiber diffraction. *J. Am. Chem. Soc.* **125,** 14300–14306 (2003).

6.   Nishiyama, Y., Langan, P. & Chanzy, H. Crystal Structure and Hydrogen-Bonding System in Cellulose Iβ from Synchrotron X-ray and Neutron Fiber Diffraction. *J. Am. Chem. Soc.* **124,** 9074–9082 (2002).

7.   Atalla, R. H. & VanderHart, D. L. Native Cellulose: A Composite of Two Distinct Crystalline Forms. *Science (80-.).* **223,** 283–285 (1984).

8.   Hearle, J. W. S. A fringed fibril theory of structure in crystalline polymers. *J. Polym. Sci.* **28,** 432–435 (1958).

9.   Somerville, C. *et al.* Toward a Systems Approach to Understanding Plant Cell Walls. *Science (80-.).* **306,** 2206–2211 (2004).

10.   Cosgrove, D. J. Growth of the plant cell wall. *Nat. Rev. Mol. Cell Biol.* **6,** 850–861 (2005).

11. Nakagaito, A. N. & Yano, H. Novel high-strength biocomposites based on microfibrillated cellulose having nano-order-unit web-like network structure. *Appl. Phys. A Mater. Sci. Process.* **80,** 155–159 (2005).

12. Marchessault, R. H., Morehead, F. F. & Walter, N. M. Liquid Crystal Systems from Fibrillar Polysaccharides. *Nature* **184,** 632–633 (1959).

13. Araki, J., Wada, M., Kuga, S. & Okano, T. Flow properties of microcrystalline cellulose suspension prepared by acid treatment of native cellulose. *Colloids Surfaces A Physicochem. Eng. Asp.* **142,** 75–82 (1998).

14. Edgar, C. D. & Gray, D. G. Induced circular dichroism of chiral nematic cellulose films. *Cellulose* **8,** 5–12 (2001).

15. Dufresne, A. Nanocellulose: A new ageless bionanomaterial. *Mater. Today* **16,** 220–227 (2013).

16. Klemm, D. *et al.* Nanocelluloses: A new family of nature-based materials. *Angew. Chemie - Int. Ed.* **50,** 5438–5466 (2011).

17. Isogai, A. Wood nanocelluloses: Fundamentals and applications as new bio-based nanomaterials. *Journal of Wood Science* **59,** 449–459 (2013).

18. Herrick, F. W., Casebier, R. L., Hamilton, K. J. & Sandberg, K. R. Microfibrillated Cellulose: Morphology and Accessibility. *J. Appl. Polym. Sci. Appl. Polym. Symp.* **37,** 797–813 (1983).

19. Azizi Samir, M. A. S., Alloin, F. & Dufresne, A. Review of recent research into cellulosic whiskers, their properties and their application in nanocomposite field. *Biomacromolecules* **6,** 612–626 (2005).

20. Fleming, K., Gray, D. G. & Matthews, S. Cellulose crystallites. *Chem. - A Eur. J.* **7,** 1831–1835 (2001).

21. De Souza Lima, M. M. & Borsali, R. Rodlike cellulose microcrystals: Structure, properties, and applications. *Macromol. Rapid Commun.* **25,** 771–787 (2004).

22. Pääkko, M. *et al.* Enzymatic hydrolysis combined with mechanical shearing and high-pressure homogenization for nanoscale cellulose fibrils and strong gels. *Biomacromolecules* **8,** 1934–1941 (2007).

23. Henriksson, M., Henriksson, G., Berglund, L. a. & Lindström, T. An environmentally friendly method for enzyme-assisted preparation of microfibrillated cellulose (MFC) nanofibers. *Eur. Polym. J.* **43,** 3434–3441 (2007).

24. Nakagaito, A. N. & Yano, H. The effect of morphological changes from pulp fiber towards nano-scale fibrillated cellulose on the mechanical properties of high-strength plant fiber based composites. *Appl. Phys. A Mater. Sci. Process.* **78,** 547–552 (2004).

25. Zimmermann, T., Bordeanu, N. & Strub, E. Properties of nanofibrillated cellulose from different raw materials and its reinforcement potential. *Carbohydr. Polym.* **79,** 1086–1093 (2010).

26. Ougiya, H. *et al.* Relationship between the Physical Properties and Surface Area of Cellulose Derived from Adsorbates of Various Molecular Sizes. *Bioscience, Biotechnology, and Biochemistry* **62,** 1880–1884 (1998).

27. Fall, A. B., Lindström, S. B., Sundman, O., Ödberg, L. & Wågberg, L. Colloidal stability of aqueous nanofibrillated cellulose dispersions. *Langmuir* **27,** 11332–11338 (2011).

28. Pääkkö, M. *et al.* Long and entangled native cellulose I nanofibers allow flexible aerogels and hierarchically porous templates for functionalities. *Soft Matter* **4,** 2492 (2008).

29. Henriksson, M., Berglund, L. a., Isaksson, P., Lindström, T. & Nishino, T. Cellulose nanopaper structures of high toughness. *Biomacromolecules* **9,** 1579–1585 (2008).

30. Nakagaito, a. N. & Yano, H. Novel high-strength biocomposites based on microfibrillated cellulose having nano-order-unit web-like network structure. *Appl. Phys. A Mater. Sci. Process.* **80,** 155–159 (2005).

31. Taniguchi, T. & Okamura, K. New films produced from microfibrillated natural fibres. *Polym. Int.* **47,** 291–294 (1998).

32. Fukuzumi, H., Saito, T., Iwata, T., Kumamoto, Y. & Isogai, A. Transparent and high gas barrier films of cellulose nanofibers prepared by TEMPO-mediated oxidation. *Biomacromolecules* **10,** 162–165 (2009).

33. Lin, N. & Dufresne, A. Nanocellulose in biomedicine: Current status and future prospect. *Eur. Polym. J.* (2014). at <http://www.sciencedirect.com/science/article/pii/S0014305714002493>

34. Habibi, Y., Lucia, L. A. & Rojas, O. J. Cellulose nanocrystals: Chemistry, self-assembly, and applications. *Chem. Rev.* **110,** 3479–3500 (2010).

35. Elazzouzi-Hafraoui, S. *et al.* The shape and size distribution of crystalline nanoparticles prepared by acid hydrolysis of native cellulose. *Biomacromolecules* **9,** 57–65 (2008).

36. Beck-Candanedo, S., Roman, M. & Gray, D. G. Effect of reaction conditions on the properties and behavior of wood cellulose nanocrystal suspensions. *Biomacromolecules* **6,** 1048–1054 (2005).

37. Liu, D., Chen, X., Yue, Y., Chen, M. & Wu, Q. Structure and rheology of nanocrystalline cellulose. *Carbohydr. Polym.* **84,** 316–322 (2011).

38. Sakurada, I., Nukushina, Y. & Ito, T. Experimental determination of the elastic modulus of crystalline regions in oriented polymers. *J. Polym. Sci.* **57,** 651–660 (1962).

39.   Revol, J. F., Bradford, H., Giasson, J., Marchessault, R. H. & Gray, D. G. Helicoidal self-ordering of cellulose microfibrils in aqueous suspension. *Int. J. Biol. Macromol.* **14,** 170–172 (1992).

40.   Edgar, C. D. & Gray, D. G. Smooth model cellulose I surfaces from nanocrystal suspensions. *Cellulose* **10,** 299–306 (2003).

41.   Viet, D., Beck-Candanedo, S. & Gray, D. G. Dispersion of cellulose nanocrystals in polar organic solvents. *Cellulose* **14,** 109–113 (2006).

42.   Iwamoto, S., Nakagaito, a. N., Yano, H. & Nogi, M. Optically transparent composites reinforced with plant fiber-based nanofibers. *Appl. Phys. A Mater. Sci. Process.* **81,** 1109–1112 (2005).

43.   Okahisa, Y., Yoshida, A., Miyaguchi, S. & Yano, H. Optically transparent wood-cellulose nanocomposite as a base substrate for flexible organic light-emitting diode displays. *Compos. Sci. Technol.* **69,** 1958–1961 (2009).

44.   Aulin, C., Salazar-Alvarez, G. & Lindström, T. High strength, flexible and transparent nanofibrillated cellulose–nanoclay biohybrid films with tunable oxygen and water vapor permeability. *Nanoscale* **4,** 6622 (2012).

45.   Olsson, R. T. *et al.* Making flexible magnetic aerogels and stiff magnetic nanopaper using cellulose nanofibrils as templates. *Nat. Nanotechnol.* **5,** 584–588 (2010).

46.   Purandare, S., Gomez, E. F. & Steckl, A. J. High brightness phosphorescent organic light emitting diodes on transparent and flexible cellulose films. *Nanotechnology* **25,** 094012 (2014).

47.   Korhonen, J. T., Kettunen, M., Ras, R. H. A. & Ikkala, O. Hydrophobic nanocellulose aerogels as floating, sustainable, reusable, and recyclable oil absorbents. *ACS Appl. Mater. Interfaces* **3,** 1813–1816 (2011).

48.   Malho, J. M., Laaksonen, P., Walther, A., Ikkala, O. & Linder, M. B. Facile method for stiff, tough, and strong nanocomposites by direct exfoliation of

multilayered graphene into native nanocellulose matrix. *Biomacromolecules* **13,** 1093–1099 (2012).

49. Jin, H. *et al.* Superhydrophobic and superoleophobic nanocellulose aerogel membranes as bioinspired cargo carriers on water and oil. *Langmuir* **27,** 1930–1934 (2011).

50. Kästner, U. The impact of rheological modifiers on water-borne coatings. *Colloids Surfaces A Physicochem. Eng. Asp.* **183-185,** 805–821 (2001).

51. Morrison, F. A. *Understanding Rheology. Oxford University Press* (2001). doi:10.3933/ApplRheol-12-233

52. Tadros, T. F. *Rheology of Dispersions: Principles and Applications. Rheology of Dispersions: Principles and Applications* (2010). doi:10.1002/9783527631568

53. Shafiei-Sabet, S., Hamad, W. & Hatzikiriakos, S. Influence of degree of sulfation on the rheology of cellulose nanocrystal suspensions. *Rheol. Acta* **52,** 741–751 (2013).

54. McKee, J. R. *et al.* Thermoresponsive nanocellulose hydrogels with tunable mechanical properties. *ACS Macro Lett.* **3,** 266–270 (2014).

55. Hogg, P. J. Composites in armor. *Science* **314,** 1100–1101 (2006).

56. Mayer, G. Rigid biological systems as models for synthetic composites. *Science* **310,** 1144–1147 (2005).

57. Fratzl, P. & Weinkamer, R. Nature's hierarchical materials. *Progress in Materials Science* **52,** 1263–1334 (2007).

58. Wegst, U. G. K. & Ashby, M. F. The mechanical efficiency of natural materials. *Philos. Mag.* **84,** 2167–2186 (2004).

59. Dunlop, J. W. C. & Fratzl, P. Biological Composites. *Annual Review of Materials Research* **40,** 1–24 (2010).

60. Fratzl, P., Gupta, H. S., Paschalis, E. P. & Roschger, P. Structure and mechanical quality of the collagen?mineral nano-composite in bone. *Journal of Materials Chemistry* **14,** 2115 (2004).

61. Fratzl, P. A Composite Matter of Alignment. *Science (80-.).* **335,** 177–178 (2012).

62. Abraham, E. *et al.* X-ray diffraction and biodegradation analysis of green composites of natural rubber/nanocellulose. *Polym. Degrad. Stab.* **97,** 2378–2387 (2012).

63. Fernandes, S. C. M. *et al.* Transparent chitosan films reinforced with a high content of nanofibrillated cellulose. *Carbohydr. Polym.* **81,** 394–401 (2010).

64. Capadona, J. R., Shanmuganathan, K., Tyler, D. J., Rowan, S. J. & Weder, C. Stimuli-responsive polymer nanocomposites inspired by the sea cucumber dermis. *Science* **319,** 1370–1374 (2008).

65. Fricke, J. & Emmerling, A. Aerogels. *J. Am. Ceram. Soc.* **75,** 2027–2036 (1992).

66. Fricke, J. & Tillotson, T. M. Aerogels: production, characterization, and applications. *Thin Solid Films* **297,** 212–223 (1997).

67. Cai, W. & Gupta, R. B. in *Kirk-Othmer Encyclopedia of Chemical Technology* (John Wiley and Sons, Inc., 2000). doi:10.1002/0471238961.0825041807211620.a01

68. Calvert, P. Hydrogels for soft machines. *Adv. Mater.* **21,** 743–756 (2009).

69. Hoffman, A. S. Hydrogels for biomedical applications. *Advanced Drug Delivery Reviews* **64,** 18–23 (2012).

70.   Qiu, Y. & Park, K. Environment-sensitive hydrogels for drug delivery. *Advanced Drug Delivery Reviews* **64,** 49–60 (2012).

71.   Hoare, T. R. & Kohane, D. S. Hydrogels in drug delivery: Progress and challenges. *Polymer* **49,** 1993–2007 (2008).

72.   Khademhosseini, A. & Langer, R. Microengineered hydrogels for tissue engineering. *Biomaterials* **28,** 5087–5092 (2007).

73.   Bhattacharya, M. *et al.* Nanofibrillar cellulose hydrogel promotes three-dimensional liver cell culture. in *Journal of Controlled Release* **164,** 291–298 (2012).

74.   Peppas, N. A., Bures, P., Leobandung, W. & Ichikawa, H. Hydrogels in pharmaceutical formulations. *European Journal of Pharmaceutics and Biopharmaceutics* **50,** 27–46 (2000).

75.   Akimov, Y. K. Fields of application of aerogels (review). *Instruments and Experimental Techniques* **46,** 287–299 (2003).

76.   Lu, X. *et al.* Thermal conductivity of monolithic organic aerogels. *Science* **255,** 971–972 (1992).

77.   Bryning, M. B. *et al.* Carbon nanotube aerogels. *Adv. Mater.* **19,** 661–664 (2007).

78.   Biener, J. *et al.* Advanced carbon aerogels for energy applications. *Energy & Environmental Science* **4,** 656 (2011).

79.   Lin, Y., Ehlert, G. J., Bukowsky, C. & Sodano, H. A. Superhydrophobic functionalized graphene aerogels. *ACS Appl. Mater. Interfaces* **3,** 2200–2203 (2011).

80.   Moreno-Castilla, C. & Maldonado-Hódar, F. J. Carbon aerogels for catalysis applications: An overview. *Carbon* **43,** 455–465 (2005).

81.   Pekala, R. W. *et al.* Carbon aerogels for electrochemical applications. *Journal of Non-Crystalline Solids* **225,** 74–80 (1998).

82.   Kettunen, M. *et al.* Photoswitchable superabsorbency based on nanocellulose aerogels. *Adv. Funct. Mater.* **21,** 510–517 (2011).

83.   Korhonen, J. T. *et al.* Inorganic hollow nanotube aerogels by atomic layer deposition onto native nanocellulose templates. *ACS Nano* **5,** 1967–1974 (2011).

84.   Cai, J., Kimura, S., Wada, M., Kuga, S. & Zhang, L. Cellulose aerogels from aqueous alkali hydroxide-urea solution. *ChemSusChem* **1,** 149–154 (2008).

85.   Fischer, F., Rigacci, A., Pirard, R., Berthon-Fabry, S. & Achard, P. Cellulose-based aerogels. *Polymer (Guildf).* **47,** 7636–7645 (2006).

86.   Hoepfner, S., Ratke, L. & Milow, B. Synthesis and characterisation of nanofibrillar cellulose aerogels. *Cellulose* **15,** 121–129 (2008).

87.   Jin, H., Nishiyama, Y., Wada, M. & Kuga, S. Nanofibrillar cellulose aerogels. *Colloids Surfaces A Physicochem. Eng. Asp.* **240,** 63–67 (2004).

88.   Granström, M. *et al.* Highly water repellent aerogels based on cellulose stearoyl esters. *Polymer Chemistry* **2,** 1789 (2011).

89.   Hamedi, M., Karabulut, E., Marais, A., Herland, A. & Nyström, G. Nanocellulose aerogels functionalized by rapid layer-by-layer assembly for high charge storage and beyond. *Angew. Chemie - Int. Ed.* **52,** 12038–12042 (2013).

90.   Miettunen, K. *et al.* Nanocellulose aerogel membranes for optimal electrolyte filling in dye solar cells. *Nano Energy* **8,** 95–102 (2014).

91.   Valo, H. *et al.* Drug release from nanoparticles embedded in four different nanofibrillar cellulose aerogels. *Eur. J. Pharm. Sci.* **50,** 69–77 (2013).

92.   Wicklein, B. *et al.* Thermally insulating and fire-retardant lightweight anisotropic foams based on nanocellulose and graphene oxide. *Nat Nano* **10,** 277–283 (2015).

93.   Bibette, J., Calderon, F. L. & Poulin, P. Emulsions: basic principles. *Reports on Progress in Physics* **62,** 969–1033 (1999).

94.   Weaire, D. L. & Hutzler, S. *The Physics of Foams.* (Clarendon Press, 2001). at <http://books.google.co.uk/books?id=mEHlZ9ZodFsC>

95.   Lee, L. J. *et al.* Polymer nanocomposite foams. *Composites Science and Technology* **65,** 2344–2363 (2005).

96.   Chevalier, Y. & Bolzinger, M. A. Emulsions stabilized with solid nanoparticles: Pickering emulsions. *Colloids Surfaces A Physicochem. Eng. Asp.* **439,** 23–34 (2013).

97.   Gonzenbach, U. T., Studart, A. R., Tervoort, E. & Gauckler, L. J. Ultrastable particle-stabilized foams. *Angew. Chemie - Int. Ed.* **45,** 3526–3530 (2006).

98.   Walther, A. & Müller, A. H. E. Janus particles. *Soft Matter* **4,** 663 (2008).

99.   Glaser, N., Adams, D. J., Böker, A. & Krausch, G. Janus particles at liquid-liquid interfaces. *Langmuir* **22,** 5227–5229 (2006).

100.   Park, B. J., Brugarolas, T. & Lee, D. Janus particles at an oil–water interface. *Soft Matter* **7,** 6413 (2011).

101.   Linder, M. B. Hydrophobins: Proteins that self assemble at interfaces. *Curr. Opin. Colloid Interface Sci.* **14,** 356–363 (2009).

102.   Szilvay, G. R. *et al.* Self-assembled hydrophobin protein films at the air-water interface: Structural analysis and molecular engineering. *Biochemistry* **46,** 2345–2354 (2007).

103.   Valo, H. K., Laaksonen, H., Peltonen, L. J., Linder, M. B. & Hirvonen, J. T. Multifunctional Hydrophobin : Toward Nanoparticles. *ACS Nano* **4,** 1750–1758 (2010).

104.   Laaksonen, P. *et al.* Interfacial engineering by proteins: Exfoliation and functionalization of graphene by hydrophobins. *Angew. Chemie - Int. Ed.* **49,** 4946–4949 (2010).

105.   Wang, Z. *et al.* Hydrophilic modification of polystyrene with hydrophobin for time-resolved immunofluorometric assay. *Biosens. Bioelectron.* **26,** 1074–1079 (2010).

106.   Ali, Z. M. & Gibson, L. J. The structure and mechanics of nanofibrillar cellulose foams. *Soft Matter* **9,** 1580 (2013).

107.   Capron, I. & Cathala, B. Surfactant-free high internal phase emulsions stabilized by cellulose nanocrystals. *Biomacromolecules* **14,** 291–296 (2013).

108.   Cervin, N. T. *et al.* Lightweight and strong cellulose materials made from aqueous foams stabilized by nanofibrillated cellulose. *Biomacromolecules* **14,** 503–511 (2013).

109.   Kalashnikova, I., Bizot, H., Cathala, B. & Capron, I. New pickering emulsions stabilized by bacterial cellulose nanocrystals. *Langmuir* **27,** 7471–7479 (2011).

110.   Kalashnikova, I., Bizot, H., Cathala, B. & Capron, I. Modulation of cellulose nanocrystals amphiphilic properties to stabilize oil/water interface. *Biomacromolecules* **13,** 267–275 (2012).

111.   Svagan, A. J., Samir, M. A. S. A. & Berglund, L. A. Biomimetic foams of high mechanical performance based on nanostructured cell walls reinforced by native cellulose nanofibrils. *Adv. Mater.* **20,** 1263–1269 (2008).

112.   Sèbe, G., Ham-Pichavant, F. & Pecastaings, G. Dispersibility and emulsion-stabilizing effect of cellulose nanowhiskers esterified by vinyl acetate and vinyl cinnamate. *Biomacromolecules* **14,** 2937–2944 (2013).

113.   Lehtiö, J. *et al.* The binding specificity and affinity determinants of family 1 and family 3 cellulose binding modules. *Proc. Natl. Acad. Sci. U. S. A.* **100,** 484–489 (2003).

114.   Finkenstadt, V. L. & Millane, R. P. Crystal Structure of Valonia Cellulose I. *Macromolecules* **31,** 7776–7783 (1998).

115.   Ougiya, H., Watanabe, K., Morigana, Y. & Yoshigana, F. Emulsion-stabilizing Effect of Bacterial Cellulose. *Biosci. Biotech. Biochem.* **61,** 1541–1545 (1997).

116.   Mitzi, D. B., Kosbar, L. L., Murray, C. E., Copel, M. & Afzali, A. High-mobility ultrathin semiconducting films prepared by spin coating. *Nature* **428,** 299–303 (2004).

117.   Wu, Z. *et al.* Transparent, conductive carbon nanotube films. *Science* **305,** 1273–1276 (2004).

118.   Chiou, B. Sen *et al.* Cold water fish gelatin films: Effects of cross-linking on thermal, mechanical, barrier, and biodegradation properties. *Eur. Polym. J.* **44,** 3748–3753 (2008).

119.   Davis, F. & Higson, S. P. J. Structured thin films as functional components within biosensors. *Biosensors and Bioelectronics* **21,** 1–20 (2005).

120.   Pavinatto, F. J., Caseli, L. & Oliveira, O. N. Chitosan in nanostructured thin films. *Biomacromolecules* **11,** 1897–1908 (2010).

121.   Roth, S. & Park, H. J. Nanocarbonic transparent conductive films. *Chem. Soc. Rev.* **39,** 2477–2483 (2010).

122.	Kontturi, E. & Al., E. Cellulose Nanocrystal Submonolyers by Spin Coating. *Langmuir* **23,** 9680 (2007).

123.	Taylor, J. F. Spin coating: An overview. *Met. Finish.* **99,** 16–21 (2001).

124.	Siemann, U. Solvent cast technology - A versatile tool for thin film production. *Prog. Colloid Polym. Sci.* **130,** 1–14 (2005).

125.	Crowell, J. E. Chemical methods of thin film deposition: Chemical vapor deposition, atomic layer deposition, and related technologies. *Journal of Vacuum Science & Technology A: Vacuum, Surfaces, and Films* **21,** S88 (2003).

126.	Pierson, H. O. *Handbook of Chemical Vapor Deposition Principles, Technology and Applications. Handbook of Chemical Vapor Deposition (CVD) (Second Edition)* (1999). at <http://man-fe.hosted.exlibrisgroup.com/primo_library/libweb/action/display.do?frbrVersion=2&tabs=viewOnlineTab&ct=display&fn=search&doc=44MAN_ALMA_DS51222143570001631&indx=1&recIds=44MAN_ALMA_DS51222143570001631&recIdxs=0&elementId=0&renderMode=poppedOut&>

127.	George, S. M. Atomic layer deposition: An overview. *Chem. Rev.* **110,** 111–131 (2010).

128.	Blinov, L. M. Langmuir films. *Sov. Phys. Uspekhi* **31,** 623–644 (1988).

129.	Zasadzinski, J. A., Viswanathan, R., Madsen, L., Garnaes, J. & Schwartz, D. K. Langmuir-Blodgett films. *Science* **263,** 1726–1733 (1994).

130.	Takamoto, D. Y. *et al.* Stable ordering in Langmuir-Blodgett films. *Science* **293,** 1292–1295 (2001).

131.	Dey, D. & Islam, M. Layer by Layer (LbL) Technique for fabrication of electrostatic Self assembled ultrathin films. *J. Pure Appl. Phys.* **4,** 39–44 (2008).

132. Whitesides, G. M. & Grzybowski, B. Self-assembly at all scales. *Science* **295,** 2418–2421 (2002).

133. Habibi, Y., Hoeger, I., Kelley, S. S. & Rojas, O. J. Development of Langmuir - Schaeffer cellulose nanocrystal monolayers and their interfacial behaviors. *Langmuir* **26,** 990–1001 (2010).

134. Habibi, Y., Foulon, L., Aguié-Béghin, V., Molinari, M. & Douillard, R. Langmuir-Blodgett films of cellulose nanocrystals: Preparation and characterization. *J. Colloid Interface Sci.* **316,** 388–397 (2007).

135. Ahola, S., Salmi, J., Johansson, L. S., Laine, J. & Österberg, M. Model films from native cellulose nanofibrils. Preparation, swelling, and surface interactions. *Biomacromolecules* **9,** 1273–1282 (2008).

136. Ahola, S., Turon, X., Österberg, M., Laine, J. & Rojas, O. J. Enzymatic hydrolysis of native cellulose nanofibrils and other cellulose model films: Effect of surface structure. *Langmuir* **24,** 11592–11599 (2008).

137. Eronen, P., Österberg, M., Heikkinen, S., Tenkanen, M. & Laine, J. Interactions of structurally different hemicelluloses with nanofibrillar cellulose. *Carbohydr. Polym.* **86,** 1281–1290 (2011).

138. Eronen, P., Laine, J., Ruokolainen, J. & Österberg, M. Comparison of Multilayer Formation Between Different Cellulose Nanofibrils and Cationic Polymers. *J. Colloid Interface Sci.* **373,** 84–93 (2012).

139. Cranston, E. D. *et al.* Determination of Young's modulus for nanofibrillated cellulose multilayer thin films using buckling mechanics. *Biomacromolecules* **12,** 961–969 (2011).

140. Cranston, E. D. & Gray, D. G. Birefringence in spin-coated films containing cellulose nanocrystals. *Colloids Surfaces A Physicochem. Eng. Asp.* **325,** 44–51 (2008).

141.	Pahimanolis, N. *et al.* Surface functionalization of nanofibrillated cellulose using click-chemistry approach in aqueous media. *Cellulose* **18,** 1201–1212 (2011).

142.	Cranston, E. D. & Gray, D. G. Morphological and optical characterization of polyelectrolyte multilayers incorporating nanocrystalline cellulose. *Biomacromolecules* **7,** 2522–2530 (2006).

143.	Majoinen, J. *et al.* Polyelectrolyte brushes grafted from cellulose nanocrystals using Cu-mediated surface-initiated controlled radical polymerization. *Biomacromolecules* **12,** 2997–3006 (2011).

144.	Habibi, Y., Chanzy, H. & Vignon, M. R. TEMPO-mediated surface oxidation of cellulose whiskers. *Cellulose* **13,** 679–687 (2006).

145.	Isogai, A., Saito, T. & Fukuzumi, H. TEMPO-oxidized cellulose nanofibers. *Nanoscale* **3,** 71–85 (2011).

146.	Saito, T., Nishiyama, Y., Putaux, J. L., Vignon, M. & Isogai, A. Homogeneous suspensions of individualized microfibrils from TEMPO-catalyzed oxidation of native cellulose. *Biomacromolecules* **7,** 1687–1691 (2006).

147.	Saito, T., Kimura, S., Nishiyama, Y. & Isogai, A. Cellulose nanofibers prepared by TEMPO-mediated oxidation of native cellulose. *Biomacromolecules* **8,** 2485–2491 (2007).

148.	Saito, T. *et al.* Individualization of nano-sized plant cellulose fibrils by direct surface carboxylation using TEMPO catalyst under neutral conditions. *Biomacromolecules* **10,** 1992–1996 (2009).

149.	Hiraoki, R., Ono, Y., Saito, T. & Isogai, A. Molecular Mass and Molecular-Mass Distribution of TEMPO-Oxidized Celluloses and TEMPO-Oxidized Cellulose Nanofibrils. *Biomacromolecules* **16,** 675–681 (2015).

150. Liimatainen, H., Suopajärvi, T., Sirviö, J., Hormi, O. & Niinimäki, J. Fabrication of cationic cellulosic nanofibrils through aqueous quaternization pretreatment and their use in colloid aggregation. *Carbohydr. Polym.* **103,** 187–192 (2014).

151. Luong, N. D. *et al.* Graphene/cellulose nanocomposite paper with high electrical and mechanical performances. *Journal of Materials Chemistry* **21,** 13991 (2011).

152. Olszewska, A. *et al.* The behaviour of cationic NanoFibrillar Cellulose in aqueous media. *Cellulose* **18,** 1213–1226 (2011).

153. Ho, T. T. T., Zimmermann, T., Hauert, R. & Caseri, W. Preparation and characterization of cationic nanofibrillated cellulose from etherification and high-shear disintegration processes. *Cellulose* **18,** 1391–1406 (2011).

154. Aulin, C., Johansson, E., Wågberg, L. & Lindström, T. Self-organized films from cellulose i nanofibrils using the layer-by-layer technique. *Biomacromolecules* **11,** 872–882 (2010).

155. Dufresne, A. Processing of polymer nanocomposites reinforced with polysaccharide nanocrystals. *Molecules* **15,** 4111–4128 (2010).

156. Lin, N., Huang, J. & Dufresne, A. Preparation, properties and applications of polysaccharide nanocrystals in advanced functional nanomaterials: a review. *Nanoscale* **4,** 3274 (2012).

157. Mertaniemi, H., Laukkanen, A., Teirfolk, J.-E., Ikkala, O. & Ras, R. H. a. Functionalized porous microparticles of nanofibrillated cellulose for biomimetic hierarchically structured superhydrophobic surfaces. *RSC Adv.* **2,** 2882 (2012).

158. Adomenas, A., Curran, K. & Falconer-Flint, M. in *Surface Coatings: Volume 1 Raw Materials and Their Usage* 179 (Chapman & Hall, 1993).

159. Mateo, C. *et al.* Immobilization of enzymes on heterofunctional epoxy supports. *Nat. Protoc.* **2,** 1022–1033 (2007).

160. Huijbrechts, a. M. L. *et al.* Synthesis and application of epoxy starch derivatives. *Carbohydr. Polym.* **79,** 858–866 (2010).

161. Majoinen, J. *et al.* Supracolloidal multivalent interactions and wrapping of dendronized glycopolymers on native cellulose nanocrystals. *J. Am. Chem. Soc.* **136,** 866–869 (2014).

162. Hayashi, T., Marsden, M. P. & Delmer, D. P. Pea Xyloglucan and Cellulose: VI. Xyloglucan-Cellulose Interactions in Vitro and in Vivo. *Plant Physiol.* **83,** 384–389 (1987).

163. Kabel, M. a., van den Borne, H., Vincken, J. P., Voragen, a. G. J. & Schols, H. a. Structural differences of xylans affect their interaction with cellulose. *Carbohydr. Polym.* **69,** 94–105 (2007).

164. Várnai, A. *et al.* Carbohydrate-Binding Modules of Fungal Cellulases. Occurrence in Nature, Function, and Relevance in Industrial Biomass Conversion. *Adv. Appl. Microbiol.* **88,** 103–165 (2014).

165. Tomme, P. & Warren, R. *Cellulose-binding domains: classification and properties. ACS Symposium Series, American Chemical Society* (1995). doi:10.1021/bk-1995-0618

166. Whitney, S. E. C., Brigham, J. E., Darke, A. H., Reid, J. S. G. & Gidley, M. J. In vitro assembly of cellulose/xyloglucan networks: ultrastructural and molecular aspects. *Plant J.* **8,** 491–504 (1995).

167. Vincken, J. P., de Keizer, a, Beldman, G. & Voragen, a G. Fractionation of xyloglucan fragments and their interaction with cellulose. *Plant Physiol.* **108,** 1579–1585 (1995).

168. Whitney, S. E. C., Gothard, M. G. E., Mitchell, J. T. & Gidley, M. J. Roles of Cellulose and Xyloglucan in Determining the Mechanical Properties of Primary Plant Cell Walls1. *Plant Physiol.* **121,** 657–664 (1999).

169. Whitney, S. E. C. *et al.* Efects of Structural Variation in Xyloglucan Polymers on Interactions With Bacterial Cellulose. *Am. J. Bot.* **93,** 1402–1414 (2006).

170. Iwamoto, S., Abe, K. & Yano, H. The effect of hemicelluloses on wood pulp nanofibrillation and nanofiber network characteristics. *Biomacromolecules* **9,** 1022–1026 (2008).

171. Bjarnestad, S. & Dahlman, O. Chemical compositions of hardwood and softwood pulps employing photoacoustic fourier transform infrared spectroscopy in combination with partial least-squares analysis. *Anal. Chem.* **74,** 5851–5858 (2002).

172. Reis, D. *et al.* Cellulose-glucuronoxylans and plant cell wall structure. *Micron* **25,** 171–187 (1994).

173. Suchy, M., Kontturi, E. & Vuorinen, T. Impact of drying on wood ultrastructure: Similarities in cell wall alteration between native wood and isolated wood-based fibers. *Biomacromolecules* **11,** 2161–2168 (2010).

174. Johansson, L.-S., Tammelin, T., Campbell, J. M., Setälä, H. & Österberg, M. Experimental evidence on medium driven cellulose surface adaptation demonstrated using nanofibrillated cellulose. *Soft Matter* **7,** 10917 (2011).

175. Linder, M. & Teeri, T. T. The roles and function of cellulose-binding domains. *Journal of Biotechnology* **57,** 15–28 (1997).

176. Abuja, P. M., Pilz, I., Claeyssens, M. & Tomme, P. Domain structure of cellobiohydrolase II as studied by small angle X-ray scattering: close resemblance to cellobiohydrolase I. *Biochem. Biophys. Res. Commun.* **156,** 180–185 (1988).

177.	Abuja, P. M. *et al.* Structural and functional domains of cellobiohydrolase I from Trichoderma reesei. *Eur. Biophys. J.* **15,** 339–342 (1988).

178.	Linder, M. & Teeri, T. T. The cellulose-binding domain of the major cellobiohydrolase of Trichoderma reesei exhibits true reversibility and a high exchange rate on crystalline cellulose. *Proc. Natl. Acad. Sci. U. S. A.* **93,** 12251–12255 (1996).

179.	Linder, M., Lindeberg, G., Reinikainen, T., Teeri, T. T. & Pettersson, G. The difference in affinity between two fungal cellulose-binding domains is dominated by a single amino acid substitution. *FEBS Lett.* **372,** 96–98 (1995).

180.	Linder, M., Nevanen, T. & Teeri, T. T. Design of a pH-dependent cellulose-binding domain. *FEBS Lett.* **447,** 13–16 (1999).

181.	Carrard, G. & Linder, M. Widely different off rates of two closely related cellulose-binding domains from Trichoderma reesei. *Eur. J. Biochem.* **262,** 637–643 (1999).

182.	Linder, M., Salovuori, I., Ruohonen, L. & Teeri, T. T. Characterization of a Double Cellulose-binding Domain. *J. Biol. Chem.* **271,** 21268–21272 (1996).

183.	Mammen, M., Choi, S.-K. & Whitesides, G. M. Polyvalent Interactions in Biological Systems: Implications for Design and Use of Multivalent Ligands and Inhibitors. *Angew. Chemie Int. Ed.* **37,** 2754–2794 (1998).

184.	Linder, M. *et al.* Identification of functionally important amino acids in the cellulose-binding domain of Trichoderma reesei cellobiohydrolase I. *Protein Sci.* **4,** 1056–1064 (1995).

185.	Levy, I. & Shoseyov, O. Expression, refolding and indirect immobilization of horseradish peroxidase (HRP) to cellulose via a phage-selected peptide and cellulose-binding domain (CBD). *J. Pept. Sci.* **7,** 50–57 (2001).

186. Levy, I., Nussinovitch, A., Shpigel, E. & Shoseyov, O. Recombinant cellulose crosslinking protein: A novel paper-modification biomaterial. *Cellulose* **9,** 91–98 (2002).

187. Levy, I. & Shoseyov, O. Cellulose-binding domains: Biotechnological applications. *Biotechnol. Adv.* **20,** 191–213 (2002).

188. Shoseyov, O., Shani, Z. & Levy, I. Carbohydrate binding modules: biochemical properties and novel applications. *Microbiol. Mol. Biol. Rev.* **70,** 283–295 (2006).

189. Ong, E., Gilkes, N. R., Warren, R. A. J., Miller, R. C. & Kilburn, D. G. Enzyme Immobilization Using the Cellulose-Binding Domain of a Cellulomonas Fimi Exoglucanase. *Bio/Technology* **7,** 604–607 (1989).

190. Laaksonen, P. *et al.* Genetic engineering of biomimetic nanocomposites: Diblock proteins, graphene, and nanofibrillated cellulose. *Angew. Chemie - Int. Ed.* **50,** 8688–8691 (2011).

191. Várnai, A., Huikko, L., Pere, J., Siika-aho, M. & Viikari, L. Synergistic action of xylanase and mannanase improves the total hydrolysis of softwood. *Bioresour. Technol.* **102,** 9096–9104 (2011).

192. Igarashi, K. *et al.* Traffic jams reduce hydrolytic efficiency of cellulase on cellulose surface. *Science* **333,** 1279–1282 (2011).

193. Rahikainen, J. L. *et al.* Inhibitory effect of lignin during cellulose bioconversion: The effect of lignin chemistry on non-productive enzyme adsorption. *Bioresour. Technol.* **133,** 270–278 (2013).

194. Linder, M. B. *et al.* Efficient purification of recombinant proteins using hydrophobins as tags in surfactant-based two-phase systems. *Biochemistry* **43,** 11873–11882 (2004).

195. Hakanpää, J. *et al.* Two crystal structures of Trichoderma reesei hydrophobin HFBI--the structure of a protein amphiphile with and without detergent interaction. *Protein Sci.* **15,** 2129–2140 (2006).

196. Cao, L. Immobilised enzymes: Science or art? *Curr. Opin. Chem. Biol.* **9,** 217–226 (2005).

197. Ahluwalia, A., De Rossi, D., Ristori, C., Schirone, A. & Serra, G. A comparative study of protein immobilization techniques for optical immunosensors. *Biosens. Bioelectron.* **7,** 207–214 (1991).

198. Rusmini, F., Zhong, Z. & Feijen, J. Protein immobilization strategies for protein biochips. *Biomacromolecules* **8,** 1775–1789 (2007).

199. Hong, S. *et al.* Covalent immobilization of P-selectin enhances cell rolling. *Langmuir* **23,** 12261–12268 (2007).

200. Wong, L. S., Khan, F. & Micklefield, J. Selective covalent protein immobilization: Strategies and applications. *Chem. Rev.* **109,** 4025–4053 (2009).

201. Chen, B., Pernodet, N., Rafailovich, M. H., Bakhtina, A. & Gross, R. a. Protein immobilization on epoxy-activated thin polymer films: effect of surface wettability and enzyme loading. *Langmuir* **24,** 13457–13464 (2008).

202. Ramos, J. *et al.* Amino-functionalized latex particles obtained by a multistep method: Development of a new immunoreagent. *J. Polym. Sci. Part A Polym. Chem.* **41,** 2404–2411 (2003).

203. Teke, a. B. & Baysal, Ş. H. Immobilization of urease using glycidyl methacrylate grafted nylon-6-membranes. *Process Biochem.* **42,** 439–443 (2007).

204. Wilchek, M. & Miron, T. Oriented versus random protein immobilization. *J. Biochem. Biophys. Methods* **55,** 67–70 (2003).

205.   Duchesne, I. *et al.* The influence of hemicellulose on fibril aggregation of kraft pulp fibres as revealed by FE-SEM and CP/MAS 13C-NMR. *Cellulose* **8,** 103–111 (2001).

206.   Centola, G. & Borruso, D. Influence of Hemicellulose on Beatability of Pulp. *Tappi* **50,** 344–347 (1967).

207.   Tenkanen, M., Puls, J. & Poutanen, K. Two major xylanases of Trichoderma reesei. *Enzyme Microb. Technol.* **14,** 566–574 (1992).

208.   Mihranyan, A., Llagostera, a. P., Karmhag, R., Strømme, M. & Ek, R. Moisture sorption by cellulose powders of varying crystallinity. *Int. J. Pharm.* **269,** 433–442 (2004).

209.   Tatsumi, D., Ishioka, S. & Matsumoto, T. Effect of Fiber Concentration and Axial Ratio on the Rheological Properties of Cellulose Fiber Suspensions. *Nihon Reoroji Gakkaishi* **30,** 27–32 (2002).

210.   Srisodsuk, M., Reinikainen, T., Penttila, M. & Teeri, T. T. Role of the interdomain linker peptide of Trichoderma reesei cellobiohydrolase I in its interaction with crystalline cellulose. *J. Biol. Chem.* **268,** 20756–20761 (1993).

211.   Ståhlberg, J., Johansson, G. & Pettersson, G. A New Model For Enzymatic Hydrolysis of Cellulose Based on the Two-Domain Structure of Cellobiohydrolase I. *Bio/Technology* **9,** 286–290 (1991).

212.   Kurašin, M. & Väljamäe, P. Processivity of cellobiohydrolases is limited by the substrate. *J. Biol. Chem.* **286,** 169–177 (2011).

213.   Phan, J. *et al.* Structural basis for the substrate specificity of tobacco etch virus protease. *J. Biol. Chem.* **277,** 50564–50572 (2002).

214.   Koncki, R., Ogończyk, D. & Głąb, S. Potentiometric assay for acid and alkaline phosphatase. *Anal. Chim. Acta* **538,** 257–261 (2005).

215. Grunfeld, F. A modular multifunctional Langmuir-Blodgett trough. *Rev. Sci. Instrum.* **64,** 548–555 (1993).

216. Roberts, G. G. Langmuir-Blodgett films. *Phys. Today* **25,** 109–128 (1990).

217. Ram, M. K. *et al.* Comparative studies on Langmuir-Schaefer films of polyanilines. *Synth. Met.* **100,** 249–259 (1999).

218. Müller, D. J. & Dufrêne, Y. F. Atomic force microscopy: A nanoscopic window on the cell surface. *Trends in Cell Biology* **21,** 461–469 (2011).

219. Rief, M. Single Molecule Force Spectroscopy on Polysaccharides by Atomic Force Microscopy. *Science* **275,** 1295–1297 (1997).

220. Vinckier, A. & Semenza, G. Measuring elasticity of biological materials by atomic force microscopy. in *FEBS Letters* **430,** 12–16 (1998).

221. Meyer, E. Atomic force microscopy. *Progress in Surface Science* **41,** 3–49 (1992).

222. Mezger, T. G. *The Rheology Handbook: For Users of Rotational and Oscillatory Rheometers.* (Vincentz Network, 2006). at <http://books.google.fi/books?id=N9Fdn0MEIDIC>

223. Miller, R. *et al.* Rheology of interfacial layers. *Colloid and Polymer Science* **288,** 937–950 (2010).

224. Krägel, J. & Derkatch, S. R. Interfacial shear rheology. *Curr. Opin. Colloid Interface Sci.* **15,** 246–255 (2010).

225. Hortin, G. L. The MALDI-TOF mass spectrometric view of the plasma proteome and peptidome. *Clinical Chemistry* **52,** 1223–1237 (2006).

226. Reyzer, M. L. & Caprioli, R. M. MALDI mass spectrometry for direct tissue analysis: A new tool for biomarker discovery. *Journal of Proteome Research* **4,** 1138–1142 (2005).

227. Karas, M. & Hillenkamp, F. Laser desorption ionization of proteins with molecular masses exceeding 10,000 daltons. *Anal. Chem.* **60,** 2299–2301 (1988).

228. Tanaka, K., Waki, H. & Ido, Y. Protein and Polymer Analyses up to m/z 100 000 by Laser Ionization Time-of-Flight Mass Spectrometry. *Rapid Commun. mass Spectrom.* **2,** 151–153 (1988).

229. Engler, C., Kandzia, R. & Marillonnet, S. A one pot, one step, precision cloning method with high throughput capability. *PLoS One* **3,** (2008).

230. Sarrion-Perdigones, A. *et al.* GoldenBraid: An iterative cloning system for standardized assembly of reusable genetic modules. *PLoS One* **6,** (2011).

231. Sunagawa, M. & Magae, Y. Transformation of the edible mushroom Pleurotus ostreatus by particle bombardment. *FEMS Microbiol. Lett.* **211,** 143–146 (2002).

232. Creighton, T. E. *Proteins: Structures and Molecular Properties*. (W. H. Freeman, 1993). at <http://books.google.fi/books?id=hu8T_kI1LrkC>

Publication I

Self-assembly of cellulose nanofibrils by genetically engineered fusion proteins. Suvi Arola, Päivi Laaaksonen, Arja Paananen, Hanna Valo, Hendrik Hähl, Timo Laaksonen and Markus Ben Linder. *Soft Matter*, 2011, 7, pp. 2402–2411*.* DOI: 10.1039/c0sm01114b

Self-assembly of cellulose nanofibrils by genetically engineered fusion proteins†

Suvi Varjonen,[ab] Päivi Laaksonen,[a] Arja Paananen,[a] Hanna Valo,[c] Hendrik Hähl,[d] Timo Laaksonen[c] and Markus Ben Linder*[a]

One central problem for the function and manufacture of materials where performance relies on nanoscale structure is to control the compatibility and interactions of the building blocks. In natural materials, such as nacre, there are examples of multifunctional macromolecules that have combined binding affinities for different materials within the same molecule, thereby bridging these materials and acting as a molecular glue. Here, we describe the use of a designed multifunctional protein that is used for self-assembly of nanofibrillar cellulose. Recent advances in the production of cellulose nanofibrils have given inspiration for new uses of cellulosic materials. Cellulose nanofibrils have mechanical and structural features that open new possibilities for performance in composites and other nanoscale materials. Functionalisation was realised through a bi-functional fusion protein having both an ability to bind to cellulose and a second functionality of surface activity. The cellulose-binding function was obtained using cellulose-binding domains from cellulolytic enzymes and the surface activity through the use of a surface active protein called hydrophobin. Using the bi-functional protein, cellulose nanofibrils could be assembled into tightly packed thin films at the air/water interface and at the oil/water interface. It was shown that the combination of protein and cellulose nanofibrils resulted in a synergistic improvement in the formation and stability of oil-in-water emulsions resulting in emulsions that were stable for several months. The bi-functionality of the protein also allowed the binding of hydrophobic solid drug nanoparticles to cellulose nanofibrils and thereby improving their long-term stability under physiological conditions.

1 Introduction

One principal approach for improving performance in materials is through control of their structure and interactions at levels of hierarchy from molecular to macro level. By fabricating nano-composites and nanostructured materials, improvements in toughness and strength of materials, new possibilities for drug delivery, biocompatibility, adhesion, *etc.* can be achieved.[1–4] One material attracting much interest is cellulose. Wood is a natural composite consisting of cellulose, hemicellulose, lignin, and some other minor components. Cellulose is a polymer formed by the repeating units of β-(1–4)-D-glucopyranose. The polymer chains are packed into fibrils that have cross-sectional dimensions of 3–20 nm and which are typically considered as the lowest level of

hierarchy in cellulose assembly.[5] As a part of the cell wall structure, these fibrils are called microfibrils. Recently, methods have been developed to disintegrate wood into the elemental microfibrils producing a material referred to as "nanofibrillar cellulose" (NFC) as a separate fraction.[6,7] NFC preparations are largely free from the other cell wall components. In this context, the term nanocellulose has also been adapted.[8,9] Depending on how the materials is produced, one can also obtain "cellulose nanocrystals" (CNC, also called cellulose nanowhiskers).[10] The main difference between the two forms is the aspect ratio, NFC can have lengths of several micrometres, whereas CNC are shorter, typically some hundreds of nanometres in length.

NFC shows promise as a novel material allowing technical solutions in a sustainable way. The long and entangled fibrils make NFC a good rheology modifier[6] and material for functional aerogels.[11] The fibrils have a high aspect ratio and excellent mechanical properties. Therefore NFC is an attractive component for reinforcement of composite materials.[7,12,13] However, to achieve a sufficient compatibility between the NFC and polymer, covalent modifications of the NFC have been required. Covalent modifications have some drawbacks such as need for solvent exchange and weakening or disintegration of the fibrils,[14] thereby loosing some of the potential advantages of NFC.

[a] VTT, Technical Research Centre of Finland Biotechnology, Tietotie 2, FIN-02044VTT, Finland. E-mail: markus.linder@vtt.fi
[b] Department of Applied Physics, Aalto University School of Science and Technology, P.O. Box 15100, FI-00076 Aalto, Finland
[c] Division of Pharmaceutical Technology, University of Helsinki, P.O. Box 56, FI-00014, Finland
[d] Department of Experimental Physics, Saarland University, 66041 Saarbrücken, Germany

† Electronic supplementary information (ESI) available: Further data on characterization and rheology. See DOI: 10.1039/c0sm01114b

One major challenge for the use of NFC and CNC is therefore to functionalise their surfaces in precise and desired ways. Through functionalisation we aim at achieving compatibility with other components, adhesiveness, or self-assembly. In this work we functionalised cellulose nanofibrils so that they would spontaneously assemble at interfaces or interact with other components through interfacial interactions. We aimed at a biomimetic approach using self-assembly rather than using covalent modification. Such functionalisation was realised using a bi-functional (or two-block) polymer. In nature, the strategy to use bi-(or multi-) functional proteins is for example found in materials such as nacre.[15] In this example, the proteins have the property of binding to both major components of nacre, aragonite and chitin, thereby acting as cross-linkers. In our approach, one block had affinity towards cellulose and the other was amphiphilic (or lipophilic). In this way, an amphiphilic function could be attached to the NFC. This polymer was made by fusing the proteins together into a single polypeptide chain by genetic engineering (Scheme 1). The cellulose-binding function

was obtained through specialised cellulose-binding domains, CBDs (also called cellulose-binding modules, CBMs), and the amphiphilic (surface active) function through an amphiphilic protein called hydrophobin (a class II hydrophobin, HFBI).

CBDs are non-catalytic parts of enzymes that degrade cellulose and plant materials.[16,17] These enzymes typically have a two-domain structure where the CBD is linked to the catalytic domain through an extended linker. The role of the CBDs is to bring the catalytic part of the enzyme close to the cellulose surface.[18] CBDs can be produced as individual polypeptides or they can be genetically fused to other proteins, *e.g.* to immobilise these to a cellulose matrix.[19] In this work, we used fungal CBDs that have a size of about 40 amino acids and bind to cellulose through one face of the molecule, which has three characteristic aromatic residues (Scheme 1). This cellulose-binding face has a length of about 3 nm.

Hydrophobins are amphiphilic proteins produced by filamentous fungi.[20–22] They are often secreted in large amounts and have several different functions as surfactants and adhesive agents in different stages of fungal growth and development. The surface activity and self-assembly of hydrophobins at interfaces are extraordinary in many ways, for example in the stable films and foams that they can form.[23,24] The surfactant properties have also been used to coat and make nanoparticles of compounds having low solubility in aqueous solution.[25] The structure of the hydrophobin used here (HFBI) shows that the protein is almost spherical and has a typical amphiphilic structure with one face of the protein consisting only of aliphatic hydrophobic side chains and the rest of the protein showing a polar surface typical for soluble proteins (Scheme 1). The HFBI-hydrophobin has a size of approximately 70 amino acids and a cross-section of about 2 nm.

In this study the functionality of this fusion protein was studied extensively to understand its interactions with cellulose and at interfaces. The fusion protein was then used in the formation of emulsions and for attaching drug nanoparticles to NFC. The goal was to study whether it was possible to bring cellulose nanofibers in a controlled manner to air/water, oil/water or solid/water interfaces by utilising the bi-functional engineered protein, HFBI–DCBD, and to study how the overall properties of the system could be affected in this manner.

2 Experimental

2.1 Production and preparation of cellulose nanofibrils (NFC) and cellulose nanocrystals (CNC)

NFC were prepared by mechanical disintegration of bleached birch pulp by ten passes through a M7115 Fluidiser (Microfluidics Corp.), essentially according to previous reports.[6] The solid content of the prepared water dispersion was 1.7%. The amount of hemicellulose (mainly xylan) in the final NFC dispersion was approximately 25–28%. For some experiments larger aggregates of NFC were removed by centrifugation. Samples were first sonicated (Soniprep 150 MSE, amplitude 24 μm, 10 minutes). After centrifugation (Beckmann Optima LE-80K, TFT 65.38 rotor, 10 000*g*), the cellulose retained in the supernatant was collected. The cellulose concentration was 0.6 g l^{-1} as determined gravimetrically.
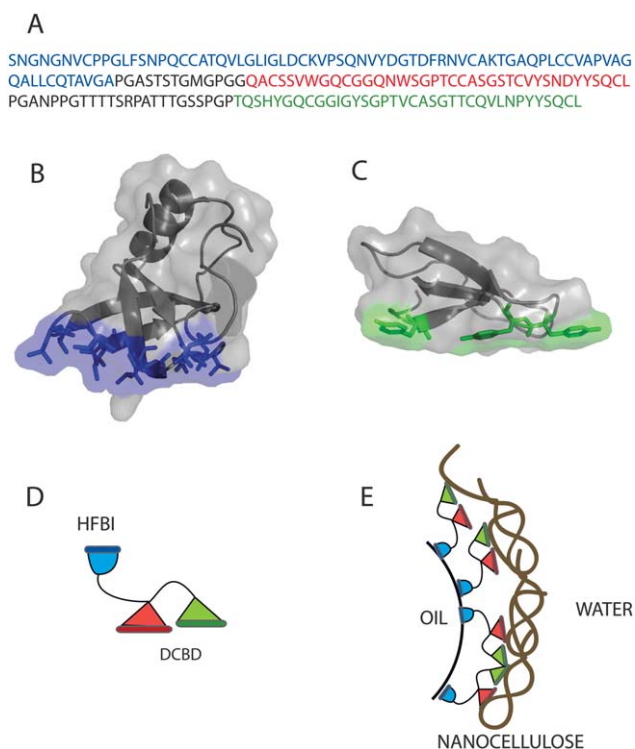
Scheme 1 (A) Amino acid sequence of the fusion protein used to functionalise cellulose. The amphiphilic protein HFBI is first in the sequence (blue), followed by two cellulose-binding sequences Cel6A-CBD (red), and Cel7A-CBD (green). The two CBD sequences are very similar in both structure and function. The domains are separated by linkers (black) to allow flexibility. (B) Structure of HFBI. The hydrophobic patch that makes the protein amphiphilic is shown in blue (PDB id 2FZ6).[38] (C) Structure of the Cel6A-CBD. The aromatic side chains that bind cellulose are show in green (PDB id 1CBH).[39] (D) Cartoon of the HFBI–DCBD fusion protein. The blue part represents HFBI, and the two CBDs (Cel6A-CBD (red), and Cel7A-CBD (green)) form the "double-CBD" (DCBD) part. (E) Schematic illustration of how the interactions of the fusion protein can lead to the assembly of nanocellulose on oil (or air)–water interfaces through the combination of interface (HFBI) and cellulose (DCBD) binding.

CNC were prepared as described previously[26,27] using Whatman 541 ash-less filter paper (Whatman, UK) as the starting material. The cellulose nanocrystals were partially hydrolysed in 4 M HCl at 80 °C for 225 minutes.

2.2 Production and purification of HFBI, HFBII, and HFBI–DCBD

The bi-functional fusion protein consisted of one hydrophobin part linked to two different CBDs in series (sequence in Scheme 1A). The HFBI-hydrophobin from *Trichoderma reesei*[28] was used and the two CBDs were from the enzymes Cel7A (previously CBHI)[29] and Cel6A (previously CBHII),[30] also from *T. reesei*. These modules of the proteins were connected by polypeptide linker regions as previously reported[31] and shown in Scheme 1. The abbreviation HFBI–DCBD was used for the fusion protein. The fusion protein was produced by recombinant means in *T. reesei* and purified by aqueous two phase extraction as described previously.[31] The protein was then purified by preparative reversed phase high performance liquid chromatography (RP-HPLC) using a water acetonitrile gradient with 0.1% trifluoro acetic acid. The identity and concentration were verified by amino acid analysis. Mass spectroscopy was used to verify the identity. HFBI and HFBII were produced using recombinant strains of *T. reesei* and purified by RP-HPLC as described previously.[32] All proteins were lyophilised before use.

2.3 Preparation of ³H-labelled HFBI–DCBD

HFBI–DCBD was labelled with tritium for interaction studies by reductive methylation as reported previously.[33,34] 1.9 mg of lyophilised HFBI–DCBD was dissolved in 1.9 ml of 0.2 M borate buffer, pH 8.96 and cooled on an ice bath. 13.2 µl of 0.37% formaldehyde and 100 mCi of ³H enriched NaBH$_4$ (10 Cimmol^{-1}, NET023H100MC, PerkinElmer) in 150 µl of 0.01 M NaOH were added and mixed for 30 minutes. The reaction was terminated by RP-HPLC. The specific activity was 0.40 Ci mmol^{-1}.

2.4 Determination of binding isotherm of HFBI–DCBD to NFC

A 100 µM stock solution of HFBI–DCBD containing 1% ³H-labelled HFBI–DCBD in 50 mM acetate buffer (pH 5.0) with 1.37 mM HFBII was prepared. Solutions with different fusion protein concentrations were made from the stock solution by diluting with the same buffer containing 1.37 mM HFBII. The excess HFBII was used to minimise nonspecific binding of the fusion protein to test tube walls and filters. 200 µl of each protein solution was mixed with 200 µl of 1 g l^{-1} NFC in MilliQ-water and stirred in ambient temperature for 1 h. Before mixing NFC with the protein solution it was dispersed with a tip ultrasonicator (Soniprep 150 MSE, 5 minutes, amplitude 24 µm). After equilibration, the suspension was filtered through a disposable filter (Millipore, Millex®-GV filter unit, PVDF, hydrophilic, 0.22 µm, 13 mm, non-sterile) and the amount of free HFBI–DCBD was determined by liquid scintillation counter (Pharmacia, Wallac 1410) from the filtrate.

2.5 Determining the stability of the HFBI–DCBD binding to NFC

A series of identical mixtures of NFC and HFBI–DCBD containing ³H-labelled HFBI–DCBD were first prepared (500 µl). The equilibrium concentration of bound protein was determined from two samples to determine the initial equilibrium point on the isotherm. The other samples were then diluted with buffer (containing no HFBI–DCBD). Dilutions from two- to ten-fold were used. The samples were filtered at different time points and analysed to determine possible release of bound protein. HFBI–DCBD was quantified from both supernatant and cellulose. To separate cellulose and supernatant, the mixture was filtered (0.22 µm Durapore membrane, Millipore). When the protein was quantified from the cellulose fraction, the filter was washed to remove unbound protein from the sample.

2.6 Formation and characterisation of monolayers on the langmuir trough

Monolayer isotherms were measured and Langmuir–Schaefer (LS) films were prepared using a KSV Minimicro trough (KSV Instruments). We use the term LS films to describe molecular layers that have transferred from the air/water interface by touching the surface with a hydrophobic material. In LS films therefore the outermost side will be the side of the surface layer that was directed towards the bulk water during film assembly. The layers were prepared by injecting protein solution, a mixture of protein and nanocellulose or solution containing only nanocellulose onto the air/water interface. The samples contained 6.25 to 25 µM protein and 0.5 to 2 g l^{-1} of NFC or CNC. After stabilisation (20–30 min), the isotherm of the monolayer was recorded by a constant rate compression of 3 mm min^{-1} at a constant temperature of 21 °C. The nanocellulose containing samples were dispersed with a tip ultrasonifier (Soniprep 150 MSE, 2 minutes, amplitude 24 µm). Samples containing only protein were dispersed mildly in an ultrasonic bath (Sonoswiss, SW3) for 30 seconds.

LS-films were prepared by first compressing the monolayer to a surface pressure of 30 mN m^{-1}. The surface films were then deposited onto pieces (10 × 10 mm) of freshly cleaved, ZYA quality, highly oriented pyrolytic graphite (HOPG), (NT-MDT Europe BV). HOPG was found suitable because it has a very flat hydrophobic surface. The LS films were then carefully rinsed with water to remove excess protein and unbound nanocellulose and dried in a vacuum desiccator.

2.7 Atomic force microscopy

Atomic force microscopy (AFM) was used to image LS films. A NanoScope IIIa Multimode (E-scanner, Digital Instruments/ Veeco) AFM instrument was used with an NSCI5/AlBS cantilever (µMASCH). All images were recorded in tapping mode in air with scan rates of 0.8–1 Hz (free amplitude was about 0.65 V). The damping ratio was around 0.7–0.85. Images were flattened to remove possible tilts in the image data.

2.8 Interfacial dilatational rheology

Dilatational rheology of the protein film, NFC film or films containing both components was studied at air/water and oil/water interfaces by an oscillating air bubble or pendant drop, respectively. Measurements were carried out by injecting an air bubble into aqueous solution containing the components under study. For oil/water interface measurements a droplet of the aqueous solution was suspended from a capillary immersed in hexadecane (Sigma-Aldrich). The droplet volume was oscillated in a sinusoidal form using a pulsating drop module (KSV PD 100, KSV Instruments Ltd.). Before rheological measurement, the interfacial tension was followed until equilibrium was reached (CAM 200, KSV Instruments Ltd.). At equilibrium, pulsation of the droplet volume at 0.1 Hz was started. The surface area and tension of the droplet were determined by recording a few oscillations at a time and by repeating the measurement a few times with several minutes interval. Rheological parameters were determined from the data with the instruments own software (OscDrop2008, KSV Instruments Ltd.).

2.9 Preparation of emulsions

Emulsions were prepared from pure hexadecane and water solutions containing different amounts of HFBI–DCBD protein, nanocellulose or combinations thereof. The volume fraction of hexadecane was kept as 10% and the total volume of the emulsions was 1 ml. Emulsions were formed by ultrasonication of mixtures of oil and water phase with an ultrasonic probe (Soniprep 150 MSE, amplitude 26 μm) for 4 × 30 seconds in an ice bath, followed by homogenisation in an ultrasonic bath for 1 hour. Creaming of the emulsions was studied by following the phase separation after homogenisation. The final volume fraction of emulsion phase was determined from separation of the clear aqueous phase from the opaque emulsion phase, observed using a digital camera.

2.10 Epifluorescence and confocal microscopy

The structure of the emulsions was studied by staining cellulose or hexadecane with fluorescent dyes. Nanocellulose was imaged by epifluorescence microscopy (Olympus BX-50) by staining cellulose with Calcofluor (Scandinavian Brewery Laboratory Ltd.) and imaging fluorescence. More information on the 3-dimensional structure of the emulsions was obtained by confocal microscopy (Radiance Plus, BIO-RAD). For verification of formation of an oil-in-water emulsion, an oil soluble stain, Nile Red (Molecular Probes), was added to the samples prior to imaging. A blue argon laser (488 nm) was used for excitation of the dye.

2.11 Drug nanoparticle preparation and binding to cellulose

An anti-solvent precipitation technique was used to form nanoparticles of a hydrophobic drug, itraconazole (ITR, Apotecnia Murcia, Spain) and hydrophobins as described previously.[25] Tetrahydrofuran (THF, p.a., Riedel-de Haën, Germany) was used as the solvent for ITR. HFBI, HFBII or HFBI–DCBD was first dissolved in water (0.6 g l⁻¹). The solution was sonicated and placed on ice. The ITR solution (12 g l⁻¹) was filtered with PVDF syringe filters (PALL, Ann Abor, USA) to remove possible dust

particles. The ITR (0.25 ml) solution was rapidly added into the hydrophobin solution (5 ml). The receiving liquid was stirred vigorously with a magnetic stirrer and the temperature of the solution was controlled by keeping the sample on ice. A white precipitate was observed as a turbid solution immediately after ITR addition, indicating the formation of the nanoparticles. The solution was stirred for 20 min.

NFC was used at a concentration of 8.4 g l⁻¹ and sonicated immediately prior to use. Nanoparticle suspensions were mixed with NFC solution to a final ITR : HFB : NFC weight ratio of 1 : 1 : 2. The ionic strength was adjusted by adding NaCl up to 300 mM. The suspensions were shaken at room temperature for 20 min before taking the first TEM samples. Characterisation of the particle size and morphology was done by transmission electron microscope (FEI Tecnai F12, Philips Electron Optics, The Netherlands). Nanoparticle dispersions were dried on formvar film-coated copper grids with mesh size 300 (Agar Scientific, Essex, UK).

3 Results and discussion

3.1 The binding isotherm for HFBI–DCBD to NFC

The affinity and capacity of HFBI–DCBD binding to NFC were determined (Fig. 1). Data were fitted using a one-site binding Langmuir adsorption model (Graph Pad, CA, USA). The affinity constant, K_d, was 2.4 μM and the binding capacity 20 μmol g⁻¹. These values are very close to previously observed ones for the binding of an individual DCBD-construct on bacterial cellulose. It was previously shown that placing two CBDs in tandem results in a synergic increase in the binding affinity compared to using individual CBDs.[35] This was the reason for choosing the DCBD as the fusion partner. The capacity converted to mass units was 0.37 g of HFBI–DCBD per gram of NFC.

The DCBD binding functionality of HFBI–DCBD was also studied using a quartz crystal microbalance (QCM, see ESI†). Injection of HFBI solution over a polystyrene (PS) surface leads to the formation of a monomolecular layer of hydrophobin, attached to the surface as described previously.[36] This was
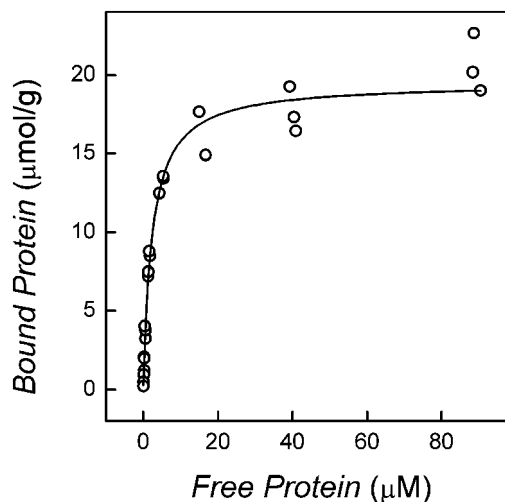

Fig. 1 Binding isotherm of HFBI–DCBD on nanofibrillar cellulose. K_d of the binding of HFBI–DCBD to NFC is 2.4 μM and the binding capacity of NFC is 20 μmol of HFBI–DCBD per gram.

observed in the QCM sensograms for both HFBI and the HFBI–DCBD fusion proteins as increase of mass of 200 ng cm^{-2} for HFBI and 650 ng cm^{-2} for HFBI–DCBD monolayer, corresponding to mean molecular areas of ∼6.3 nm^2 for HFBI and ∼4.7 nm^2 for HFBI–DCBD (see Fig. S3†). After rinsing with buffer, CNC was injected. The mass bound to the HFBI layer was 900 ng cm^{-2} whereas HFBI–DCBD bound approximately 3 μg cm^{-2}. The masses of CNC layers are only rough estimates due to limitations of the QCM method (discussed in the ESI†). It appears that the monolayer of HFBI is able to bind some CNC non-specifically or that a small amount of CNC sediments on the sensor chip. However, the amount of CNC that binds to the fusion protein is significantly higher than the mass bound to HFBI, showing a specific interaction between CNC and the CBD units.

3.2 Non-equilibrium desorption of HFBI–DCBD from NFC

We investigated the rate of release of HFBI–DCBD from cellulose to understand how stable the modification would be under changing conditions. Mixtures of HFBI–DCBD and NFC were first equilibrated and then diluted with buffer, increasing the volume to 2–10 times the original. If the binding of HFBI–DCBD to NFC would be reversible, a dilution of the sample should result in the formation of a new equilibrium point along the binding isotherm in a time comparable to the binding event. If binding were irreversible or show a very slow desorption, the concentration of free protein should decrease due to the dilution, but the amount of cellulose-bound protein would have remained essentially unchanged. The results showed that in two hours, only a little HFBI–DCBD desorbed from the cellulose in diluted samples and thus desorption was slow (Fig. 2). Over 96% of the bound protein remained bound when the equilibrated NFC/

protein suspension was diluted by a factor of 2 and allowed to reach a new equilibrium (data not shown) and over 80% was found bound after dilution by a factor of 10. The amount of bound protein was found to decrease slightly with time with the greater dilution and after 20 minutes of incubation in room temperature. The amount of HFBI–DCBD was measured both as bound to cellulose and as free in solution. Both ways of measuring gave the same results.

3.3 Formation of self-assembled films

The functionality of the HFBI–DCBD fusion protein at the air/water interface was investigated by studying its behaviour in combination with NFC in a Langmuir trough.[37] In Fig. 3, the surface pressure–area isotherms for the interfacial protein films are shown. The HFBI–DCBD fusion protein showed a slightly lower mean molecular area of ∼1.8 nm^2 than the HFBI control which was ∼2.6 nm^2. The reason is not directly evident since the bulkier DCBD part could be expected to increase the molecular dimensions. However, since the DCBD fusion part increases the size of the hydrophilic part of the fusion protein, the reason may be a decreased tendency to assemble at the surface, or different packing arrangements (AFM images of surfaces in Fig. S1, ESI†).

The formation of monolayers at the air/water interface was also studied by ellipsometry to verify the results (see Fig. S2†). The experiments showed that both proteins formed a full monolayer at the air/water interface even without compression. The mean molecular areas from ellipsometry measurements were ∼3.6 nm^2 and ∼6.0 nm^2 for HFBI and HFBI–DCBD respectively, which are very close to the crystallographic dimensions of the proteins.[38,39] The differences in the mean molecular areas obtained by Langmuir trough and ellipsometry can be caused by the differences in the preparation of the interfacial film. In ellipsometry the interfacial film is formed by free adsorption of the protein from the bulk and in Langmuir trough the protein is
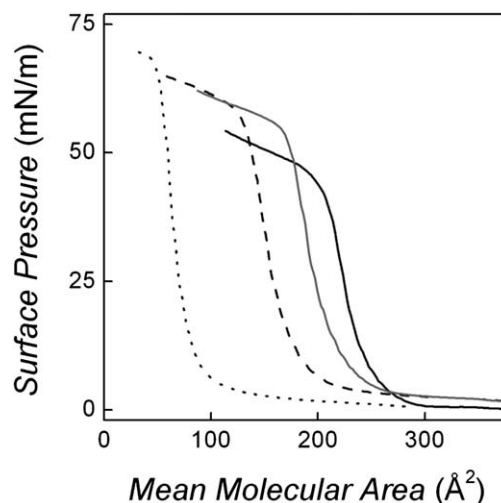

Fig. 2 Summary of dilution driven desorption of HFBI–DCBD from NFC. The columns represent the measured amount of bound HFBI–DCBD per gram of NFC. Time 0 corresponds to the situation before the 10× dilution. After dilution the amount of cellulose bound HFBI–DCBD was measured at times 1, 20 and 120 minutes (columns). The open circles show how much bound protein is expected based on the adsorption binding curve (Fig. 1). The observed bound amount of HFBI–DCBD decreases only slightly showing that the desorption kinetics is very slow. The initial concentration of HFBI–DCBD was 5 μM.

Fig. 3 Isotherms of the interfacial molecular films at air/water interface. The surface pressure as a function of the mean molecular area of HFBI (solid line), HFBI–DCBD (dashed line), 1 : 1 molar ratio mixture of HFBI and HFBI–DCBD (gray line) and the combination of HFBI–DCBD and NFC (dotted line) measured at 21 °C. Mean molecular area was calculated from the amount of injected protein.

injected dropwise onto the interface and compressed to form the film. By compressing the film it is possible that a denser arrangement of protein in the film is achieved and thus a smaller value for mean molecular area compared to ellipsometry. In ellipsometry the proteins are adsorbing freely from the bulk and thus the DCBD part of the fusion protein can interfere in the adsorption of the fusion protein and lead to a larger mean molecular area compared to HFBI.

Addition of nanocellulose (NFC or CNC) to HFBI–DCBD before film formation resulted in changes in the surface pressure–area isotherms compared to only HFBI–DCBD (Fig. 3, data for CNC not shown). The film was prepared from a mixture of 25 μM HFBI–DCBD and 0.5 mg ml^{-1} NFC. In these conditions, ~30% of the protein adsorbed to NFC and the concentration of the free protein remaining was ~17 μM. The surface pressures for film collapse of the NFC containing film were slightly higher than those of the protein films, but the presence of NFC was not otherwise observable in experiments using the Langmuir trough. On the other hand, binding of the protein decreased the amount of free protein at the interface shifting the isotherm towards smaller molecular area (~30% was bound to cellulose at these conditions). To analyse how NFC had been incorporated in the interfacial film, samples of the surface films were deposited on HOPG using the LS technique and imaged by AFM, as described above. As seen in Fig. 4A, a mesh of nanocellulose fibrils has packed as a thin layer on top of the protein film. The NFC density was not uniform across the interfacial film. Similar results were obtained for CNC, as seen in Fig. 4B. Control experiments with only NFC or CNC (lacking protein) did not result in any sort of interfacial film.

3.4 Rheology of the fusion protein/nanocellulose surface films

Surface shear rheological properties of self-assembled films of protein and its combination with NFC at air/water interface were investigated next. In surface shear rheological measurements, the viscoelastic moduli of HFBI and HFBI–DCBD at constant shear and frequency were followed as a function of time (Fig. S4†). Results showed that the interfacial film of HFBI–DCBD formed slower and had smaller moduli than HFBI. Elastic moduli, G', were dominant for all studied interfacial films indicating that they are elastic rather than viscous in nature. The high G' value, ~1.2 N m^{-1}, obtained for HFBI was comparable to the one previously reported in literature.[21,24] The G' value for HFBI–DCBD, ~0.2 N m^{-1}, although an order of magnitude lower than that for HFBI, it

is high compared to other proteins reported in literature.[40,41] The high values of rheological moduli for wild type HFBI are most likely due to the mechanism by which the hydrophobin functions, that is through strong lateral interactions between the molecules. For HFBI–DCBD, the values are significantly lower probably because the normal functional tight packing of the HFBI is sterically hindered by the DCBD fusion partner. A contributing effect for the decrease in G' value for HFBI–DCBD can also be an altered interfacial packing arrangement as compared to HFBI. By ellipsometry, it is seen that the packing density is different for HFBI–DCBD and HFBI, showing mean molecular areas of ~6 nm^2 and ~3.6 nm^2 respectively. It can therefore be expected that the interactions of the molecules are different at the interface, explaining the differences in the G' value. The differences in the adsorption rates for HFBI and the fusion protein are probably due to the size difference of the proteins (HFBI–DCBD ≈ 18 500 Da, HFBI ≈ 7200 Da), giving a significant lowering of the diffusion rate of the larger molecule.

Addition of NFC to the interfacial HFBI–DCBD film caused a slight increase in viscoelastic moduli, but also a large increase in the variation between measurements (See, Fig. S4–S7, ESI†, and Table S1†). The absolute moduli of the hybrid film containing both HFBI–DCBD and NFC do not significantly differ from the values for the film of HFBI–DCBD only indicating that the protein forms a stable interfacial layer, which the NFC does not disturb. However, the deviation of measured curves increases, probably due to variation in the density of NFC fibrils that are attached to the HFBI–DCBD film at the interface.

Dilatational surface rheology of HFBI–DCBD ± NFC hybrid films at air/water and hexadecane/water interfaces was studied by an oscillating pendant drop method. Initially equilibrium was allowed to form. Assembly of HFBI–DCBD led to a significant decrease of surface tension at air/water interface, from initial ~72 mN m^{-1} to final 55 mN m^{-1}. Similarly values decreased from 30 mN m^{-1} to 9 mN m^{-1} at the oil/water interface. Adsorption of NFC to the interfaces did not decrease the interfacial tension as much as the protein did (see Table 1). Under these conditions, ~7% of the protein was bound to the cellulose (calculated from the binding isotherm (Fig. 1)). The values of dilatational moduli for pure NFC at oil/water interface are significantly larger than the ones at air/water interface, which implies that NFC itself has a tendency to adsorb at the oil/water interface.

Dilatational rheological measurements are summarised in Table 1. A low phase lag was observed for all the film types, implying the formation of elastic films. At the air/water interface,
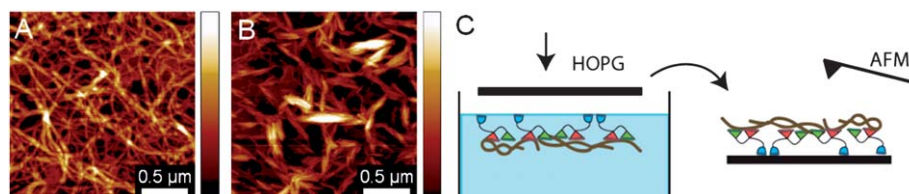

Fig. 4 AFM topography images of self-assembled protein/cellulose films picked up from air/water interface at surface pressure 30 mN m^{-1}. (A) An interfacial film formed from a combination of HFBI–DCBD and NFC. (B) An interfacial film formed from a combination of HFBI–DCBD and CNC. In both cases a well-defined two-layered hierarchical structure was obtained. The height scale in both images is 30 nm. (C) Schematic representation of how samples were prepared. First the fusion protein was allowed to assemble on the air/water interface together with NFC or CNC. Then the surface layer was lifted off from the surface by touching with a piece of HOPG. HOPG with the surface layer attached was then imaged with AFM.

Table 1 Values of interfacial tension, viscoelastic moduli and phase lag at air/water and hexadecane/water interfaces in the presence of 0.1 gl^{-1} HFBI–DCBD protein, light fraction of NFC and their combination

	Surface/interfacial tension/mN m^{-1}	$|E|$/mN m^{-1}	E'/mN m^{-1}	E''/mN m^{-1}	Phase lag/deg
HFBI–DCBD (air/w)	57	235	234	6	−1
HFBI–DCBD (o/w)	9	33	32	5	8
NFC (air/w)	63	8	8	0	1
NFC (o/w)	15	21	20	4	11
HFBI–DCBD + NFC (air/w)	53	146	145	16	6
HFBI–DCBD + NFC (o/w)	9	14	14	1	5

the value of dilatational elastic modulus E' was very high for pure protein, but low for pure NFC. NFC together with protein had intermediate E' values. HFBI results were comparable to earlier observations from a Langmuir trough method.[41] At the oil/water interface the absolute moduli values were much smaller and samples with only protein had the highest values. The behaviour of the hybrid film at the oil/water interface deviated from the air/water interface and showed the lowest E' value. This is probably due to NFC's different behaviour at the two interfaces. Since NFC was observed to form a film at the oil/water interface, there may be competitive adsorption of NFC and HFBI–DCBD leading to less-ordered film than at the air/water interface, where formation of a stable hydrophobin layer is very favourable and practically no NFC adsorption was observed. A reason for the assembly of NFC might be their high surface energy, which makes them very sensitive towards other solvents than water. It has been shown that the dispersed nanofibrillar structure may collapse in the contact with organic solvents.[42] On the other hand, low elastic moduli of the protein/NFC films imply to restricted dilatation of the film containing cellulose. The interface between pure water and hexadecane was studied as a reference and was also elastic in nature, but had a lower modulus $|E|$ than the other interfaces.

We conclude that the NFC alters the rheological properties of interfacial films to some extent but that the properties are still dominated by the properties of hydrophobin.

3.5 NFC and HFBI–DCBD as emulsion stabilisers

Emulsions of hexadecane and water in the presence of HFBI–DCBD and/or nanocellulose were studied. As shown above the self-assembly of HFBI–DCBD and NFC led to interfacial films and we investigated how the possible formation of such films could affect the properties of emulsions. Effects could include the stabilisation of interfaces, and thereby increased stability of emulsions. Emulsion structures were studied by microscopy and they were confirmed to be of oil-in-water type by staining the oil phase with a lipophilic dye (Nile Red) (see Fig. S8 and S9†). Oil droplets could also be observed by bright field microscopy and their size varied from tens of micrometres to some hundreds of nanometres for different samples and emulsion types. Fig. 5A shows an example of an emulsion formed by NFC alone. NFC is stained with Calcofluor and is clearly visible as bright blue surrounding the *ca.* 10–20 μm oil droplets. The droplets in HFBI–DCBD containing emulsions were much smaller, about 600 nm in diameter. In emulsions containing both NFC and the protein, the droplets were also small and they were coated by a thin layer of cellulose, which was observed by their

fluorescence. The fluorescence intensity of droplets containing NFC increased with increased NFC content. As the cellulose concentration was increased, a continuous cellulose matrix was formed in the aqueous phase. Association of the submicron oil droplets to the cellulose fibrils was observed as shown in Fig. 5B and C. Similar structures were observed for CNC (see Fig. S10†).

The stability of the emulsions was studied by following separation of the emulsion phase from the aqueous phase due to creaming. The results are presented as the emulsion stability index (*ESI*), which is calculated from the volume of separated water and the total amount of water as follows.

$$ESI = \left[1 - \frac{V_{w,separated}}{V_{w,total}} \right] \times 100\% \qquad (1)$$

The equilibrium *ESI*, measured 28 days after formation of the emulsions are shown in Fig. 6. The stability was rechecked under a period of 6 months with no visible change. The stability of the cellulose-containing emulsions was generally dependent on the concentration of nanocellulose, which is probably caused by both the increasing viscosity of the water phase as a function of the nanocellulose content and by the increasing amount of NFC available for encapsulating the oil droplets. The stability of the emulsions was further enhanced by addition of the fusion protein. In Fig. 6A, a comparison of an emulsion series stabilised with varying amount of NFC without protein and with added 1 g l^{-1} of HFBI–DCBD is presented. The data show that full stability of the emulsion could be reached at conditions where the NFC concentration was ~1.25 g l^{-1} and protein concentration 1 g l^{-1}. In the case of plain NFC, the most stable emulsion at the studied concentration range (2 g l^{-1}) had volume of ~80% of the total volume. The protein itself was observed to stabilise emulsions rather well even in the absence of nanocellulose, but the equilibrium volume above 80% could not be reached (see Fig. S11A†). The *ESI* value for the control emulsion containing 1 g l^{-1} of HFBI and 1 g l^{-1} NFC was 54%. Stabilisation of emulsions was also studied with CNC, but their ability to stabilise emulsions was much lower (see Fig. S11B†).

From the above observations, two possible reasons for enhanced emulsion stability are proposed. On the one hand, it can be expected that NFC acts as a thickener of the continuous phase slowing down the diffusion of the emulsion droplets when the phases separate due to their density difference. On the other hand, addition of HFBI–DCBD showed a clear enhancement of emulsion stability. One reason for more stable emulsions may be assembly of HFBI–DCBD at the interfaces of the oil droplets, which decreases their size. However, control emulsions containing wild type HFBI and NFC were less stable than the ones containing same amount of NFC and HFBI–DCBD. HFBI
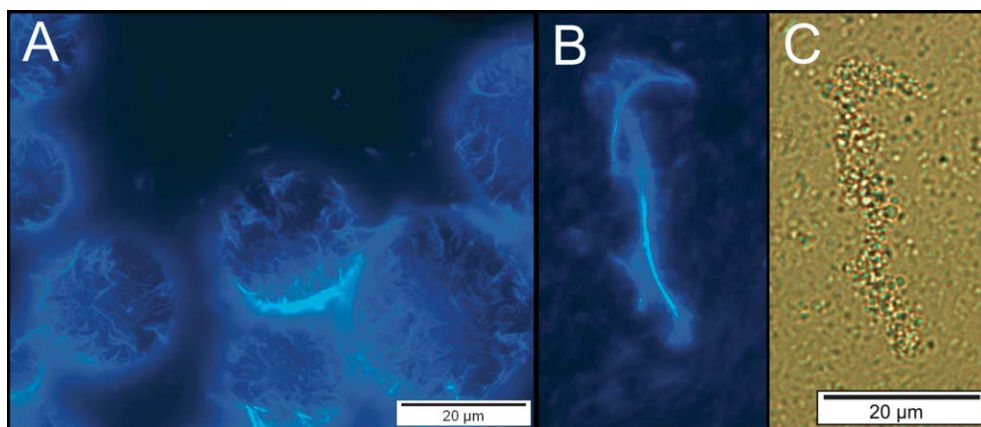
Fig. 5 Epifluorescence microscope images of emulsions. Cellulose has been stained with Calcofluor. (A) An image of emulsion stabilised by 0.1 g l^{-1} of NFC. (B) An image of emulsion stabilised by NFC/HFBI–DCBD. Structures consisting of bundled cellulose fibrils are clearly visible. (C) A bright field microscope image of the same structure. Droplets are seen as small granules following the cellulose structures. Concentrations of NFC and HFBI–DCBD were 0.025 g l^{-1} and 1.0 g l^{-1} respectively.

assembles the oil/water interface, but does not bind to cellulose specifically. These data and the microscope examination of the emulsions indicate that there is interaction between the NFC fibrils and the HFBI–DCBD-coated oil droplets leading to highly stable emulsions. The synergetic effect between the protein and nanocellulose was studied further by examining the measured *ESI* values of emulsions containing NFC and HFBI–DCDB as a function of different variables, such as amount of NFC, total protein, unbound protein and bound protein. The only variable showing a general trend (Fig. 6B) was the amount of HFBI–DCBD bound to NFC, which was calculated from the binding isotherm. For comparison, the inset shows the data plotted against the amount of free protein (see Fig. 6B inset), which shows no clear dependency. According to this observation, the best stabilisation occurs when largest amount of the HFBI–DCBD + NFC complex is present.

Cellulose derivates and modified cellulose have been used widely in emulsions and other drug and food formulations but only few reports on using unmodified cellulose as an emulsion stabiliser have been published.[43–46] The surface of cellulose is hydrophilic, but nanocelluloses (NFC and CNC) have low colloidal stability, leading to bundling of the fibrils and collapse of CNC.[10] Yet, nanocellulose is not amphiphilic and its ability to stabilise emulsions has not been reported widely. Only one report, describing structures similar to our observations where unmodified bacterial nanocellulose has formed a mechanical barrier surrounding oil droplets has been published.[45] The reasons for deposition of mesh of unmodified nanocellulose at the oil/water interface cannot be associated with self-assembly of nanocellulose at the interface, since there was no detectable lowering of interfacial tension in the presence of NFC alone. The reason for oil encapsulation is most probably due to collapse and bundling of
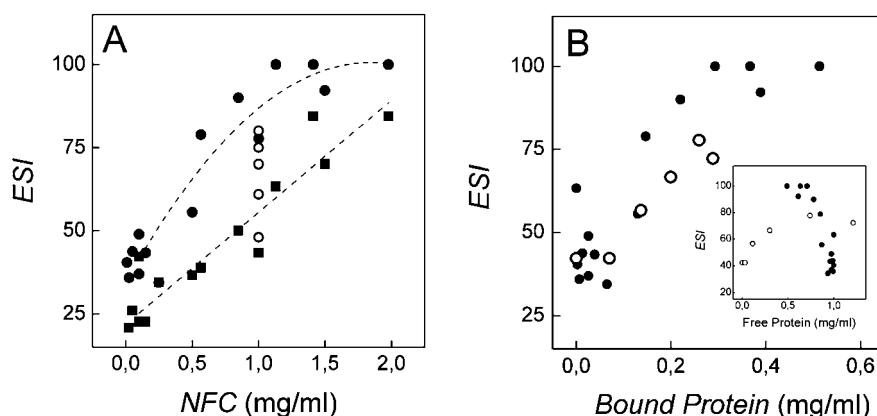

Fig. 6 Emulsion stability indices (*ESI*) of emulsion containing NFC. (A) *ESI* of emulsions stabilised by NFC (filled squares) and combinations of varying amount of NFC and 1 g l^{-1} HFBI–DCBD protein (filled circles) as a function of NFC concentration. A series of emulsions containing 1.0 g l^{-1} of NFC and a varying amount of protein (from 0.1 to 1.5 g l^{-1}) (unfilled circles) showed an intermediate behaviour between pure NFC and the emulsions containing 1.0 g l^{-1} of protein with varying amount of NFC. The dashed lines do not have theoretical meaning but are plotted as a guide to the eye. (B) *ESI* of all emulsions containing combinations of NFC and HFBI–DCBD as a function of bound protein concentration. The data are the same as presented in (A), the emulsions with varying amount of NFC and 1 g l^{-1} HFBI–DCBD protein (filled circles) and the emulsions containing 1.0 g l^{-1} of NFC and a varying amount of protein (unfilled circles). Inset: the same data presented as a function of free protein concentration, showing that there is no meaningful correlation between *ESI* and the amount of free protein.

the nanofibrils at the interface when they were forced in contact with hexadecane during the emulsification.[42] On the other hand, the emulsions high stability might imply the formation of Pickering emulsions, where solid particles assemble at the oil/water interface forming very likely highly stable emulsions.[47]

The behaviour of the HFBI–DCBD containing emulsions shows a difference to emulsions formed by only NFC that can be explained through the dual function of HFBI–DCBD. Formation of oil-droplets by the fusion protein both in the absence and presence of NFC implies that the protein's assembly at the oil/water interface is rapid and that cellulose does not significantly interfere with the assembly or protein orientation. This implies that the structure of the interfacial films in the emulsions is the same two-layered structure that was observed at the flat air/water interface.

3.6 Functionalisation of drug nanoparticles for binding to NFC

The amphiphilic structure of hydrophobin allows it to be used to produce and coat nanoparticles of compounds that have low solubility in aqueous solution, such as some drug compounds.[25] We previously showed when a compound of low solubility in water (here itraconazole (ITR)) was dissolved in a suitable solvent (here tetrahydrofuran (THF)) and then dispersed in an aqueous solution of hydrophobin, nanoparticles were formed (Fig. 7A). Such nanoparticles have many desirable effects such as improved solubility and bioavailability, but the long term stability of the particles can be low, especially in physiological conditions. In Fig. 7B, it can be seen that particles have aggregated and their morphology has changed after five days in aqueous solution.

Next we investigated how a cellulose-binding functionality could be added to the nanoparticles through the use of HFBI–DCBD. The use of HFBI–DCBD resulted in morphologically identical particles as with the HFBII as observed by TEM. The cellulose binding capacity of the nanoparticles was studied by mixing NFC and the nanoparticle solution. HFBI coated nanoparticles were used as the control. It was found that particles associated to NFC, but in a solution dependant manner. At low ionic strength, both HFBI and HFBI–DCBD coated particles were found to associate with NFC (Fig. S12†). However, increasing the ionic strength by adding NaCl up to 300 mM revealed a clear difference between particles with DCBD function and those without, as shown in Fig. 8. Freshly prepared mixtures of particles and NFC showed little difference and
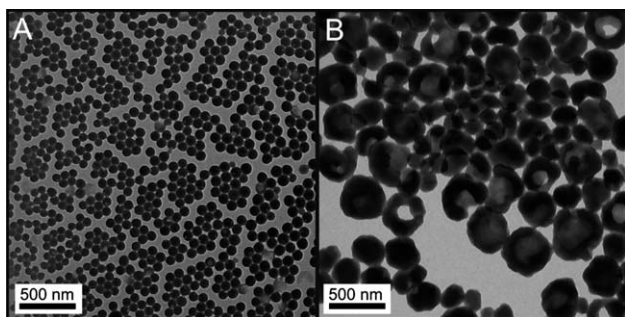

Fig. 7 (A) TEM image of freshly prepared ITR filled nanoparticles coated with hydrophobin (HFBII). (B) The particles are unstable and storage in aqueous solution leads to disruption and disproportionation, as shown here for a five-day old sample.
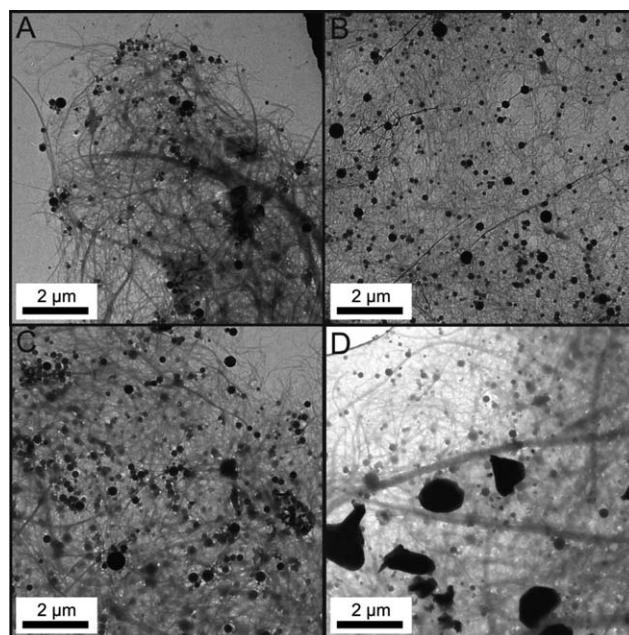

Fig. 8 TEM images of (A) ITR–HFBI–DCBD–NFC sample made in 0.3 M NaCl, (B) ITR–HFBI–NFC sample made in 0.3 M NaCl. Both samples were stored in suspension for 12 days. (C) After storage the morphology of the sample prepared with HFBI–DCBD showed no change, (D) the sample prepared with only HFBI showed strong aggregation.

particles associated with the cellulose could be identified on TEM images. However, upon aging of the samples they behaved distinctly differently. The particles prepared with only HFBI showed strong aggregation and coalescence of particles, with their size growing from *ca.* 50–100 nm to above micrometres after 12 days. In contrast, particles prepared using HFBI–DCBD showed very little change after the same storage. The particles were still attached to the NFC network and well dispersed. Steric stabilisation using polymers has been considered an effective mechanism to shelter drug nanoparticles against aggregation and degradation. It can be more effective than ionic stabilisation because of the high ionic strength and variation in pH in the human body. Therefore, HFBI–DCBD fusion protein ability to bind to NFC with high affinity, regardless of the high ionic concentration, was considered as an integral part of protective matrix for drug nanoparticles.

4 Conclusions

In this work we have demonstrated a way to use specific protein interactions to functionalise nanocellulose. Through this functionalisation, NFC could be self-assembled at the air/water interface, forming thin layers of tightly packed fibrils. The combination of NFC and HFBI–DCBD gave a synergistic effect in the formation and stability of an oil-in-water emulsion. The bifunctional adhesive properties of HFBI were also shown to improve the attachment of drug nanoparticles to NFC and thus improve their stability during storage.

In nature there are innumerable examples of how specific protein interactions control the architecture of cells, tissues and other structures, thereby creating highly functional assemblies.

To achieve a similar level of control of structures is a major goal of materials science and molecular nanotechnology.[48,49] It can be instructive to view the HFBI–DCBD as a block copolymer as it consists of blocks of different functionalities. The interactions of the different blocks lead to self-assembly of the system. In principle such block-copolymers could be produced in a completely non-biological manner if blocks with suitable functionality would be available. However, we are not aware of the existence of non-biological blocks that would function with similar efficiency as the protein blocks used here. We suggest that protein-based block copolymers have the significant advantage that their structures can be engineered on a molecular level in a significantly more precise way than any synthetic system, leading to more specific interactions and higher degree of control. The main drawback of amino acid based systems is that we are currently limited to the 20 naturally occurring ones. However, with the rapid development of molecular and synthetic biology, it is likely that this limitation will be overcome in the future.

The use of genetic engineering allows the production of a vast number of molecular functionalities and combinations thereof, opening an enormous resource for materials engineering on the nano and molecular scale. Nature provides examples of interactions that can be used, such as the ones used in this work. However, we can also fine tune these biological compounds or find entirely new interactions and molecular functions in the laboratory by using methods such as directed evolution.[50] In this way, similar protein-based approaches for structural assembly can be extended to any system, biologic or non-biologic.

Acknowledgements

References

1 I. Siro and D. Plackett, *Cellulose*, 2010, **17**, 459–494.
2 S. J. Eichhorn, A. Dufresne, M. Aranguren, N. E. Marcovich, J. R. Capadona, S. J. Rowan, C. Weder, W. Thielemans, M. Toman, S. Renneckar, W. Gindl, S. Veigel, J. Keckes, H. Yano, K. Abe, M. Nogi, A. N. Nakagaito, A. Mangalam, J. Simonsen, A. S. Benight, A. Bismarck, L. A. Berglund and T. Peijs, *J. Mater. Sci.*, 2010, **45**, 1–33.
3 K. Riehemann, S. W. Schneider, T. A. Luger, B. Godin, M. Ferrari and H. Fuchs, *Angew. Chem., Int. Ed.*, 2009, **48**, 872–897.
4 D. J. Gardner, G. S. Oporto, R. Mills and M. A. S. A. Samir, *J. Adhes. Sci. Technol.*, 2008, **22**, 545–567.
5 D. Klemm, B. Heublein, H. Fink and A. Bohn, *Angew. Chem., Int. Ed.*, 2005, **44**, 3358–3393.
6 M. Pääkkö, M. Ankerfors, H. Kosonen, A. Nykänen, S. Ahola, M. Österberg, J. Ruokolainen, J. Laine, P. T. Larsson, O. Ikkala and T. Lindström, *Biomacromolecules*, 2007, **8**, 1934–1941.
7 A. N. Nakagaito and H. Yano, *Appl. Phys. A: Mater. Sci. Process.*, 2004, **80**, 155–159.
8 M. Ioelovich, *Curr. Trends Polym. Sci.*, 2008, **12**, 43–48.
9 M. Pääkkö, J. Vapaavuori, R. Silvennoinen, H. Kosonen, M. Ankerfors, T. Lindström, L. A. Berglund and O. Ikkala, *Soft Matter*, 2008, **4**, 2492–2499.
10 J. F. Revol, L. Godbout, X. M. Dong, D. G. Gray, H. Chanzy and G. Maret, *Liq. Cryst.*, 1994, **16**, 127–134.
11 R. T. Olsson, M. A. S. Azizi Samir, G. Salazar-Alvarez, L. Belova, V. Ström, L. A. Berglund, O. Ikkala, J. Nogues and U. W. Gedde, *Nat. Nanotechnol.*, 2010, **5**, 584–588.
12 Q. Wu, M. Henriksson, X. Liu and L. A. Berglund, *Biomacromolecules*, 2007, **8**, 3687–3692.
13 L. A. Berglund and T. Peijs, *MRS Bull.*, 2010, **35**, 201–207.
14 C. Gousse, H. Chanzy, G. Excoffier, L. Soubeyrand and E. Fleury, *Polymer*, 2002, **43**, 2645–2651.
15 M. Suzuki, K. Saruwatari, T. Kogure, Y. Yamamoto, T. Nishimura, T. Kato and H. Nagasawa, *Science*, 2009, **325**, 1388–1390.
16 M. Linder and T. T. Teeri, *J. Biotechnol.*, 1997, **57**, 15–28.
17 E. A. Bayer, E. Morag and R. Lamed, *Trends Biotechnol.*, 1994, **12**, 379–386.
18 H. Palonen, M. Tenkanen and M. Linder, *Appl. Environ. Microbiol.*, 1999, **65**, 5229–5233.
19 M. Linder, T. Nevanen, L. Söderholm, O. Bengs and T. T. Teeri, *Biotechnol. Bioeng.*, 1998, **60**, 642–647.
20 M. B. Linder, *Curr. Opin. Colloid Interface Sci.*, 2009, **14**, 356–363.
21 K. Scholtmeijer, J. G. H. Wessels and H. A. B. Wosten, *Appl. Microbiol. Biotechnol.*, 2001, **56**, 1–8.
22 J. G. H. Wessels, *Adv. Microb. Physiol.*, 1997, **38**, 1–45.
23 A. R. Cox, D. L. Aldred and A. B. Russell, *Food Hydrocolloids*, 2008, **23**, 366–376.
24 A. R. Cox, F. Cagnol, A. B. Russell and M. J. Izzard, *Langmuir*, 2007, **23**, 7995–8002.
25 H. K. Valo, P. H. Laaksonen, L. J. Peltonen, M. B. Linder, J. T. Hirvonen and T. J. Laaksonen, *ACS Nano*, 2010, **4**, 1750–1758.
26 C. D. Edgar and D. G. Gray, *Cellulose*, 2003, **10**, 299–306.
27 J. Araki, M. Wada, S. Kuga and T. Okano, *J. Wood Sci.*, 1999, **45**, 258–261.
28 T. Nakari-Setälä, N. Aro, N. Kalkkinen, E. Alatalo and M. Penttilä, *Eur. J. Biochem.*, 1996, **235**, 248–255.
29 T. T. Teeri, P. Lehtovaara, S. Kauppinen, I. Salovuori and J. Knowles, *Gene*, 1987, **51**, 43–52.
30 T. Teeri, I. Salovuori and J. Knowles, *Bio/Technology*, 1983, **1**, 696–699.
31 M. B. Linder, M. Qiao, F. Laumen, K. Selber, T. Hyytiä, T. Nakari-Setälä and M. E. Penttilä, *Biochemistry*, 2004, **43**, 11873–11882.
32 M. Linder, K. Selber, T. Nakari-Setälä, M. Qiao, M. Kula and M. Penttilä, *Biomacromolecules*, 2001, **2**, 511–517.
33 G. E. Means and R. E. Feeney, *Anal. Biochem.*, 1995, **224**, 1–16.
34 N. Jentoft and D. G. Dearborn, *J. Biol. Chem.*, 1979, **254**, 4359–4365.
35 M. Linder, I. Salovuori, L. Ruohonen and T. T. Teeri, *J. Biol. Chem.*, 1996, **271**, 21268–21272.
36 Z. Wang, M. Lienemann, M. Qiau and M. B. Linder, *Langmuir*, 2010, **26**, 8491–8496.
37 G. R. Szilvay, A. Paananen, K. Laurikainen, E. Vuorimaa, H. Lemmetyinen, J. Peltonen and M. B. Linder, *Biochemistry*, 2007, **46**, 2345–2354.
38 J. Hakanpää, G. R. Szilvay, H. Kaljunen, M. Maksimainen, M. Linder and J. Rouvinen, *Protein Sci.*, 2006, **15**, 2129–2140.
39 P. J. Kraulis, G. M. Clore, M. Nilges, T. A. Jones, G. Pettersson, J. Knowles and A. M. Gronenborn, *Biochemistry*, 1989, **28**, 7241–7257.
40 R. Ipsen and J. Otte, *Annu. Trans. Nord. Rheol. Soc.*, 2003, **11**, 89–93.
41 T. B. J. Blijdenstein, P. W. N. de Groot and S. D. Stoyanov, *Soft Matter*, 2010, **6**, 1799–1808.
42 H. Jin, Y. Nishiyama, M. Wada and S. Kuga, *Colloids Surf., A*, 2004, **240**, 63–67.
43 E. Melzer, J. Kreuter and R. Daniels, *Eur. J. Pharm. Biopharm.*, 2003, **56**, 23–27.
44 L. W. Chan, P. W. S. Heng and L. S. C. Wan, *J. Microencapsulation*, 1997, **14**, 545–555.
45 H. Ougiya, K. Watanabe, Y. Morinaga and F. Yoshinaga, *Biosci., Biotechnol., Biochem.*, 1997, **61**, 1541–1545.
46 M. Andresen and P. Stenius, *J. Dispersion Sci. Technol.*, 2007, **28**, 837–844.
47 R. Aveyard, B. P. Binks and J. H. Clint, *Adv. Colloid Interface Sci.*, 2003, **100–102**, 503–546.
48 M. Muthukumar, C. K. Ober and E. L. Thomas, *Science*, 1997, **277**, 1225–1232.
49 J. Lehn and P. Ball, Supramolecular Chemistry, in The New Chemistry, ed. N. Hall, Cambridge University Press, Cambridge, 2000, pp. 300–351.
50 M. Sarikaya, C. Tamerler, A. K. Jen, K. Schulten and F. Baneyx, *Nat. Mater.*, 2003, **2**, 577–585.

Supporting Information for

Self-Assembly of Cellulose Nanofibrils by Genetically Engineered Fusion Proteins

Suvi Varjonen[1], Päivi Laaksonen[1], Arja Paananen[1], Hanna Valo[2], Hendrik Hähl[3], Timo Laaksonen[2], Markus B. Linder[1*]

[1]Nanobiomaterials, VTT Technical Research Centre of Finland, Tietotie 2, P.O. Box 1000, FI-02044 VTT, Finland, [2]Division of Pharmaceutical Technology, University of Helsinki, P.O. Box 56, FI-00014 University of Helsinki, Finland, [3]Department of Experimental Physics, Saarland University, 66041 Saarbrücken, Germany.

LS films of proteins

Protein monolayers were studied by pipetting a known amount of HFBI and HFBI-DCBD on top of the subphase on a Langmuir trough. The films were compressed to surface pressure 30 mN/m and then picked up on a HOPG substrate. Films were then imaged by AFM (Figure S1).
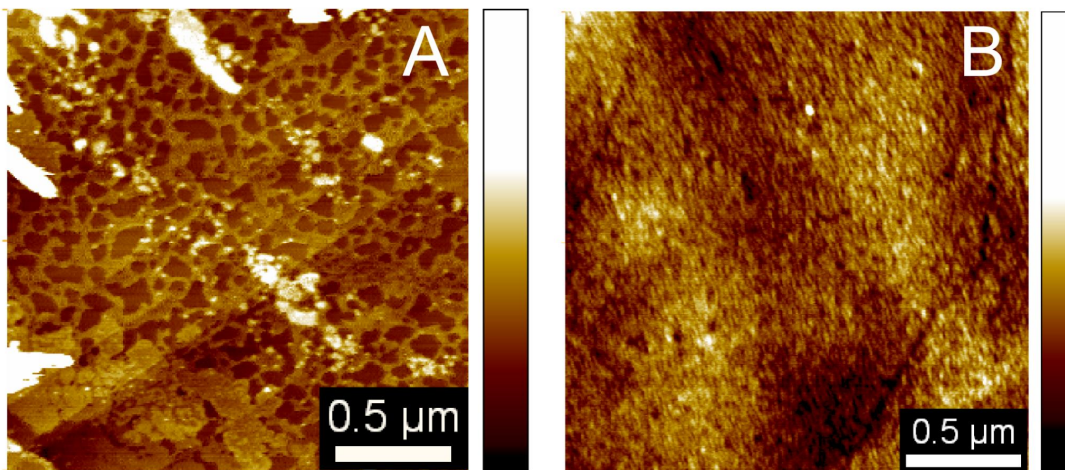
Figure S1. AFM topography images of self-assembled protein films picked up from air/water interface at surface pressure 30 mN/m. A) A monolayer of HFBI. B) A monolayer of HFBI-DCBD.

Ellipsometry

Ellipsometric measurements were carried out using a multi-wavelength ellipsometer (EP3, Nanofilm, Göttingen, Germany) operated at a single wavelength of 532 nm. The device was set up in a PCSA (polarizer-compensator-sample-analyzer) configuration with an angle of incidence of 54° to the surface normal. The air/water interface is realized by a round Teflon trough filled with buffer solution (10 mM acetate buffer, pH 5). Care was taken on choosing the optimal trough diameter, large enough to minimize meniscus curvature in the middle region, where the laser light probes (or: is reflected by) the liquid/air interface. To minimize evaporation, the trough was covered by a hood with a small slit for incident and reflected light beam.

The ellipsometric angles Ψ and Δ were recorded via the nulling ellipsometry principle in two zones[i] thus balancing between measurement time and accuracy of the

measurement. A sampling rate of ca. 1.5 min^{-1} was chosen for the time resolved measurements of the adsorption kinetics.

For the evaluation of the recorded data, an optical box model was applied consisting of the buffer solution (whose refractive index n_s was determined before), the protein film (assumed as homogeneous layer with a fixed refractive index n_f) and the ambient air (simulated as vacuum, $n_v = 1$). This model yields the protein layer thickness d_f as a function of time, yet with a fixed refractive index. The absolute amount of adsorbed protein Γ can be determined with de Feijter's formula

$$\Gamma = d_f \frac{n_f - n_s}{dn/dc} \qquad\qquad \text{(Eq S1)}$$

assuming that the refractive index of a protein is a linear function of its concentration, and with dn/dc as the increment of the refractive index due to concentration increase, fixed to a value of 0.183 cm^3g^{-1}.[ii,iii] Since for layer thicknesses smaller than 5 nm it is not possible to determine thickness and refractive index of a layer unambiguously[iv,i], the adsorbed amount Γ is the more reliable value.
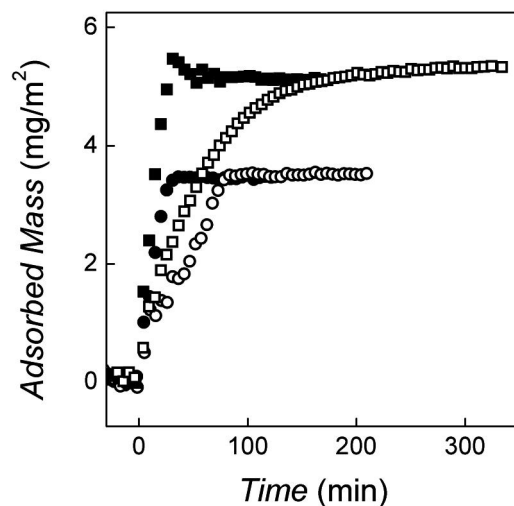
Figure S2. Adsorbed mass of HFBI (circles) and HFBI-DCBD (squares) at the air/water interface as a function of time. Closed symbols correspond to protein concentrations 1 μM and open symbols to 0.5 μM.

Adsorption HFBI and HFBI-DCBD at air/water interface was studied by injecting certain amounts of the proteins into water and measuring the evolution of a surface film. After observing a constant baseline indicating constant ambient conditions, the measurements were started by exchanging 10 ml of the buffer with the protein solution. Complete mixing was achieved by injecting the protein solution into the bulk water at velocities sufficiently high for turbulent flow behavior. Measurement was repeated with protein concentrations 0.5 μM and 1.0 μM (Figure S2.). The final adsorbed masses of HFBI (M = 7.54 kDa) and HFBI-DCBD (18.50 kDa) were ∼ 3.5

mg/m^2 and 5.1 ~ mg/m^2, respectively. These correspond to monolayers with mean molecular areas 3.6 nm^2 and 6.0 nm^2.

QCM Analysis of Functionality of the HFB-DCBD Fusion Protein.

Sensograms of the QCM binding studies are shown in Figure S3. The experiment can be divided into three regions, the initial equilibration (baseline), injections of the protein (first vertical line) and CNC (second vertical line). In addition, the surfaces were washed with buffer after each injection. The amount of bound masses were estimated from the frequency change by Sauerbrey equation

$$\Delta m = -\frac{C\Delta f}{n}$$ (Eq S2)

where *C* is a constant 17.7 ngHz^{-1}cm^{-2} arising from the properties of the quartz crystal, Δf is the frequency change and *n* is the overtone of the oscillations.

Injecting of HFBI over a PS surface is known to lead to formation of a monomolecular layer of hydrophobin on the surface. This can be seen for the initial parts of the QCM sensograms for both HFBI and the HFBI-DCBD fusion proteins. Mass of bound HFBI was 200 ng/cm^2 and the HFBI-DCBD bound to a level of 650 ng/cm^2. The bound amounts correspond to mean molecular area of ~ 6.3 nm^2 for HFBI and ~ 4.7 nm^2 for HFBI-DCBD. After protein injection and rinsing, a solution of CNC was injected. The Sauerbrey mass of bound CNC on the HFBI layer was 900 ng/cm^2 and the mass bound to HFBI-DCBD was approximately 3.0 µg/cm^2. Sauerbrey equation is only valid for thin, rigid films, assuming negligible dampening

of the oscillations. The measured dissipation (ΔD) values for CNC binding, however, were significant (12 and 30 $\times$ 10^{-6} to HFBI and HFBI-DCBD respectively) and thus their calculated masses are most likely underestimated. The larger the ΔD value, the larger the underestimation is. Nonetheless we can use the Sauerbrey masses as estimations and draw the conclusion that the monolayer of HFBI-DCBD fusion protein has a much higher capability of binding cellulose than wild-type HFBI.
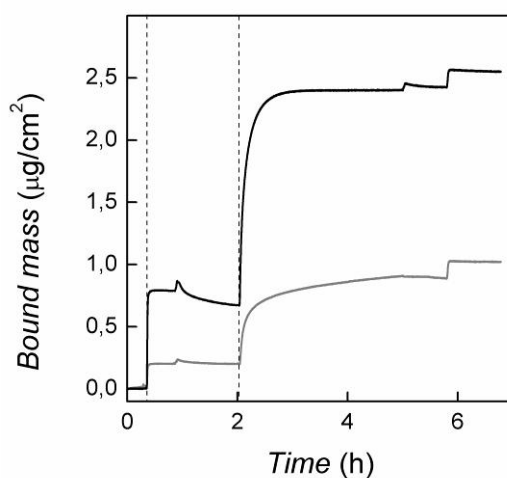

Figure S3. A QCM sensogram of consecutive binding of HFBI (grey line) and HFBI-DCBD (black line) to PS surface and CNC to the resulting protein layers. Injection times of protein and CNC solutions are marked with vertical lines to the image.

Interfacial Shear Rheology

Interfacial shear rheology was measured using TA Instruments AR–G2 controlled stress rheometer equipped with a Du Noüy –ring geometry. The experiments were made on air/water interface at 20 °C. The interfacial films of 0.54 μM HFBI-DCBD with and without nanocellulose were aged in the measuring cup for 20 h. For 1.3 μM

HFBI and HFBI-DCBD the interfacial films were not aged before the measurement, instead the evolution of the interfacial film was measured. Rotational and oscillatory mappings were done before each measurement. The ring was carefully placed onto the interface, immersed into the sample and then brought back onto the interface by automatic control of the geometry height. Three different measurement types were performed for the aged interfacial films: A time dependent experiment at constant frequency (0.1 Hz) and strain (0.01 %), a frequency dependent experiment at constant strain (0.01%) and a strain dependent experiment at constant frequency (0.1 Hz). The frequency dependent experiment was done after the time dependent measurement for the same interfacial film, since the films remained stable. The strain in the above experiments was set to 0.2 % to ensure that the experiments were done in the linear viscoelastic regime. The strain value was selected from a strain dependent experiment where strain was varied from 0.001 to 10 % at a constant 0.1 Hz frequency.

Viscoelastic shear moduli resulting from the adsorption of HFBI and HFBI-DCBD as a function of time are shown in Figure S4. In the case of HFBI–DCBD the G' value after tree hours is almost an order of magnitude lower compared to HFBI. The HFBI–DCBD film forms slower than the film of HFBI in consistency with the observations done by ellipsometry. The G' of HFBI-DCBD starts to increase 75 minutes after starting the measurement , whereas G' of HFBI starts to evolve after ~ 20 minutes.
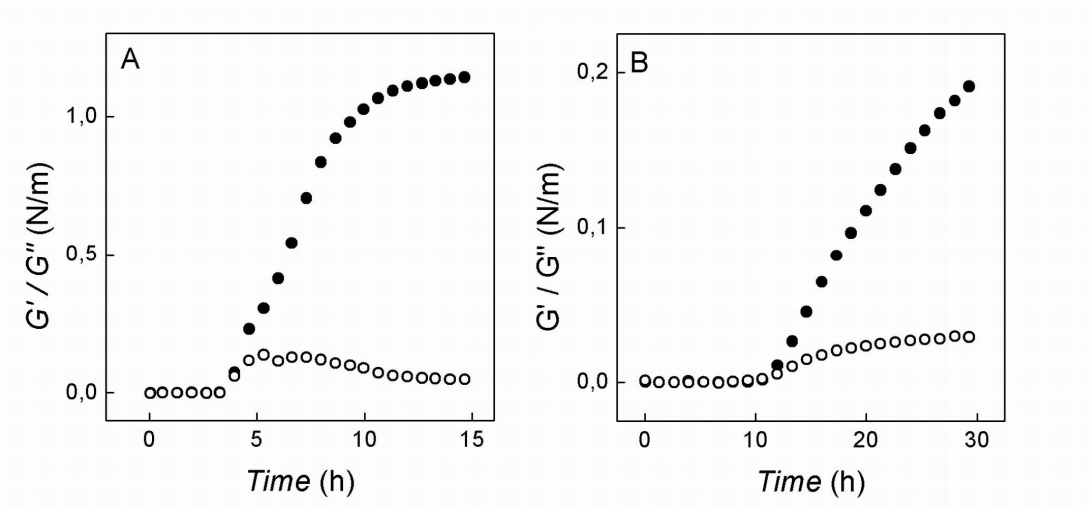
Figure S4. Surface shear moduli of 1.3 µM HFBI (A) and HFBI–DCBD (B) as a function of time. Elastic modulus G' is plotted as the closed circles and viscous modulus G'' as the open circles. Measurements were carried out using constant 0.2 % strain and 0.1 Hz frequency.

Time dependent changes in aged films of 0.54 µM HFBI-DCBD and its mixture with 0.025 mg/ml NFC were studied by exposing them to constant strain and frequency (Figure S5). Addition of NFC to the interface increased the G' values slightly, but the most prominent change was in the increased deviation between parallel experiments done on the NFC containing films. The studied ratio of HFBI-DCBD to NFC represents a situation where ~ 50 % of HFBI-DCBD is associated with NFC; the free HFBI-DCBD concentration being roughly 12 µM and the amount of bound HFBI-DCBD being approximately 5 µmol/g (not fully saturated).
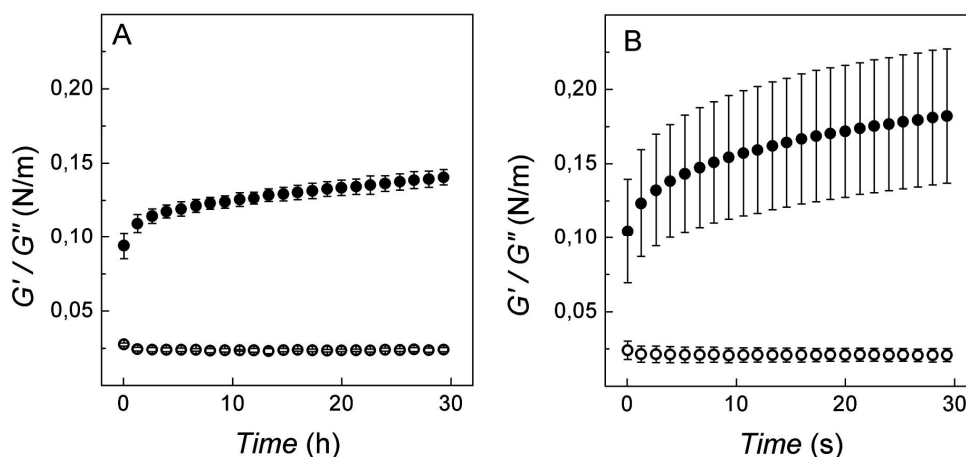
Figure S5. Surface shear moduli of 0.54 µM HFBI-DCBD (A) and 0.54 µM HFBI-DCBD with 0.025 g/l NFC light fraction (B) as a function of time. Elastic modulus G' is plotted as the closed circles and viscous modulus G'' as the open circles. Error bars are calculated from the standard deviation of 3-5 measurements. Measurements were carried out using constant 0.2 % strain and 0.1 Hz frequency.

In the frequency dependent measurement one can note that the G' value of both film types increased monotonically over the investigated frequency range and interfacial shear viscosity |η*| of both samples decreased (Figure S6). Logarithm of the interfacial viscosity is inversely proportional to the frequency on logarithmic scale and indicates shear thinning behavior. Both interfacial shear viscosity and viscoelastic moduli had a power law dependency on frequency (eg. $G' \propto \omega^{n'}$). Power law constants N, n' and n'' extracted from the slopes of viscosity, G' and G'' on log-log scale are summarized in table S1.

9

Table S1. Power law constants for HFBI-DCBD and HFBI-DCBD/NFC films.

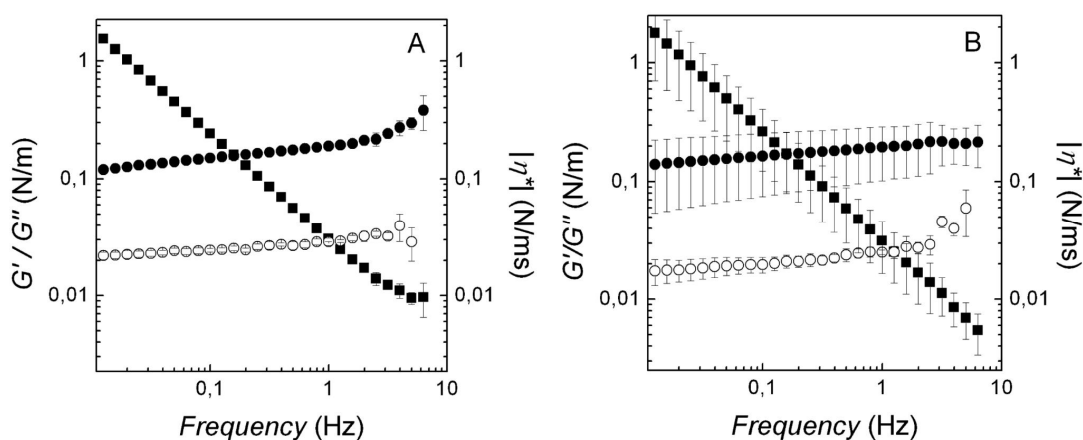|	HFBI-DCBD	HFBI-DCBD + NFC
N (viscosity)	-0.86	-0.92
n'	0.12	0.12
n''	0.07	0.07

Fig S6. Surface shear moduli and interfacial shear viscosity of 0.54 µM HFBI-DCBD (A) and 0.54 µM HFBI-DCBD with 0.025 mg/ml NFC light fraction (B) as a function of frequency. Elastic modulus G' is plotted as the closed circles, viscous modulus G'' as the open circles and interfacial viscosity as squares. Error bars are calculated from the standard deviation of 3-5 measurements. Measurements were carried out using constant 0.2 % strain. The power law constant of the shear viscosity was -0.86 for HFBI-DCBD and -0.92 for the combination.

In the strain dependent measurements one can see the collapse of the viscoelastic moduli at strain 0.25 % (Figure S7). Absolute values of G' is again higher for the

NFC containing film, but more or less similar effect of increasing strain indicates that NFC does not otherwise affect on the interfacial properties of the protein film.
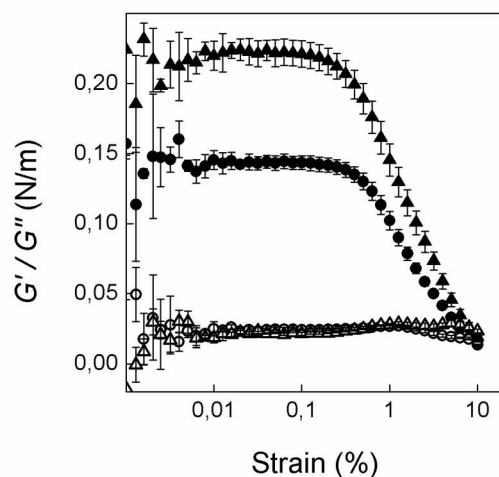

Fig S7. Surface shear moduli of 0.54 µM HFBI–DCBD (circles) and its combination with 0.025 g/l NFC (triangles) as a function of % strain. Elastic modulus G' is plotted as the closed symbols and viscous modulus G'' as the open symbols. Error bars are calculated from the standard deviation of 3-5 measurements. Measurements were carried out using a constant 0.1 Hz frequency.

Emulsification Experiments

Emulsions stabilized with NFC were imaged with optical microscopy. The oil/water interface is clearly visible in bright field images as circular lines (Figure S8A). For verification that an oil-in-water type emulsions were indeed formed, the oil phase was stained with a lipophilic dye (Nile Red) and the emulsion was imaged with a confocal microscopy. In Figure S8B it clearly seen that the droplets were colored and the continuous phase remained unstained. Emulsions stabilized with combinations of

NFC, CNC and HFBI-DCBD were imaged similarly and are presented in Figures S9 and S10. The structure of all emulsions appear more or less similar, but the droplet size in emulsions including HFBI-DCBD was much smaller, only hundreds of nanometers (Figure S9). In Figures S9A, S10A and S10C cellulose has been stained with Calcofluor.
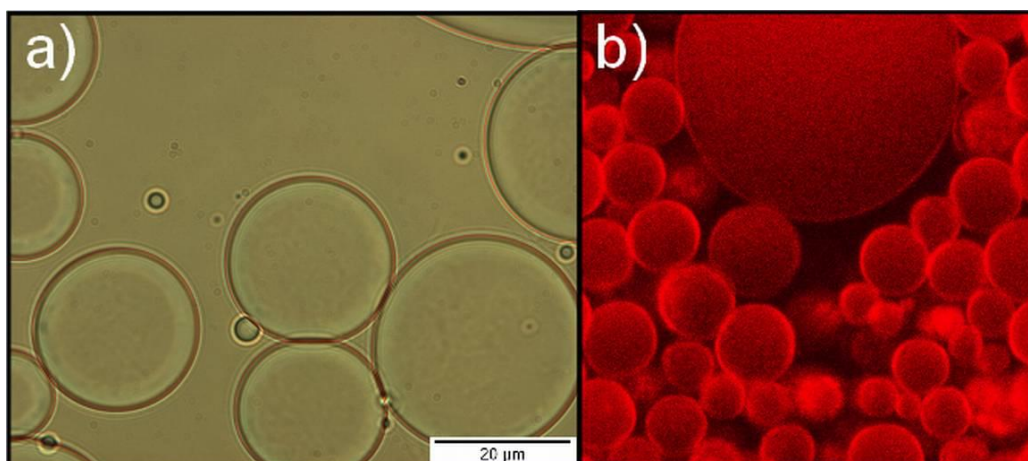
Figure S8. Emulsions stabilized with NFC. A) A bright field microscopy image of emulsion droplets. B) A confocal microscopy image where the oil phase has been stained with Nile Red. Image size is 26×26 μm.
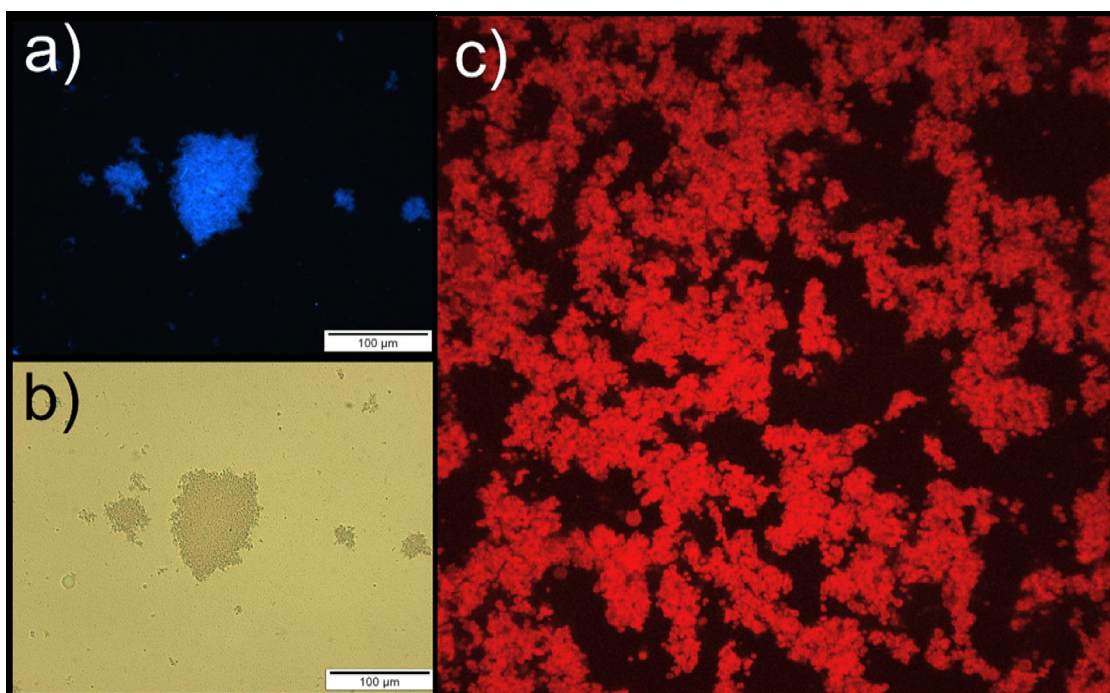
Figure S9. Emulsios stabilized with NFC and HFBI-DCBD. An epifluorescence (A) and a bright field (B) image of emulsion containing nanodroplets associated into larger agglomerates. C) A confocal microscopy image of an emulsion where oil phase has been stained with Nile Red. Image size is 128×228 μm.
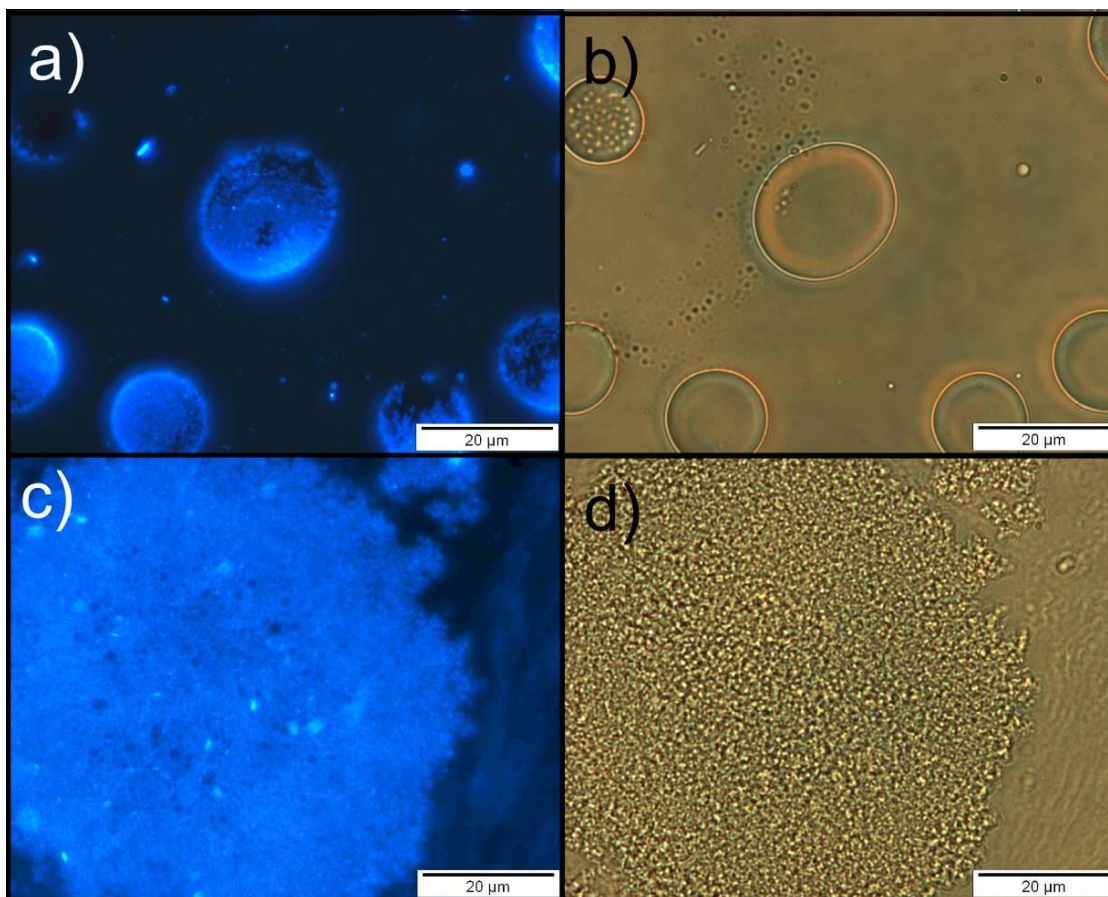
Figure S10. Emulsions stabilized by cellulose nanowhiskers. An epifluorescence (A) and bright field image (B) of an emulsion stabilized by CNC. An epifluorescence (C) and bright field image (D) of an emulsion stabilized by CNC and HFBI-DCBD. Cellulose was stained with Calcofluor.

Stability of emulsions containing only HFBI-DCBD, cellulose nanowhiskers or both in water-hexadecane mixtures was also studied. Emulsion stability indices for these systems are presented in Figure S11. Since hydrophobins are amphiphilic and assemble at oil/water interface, they are also able to stabilize emulsions. In Figure S11A, it is clearly seen that stability of emulsions is increased as the concentration of HFBI-DCBD is increased and reaches a limiting value of about 80 vol-% at concentration 1.5 mg/ml. When cellulose nanowhiskers are added to the system containing 1 mg/ml HFBI-DCBD, a significant decrease in emulsion stability is

observed (Figure S11B). However, compared to emulsions stabilized with only CNC, the combination with protein shows better emulsification ability, by increasing the final volume from about 30 % to 50 %.
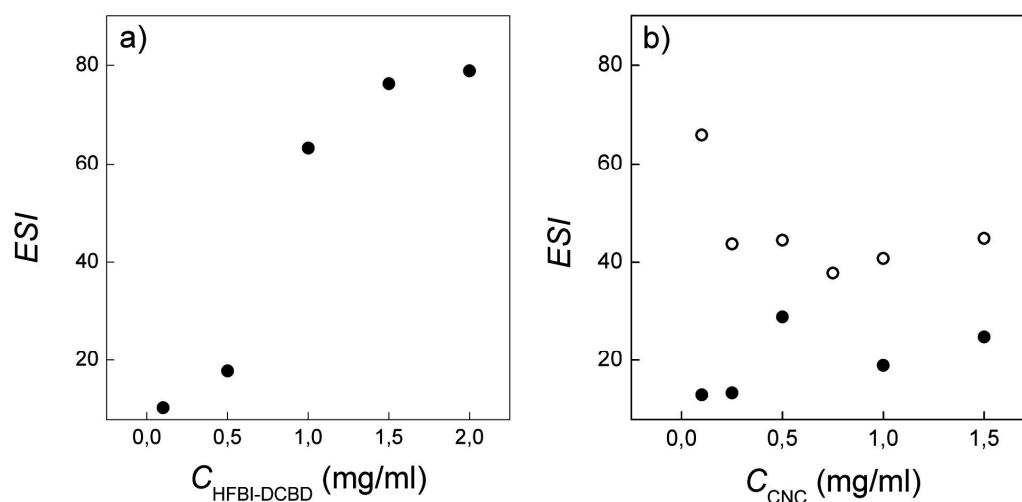

Figure S11. ESI of emulsions stabilized by varying amount of HFBI-DCBD (A), cellulose nanowhiskers (B, black dots) and 1 mg/ml HFBI-DCBD and varying amount of cellulose nanowhiskers (B, open dots).

Binding of Drug Nanoparticles to NFC

For cellulose binding studies, the particles were either prepared with HFBI or HFBI-DCBD coatings. When the nanoparticles were mixed with cellulose, the particles spontaneously attached to the cellulose nanofibrils (Figure S12). This happened with both HFBI and HFBI-DCBD coatings. The lifetime of the particles increased dramatically, and no degradation was observed within 4 weeks. Even though the particles slowly sediment to the bottom of the vial during storage when bound to NFC, they can be readily redispersed with no apparent degradation. The particles are not removed even with mechanical activation, e.g. when subjected to concentration, drying and redispersion in water.
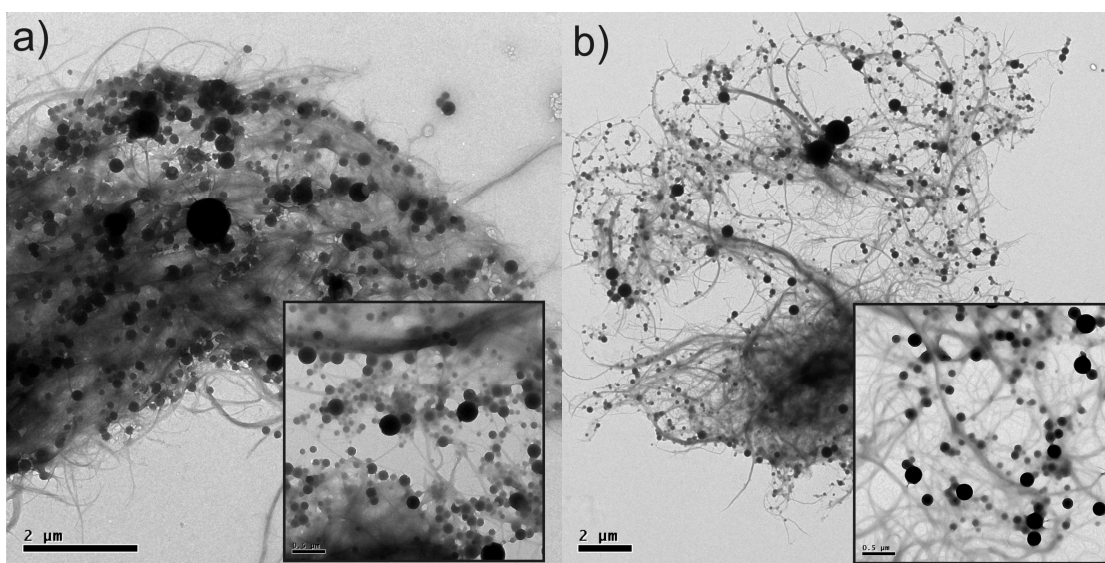
Figure S12. TEM images of a) ITR-HFBI-NFC samples and b) ITR-HFBI-DCBD-NFC samples. Insets show close-ups of the particles.

References

i Tompkins, H. G., & Irene, E. A. (Eds.), Handbook of ellipsometry (2005) Heidelberg, Springer.

ii de Feijter, J. A., Benjamins, J., & Veer, F. A. Ellipsometry as a Tool to Study the Adsorption Behavior of Synthetic and Biopolymers at the Air-Water Interface, Biopolymers (1978) 17, 1759.

iii Ball, V., & Ramsden, J. J. Buffer Dependence of Refractive Index Increments of Protein Solutions. Biopolymers (1998) 46 (7) 489.

iv Azzam, R. M., & Bashara, N. M. Ellipsometry and Polarized Light (1977) Amsterdam: North-Holland.

Publication II

Immobilization−Stabilization of Proteins on Nanofibrillated Cellulose Derivatives and Their Bioactive Film Formation. Suvi Arola, Tekla Tammelin, Harri Setälä, Antti Tullila and Markus B. Linder. *Biomacromolecues,* 2012, 13 (3), pp. 594–603. DOI: 10.1021/bm201676q

Immobilization−Stabilization of Proteins on Nanofibrillated Cellulose Derivatives and Their Bioactive Film Formation

Suvi Arola,*,[†,‡] Tekla Tammelin,[§] Harri Setälä,[§] Antti Tullila,[†] and Markus B. Linder[†]

[†]VTT, Technical Research Centre of Finland, Bio and Process Technology, Tietotie 2, P.O. Box 1000, FIN-02044 VTT, Finland
[§]VTT, Technical Research Centre of Finland, Energy and Pulp and Paper, Biologinkuja 7, P.O. Box 1000, FIN-02044 VTT, Finland
[‡]Department of Applied Physics, Aalto University School of Science and Technology, P.O. Box 15100, FI-00076 Aalto, Finland

Ⓢ *Supporting Information*

ABSTRACT: In a number of different applications for enzymes and specific binding proteins a key technology is the immobilization of these proteins to different types of supports. In this work we describe a concept for protein immobilization that is based on nanofibrillated cellulose (NFC). NFC is a form of cellulose where fibers have been disintegrated into fibrils that are only a few nanometers in diameter and have a very large aspect ratio. Proteins were conjugated through three different strategies using amine, epoxy, and carboxylic acid functionalized NFC. The conjugation chemistries were chosen according to the reactive groups on the NFC derivatives; epoxy amination, heterobifunctional modification of amino groups, and EDC/s-NHS activation of carboxylic acid groups. The conjugation reactions were performed in solution and immobilization was performed by spin coating the protein−NCF conjugates. The structure of NFC was shown to be advantageous for both protein performance and stability. The use of NFC allows all covalent chemistry to be performed in solution, while the immobilization is achieved by a simple spin coating or spreading of the protein−NFC conjugates on a support. This allows more scalable methods and better control of conditions compared to the traditional methods that depend on surface reactions.
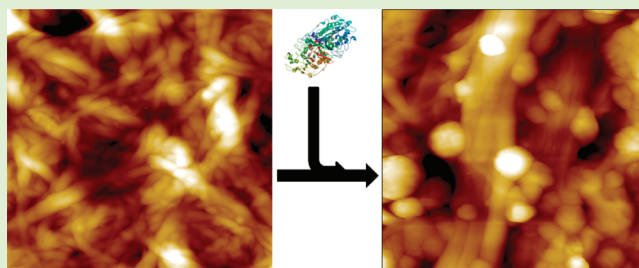
INTRODUCTION

The immobilization of proteins and other biomolecules is an essential technique in several biotechnical applications.[1−4] For the use of enzymes to catalyze industrial processes, immobilization enables enzyme reuse, continuous processes, and can markedly increase their stability. Diagnostic applications also rely largely on immobilization of antigens or antibodies using a number of different formats from microtiter plates to different types of strips. There is a continuous need to improve and diversify technologies for immobilization for the development of new formats, better economy, and performance.[2,4] Several techniques have been developed for protein immobilization. These can broadly be grouped in the following categories based on mechanisms: (i) physical interactions or adsorption, (ii) chemical covalent bonds, or (iii) high affinity interactions between biological molecules.[4] For industrial enzymes the most preferred method for immobilization is the use of covalent coupling. For this, great efforts have been made to produce feasible protocols that yield reproducible results and stabile enzymes.[3,5] It has been found that the environment around and on the solid support as well as the chemistry used in the immobilization have a great impact on the stability and performance of the enzymes.[2] In most cases, the molecules to be immobilized are covalently coupled directly onto the solid supports. With this approach it is often found that the efficiency of immobilization is restricted by the surface chemistry of the

immobilization platform.[5,6] Also, the fact that the immobilization often occurs randomly in respect to protein orientation is one of the drawbacks of these systems. Proteins tend to unfold when they are assembled on surfaces, which leads to loss of activity.[4] Another drawback is that procedures for direct covalent linking on surfaces can be problematic to scale for large areas.

Cellulose has been studied as a carrier material for protein immobilization previously mostly because of the possibility to use specific cellulose-binding proteins that bind and therefore immobilize spontaneously to cellulose materials.[7] In other cases, different types of regenerated celluloses have been used as a carriers.[8] In this work, we take advantage of recent developments in cellulose technology to design new techniques for surface immobilization of biomolecules. Cellulose is a homopolymer formed by repeating units of D-glucose linked together by β-(1−4) glycosidic bonds. In natural cellulose materials, such as wood, the polymer chains are packed together to form elemental fibrils with a cross-section of 3−5 nm. These elemental fibrils are usually considered to be the lowest level of hierarchy in cellulose assembly.[9] In the wood structure, these elemental fibrils are packed further to form

microfibrils that range in size from 15–20 nm which further aggregate in to larger fibril bundles and finally to wood fibers.[10,11] It has been shown that cellulose pulp can be disintegrated to the nanosized microfibrils with mechanical and biological methods and in this context the term nanofibrillated cellulose (NFC) has also been adopted.[12,13] The very long aspect ratio and the high stiffness of the fibrils are important for giving NFC its properties. The surface of the fibrils are dominated by hydroxyl groups that make the surface hydrophilic, but also result in hydrogen bonding interactions between adjacent fibrils. These properties lead to gel formation in aqueous suspensions that are strongly stabilized by these network interactions. Already, at 2% dry weight, such suspensions have a very high viscosity, leading to applications of NFC as rheology modifiers and in the dried form as aerogels.[14–17] The gel-like behavior also makes NFC difficult to handle at high concentrations. Other applications that take advantage of the properties of NFC are in nanocomposite materials as reinforcing elements and as templates for functional nanostructures.[14,18–20] NFC also has an ability to form strong thin films that have nanoporous structures and good adhesion to underlying structures.[14,21–23] The film forming capabilities also depend on strong fibril networks that are formed by the characteristic properties of high aspect ratio, stiffness of the fibrils and interacting hydroxyl groups.[21] NFC thin films are readily made, for example, by spin coating from aqueous media and have been used as model films to study native cellulose I behavior at surfaces.[21,24] It has also been shown that NFC films can be used as paper coatings to reinforce paper and increase the barrier properties such as air permeability.[25,26]

Due to the high amount of reactive hydroxyl groups on the fibril surface, NFC has an ability to absorb more water than other cellulose model films.[21] The hydroxyl groups on the surface of the fibrils also provide possibilities for chemical modifications of the NFC. One very efficient way of modifying surface hydroxyl groups is through oxidation using TEMPO (2,2,6,6-tetramethylpiperidine-1-oxyl), resulting in the formation of carboxyl groups on the fibril surface.[27,28] The reaction also leads to a more easy disintegration, giving very thin fibrils with a diameter of 3–5 nm[27,28] but which also have altered properties due to their high negative charge on the surface.

The possibility to covalently modify and the efficient film forming properties of NFC inspired us to investigate how NFC would function as a support for protein immobilization. The advantage of this approach is that the conjugation reactions could be performed in solution compared to the conventional methods that use surface chemistry, making the reactions more reproducible and scalable. After the conjugation reaction, the protein immobilization to the solid support could be achieved by different spreading techniques such as spin coating. The ability of cellulose to take up water is also pronounced in NFC, which is likely to be advantageous for immobilized proteins.[3]

In this work, we investigated the effect of different conjugation strategies and, for that, three different NFC derivatives were made: epoxy functionalized, amine functionalized, and carboxylic acid functionalized NFC. The three different NFC derivatives demanded different conjugation strategies. As model proteins, we used alkaline phosphatase (AP) and anti-hydrocortisone antibody. The two proteins used in this study were chosen for their specific bioactivities but also because of the difference in their substrate size. AP gives a colored reaction with a soluble substrate that has a small size

compared to proteins. Anti-hydrocortisone antibody on the other hand is more relevant in its bioactivity to recognize hydrocortisone.
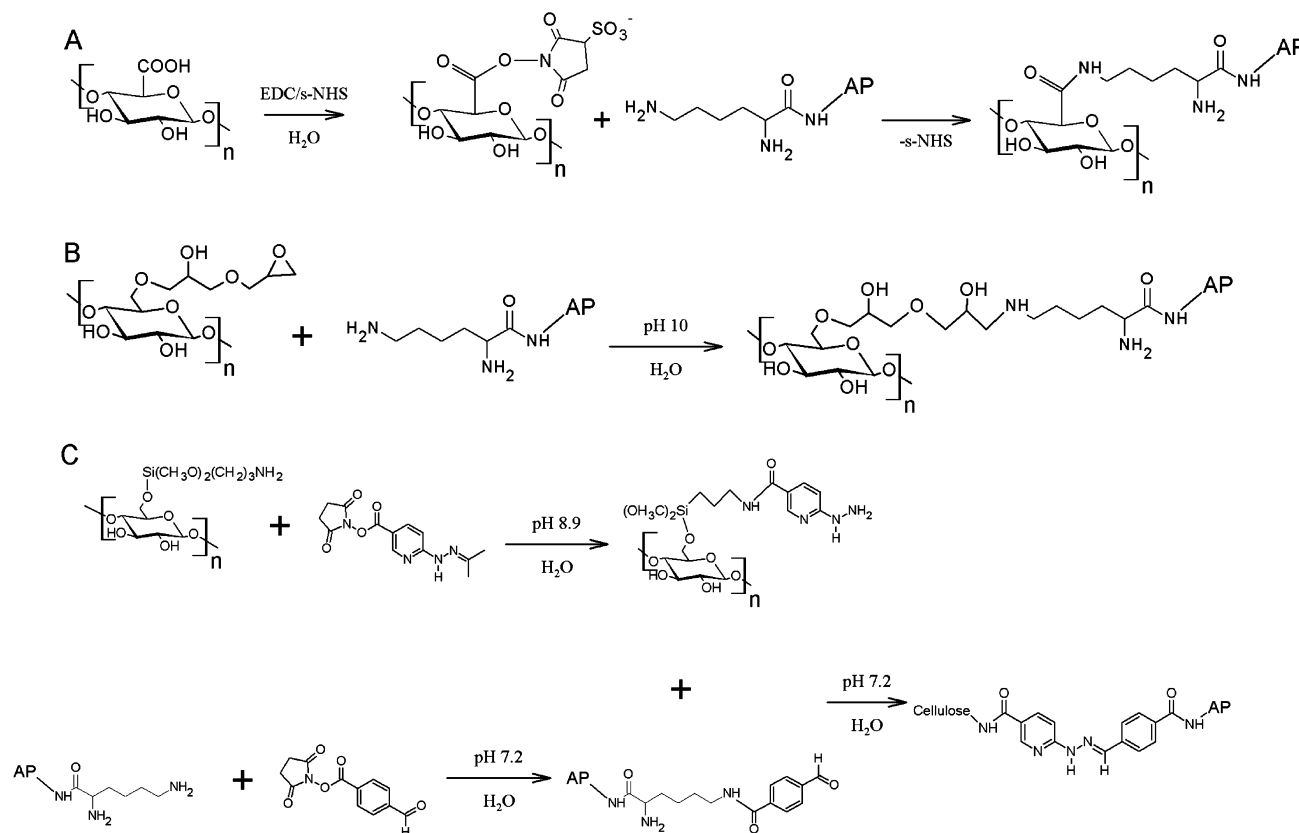
◼ EXPERIMENTAL SECTION

Materials and Methods. *Preparation of Epoxy Functionalized Nanofibrillated Cellulose (epoxy-NFC).* The first step for the epoxy functionalization of cellulose was through an allylation step. Briefly, 250 mL of butyl glycidyl ether and 100 mL of allyl glycidyl ether were added to 500 g of never-dried bleached birch kraft pulp fibers (29.1%) in 90% aqueous *t*-butanol (1.5 L) in alkaline conditions (114 mL, 10 M NaOH + 600 mL water) at 60 °C overnight. Sulfuric acid was then added until the pH was 7. The fibers were washed with ethanol and water by filtration and then ground using a Masuko refiner (Masuko Sangyo, Japan). The obtained microfibrillated cellulose (MFC, dry matter content 2–3%) was then repeatedly centrifuged and washed by resuspending with acetone. After this solvent exchange step, the dry matter content was 6.0% and water content 2–5%. Next, allyl glycidyl ether (3 mol/L mol anhydroglucose unit (AGU)) was added to 165 g of the solvent-exchanged MFC and allowed to react at 65 °C overnight. Fibers were filtered and washed with ethanol and water. The degree of substitution was determined by ¹³C cross-polarized magic angle spinning nuclear magnetic resonance (CP/MAS NMR) spectroscopy[29] and also by a method published by Heinze et al.,[30] where allyl groups were brominated and the bromine content was determined.

The epoxy functionalization of allylated MFC was performed using the procedure published by Huijbrechts and et al.[31] Allylated MFC (dry matter content 4.7%) was reacted in sodium carbonate/bicarbonate buffer solution with acetonitrile and 30% hydrogen peroxide overnight at 30 °C. The cellulose was separated by filtration, and washed with water and ethanol to yield epoxy-MFC. The epoxy content of epoxy-MFC was analyzed using the slightly modified method published by Huijbrechts et al.[31] Freeze-dried epoxy-MFC fibers were suspended in water and reacted with 4,4′-diaminodiphenyl-methane in ethanol overnight at 30 °C. The product was isolated by centrifugation, and washed with ethanol and water. The DS value for epoxy groups was calculated from the amount of nitrogen analyzed by the Kjeldahl method (Vario MAX CHN, Maxitech Corporation, Pakistan). Epoxy-MFC was then fluidized to nanofibrillated cellulose (NFC) with a pressure of 1600 bar and 15 passes (M110EH, Microfluidics, MA, U.S.A.) to yield epoxy-NFC (dry matter content 1.6%).

Preparation of Amine-Functionalized Nanofibrillated Cellulose (amine-NFC). Never-dried bleached birch kraft pulp was fluidized (dry matter content ~2%) with a pressure of 1600 bar with eight passes as described above to give NFC. The solvent for NFC was exchanged via acetone to dimethyl acetamide (DMA) by five centrifugation and redispersing steps for each solvent. Amine functionalization was conducted via silylation reactions using a protocol originally tailored for dissolved cellulose.[32–34] First, 0.75 g of solvent-exchanged NFC was suspended into 100 mL of DMA. Nitrogen was bubbled into the suspension for 1 h after which it was heated to 80 °C. Then, 15 mL of 3-aminopropyl trimethoxysilane was added and the reaction was allowed to proceed overnight at 80 °C. The product was washed by centrifugation and redispersed with methanol. Finally, the solvent for amine-NFC was exchanged to water by centrifuging and redispersing five times. The degree of amine functionalization was calculated from the surface silicon and surface nitrogen content analyzed by x-ray photoelectron spectroscopy (XPS), as described in Johansson et al.[35,36] The dry matter content of the resulting amine-NFC was 1.6%.

Preparation of 2,2,6,6,-Tetramethylpiperidine-1-oxyl Oxidized Nanofibrillated Cellulose (TEMPO-NFC). NFC functionalized with carboxylic acid groups (TEMPO-NFC) was prepared as described by Saito et al.[28] Shortly, never-dried, bleached birch pulp at 1 g L⁻¹ concentration was subjected to 2,2,6,6-tetramethylpiperidine-1-oxyl (TEMPO)-catalyzed oxidization (0.3 weight ratio of TEMPO to pulp) for 4 h at room temperature. The product was purified from residual reaction chemicals by centrifugation and redispersing with deionized

Scheme 1. Reaction Schemes of Alkaline Phosphatase Conjugation to Different NFC Derivatives[a]

[a](A) Reaction of lysine residues on AP surface with epoxy groups on epoxy-NFC through a ring-opening reaction. (B) Carboxylic acid groups on TEMPO−NFC were first activated using EDC and s-NHS. The activated carboxylic acid groups react with lysine groups on AP forming stable peptide bonds. (C) Amino groups on amine-NFC were modified with SANH to yield hydrazine/hydrazide reactive species (SANH−NFC). Lysine groups on AP were reacted with SFB to yield an aldehyde modified AP (SFB−AP). The aldehyde on SFB−AP and the hydrazine/hydrazide on SANH−NFC reacted forming a stable hydrazone bond.

water. The centrifugation and washing step was repeated twice. The resulting TEMPO-NFC was then fluidized twice using 1300 and 1900 bar pressure, respectively, with a fluidizer (Microfluidics M110EH). The DS value for TEMPO-NFC (dry matter content 0.9%) was determined by conductometric titration of carboxylic acid groups.

Conjugation of AP to Epoxy−NFC. The reaction was performed through epoxy amination in alkaline conditions where the amino groups of lysine amino acids on the enzyme alkaline phosphatase (AP; Sigma, P5931-500U) react with the epoxy group of epoxy-NFC in a ring-opening reaction (Scheme 1A).[37] A total of 200 μg of AP (final concentration 7.9 μM) was reacted with 600 μg of epoxy-NFC (final concentration 1.13 g L^{-1}) in 0.1 M NaHCO$_3$/Na$_2$CO$_3$ pH 10 buffer for 24 h at 22 °C. Negative controls for the conjugation were made by first blocking the epoxy groups with excess of diethanolamine (DEA, final concentration of 1 M) and then reacting them with AP. The effect of 0.5 μL of catalyst triethylamine was tested for the epoxy amination reaction.

Conjugation of AP to TEMPO−NFC. AP was coupled to TEMPO-NFC through a peptide bond forming reaction (Scheme 1B).[37] A minor amount of aldehyde groups are present on TEMPO-NFC and may react through a different reaction mechanism than that of carboxylic acids.[38] A 1:2.5 molar ratio mixture of 1-ethyl-3-[3-dimethylaminopropyl]carbodiimide hydrochloride (EDC, Pierce 22980, final concentration 2.5 mM) and N-hydroxysulfosuccinimide (s-NHS, Pierce 24510, final concentration 5 mM) was reacted with 53.2 μg of TEMPO-NFC (final concentration 0.133 g L^{-1}) in aqueous solution, pH ∼ 5, for 15 min at 22 °C. Activated TEMPO-NFC (final concentration 0.1 g L^{-1}) and AP (final concentration of 7.9 μM) were then conjugated by mixing in 25 mM borate buffer pH 8 for 3 h at 22

°C. A negative control was made by leaving out EDC and s-NHS and performing reactions otherwise, as described above.

Conjugation of AP to Amine−NFC. The conjugation of AP to amine-NFC was performed by a three-step reaction procedure (Scheme 1C).[39] First, 2 mL of 1.5 g L^{-1} amine-NFC in 25 mM borate buffer pH 8.9 was reacted with 10 μL of 20 g L^{-1} succinimidyl-4-hydrazinonicotinate acetone hydrazone (SANH, Thermo Scientific 22400) dissolved in dimethylsulfoxide (DMSO) for 3 h at 22 °C to yield a hydrazine/hydrazide reactive species on the amine-NFC (later referred to as SANH-NFC). The SANH-NFC was washed with Milli-Q water using a concentration tube (Amicon Ultra 10K 4 mL, Millipore). The benzaldehyde reactive AP (later referred to as SFB−AP) was made by mixing 250 μL of 3.2 g L^{-1} AP in phosphate buffer saline (PBS) pH 7.2 and 5 μL of 20 g L^{-1} succinimidyl-4-formylbenzoate (SFB, Thermo Scientific 2249) in DMSO for 3 h at 22 °C. The SFB−AP was washed with Milli-Q water as above (Amicon Ultra 10K 0.5 mL, Millipore). In the final step of the conjugation reaction, SFB−AP (0.14 g L^{-1}) and SANH-NFC (1.13 g L^{-1}) were allowed to react in PBS pH 7.2 overnight at 22 °C. Residual amine reactive groups were quenched by adding 1 M Tris buffer saline (TBS) pH 7.2 to a final concentration of 0.1 M and incubating for 65 h at +4 °C. Control samples were made using unmodified AP and amine-NFC in the final step.

Matrix-assisted laser desorption/ionization−time-of-flight mass spectrometry (MALDI−TOF MS, Bruker autoflex II MALDI−TOF) was used to study the extent of SFB modification of AP as described in Supporting Information (S1).

Preparation of Bioactive Films from AP−NFC Conjugates. AP−NFC films were prepared by spin coating a 50 μL aliquot of the different conjugates onto a silicon surfaces (Okmetic Oy, Vantaa,

Finland, 1 cm² pieces). Prior to use, the silica surfaces were washed three times with ethanol and Milli-Q water, dried in nitrogen flow, and spin coated with 50 μL of 1 g L^{-1} polyethyleneimine (PEI, Sigma-Aldrich) in water using an Autolab spin coater (Autolab, The Netherlands). PEI was used as an anchoring polymer to ensure sufficient adherence of NFC to the silica surface.[21] The procedure of spin coating the AP–NFC conjugates was repeated 1–11 times. After immobilization of AP–NFC films, the surfaces were washed (3 × 2 mL) for 3–4 h with buffer (0.1 M TRIS 50 mM MgSO$_4$ 0.2 M NaCl buffer pH 8.8) to remove noncovalently bound AP.

Determining Enzymatic Activity of AP–NFC Bioactive Films. The enzymatic activity of AP–NFC films was measured using a small chromogenic substrate 4-nitrophenyl phosphate sodium hexahydrate (p-NPP). A total of 500 μL of enzyme reaction buffer (0.1 M TRIS 50 mM MgSO$_4$ pH 8.8) and 500 μL of freshly prepared solution of p-NPP (2 g L^{-1}) in diethanolamine MgCl$_2$ buffer (Reagena Oy Ltd., Finland) was incubated with NFC film samples that had been spin coated on silicon surfaces. Absorbance at 405 nm of the enzyme reaction solution at a specific time points were measured with a spectrophotometer (Varioscan, Thermo Electron Corporation), and the amount of AP was calculated using a standard curve determined for nonconjugated AP in solution.

Long-Term Stability of AP on Different AP–NFC Films. To study if the conjugation of AP to the different NFC derivatives affected the stability of AP, the enzymatic activity of a series of samples incubated at elevated temperatures were studied. Silicon surfaces having two spin coated layers of all three different AP–NFC conjugates were kept in enzyme reaction buffer at either room temperature or +37 °C. The enzymatic activity of the films was measured at time points of 16, 24, 48, and 168 h. Solutions of AP (0.43 μM) in enzyme reaction buffer were used as controls and they were stored in the same conditions and enzyme reaction were performed similarly as to immobilized AP.

Conjugation of Hydrocortisone to AP. Hydrocortisone 3-oxime (Sigma-Aldrich, H6635) was conjugated to AP using EDC and s-NHS (Thermo Scientific, 22980 and 24510, respectively) as above. The formed hydrocortisone–AP conjugate was purified from unreacted hydrocortisone 3-oxime, EDC, and s-NHS using desalting column. Protein concentrations were measured using BCA Protein Assay Kit (Pierce, 23225). MALDI-TOF MS was applied to determine the extent of chemical conjugation degree of the haptens to the carrier protein as described previously for SFB–AP (Supporting Information, S1).

Production and Purification of Anti-Hydrocortisone Antibody. An anti-hydrocortisone Fab-fragment antibody (anti-hydrocortisone antibody) that had been selected from immunized mouse antibody phage display library against the hydrocortisone–AP conjugate was used.[40,41] The hydrocortisone specific antibody fragment clone, anti-hydrocortisone, was cloned into pKKtac expression vector containing His$_6$ tag for Fab-protein purification.[42] Protein production of anti-hydrocortisone Fab fragment was performed in *Escherichia coli* bacteria strain RV308 (ATCC 31608) and purified by metal affinity chromatography[43] followed by dialysis into PBS.

Conjugation of Anti-Hydrocortisone Antibody to TEMPO-NFC and Its Immobilization onto Solid Support. The antibody conjugation and immobilization was performed as described for AP above. Briefly, 200 μL of 0.133 g L^{-1} EDC/s-NHS activated TEMPO–NFC and 100 μg of anti-hydrocortisone antibody were reacted in PBS buffer pH 7.2 for 4 h at 22 °C. Bioactive films were spin coated as described above for AP–NFC conjugates. Silicon surfaces having one or two layers of antibody–NFC conjugate were prepared. One or two layers of only TEMPO–NFC were also spin coated as negative controls. The conjugation of antibody to TEMPO–NFC was studied by how much antigen was bound to the surfaces. The antigen, that is, hydrocortisone, had been conjugated to AP to facilitate its detection. The antibody-NFC surfaces were incubated with 100 μL of hydrocortisone–AP conjugate (10 mg L^{-1}) in PBS buffer pH 7.2 for 2 h at 22 °C and washed with of PBS buffer pH 7.2 overnight at +4 °C to remove any nonspecifically bound hydrocortisone–AP conjugate. The activity of AP bound to antibody-NFC surfaces was detected as previously described for immobilized AP.

Atomic Force Microscopy (AFM) Imaging. AFM was used to analyze the morphology of the NFC derivatives before and after AP conjugation and immobilization. AFM was also used to characterize the structural features of the different NFC derivatives. A NanoScope IIIa Multimode AFM instrument (E-scanner and J-scanner, Digital Instruments/Veeco) was used with an NSCI5/AlBS cantilever (μMASCH, U.S.A.). All images were recorded in tapping mode in air with scan rates of 0.8–1 Hz (free amplitude was about 0.65 V). The damping ratio was around 0.7–0.85. Images were flattened to remove possible tilts in the image data. Otherwise, no further processing of the images was done.
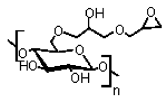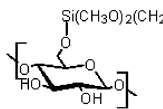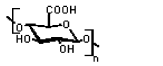
Quartz Crystal Microbalance with Dissipation (QCM-D). QCM-D (E4 instrument, Q-Sense AB, Sweden) was used to determine nonspecific adsorption of proteins to unmodified NFC surfaces and PEI surfaces. With QCM-D, the changes in frequency (Δf) and dissipation (ΔD), that is, changes in mass and viscoelastic properties on the sensor surface, are followed simultaneously as a function of time at the fundamental resonance frequency (5 MHz) and its overtones. The interpretation of QCM-D data has been discussed in detail elsewhere.[44,45] Quartz crystals coated with silica (QSX 303, mass sensitivity constant C = 0.177 mg m^{-2} Hz^{-1}) were used. Prior to use, the sensor crystals were washed for 30 min at room temperature in 2% SDS solution, rinsed with Milli-Q water, and dried in a nitrogen flow. The NFC layers were spin coated with NFC prepared as described previously.[19] The proteins studied were AP, bovine serum albumin (BSA), SFB–AP and hydrocortisone–AP conjugates. Spin-coated crystals were stabilized in the QCM-D chambers for 24 h against PBS buffer pH 7.2 before the measurements were started. The nonspecific protein binding of all the four proteins were tested on both PEI and NFC.

■ RESULTS

Estimation of the Degree of Substitution for Epoxy-Functionalized NFC. The functionalization of NFC was characterized by ^{13}C CP/MAS NMR and the Kjeldahl method. The first allylation step lead to the removal of approximately 40% of hemicelluloses and a 0.01 degree of substitution (DS) for modification by butyl and allyl functionalities, as determined by ^{13}C CP/MAS NMR (see Supporting Information, Figure S2). The final degree of substitution after second allylation step was estimated by integrating the combined area of both peaks from allyl groups and the area of the anomeric C1 carbon in cellulose (see Supporting Information, Figure S2). Because the NMR results are semiquantitative, they were verified for the final product using bromination of double bonds, as described by Heinze et al.[30] The results of both methods agreed well and gave the DS values for allyl groups after two allylation steps of 0.055 by NMR and 0.066 by bromination. The subsequent functionalization of allyl groups to epoxy groups was followed by the Kjeldahl method. For this measurement epoxy groups were first aminated. According to this method the amount of epoxy groups was 0.64 mmol g^{-1} cellulose and corresponds to a degree of substitution for epoxy groups 0.061 (Table 1). The results show that the allyl groups were converted to epoxy groups almost quantitatively.

Estimation of the Degree of Substitution for Amine-Functionalized NFC. XPS was used for the determination of the DS[35,36] for silylated amine modified NFC. XPS spectra and data are shown in Supporting Information, Figure S3 and Table S3. The degree of amination on the fibril surface was calculated from the nitrogen and silicon content. The surface content of nitrogen was 1.7% and the surface content of silicon was 1.5%, corresponding to surface substitution values of 0.21 for the nitrogen marker and 0.19 for the silica marker (Table 1). The degree of substitution was calculated to be 1.24 mmol of functional groups per gram of cellulose.

Table 1. Different Functionalizations of NFC, the DS Values Obtained for the Different Derivatives and the Degree of Derivatization in Relation to the Total Amount of Cellulose

Functionalized NFC	Degree of substitution (maximum DS)	Degree of derivatization (mmol g^{-1} cellulose)
Epoxy functionalized NFC	DS_{epoxy} 0.061 ($DS_{max} = 3$)[a] DS_{allyl} 0.066 ($DS_{max} = 3$)[b] DS_{allyl} 0.055 ($DS_{max} = 3$)[c]	0.64[g]
Amine functionalized NFC $Si(CH_3O)_2(CH_2)_3NH_2$	DS_{Si} ~0.2 ($DS_{max} = 3$)[d] DS_N ~0.2 ($DS_{max} = 3$)[e]	1.24[h]
TEMPO oxidized NFC	Surface charge ~0.9 meq g^{-1} pulp, corresponds to 57% efficiency in oxidation of C–6 hydroxyls of wood cellulose crystal[f]	0.9[i]

[a]Degree of substitution for epoxy groups per anhydroglucose units (AGUs) calculated from results of Kjeldahl method. [b]DS for allyl groups per AGU determined by ^{13}C/CP MAS NMR. [c]DS for allyl groups per AGU analyzed by bromination of double bonds. [d]DS per AGU analyzed from XPS silica marker.[35,36] [e]DS per AGU analyzed from XPS nitrogen marker.[35,36] [f]Degree of surface charge and oxidation efficiency determined by conductometric titration of carboxylic acid groups, the theoretical maximum for wood cellulose crystal is 1.5 meq g^{-1}, which corresponds to every second glucose unit on the surface of cellulose crystal carrying a carboxylic acid group.[27] TEMPO oxidation is selective to primary alcohols (cellulose C6 position), and thus, there is only 1 reactive unit per 2 AGUs available on the crystal surface. [g]Result from Kjeldahl method. [h]Result estimated from XPS data. [i]Result from conductometric titration of carboxylic acid groups.

Estimation of the DS for TEMPO-oxidized NFC. The amount of carboxylic acid groups on TEMPO-oxidized pulp was determined by conductometric titration. For the sufficient fibrillation, the content of the carboxylic acid groups has to be higher than 0.7 meq g^{-1} of pulp, and the theoretical maximum of wood cellulose crystal is ~1.5 meq g^{-1}.[27] The content of the carboxylic acid groups of the TEMPO-oxidized pulp was over 0.9 meq g^{-1} of pulp (Table 1). The result corresponds to about 57% efficiency of oxidization of available C-6 hydroxyl groups on the surface of crystalline cellulose.[28]

Structural Analysis of Functionalized Fibrils by AFM. The morphology and fine structure of the spin-coated films of functionalized NFC were studied by AFM (Figure 1A, C, and F). The AFM images show that there are clear morphological differences between the different NFC types. Especially pronounced was the very fine structure of TEMPO–NFC, which is seen only in the small 1 × 1 μm image (Figure 1E, inset) compared to the more coarse amine–NFC and epoxy–NFC. The TEMPO–NFC fibers were more homogeneous in size and have fibrils of approximately 4 nm in diameter. Both amine–NFC and epoxy–NFC were more coarse and had larger variation in fibril heights (diameters) ranging from ~10 to 100 nm. However, the amine–NFC seemed to form a more densely packed and tighter film with more fiber–fiber interactions than epoxy–NFC. From AFM analysis we can conclude that all the NFC films were fully covering and porous.
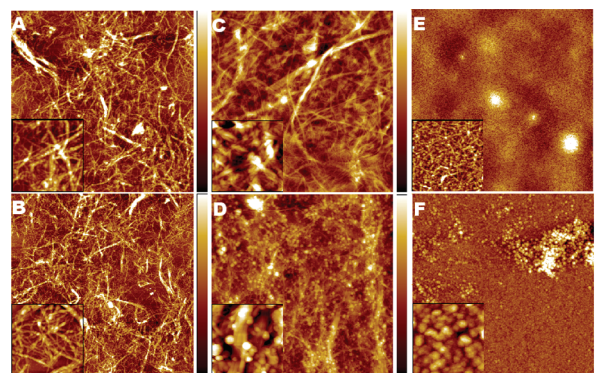

Figure 1. AFM topography images (10 × 10 μm) of surfaces made from negative controls without AP and from AP–NFC conjugates. Inserts are 1 × 1 μm magnifications of the images: (A) Epoxy–NFC control (maximum height 40 nm, insert maximum height 20 nm); (B) AP–epoxy–NFC conjugate (maximum height 40 nm, insert maximum height 25 nm); (C) Amine–NFC control (maximum height 200 nm, insert maximum height 50 nm); (D) AP–amine–NFC conjugate (maximum height 400 nm, insert maximum height 100 nm); (E) TEMPO–NFC control (maximum height 8 nm insert maximum height of 8 nm; (F) AP–TEMPO–NFC conjugate (maximum height of 100 nm, insert maximum height 50 nm).

Characterization of SFB–AP. Primary amines on the surface of AP were activated using SFB (see Scheme 1). The reaction between SFB and AP was confirmed by MALDI–TOF MS (Figure S1). Peak masses of AP ($m/z = 47202.5$) and SFB–AP ($m/z = 48693.1$) showed that on average 11.3 formylbenzoate ($M = 132.109$ Da) moieties were introduced per AP molecule. AP contains 29 Lys residues on its surface and, therefore, the efficiency of Lys modification was ~39%. Additionally a $m/z = 97273.1$ peak was detected, corresponding to a covalently cross-linked dimer of SFB–AP. Larger oligomers of SFB–AP were not seen and would likely be difficult to detect with MALDI–TOF. The concentration of SFB–AP was 1.13 g L^{-1}.

Characterization of AP Conjugated to NFC by the Different Routes. The three different (TEMPO, epoxy, and amine) AP–NFC conjugates were characterized by first spin coating the AP–NFC suspensions on silica surfaces. Negative controls prepared with NFC as described above were also made. Surfaces were assayed for enzymatic activity using the *p*-NPP substrate. The amount of immobilized AP was calculated from its activity compered to nonconjugated AP. The yield of conjugation reaction for AP was less than 1% because a large excess of AP was used in the reactions and reaction conditions were not optimized for this parameter.

The volume and amount of AP–NFC conjugate that was applied by spin coating was restricted by practical considerations. Too large volumes of NFC tended to give uneven surfaces, as did too high concentrations of NFC. In practice, the useful maximum concentration was for TEMPO 0.1 mg L^{-1} and for both epoxy– and amine–NFC 1.13 mg L^{-1}. The volume for all was 50 μL.

The spin coating procedure was repeated up to 11 times. Samples having different numbers of layers were then compared to each other. In Figure 2, the total amount of protein bound to the silicon surface after each successive coating layer is shown. The amount of protein added during each successive layer per mass of NFC is shown in Figure 3. For each of the different NFC derivatives there was an increase in
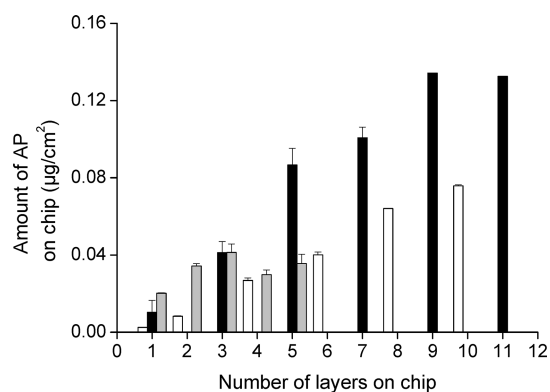
Figure 2. Enzymatic activity of spin-coated AP−NFC films showing the effect of spin coating multiple layers. The amount of AP increased for each successive spin-coated layer. The white bars represent epoxy−NFC, black bars represent TEMPO−NFC, and gray bars represent amine−NFC.
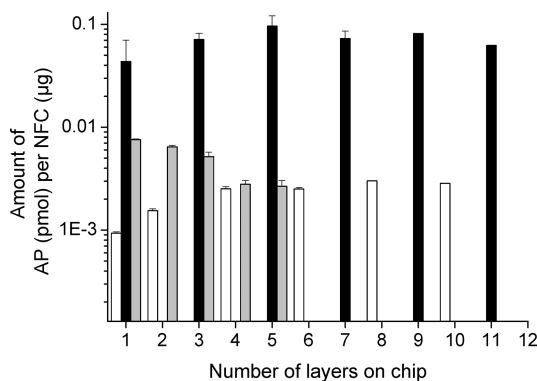

Figure 3. Immobilization density of AP (pmol) on each NFC derivative (μg). The values are calculated by determining the total activity of AP after each successive layer and dividing by the total NFC amount. White bars represent epoxy−NFC, black bars represent TEMPO−NFC, and gray bars represent amine−NFC.

activity for each successive layer. All three NFC derivatives showed good adhesion to underlying layers and to the PEI primed silicon surface. For each successive step, the limiting factor for the amount of NFC added was the practical limits set by the spin coating process. For the first three layers, the amine−NFC performed very well and allowed the largest amount of AP to be immobilized. Addition of more layers of amine−NFC after the first three ones did not increase activity. The TEMPO−NFC showed a linear increase in activity for each layer up to 11 layers. The epoxy−NFC showed less immobilized AP than the TEMPO, but unlike the amine−NFC, it showed a linear increase up to 10 subsequent layers. By comparing different samples, it could be concluded that the catalyst triethylamine, had no significant impact on the amount of conjugated AP for the epoxy−NFC.

TEMPO−NFC contained significantly higher amounts of reactive groups compared to the two other NFC derivatives (Table 1). The effect of higher degree of substitution is seen in over 10× higher capacity of bound protein (Figure 3, note logarithmic scale) per weight of cellulose. The higher surface to bulk ratio of TEMPO−NFC allowed a higher degree of AP conjugation, but the finely divided structure allowed application of only a much smaller amount of material in the spin coating. Therefore the total amount of protein that was possible to

apply on the surface (Figure 2) was not as much higher as could have been expected based on the capacity (Figure 3).

Characterization by AFM (Figure 1) showed some additional differences between the different conjugates. Especially the TEMPO−NFC differed most markedly from the others by its distinct fine structure (Figure 1E). A difference between the different NFC derivatives is also that objects with a size corresponding to small clusters of protein molecules can be seen in the amine−NFC and TEMPO−NFC but not in the epoxy−NFC. This may be due to the difference in the chemistry used for the conjugation as discussed below.

The negative controls were analyzed for the possibility that noncovalently bound protein may be either physically entrapped in the NFC matrix or noncovalently coupled to the NFC by, for example, charge−charge interactions. In all the control surfaces, the AP activity was below the detection limits after washing the surfaces similarly as for the other samples. We noted, however, that if the surfaces were not properly washed (less than 1 h in buffered solution), a slight AP activity could be measured. It was also noted that the enzyme responsible for the activity was desorbing from the surfaces during activity measurements.

Long-Term Stability and Activity of AP−NFC Conjugates. The effect of the conjugation on the stability of AP with the different functionalized NFC was studied. Spin-coated films were stored in buffer at elevated temperatures and their activities monitored. Initial experiments showed that free AP in solution was stable at +4 °C for several months, but at 21 and 37 °C, the activity decreased rapidly. The activity decreased by 90% after 16 h at 21 °C and over 95% after 16 h in +37 °C. After 24 h at these temperatures, almost no activity could be detected. In contrast, all conjugated AP−NFC combinations showed a marked increase in stability. After 168 h at 21 °C, all three conjugates showed no decrease in AP activity compared to the initial AP activity on the films measured immediately after spin coating and washings. After 168 h at 37 °C, the AP TEMPO−NFC, AP amine−NFC, and AP epoxy−NFC conjugates showed 27, 18, and 26% of their original activity, respectively.

Conjugation of hydrocortisone to AP, and anti−hydrocortisone antibody purification. MALDI−TOF MS data showed that hydrocortisone−AP conjugates had the conjugation degree of 6−10 hydrocortisones per 1 AP monomer. After purifications, the concentration of the final hydrocortisone−AP conjugate was 1.36 g L^{-1} in PBS. The anti−hydrocortisone antibody concentration after metal affinity chromatography purification was 3 g L^{-1} in PBS.

Antibody Conjugation to TEMPO−NFC and Its Immunological Detection. Based on the efficiency of conjugating and immobilizing AP, TEMPO−NFC was chosen for further studies for immobilizing antibodies to surfaces. Anti-hydrocortisone antibody was conjugated to TEMPO−NFC and spin-coated with one and two layers on a silicon surface. Hydrocortisone conjugated to AP was used as the antigen for analyzing the functionality of the anti-hydrocortisone antibody conjugated to TEMPO−NFC. The use of this AP conjugate gave the advantage that bound hydrocortisone could be detected directly by the AP + p-NPP reaction. In a negative control, the anti-hydrocortisone antibody was left out. The results of the functional analysis are shown in Figure 4. The bound hydrocortisone−AP conjugate was estimated to be 11 ng on both one and two layered surfaces based on the enzymatic activity of AP (Figure 4). The negative control
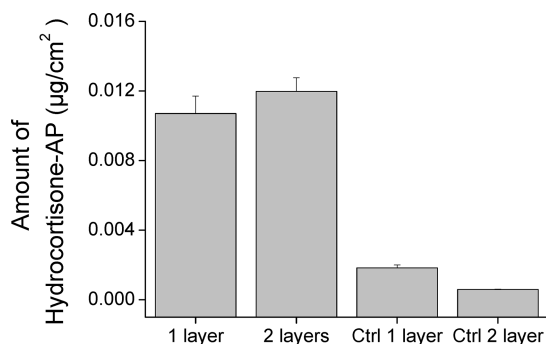
Figure 4. Immobilization of anti-hydrocortisone antibody onto a surface by TEMPO-oxidized NFC and its detection with hydro-cortisone−AP conjugate. The amount of hydrocortisone−AP conjugate per surface area on both one- and two-layered silicon surfaces is very similar.

without anti-hydrocortisone antibody showed between 24 (two layers) and 6 (one layer) times lower activity compared to the samples containing all components. The higher background for the sample with one coating may be due to some residue exposure of the underlying PEI surface.

Nonspecific Binding of Proteins to NFC and PEI Surfaces, a QCM-D Study. The nonspecific adsorption of proteins, in our case, BSA, AP, SFB−AP, and hydrocortisone−AP, to unmodified NFC and PEI surfaces was studied using QCM-D. Results presented in Table 2 showed very low

Table 2. Amounts of BSA, AP, Hydrocortisone−AP, and SFB−AP Bound nonspecifically to PEI and NFC Surfaces in PBS pH 7.2[a]

protein	$\Delta f/\Delta D$ on PEI	$\Delta f/\Delta D$ on NFC	ng/cm^2 PEI/NFC[b]
BSA	−1.3/0.15	−0.6/0.04	23.0/10.6
AP	−2.16/0.05	−1.1/-0.04	32.2/19.5
hydrocortisone−AP	−0.33/-0.01	0/0.01	5.84/0
SFB−AP	−0.9/0.06	−0.45/0.04	15.9/7.97

[a]f_0 = 5 Hz, n = 3, f_3/n, time 2−3 h, C = 0.177 mg m^{-2} Hz^{-1}. [b]Values calculated by Sauerbrey equation $\Delta m = -(C\Delta f/n)$.[44]

adsorption of all the proteins on NFC and also on PEI. The negative change in frequency, which indicates the positive mass change detected on the sensor surface, was less than 2.2 Hz for all protein samples during the contact time of 2−3 h time, indicating no significant adsorption. This very low adsorption of proteins to cellulose surface show that NFC itself has a low background effect in assays where proteins are immobilized for example on solid surfaces.

■ DISCUSSION

We show here that nanocellulose provides an efficient strategy for immobilizing proteins on surfaces. The properties of NFC allow an approach that is different from typical immobilization protocols[5,7,8] because the covalent linkage of the protein can be performed in solution using suspended NFC and the immobilization itself relies on the physical interactions of NFC that lead to film formation on surfaces. The physical interactions of NFC are based on the noncovalent networks that the long cellulose fibrils form when spread on surfaces and their interactions through hydrogen bonding.

The protein−NFC films had a nanoporous structure that had an influence on how molecules of different sizes can interact with the immobilized proteins. The chemistry of how NFC was functionalized had a significant impact on how the protein was immobilized and how the bioactive films were formed, but the immobilized protein itself did not significantly alter the film-forming capability of NFC. The way NFC formed films and coatings depended significantly on its size distribution, that is, processing history. Also, the three alternative ways of introducing functional groups on the NFC surface all lead to a different characteristic of the resulting NFC−protein conjugates. The amount of reactive groups, fibril dimensions (specific surface area), and conjugation chemistry used for linking enzymes to NFC derivatives all have an impact on the degree of conjugation.

The degree of functionalization for the different NFC derivatives was determined according to the most suitable method for each functional group. Although the methods differed from one another, we can compare the amount of functional groups on the different NFC derivatives as follows. In the case of epoxy−NFC, the degree of functionalization of 0.06 corresponds to 6% of modified anhydroglucose units (AGUs). In the case of amine−NFC, the DS of 0.2 corresponds to 20% of modified AGUs. In the case of TEMPO−NFC, the reaction is regioselective to primary alcohols (in cellulose C6 hydroxyls) and the reaction acts only on the fibril surface. Thus, the degree of functionalization only considers surface C6 hydroxyls. The degree of surface functionalization of ∼0.9 meq g^{-1} pulp corresponds to roughly 57% of modified primary alcohols on cellulose crystal.[27] In our case, therefore, the TEMPO−NFC was the most highly substituted and epoxy−NFC was the least.

The procedures of conjugating protein to both TEMPO−NFC and amine-functionalized NFC involve several reaction steps, while the conjugation to epoxy-functionalized NFC proceeded in a single step (Scheme 1). The reaction times for conjugation to amine- and TEMPO-functionalized NFC was much faster than the conjugation to epoxy-functionalized NFC. The epoxy route also gave the lowest density of immobilized AP. From literature, it is previously known that the reactions to epoxy-activated supports are very slow, leading for example to attempts to increase reaction rates by salt-induced aggregation.[6] The efficiency of epoxy immobilization in this work was comparable to previously published results .[46]

Comparing the AFM images of the protein−NFC films (Figure 1), we note that the surfaces with proteins conjugated to amine- and TEMPO-functionalized NFC show globular aggregates of molecules with the diameter of about 70 nm. Such aggregates are not seen in the epoxy-functionalized NFC. Because the sizes of the aggregates are larger than is expected for the natural dimeric form of AP (5−6 nm), it is likely that these aggregates are small clusters of AP enzyme. In both strategies for immobilizing to amine and TEMPO-functional-ized NFC, the side reactions can lead to the formation of chemically cross-linked AP enzyme. When immobilizing to amino groups, the intermediate step of making SFB−AP leads to the modification of about 40% of the lysine residues in AP. As the formed formylbenzoate group is reactive toward amino groups, the cross-linking of individual SFB−AP molecules to larger oligomers is possible and at least the dimer form of AP was confirmed by MALDI−TOF (see Figure S1). This cross-linking is likely to lead a mechanism where the immobilized units are oligomeric clusters instead of monomers of AP to

SANH−NFC. Similarly, in the case of TEMPO−NFC, a carboxyl acid activating reagent EDC/s-NHS mixture was used. Excess activator was not removed prior to addition of AP because of the poor stability of the activated carboxylic acid group in aqueous solution. As AP was added to the activation mixture it is possible that some excess of activator reacted with surface exposed aspartic and glutamic acid residues on AP (see Figure S6) and, thus, resulting in cross-linking of AP protein molecules to larger clusters. Such clusters of AP or individual AP molecules could not be identified in epoxy−NFC films. The clustering is not expected in the epoxy−NFC case due to the nature of the chemistry used for conjugation. Individual AP molecules would probably be hard to identify in the fibril network due to their small size and much lower modification density compared to amine- and TEMPO-functionalized NFC.

The formation of such small clusters would explain the globular aggregates seen in the AFM images and could also partly explain the increased efficiency of immobilization to amine and TEMPO functionalized NFC, since for every functional group a cluster of AP could bind instead of individual molecules as in the epoxy functionalized case. The cross−linking of enzymes together can also aid the stabilization and preservation of enzyme activity. Both conjugation methods on TEMPO− and amine−NFC combine two features that are thought to be very effective in protein immobilization and enzyme stability preservation; the multipoint covalent immobilization of protein[5] and carrier-bound cross-linked enzymatic aggregation.[2] In our case, the multipoint covalent attachment occurs both between individual enzyme molecules and between the enzyme and the solid support (in our case, NFC), resulting in a system where the protein is simultaneously covalently bound to the carrier as well as cross-linked to small clusters. However, increased stability of AP was also seen for the epoxy−NFC, which shows that the NFC structure is a generally biocompatible environment for proteins. It is likely that the hydrophilic nature of cellulose and its rigid structure are reasons for this. It was also shown that the NFC films have very low nonspecific binding which is a clear advantage over many polymer matrixes and other functional surfaces used for immobilization.[47] The low protein binding to NFC may also be a contributing factor for the biocompatibility of the NFC. Another clear effect of the protein conjugation to NFC was the observed increase in stability. Increase in stability has been described to occur for several enzymes and has been attributed to intramolecular cross-linking.[2] In this work, we did not investigate mechanism of the increase of stability in a systematic way. However, we observe that in accordance with published work, multipoint cross-linking[5] can result in increased stability and that this conclusion is in accordance with the other results of this work. Previously has also been shown that the cross-linking chemistry and the microenvironment of the carrier has an effect on the inactivation and stabilization of enzymes.[3] It has been shown that for better stability covalent immobilization is a more advantageous immobilization method over adsorption and that hydrophilic carriers are more advantageous that hydrophobic ones. These results are in line with our findings of increased stability with protein conjugation to NFC.

When applying layers of AP−NFC by spin coating an increase in enzymatic activity was seen for each successive layer. As a general trend, the measured activity of AP with p-NPP as the substrate increased with successive layers, suggesting that the layers had a porous structure that allowed the transport of the small substrate through the network and that underlying layers contributed to the total activity (Figures 2 and 3). However, clear differences between the different types of NFC were observed. Initially the NFC with AP coupled to amine−NFC showed a greater amount of AP activity, but after about four layers the efficiency declined (Figure 3). The reason for this is likely to be that a densely packed film was formed which did not allow the penetration of even the small p-NPP molecule deeper into the structure of the film. Therefore the response was seen only from the topmost layers. The tighter packing of amine functionalized NFC fibrils in the film can be seen in the AFM images (Figure 1). On the other hand, the epoxy−NFC and TEMPO−NFC showed a linear and continuous increase in the amount of immobilized protein, suggesting a more porous or loosely packed film. TEMPO−NFC has a large aspect ratio, is very even in size distribution, and contains a large number of carboxyl groups on its surface. The finer structure of the TEMPO−NFC is also clear from the AFM images (Figure 1), thus, making the film forming and swelling properties very good. The apparently less dense film structure of epoxy−NFC compared to amine−NFC may be that the chemical modification of epoxy−NFC lead to a greater reduction of hemicelluloses (alkaline treatment) as well as to an introduction of hydrophobic groups on the fibrils and, therefore, to a poorer or more coarse film structure compared to amine−NFC.[48]

The experiments using immobilized antibodies did not show a significant increase in binding of antigens with additional deposited layers of antibody−NFC conjugate. The density of immobilization detected for the first layer (11 ng on antibody conjugated TEMPO−NFC) corresponded to the density achieved using the direct immobilization of AP. Because additional layers did not increase the response, we conclude that large proteins (such as AP) do not diffuse through the TEMPO−NFC film structure. An AP monomer is a globular protein with a diameter of approximately 5−6 nm in its active dimer form. This shows that, although the NFC conjugation and immobilization is versatile in functioning for different types of targets, the porosity[21] of the NFC layer and the structure of the analytes have a dependency that affects the overall performance of the system and should be taken into account in the design. Thus, the TEPMO−NFC immobilization can be advantageous in systems where a large density is achieved due to the porosity of the surface layer and its availability for small molecules. The exclusion of macromolecules can be beneficial when targeting small molecules, but may be a limitation in applications where macromolecules are targeted.

CONCLUSIONS

In this work we have shown that NFC derivatives can be used as matrixes for conjugation and stabilization of enzymes and proteins and that bioactive films immobilizing the proteins on surfaces are readily formed by these protein−NFC conjugates. Typically it is technically challenging to perform chemical reactions on surfaces or on surface-immobilized polymers because of slow kinetics and difficulties to mix reagents efficiently, leading to slow reactions and low yields. Scale-up and process design is also problematic for large solid surfaces. We therefore propose that the procedure described here, to first perform chemical reactions in solution and then spread the mixture on the target surface, will provide a technically more feasible procedure. The conjugation reactions can be performed under well-controlled mild aqueous conditions, mixing, and temperature, while spreading of the mixture for immobilization

could be readily automated by various printing or coating technologies. The work is also a demonstration that cellulose in its highly fibrillated NFC form shows highly desirable properties that lead to new methods in technology.

■ ASSOCIATED CONTENT

Ⓢ Supporting Information

(Figure S1) MALDI–TOF MS sample preparation for SFB–AP with MALDI–TOF MS spectra of AP and SFB–AP (Figure S1 and S2); description of allylation of MFC prior to epoxidation and the ^{13}C CP/MAS NMR spectra of allylated MFC (Figure S2 and S3); descriptions of the determination of functionalization degree of amine–NFC accompanied by XPS spectra (Figure S3); and elemental concentrations (Table S3) of NFC and amine–NFC. This material is available free of charge via the Internet at http://pubs.acs.org.

■ AUTHOR INFORMATION

Corresponding Author

*Tel.: +358 40 180 3812. Fax: +385 02 722 7071. E-mail: ext-suvi.arola@vtt.fi.

Notes

The authors declare no competing financial interest.

■ ACKNOWLEDGMENTS

■ REFERENCES

(1) Stephanopoulos, N.; Francis, M. B. *Nat. Chem. Biol.* **2011**, *7*, 876–884.

(2) Cao, L. *Curr. Opin. Chem. Biol.* **2005**, *9*, 217–226.

(3) Hwang, S.; Lee, K.-T.; Park, J.-W.; Min, B.-R.; Haam, S.; Ahn, I.-S.; Jung, J.-K. *Biochem. Eng. J.* **2004**, *17*, 85–90.

(4) Rusmini, F.; Zhong, Z.; Feijen, J. *Biomacromolecules* **2007**, *8*, 1775–1789.

(5) Mateo, C.; Grazu, V.; Palomo, J. M.; Lopez-Gallego, F.; Fernandez-Lafuente, R.; Guisan, J. M. *Nat. Protoc.* **2007**, *2*, 1022–1033.

(6) Wheatley, J. B.; Schmidt, D. E. Jr *J. Chromatogr., A* **1993**, *644*, 11–16.

(7) Ong, E.; Gilkes, N. R.; Warren, R. A. J.; Miller, R. C.; Kilburn, D. G. *Nat. Biotechnol.* **1989**, *7*, 604–607.

(8) Kumar, S.; Nahar, P. *Talanta* **2007**, *71*, 1438–1440.

(9) Klemm, D.; Heublein, B.; Fink, H.-P.; Bohn, A. *Angew. Chem., Int. Ed.* **2005**, *44*, 3358–3393.

(10) Fengel, D.; Wegener, G. *Wood: Chemistry, Ultrastructure, Reactions*; Walter de Gruyter: Berlin, NY, 1984; pp 6–25.

(11) Klemm, D.; Kramer, F.; Moritz, S.; Lindström, T.; Ankerfors, M.; Gray, D.; Dorris, A. *Angew. Chem., Int. Ed.* **2011**, *50*, 5438–5466.

(12) Nakagaito, A. N.; Yano, H. *Appl. Phys. A: Mater. Sci. Process.* **2005**, *80*, 155–159.

(13) Pääkkö, M.; Ankerfors, M.; Kosonen, H.; Nykänen, A.; Ahola, S.; Österberg, M.; Ruokolainen, J.; Laine, J.; Larsson, P. T.; Ikkala, O.; Lindström, T. *Biomacromolecules* **2007**, *8*, 1934–1941.

(14) Paakko, M.; Vapaavuori, J.; Silvennoinen, R.; Kosonen, H.; Ankerfors, M.; Lindstrom, T.; Berglund, L. A.; Ikkala, O. *Soft Matter* **2008**, *4*, 2492–2499.

(15) Zugenmaier, P. *Prog. Polym. Sci.* **2001**, *26*, 1341–1417.

(16) Herrick, F. W.; Casebier, R. L.; Hamilton, J. K.; Sandberg, K. R. *J. Appl. Polym. Sci.: Appl. Polym. Symp.* **1983**, *37*, 797–813.

(17) Turbak, A. F.; Snyder, F. W.; Sandberg, K. R. *J. Appl. Polym. Sci.: Appl. Polym. Symp.* **1983**, *37*, 815–827.

(18) Olsson, R. T.; Azizi Samir, M. A. S.; Salazar Alvarez, G.; Belova, L.; Strom, V.; Berglund, L. A.; Ikkala, O.; Nogues, J.; Gedde, U. W. *Nat. Nanotechnol.* **2010**, *5*, 584–588.

(19) Varjonen, S.; Laaksonen, P.; Paananen, A.; Valo, H.; Hahl, H.; Laaksonen, T.; Linder, M. B. *Soft Matter* **2011**, *7*, 2402–2411.

(20) Eichhorn, S.; Dufresne, A.; Aranguren, M.; Marcovich, N.; Capadona, J.; Rowan, S.; Weder, C.; Thielemans, W.; Roman, M.; Renneckar, S.; Gindl, W.; Veigel, S.; Keckes, J.; Yano, H.; Abe, K.; Nogi, M.; Nakagaito, A.; Mangalam, A.; Simonsen, J.; Benight, A.; Bismarck, A.; Berglund, L.; Peijs, T. *J. Mater. Sci.* **2010**, *45*, 1–33.

(21) Ahola, S.; Salmi, J.; Johansson, L. S.; Laine, J.; Österberg, M. *Biomacromolecules* **2008**, *9*, 1273–1282.

(22) Wagberg, L.; Decher, G.; Norgren, M.; Lindstrom, T.; Ankerfors, M.; Axnas, K. *Langmuir* **2008**, *24*, 784–795.

(23) Henriksson, M.; Berglund, L. A.; Isaksson, P.; Lindström, T.; Nishino, T. *Biomacromolecules* **2008**, *9*, 1579–1585.

(24) Ahola, S.; Turon, X.; O'sterberg, M.; Laine, J.; Rojas, O. J. *Langmuir* **2008**, *24*, 11592–11599.

(25) Nakagaito, A.; Yano, H. *Cellulose* **2008**, *15*, 323–331.

(26) Syverud, K.; Stenius, P. *Cellulose* **2009**, *16*, 75–85.

(27) Saito, T.; Kimura, S.; Nishiyama, Y.; Isogai, A. *Biomacromolecules* **2007**, *8*, 2485–2491.

(28) Saito, T.; Nishiyama, Y.; Putaux, J.-L.; Vignon, M.; Isogai, A. *Biomacromolecules* **2006**, *7*, 1687–1691.

(29) Maunu, S. L. *Prog. Nucl. Magn. Reson. Spectrosc.* **2002**, *40*, 151–174.

(30) Heinze, T.; Lincke, T.; Fenn, D.; Koschella, A. *Polym. Bull.* **2008**, *61*, 1–9.

(31) Huijbrechts, A. M. L.; Haar, R. t.; Schols, H. A.; Franssen, M. C. R.; Boeriu, C. G.; Sudhölter, E. J. R. *Carbohydr. Polym.* **2010**, *79*, 858–866.

(32) Holmberg, M.; Berg, J.; Stemme, S.; Ödberg, L.; Rasmusson, J.; Claesson, P. *J. Colloid Interface Sci.* **1997**, *186*, 369–381.

(33) Schaub, M.; Wenz, G.; Wegner, G.; Stein, A.; Klemm, D. *Adv. Mater.* **1993**, *5*, 919–922.

(34) Tammelin, T.; Saarinen, T.; Österberg, M.; Laine, J. *Cellulose* **2006**, *13*, 519–535.

(35) Johansson, L.-S.; Tammelin, T.; Campbell, J. M.; Setala, H.; Osterberg, M. *Soft Matter* **2011**, *7*, 10917–10924.

(36) Andresen, M.; Johansson, L.-S.; Tanem, B. S.; Stenius, P. *Cellulose* **2006**, *13*, 665–677.

(37) Hermanson, G. T. *Bioconjugate Techniques*, 2nd ed.; Academic Press: New York, 2008; pp 582–626.

(38) Azzam, F.; Heux, L.; Putaux, J.-L.; Jean, B. *Biomacromolecules* **2010**, *11*, 3652–3659.

(39) Hermanson, G. T. *Bioconjugate Techniques*, 2nd ed.; Academic Press: New York, 2008; p 666–706.

(40) Pulli, T.; Höyhtyä, M.; Söderlund, H.; Takkinen, K. *Anal. Chem.* **2005**, *77*, 2637–2642.

(41) Turunen, L.; Takkinen, K.; Söderlund, H.; Pulli, T. *J. Biomol. Screen.* **2009**, *14*, 282–293.

(42) Takkinen, K.; Laukkanen, M.-L.; Sizmann, D.; Alfthan, K.; Immonen, T.; Vanne, L.; Kaartinen, M.; Knowles, J. K. C.; Teeri, T. T. *Protein Eng., Des. Sel.* **1991**, *4*, 837–841.

(43) Nevanen, T. K.; Söderholm, L.; Kukkonen, K.; Suortti, T.; Teerinen, T.; Linder, M.; Söderlund, H.; Teeri, T. T. *J. Chromatogr., A* **2001**, *925*, 89–97.

(44) Höök, F.; Rodahl, M.; Brzezinski, P.; Kasemo, B. *Langmuir* **1998**, *14*, 729–734.

(45) Rodahl, M.; Hook, F.; Krozer, A.; Brzezinski, P.; Kasemo, B. *Rev. Sci. Instrum.* **1995**, *66*, 3924–3930.

(46) Chen, B.; Pernodet, N.; Rafailovich, M. H.; Bakhtina, A.; Gross, R. A. *Langmuir* **2008**, *24*, 13457–13464.

(47) Ahluwalia, A.; De Rossi, D.; Ristori, C.; Schirone, A.; Serra, G. *Biosens. Bioelectron.* **1992**, *7*, 207–214.

(48) Iwamoto, S.; Abe, K.; Yano, H. *Biomacromolecules* **2008**, *9*, 1022−1026.

Supporting Information for

Immobilization–stabilization of proteins on nanofibrillated cellulose derivatives

Suvi Arola*[ac], Tekla Tammelin[b], Harri Setälä[b], Antti Tullila[a] and Markus B. Linder[a]

[a]VTT, Technical Research Centre of Finland, Bio and process technology, Tietotie 2, FIN–02044 VTT, Finland, [b]VTT, Technical Research Centre of Finland, Energy and Pulp&Paper, Biologinkuja 7, FIN–02044 VTT, Finland, [c]Aalto University School of Science and Technology, Department of Applied Physics, P.O. Box 15100, FI–00076 Aalto, Finland

Ext-suvi.arola@vtt.fi

RECEIVED DATE (to be automatically inserted after your manuscript is accepted if required according to the journal that you are submitting your paper to)

Suvi Arola (née Varjonen), VTT Technical Research Centre of Finland, Tietotie 2, FIN–02044 VTT, Finland, Mobile: +358 40 180 3812, Fax: +385 02 722 7071, Email: Ext-suvi.arola@vtt.fi

Supporting Information

Supporting information contains S1) MALDI–TOF MS sample preparation for SFB–AP with MALDI–TOF MS spectra of AP and SFB–AP (Figure S1), S2) description of allylation of MFC prior to epoxidation and the ^{13}C CP/MAS NMR spectra of allylated MFC (Figure S2), and S3) descriptions of the determination of functionalization degree of amine–NFC accompanied by XPS spectra (figure S3) and elemental concentrations (Table S3) of NFC and amine–NFC.

S1 MALDI–TOF analysis of AP and SFB–AP. In order to prepare the MALDI–TOF samples of AP and SFB–AP TA–solution was prepared by diluting 0.1 % trifluoroacetic acid in MilliQ–water in 1:1 proportion to acetonitrile. A saturated solution of sinapic acid (Fluka, 49508–10MG–F) in TA–solution was used as matrix. Protein samples were diluted in TA–solution. 1 µl of 1:1 ration of protein/matrix mixture was spotted on a ground steel target plate and flight times were measured. The standard used in the measurements was Protein Calibration Standard II (Brukser Daltonics, 207234). The MALDI–TOF spectra of SFB–AP and AP are shown in figure S6. From the spectra we can see that the difference in mass between AP and SFB–AP is m/z 1496.4. The reaction of SFB and lysine residues attaches formylbenzoate to the lysine residue via peptide bondage. One attached formylbenzoate yields a rise of mass by 132.1 Da. This means that in average there are 11.3 modified lysine groups on each AP molecule. In the SFB–AP spectra there is another peak at m/z 97273.143. This can correspond to a dimmer of AP with 21.8 modified lysines. As aldehydes can react with primary amines to produce imines the formation of covalently bound dimers and even larger oligomers is possible in the case of SFB–AP.
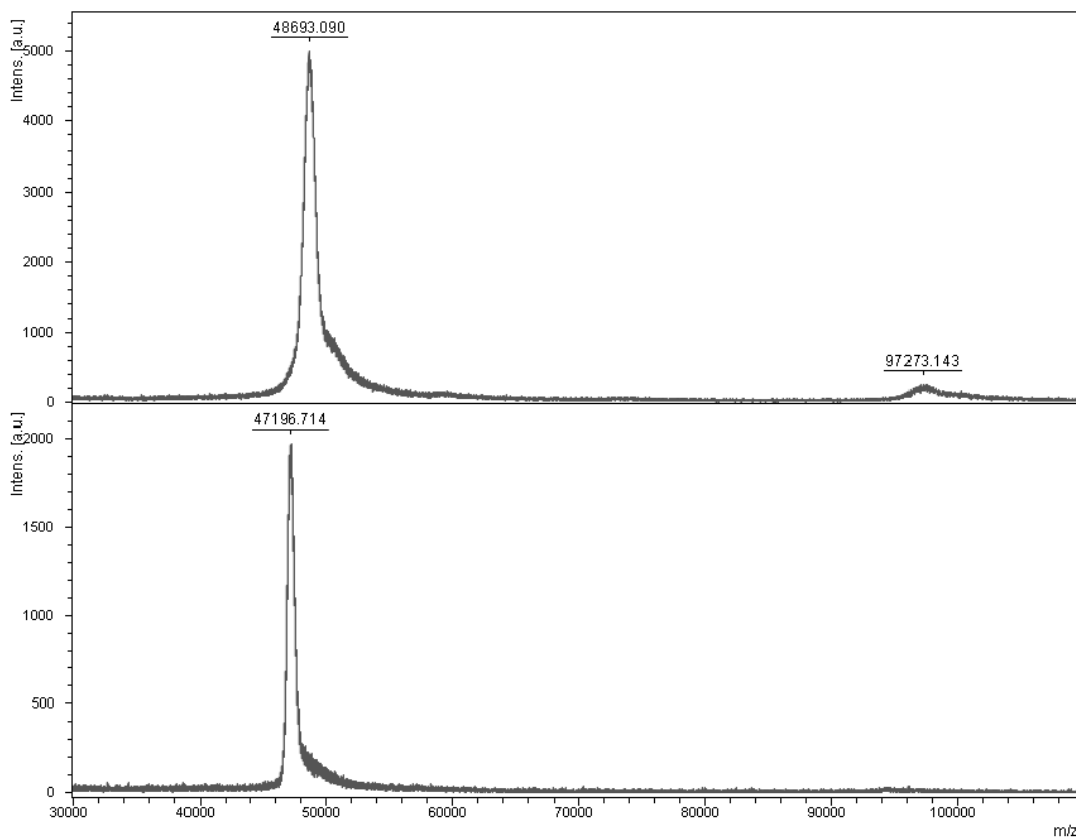
Figure S1. MALDI–TOF spectra of SFB–AP (top) and AP (bottom). SFB–AP monomer carrying ~11.3 formylbenzoate molecules is seen at m/z 48693.090 and a dimer of it at m/z 97273.143. AP molecule is seen at m/z 47196.714.

S2 ^{13}C CP/MAS NMR spectra of epoxy functionalized microfibrillated cellulose (epoxy–MFC). The allylation of MFC was done in two steps because in the first reaction the soluble hemicelluloses disturb the reaction. In the first step 40% of hemicelluloses are removed and a very low yield of butyl and allyl modification is achieved ($DS_{butyl+allyl} = 0.01$) which can be seen from the left hand side NMR spectra. The amount of allyl groups is very low and it falls below the detection limits of the method thus butyl peaks are used for the determination of modification extent. After the second allylation step the extent of allyl modification can be determined from the allyl peaks at 140–120 ppm. The DS_{allyl} after two step allylation was calculated to be 0.066 by combining the integrated areas of both allyl peaks and comparing it to the anomeric C1 peak in cellulose.
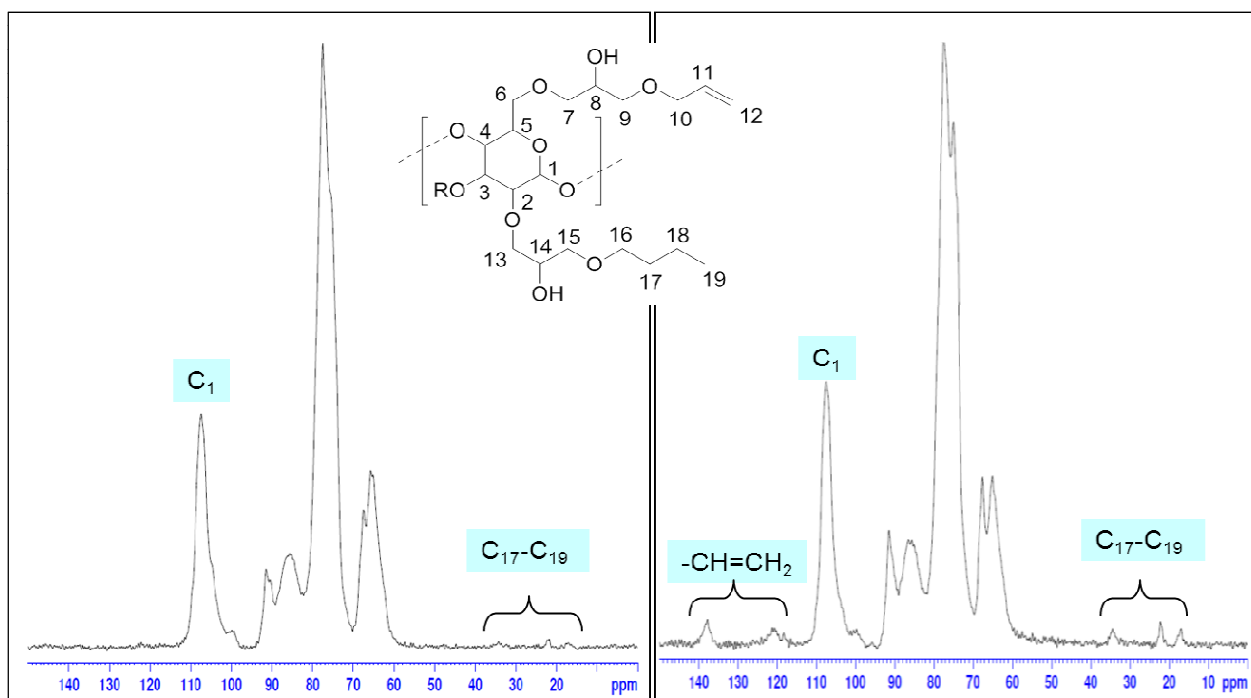

Figure S2. The ^{13}C CP/MAS NMR spectra of MFC fibers after the first allylation step (left) and after the second allylation step (right). A schematic drawing of the functional groups attached on a glucose unit of cellulose chain is presented to ease the interpretation of the spectra.

S3 Determining the degree of functionalization of amine functionalized nanofibrillated cellulose (amine–NFC). The degree of amine functionalization was calculated from the surface silicon and surface nitrogen content analyzed by X–Ray photoelectron spectroscopy (XPS) as described in Johansson et al.[1] Figure S2 shows XPS survey spectra peaks due to emission of O 1s, C 1s, N 1s, Si 2s and Si 2p electrons. Survey scans were used in determination of surface elemental concentrations. O 1s (oxygen) and C 1s (carbon) originate from cellulose whereas N 1s (nitrogen), Si 2s and Si 2p (silica) are markers for successfully aminated nanocellulose samples. Table S2 shows the elemental concentrations and relative abundance of different carbon bonds achieved by curve fitting of carbon C1 s spectra.[2,3] The degree of amination was calculated from the nitrogen and silicon content. The surface content of nitrogen was 1.7 % and the surface content of silicon was 1.5 % for amine–NFC, corresponding to surface substitution values of 0.21 for nitrogen marker and 0.19 for silica marker, respectively.
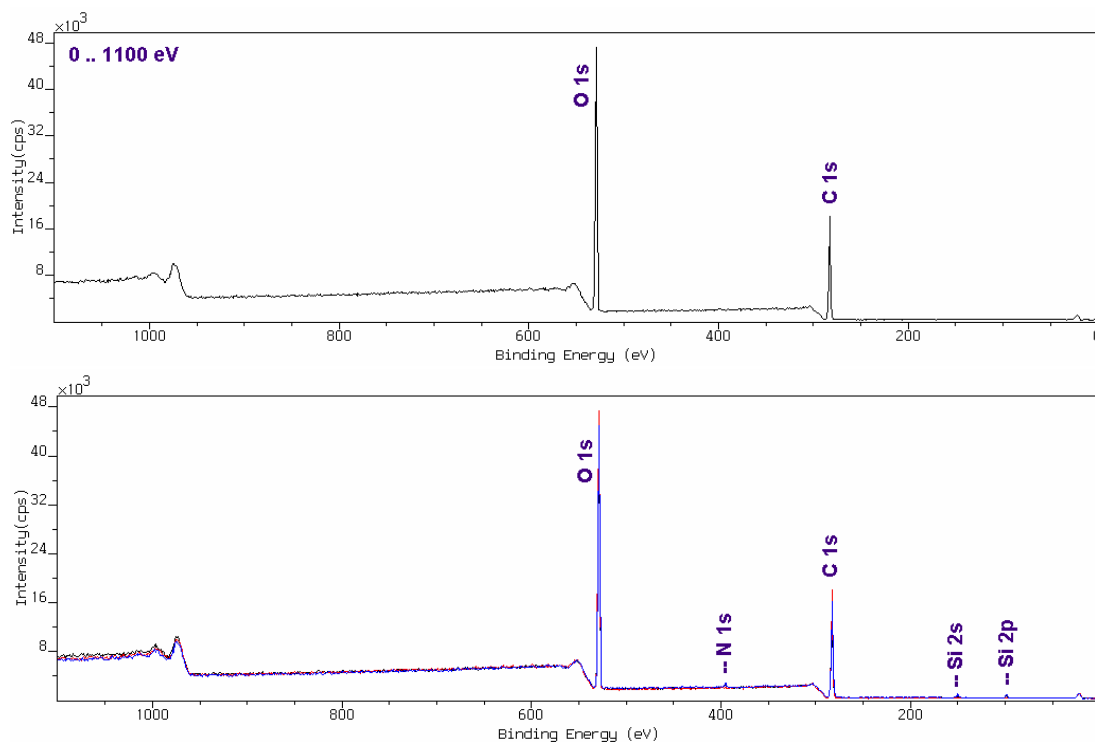

Figure S3. Low resolution XPS survey spectra recorded for unmodified fluidized NFC (top panel) and for amine–NFC (bottom panel).

Table S3. XPS data for NFC and amine–NFC.

Sample	Elemental concentration (at-%)				Relative abundance of carbon bonds (at-%)			
	O 1s	C1s	N1 s	Si 2p	C-C	C-O	O-C-O	C=O
Unmodified NFC	43.4	56.4	0.1	0	3.8	76.8	18.6	0.8
Aminated-NFC	41.5	55.3	1.7	1.5	8.9	72.9	17.4	0.8

References

(1)	Johansson, L.-S.; Tammelin, T.; Campbell, J. M.; Setala, H.; Osterberg, M. *Soft Matter* **2011**, *7*, 10917-10924.
(2)	Beamson, G.; Briggs, D. *High resolution XPS of organic polymers : the Scienta ESCA300 database*; Wiley: Chichester [England]; New York, 1992.
(3)	Koljonen, K.; Österberg, M.; Johansson, L. S.; Stenius, P. *Colloids Surf., A* **2003**, *228*, 143-158.

Publication III

The role of hemicellulose in nanofibrillated cellulose networks. Suvi Arola, Jani-Markus Malho, Päivi Laaksonen, Martina Lille and Markus B. Linder. *Soft Matter*, 2013, 9, pp. 1319–1326. DOI:10.1039/C2SM26932E

The role of hemicellulose in nanofibrillated cellulose networks

Suvi Arola,†[*ab] Jani–Markus Malho,[a] Päivi Laaksonen,[a] Martina Lille[a] and Markus B. Linder[*ac]

Cellulose nanofibrils show remarkable properties with applications in several fields of materials science, such as for composites, hydrogels, aerogels, foams, and coatings. Cellulose nanofibrils are typically produced by mechanical and enzymatic processing leading to fibrils having a width in the nanometer range and very high aspect ratios. The formation of percolating networks and interactions between fibrils lead to useful properties in for example gel formation and composites. In this work we studied how the residual xylan that is found in cellulose nanofibrils that have been produced from hardwood pulp affects these properties. We used enzymatic hydrolysis to specifically remove xylan and studied rheological properties, morphological features, and properties of paper-like films of cellulose nanofibrils. We found that removal of xylan enhances the formation of fibril networks, resulting in both stiffer gels and stronger films. However xylan also stabilizes the fibrils against flocculation. Also the history of processing of the preparations affects the results significantly.

Introduction

New developments for processing cellulose into fibrils with widths in the nanometer range have widely expanded its potential for use in materials science. As a polymer chain, cellulose is a homopolymer formed by the repeating unit of β-(1-4)-D-glucopyranose. In natural materials such as wood the cellulose polymer is packed into fibrils with a diameter of 3–5 nm. These fibrils are referred to as elemental fibrils and they are further packed together with hemicellulose to form what is known as microfibrils with a diameter of ~10 to 20 nm.[1] The microfibrils are packed further into larger fibrils finally forming macroscopic wood cellulose fibres.[2,3] The processing methods for the production of native fibrillar nanocellulose materials are based on disintegration of fibres mechanically and biochemically into high aspect ratio nanosized fibrils.[4] The resulting fibrils are 3–20 nm in diameter and microns long and referred to as nanofibrillated cellulose (NFC) or microfibrillated cellulose (MFC). The high aspect ratio and the excellent mechanical properties of the fibrils make NFC special as a material.[1,5] It is also possible to obtain high strength NFC fibrils by other means such as TEMPO-oxidation which are reviewed elsewhere.[6] The stiffness of individual cellulose I crystals is very high, measured to be between 134 and 143 GPa and the strength in the GPa range.[7,8]

NFC has been shown to form excellent stiff gels as aqueous dispersions at low solid content,[4] flexible and tough aerogels,[9] composite materials,[10,11] foams,[12] stabilizing emulsions and dispersions,[13–15] biomedical applications[16] with applications for different types of materials even for oil recovery.[17] Many of these applications rely on the stiffness and the high aspect ratio of the fibrils in NFC materials which leads to percolating networks that are further influenced by fibril entanglement and interactions between fibrils.[9,18]

Depending on the origin and the processing history, there can be up to 30% of hemicellulose present in NFC.[19] In softwood NFC, the main hemicellulose is galactoglucomannan and in hardwood NFC it is glucuronoxylan.[20] It is known that the fibrillation of pulp into microfibrillated cellulose is aided by the presence of hemicellulose, which is most likely due to the negative charges on hemicellulose that lead to charge repulsion between the fibrils.[21] The drying of pulp has a negative effect on the fibrillation process.[21] This is most likely due to irreversible coalescence of fibrils together[22–24] which could be driven by the formation of strong hydrogen bonding and contamination of the fibril surface during the drying process making the cellulose surface passive, *i.e.* less reactive.[25] It has been shown that the more hemicellulose is present in the material the less drying affects the fibrillation and other properties of pulp.[21]

A full understanding is still lacking of how the hemicellulose is located in the fibril structure and how it affects the NFC material properties in solution or in the dried state. It is

[a]VTT Technical Research Centre of Finland, Bio and Process Technology, Tietotie 2, Espoo P.O. Box 1000, FI-02044 VTT, Finland. E-mail: Markus.Linder@vtt.fi; Fax: +358 20 722 7071; Tel: +358 400 971 207

[b]Department of Applied Physics, Aalto University School of Science and Technology, P.O. Box 15100, FI-00076 Aalto, Finland

[c]Department of Biotechnology and Chemical Technology, Aalto University School of Chemical Technology, P.O. Box 16100, FI-00076 Aalto, Finland. E-mail: Markus. Linder@aalto.fi; Tel: +358 50 431 5525

† née Varjonen.

expected that at least part of the hemicellulose is on the surface of the fibrils.[26,27] Previous studies on total enzymatic hydrolysis of cellulosic material, also NFC, have shown that hemicellulases especially xylanases are crucial for the efficient hydrolytic solubilisation of cellulosic materials.[28] Xylanases are enzymes that specifically hydrolyse xylans to xylose and small xylo-oligomers leaving cellulose intact.[29] The results suggest that hemicelluloses are associated in the fibril structure in such a way that they prevent cellulases to freely access the cellulose.[28] Other studies on hard wood pulp materials have shown that only some 35% of xylan can be solubilized from the materials by using xylanases demonstrating that not all the xylan in pulp is accessible for the enzyme.[30] The rest of the hemicellulose is most probably located within the fine structure of fibrils in between elemental fibrils. Therefore it is unclear how much hemicellulose can be solubilized from fibrillated material such as NFC where still elemental fibrils are closely associated and protecting at least some fraction from hydrolysis.

The adsorption of different hemicelluloses has been studied on a variety of cellulosic materials.[31–33] There are certain structural features, such as a critical length of the hemicellulose back-bone and the substitution degree that determine the affinity of hemicellulose on the cellulose surface.[31,32] For example, it has been shown that the shortest xyloglucan that can adsorb onto Avicel cellulose must be at least 12 sugar units long.[32] The critical length for xylan adsorption onto bacterial cellulose has been shown to be 15 xylose units.[31] It has also been shown that the more substituents the hemicellulose has the less it will adsorb onto the cellulose surface.[31] The two major xylanases from the filamentous fungi *Trichoderma reesei* hydrolyse xylan to xylose and 2–7 unit xylo-oligomers and are thus expected to release the hemicellulose from the cellulose surface.[34]

In this work we were interested in understanding how the percolating networks in NFC dispersions are affected by the presence of hemicellulose and how hemicellulose may affect interactions between cellulose fibrils and thereby nodes of interactions between fibrils that affect the rheological properties. Hemicellulose (in our case xylan) was partially hydrolysed by an enzymatic treatment and the effect of xylan hydrolysis on fibril interactions in the NFC dispersion was studied by rheological measurements and microscopy. More information on the organisation of the fibrils was obtained by studying the performance of dry films prepared from the NFC dispersions.

Experimental

Preparation of nanofibrillated cellulose

NFC was prepared by mechanical disintegration of bleached birch kraft pulp by ten passes through a M7115 Fluidizer (Microfluidics Corp.), essentially according to previous reports.[4] The solid content of the prepared water dispersion was ∼1.9%.

Total hydrolysis of NFC and the analysis of sugar content

A total hydrolysis of the NFC suspension (dry weight 1.9%) was performed to determine its total xylan content.[35] An enzyme mixture containing four different commercial enzyme products was used (Econase (cellulase, Roehm Enzyme Finland) 20 mL, Ecopulp X-200 (xylanase, Roehm Enzyme Finland) 50 mL, Gamanase (mannanase, Novo) 100 mL and Novozyme 188 (β-glucosidase, Novo) 50 mL). The mixture was then diluted with 200 mL of 50 mM sodium acetate buffer pH 5 and desalted using a Biogel P-6 gel (Bio-Rad) column using the same buffer. The total activity of the mixture was 29.8 FPU (filter paper units) mL^{-1}. The load of enzyme used for total hydrolysis of NFC was 50 FPU g^{-1} and the reaction was allowed to proceed for 48 h at 40 °C (stirring 250 rpm), after which an additional 10 FPU g^{-1} amount of enzyme cocktail was added and the reaction continued for another 18 h to ensure total hydrolysis of the sample. The mixture was cleared by centrifugation (4000 rpm, 10 min, Eppendorf), supernatant was boiled for 5 min to inactivate enzymes and centrifuged again. Monosaccharides were determined by chromatography (DIONEX ISC-5000, CarboPac PA20) from the second supernatant. The dry weight of the first pellet from the total hydrolysis reaction was also determined.

NFC sample preparation

A stock solution of NFC was prepared as described previously.[15] For experiments, an aliquot of the stock solution was diluted with 50 mM sodium acetate pH 5 to a concentration of 4.55 g L^{-1} while mixing with a magnetic stirrer (<1000 rpm). Mixing was continued for about 30 seconds after which the solution was sonicated with an ultrasonifier (Vibra-Cell VXC 750, Sonics and Materials Inc., U.S.A.) using a standard tip (20%, 5 min). After sonication the solution was again mixed with the magnetic stirrer for about ∼30 s. After this pre-treatment, xylan was hydrolysed using purified pI9 xylanase from *T. reesei*.[34] The total volume of the reactions was 3.52 mL with a final concentration of 0.4% NFC and an enzyme dosage of 3 mg g^{-1}. The samples were incubated at 45 °C for 24 h. Part of the samples were mixed with a magnetic stirrer (800 rpm) and part were allowed to react without stirring. Control samples were treated identically except that buffer was added instead of enzyme.

Analysis of xylan released from NFC

Samples were first clarified by centrifugation (20 000 rpm, 20 min). The clarified samples were then subjected to further enzymatic hydrolysis to break down possible oligosaccharide products into constituent monosaccharides. The following enzyme mixture was used: endoglucanase (24 nk at mL^{-1}), xylanase (187 nk at mL^{-1}), mannanase (18 nk at mL^{-1}), β-xylosidase (1 nk at mL^{-1}), β-mannosidase (18 nk at mL^{-1}), β-glucosidase (4 nk at mL^{-1}), α-galactosidase (11 nk at mL^{-1}), arabinosidase (6 nk at mL^{-1}), and α-glucuronidase (9 nk at mL^{-1}). A 1 : 4 ratio of enzyme to sample was used and sodium acetate buffer pH 5 (100 mM) was used for dilutions. Incubation was continued for 24 h at 45 °C. Finally the samples were boiled for 5 min to inactivate the enzymes and then centrifuged. The monosaccharide composition was analysed from the supernatant by chromatography as described above.

Rheological characterization of NFC suspensions

Xylanase treated and control samples were characterized for their rheological properties using cylinder and cup geometry (CC15, gap between the cup wall and bob 0.5 mm), with a stress controlled rheometer (StressTech, Reologica Instruments Ab, Sweden). Viscoelastic properties of the NFC dispersions were measured by oscillatory stress sweep tests (0.01–1 Pa) under a constant frequency of 0.1 Hz and by frequency sweep tests (0.01–10 Hz) at a constant stress amplitude of 0.03 Pa. Three samples were analysed for each treatment. The error of the measurements was calculated from the set of samples and it represents the accuracy of the sample preparation, *i.e.* how reproducible the sample preparation was. After the xylanase treatment the samples were allowed to equilibrate to room temperature for 3 h prior to rheological measurements. 3 mL of each sample was pipetted into the measuring cup and the bob was lowered to the measuring position. The sample was allowed to relax for 5 min before the measurement was started.

Preparation and characterization of dried NFC films

Xylanase treated NFC and control samples were used to make thin, paper-like films. The films were prepared passing NFC dispersion (1 mL, 4 g L^{-1}) through a membrane (Durapore GVWP, 0.22 μm, Millipore, US) in a vacuum filtering device whereby the NFC deposited on the membrane as a film. The deposited NFC film was peeled off from the supporting membrane and gentle pressure was applied on it using a 300 g load for 10 min. Films were dried overnight at 65 °C, and then allowed to stabilize at 50% humidity at 21 °C before tensile testing under ambient conditions. For the tensile testing, a mini tensile tester (Deben, UK) was used. A 20 N load cell was used with a nominal strain rate of 0.5 mm min^{-1}. At least 4 duplicates were made from each sample. The films were cut into strips of 2 mm × 20 mm and had a thickness of about 7–10 μm. A micrometer slide calliper was used to determine the widths of the samples. The thickness was measured with a scanning electron microscope (JEOL JSM-7500F FEG, Japan) using an acceleration voltage of 1–15 kV depending on the sample. Samples were sputtered with palladium to enhance imaging conditions and prevent the charging of the samples. For the thickness measurements, films were aligned perpendicular to the electron beam. At least 8 measures were made from different places of the film cross-section.

Cryogenic transmission electron microscopy (Cryo-TEM) imaging of NFC fibrils

Cryo-TEM was used to analyse the morphology of the NFC fibrils in solution. NFC dispersions were diluted 1 : 10 and vitrified by purging in a liquid propane–ethane mixture on c-flat grids using a vitrobot (FEI, U.S.A.). Imaging was performed with a JEOL JEM-3200FSC Cryo-TEM 300 kV.

Atomic force microscopy (AFM)

NFC samples were diluted 1 : 400 with water and a 30 μL aliquot was spread on freshly cleaved mica (Electron Microscopy Sciences). The samples were allowed to dry for 24 h, attached on steel supports with double-sided tape (Scotch) and imaged using a NanoScope IIIa Multimode AFM instrument (E-scanner, Digital Instruments/Veeco) with an NSCI5/AlBS cantilever (μMASCH, USA). All images were recorded in tapping mode in air with scan rates of 0.8–1 Hz (free amplitude was about 0.65 V). The damping ratio was around 0.7–0.85. Images were flattened to remove possible tilts in the image data. Otherwise no further processing of the images was done.

Dynamic vapour sorption (DVS) measurement of NFC films

Dynamic water vapour sorption of NFC films was done with a DVS-1 instrument (Surface Measurement Systems, UK) to investigate if the amount of xylan within the films has an effect on the water sorption capability of NFC. NFC films were dried overnight at 60 °C in a desiccator containing phosphorus pentoxide before the measurement. The measurement had five 16 hour steps at 0%, 25%, 50%, 75% and 90% relative humidity. The amount of water vapour content was measured during the whole experiment.

Results

Total xylan content and release of xylan from NFC

Table 1 summarises the sugar content results from total enzymatic hydrolysis of NFC analysed by chromatographic methods. In addition to solubilised sugars there were 1.7% of non-soluble materials such as lignin.

We conclude that ~27% of the NFC sample consisted of xylan (xylose, methylglucuronic acid and xylotrioses), ~71% of cellulose (glucose), ~0.3% of glucomannan (2 : 1 mannose to glucose[20]) and 1.7% of insoluble materials. The hydrolysis with only pI9 xylanase for 24 hours at 45 °C (with stirring and without) showed that only part of the total xylan was accessible to the enzyme releasing 32–36% of the total xylan as soluble saccharides. There were no significant differences between samples that had been stirred or not. The release of xylan during the hydrolysis corresponded to approximately a 10% reduction of total mass. Experiments showed that increasing enzyme load or hydrolysis time did not increase the release of xylan.

Effect of xylan removal and continuous mixing on NFC dispersion rheology

Stress sweep measurements were performed on xylanase-treated samples that had been mixed or not mixed during the

Table 1 The amount of mono- and oligosaccharides released from NFC by total enzymatic hydrolysis

Mono-/oligosaccharide[a]	Glu	Xyl	Man	Me-gluA	Xyl$_3$
Amount solubilised (%)	71	26.2	0.2	0.6	0.3

[a] Glu = glucose, Xyl = xylose, Man = mannose, Me-gluA = methylglucuronic acid, and Xyl$_3$ = branched xylotrioses (hexenuronic acid xylotriose and 2-*O*-(4-*O*-methyl-3-L-idopyranosyluronic acid)-xylotriose).

hydrolysis. The elastic modulus (G'), viscous modulus (G'') and phase angle of a typical measurement (NFC) are presented in Fig. 1A. The average G' and G'' values in the linear viscoelastic region and the critical stress at the onset of non-linear behaviour were determined from the curves (Fig. 1B). From Fig. 1B it is seen that G' values are an order of magnitude higher than G'' values and thus the systems are all predominantly elastic. Xylan hydrolysis had a clear effect on the elastic modulus, but the effect was dependent on the treatment procedure. Letting the xylan hydrolysis proceed without mixing resulted in a higher G' than the corresponding control sample without xylanase. Mixing with a magnetic stirrer during the hydrolysis on the other hand led to a significant decrease in G'. This lowering of G' was more pronounced when xylan had been removed. The critical stress values present the onset of elastic-to-viscous transition and clearly show that this phenomenon occurs at lower stress values for samples that are mixed compared to those that are not mixed. From the samples that are mixed the one treated with xylanase stands a significantly lower stress value than the one not treated with xylanase. Xylan hydrolysis increases the critical stress value compared to native NFC.

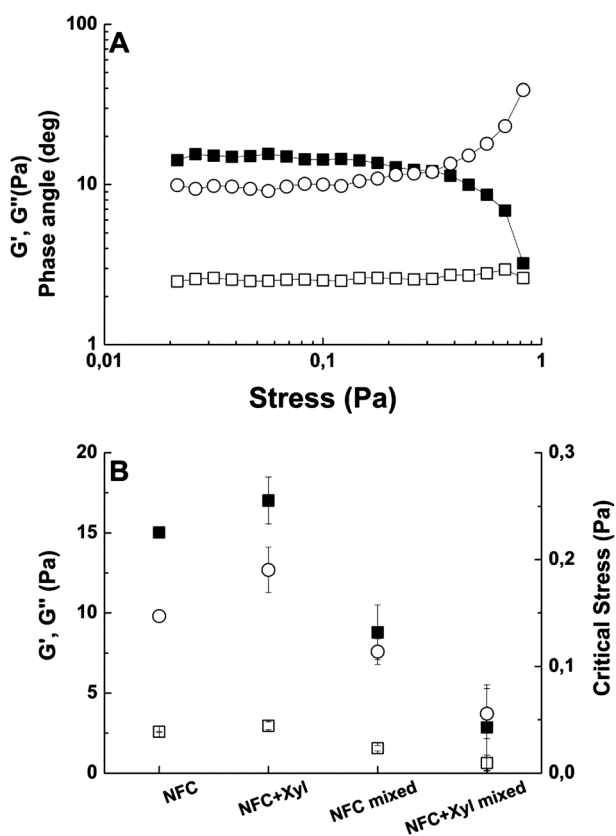No significant differences were observed in frequency dependent behaviour of the different NFC samples. The modulus of all NFC solutions rose as a function of frequency with an equal slope (data not shown).

Effect of xylan removal and continuous mixing on NFC fibril morphology

Cryo-TEM and AFM images were taken for samples (Fig. 2) that had been treated with xylanase with and without mixing and controls. No differences between treatments were observed compared to non-treated controls. Xylanase treatment or continuous mixing does not seem to have an effect on the morphology of the fibrils; no shortening of the fibrils or significant differences in bundling can be seen in any of the samples. The fibril diameters, *i.e.* heights, from the AFM images are very similar for all samples; NFC 6.8 ± 4.0 nm, mixed NFC 9.1 ± 4.2 nm, xylanase treated NFC 9.0 ± 4.3 nm and xylanase treated mixed NFC 9.6 ± 3.4 nm. The heights and deviations were calculated from heights obtained from the cross-section of 20 fibrils in different images.

Preparation and characterization of thin paper-like films

Films of NFC were made using samples that had been treated with xylanase and controls without xylanase. Each set included samples that had been mixed or not mixed during the treatment. Although the film preparation followed an identical procedure, the different NFC treatments resulted in different film thicknesses and thus different film densities. The film thicknesses and densities are summarised in Table 2.

Typical stress–strain curves for differently processed NFC film samples are shown in Fig. 3. The mechanical properties of
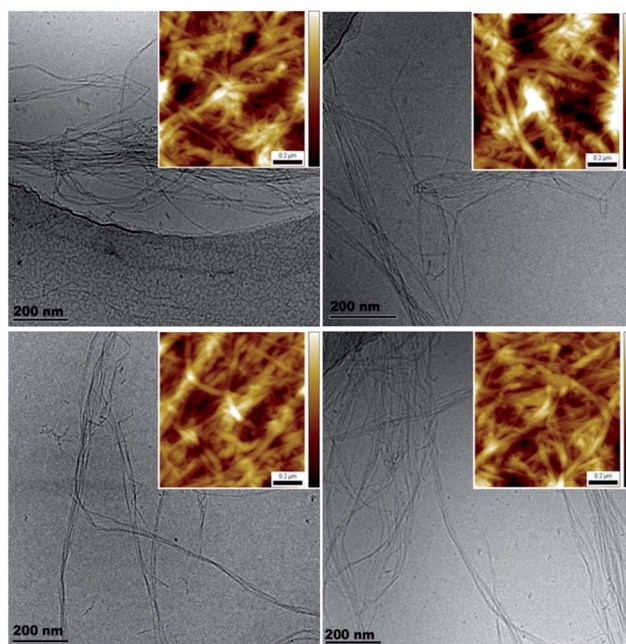

Fig. 1 Effects of xylanase treatment and continuous mixing on rheological properties of NFC dispersion. (A) A typical stress sweep test for NFC dispersion showing the behaviour of elastic and viscous moduli (G', G'') and phase angle. (B) Elastic moduli (G'), viscous moduli (G'') and the critical stress values of the different samples. In graph (A) ■: G', □: G'', and ○: phase angle. In graph (B) ■: G', □: G'', and ○: critical stress.

Fig. 2 Cryo-TEM images of NFC suspensions: top left, NFC; top right, NFC mixed; bottom left, NFC treated with xylanase; and bottom right, NFC treated with xylanase and mixed. Insets: AFM height images of the corresponding samples spread and dried on freshly cleaved MICA. Scan size 1 × 1 μm and height 60 nm.

Table 2 Thickness and average density of differently treated NFC films

	NFC	NFC–Xyl[a]	NFC mixed[b]	NFC–Xyl mixed[c]
h (μm)	12.2 ± 1.45	8.2 ± 0.90	8.5 ± 0.84	9.4 ± 0.83
ρ (mg mm^{-3})	1.2	1.6	1.8	1.4

[a] Xylanase treated NFC. [b] Continuously mixed NFC. [c] Continuously mixed NFC that was treated with xylanase.
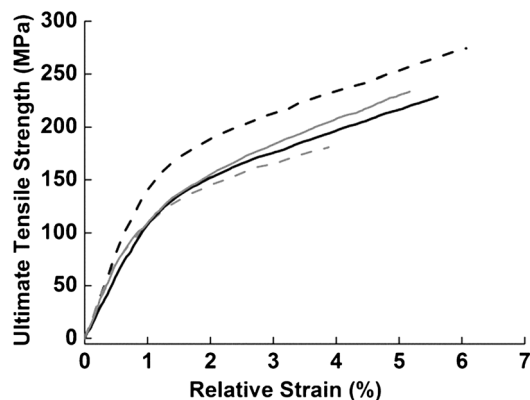

Fig. 3 Typical stress–strain curves for the differently processed NFC films. NFC (solid black line), continuously mixed NFC (dashed black line), NFC treated with xylanase (solid grey line), and continuously mixed NFC treated with xylanase (dashed grey line).

Table 3 Mechanical properties of differently treated NFC films

	Ultimate tensile strength (MPa)	Young's modulus (GPa)	Strain-to-failure (%)	Yield strength (MPa)
NFC	199 ± 35	10.0 ± 3.1	5.24 ± 0.6	113 ± 22
NFC–Xyl[a]	243 ± 38	13.1 ± 1.9	4.81 ± 0.3	126 ± 24
NFC mixed[b]	252 ± 17	14.6 ± 1.3	5.55 ± 0.4	149 ± 6.3
NFC–Xyl mixed[c]	166 ± 34	11.1 ± 1.3	3.80 ± 0.6	100 ± 26

[a] Xylanase treated NFC. [b] Continuously mixed NFC. [c] Continuously mixed NFC that was treated with xylanase.

the four NFC films are summarised in Table 3. Treatments showed in general significant effects on the mechanical properties. The measured parameters (stiffness (Young's modulus), yield strength, ultimate tensile strength, and strain to failure) show dependence on both mixing and xylanase treatment of the samples. A general trend is that in mixed samples the xylanase treatment weakened the mechanical properties and in non-mixed samples the xylanase treatment improved mechanical properties. However for the values for strain to failure, the xylanase treatment generally led to lower values.

Dynamic water sorption measurement of NFC films

Water uptake was used as a way of identifying differences between xylanase treated and non-treated NFC films. Control samples and samples with xylanase treatment either with or without mixing showed very similar water uptake profiles
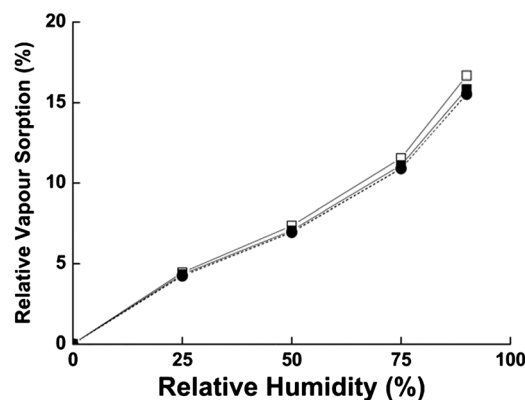

Fig. 4 Relative water vapour uptake by paper-like films made of differently treated NFC. –□– NFC, –○– xylanase treated NFC, –■– continuously mixed NFC and –●– continuously mixed xylanase treated NFC. Treating NFC with xylanase with or without mixing did not significantly change moisture uptake compared to controls without xylan treatment.

(Fig. 4). In total a 16% mass gain was reached at 90% relative humidity in all films.

Discussion

NFC prepared from hard and softwood has been widely used for developing new innovative materials and has proven to be very promising for many applications. In this work we addressed the question of how the hemicellulose content of the NFC can affect its properties. We used a type of NFC preparation that has been widely used in other studies.[9,11,13,17,36–54]

Initially we found that 27% of the NFC preparation consisted of xylan, the major hemicellulose in hardwood. Treating the NFC with a purified xylanase (pI 9 variant from *T. reesei*) released 32–35% of xylan. Extending hydrolysis time or enzyme dosage did not release more xylan indicating that the remaining xylan was not accessible. Xylan is naturally found between elementary microfibrils of cellulose in the plant cell walls. Most likely the xylan that was hydrolyzed and removed in the current experiments was located easily accessible on the surface of the small bundles of microfibrils that form the NFC. The xylan that was not hydrolysed by the enzyme was most likely in between the microfibrils of the NFC. Interestingly, the hydrolysis of xylan did not result in any notable change in the dimensions or shape of the NFC as analyzed by both Cryo-TEM and AFM. It is therefore difficult to estimate exactly how the xylan is associated with the cellulose, if it was thinly and evenly spread out along the fibrils or only as loosely associated. The water sorption behaviour was performed to detect possible changes in the cellulose fibril structure during xylan hydrolysis. Previously it has been shown that the water sorption capability of cellulosic material is dictated by the crystallinity of the materials below RH 75% and by structural features such as porosity above RH 75%.[55] In our work we saw no differences in water sorption behaviour of the different samples suggesting that the xylanase has not altered the cellulose structure.

Rheological measurements showed significant differences between xylanase treated and non-treated NFC samples.

However, it was found already in preliminary experiments that the viscoelastic properties of NFC dispersions are very much dependent on their shearing history even in the absence of xylanase, which is probably related to shear-induced changes in the floc structure of the dispersions.[56] In our work, we also observed a marked difference in G' between the mixed and non-mixed NFC dispersions without xylanase (Fig. 1B), although they had identical chemical composition. This highlighted the necessity of developing a pre-treatment protocol involving initial break-up of aggregates and networks by sonication and mixing prior to enzymatic treatment. This pre-treatment protocol served very well to achieve a reproducible base-level to which different treatments could be performed and reduced significantly the variation between experiments.

The enzymatic hydrolysis of xylan led to a clear increase in the elastic modulus of the sample when the sample was not mixed (Fig. 1B). Continuous mixing lowered the modulus of the non-treated samples but the samples that were both mixed and treated with xylanase resulted in the lowest modulus values overall. Interpretation of the results is difficult because apparently several different effects are occurring simultaneously. The initial pre-treatment of the samples involving sonication is expected to open up bundles of fibrils and increase fibril entanglement and therefore interaction nodes between fibrils. We also note that this non-enzyme treated, non-mixed sample gave high modulus values. Treating the sample with xylanase, but not mixing increased the modulus further. We interpret this change as an increase of interactions between fibrils resulting in a stronger percolating network. On the other hand, the continuous mixing of samples without the addition of xylanase significantly decreased the modulus. The mechanism behind this is most likely related to less effective percolation due to the formation of flocs as a result of the shear forces during mixing.[18] The bundling might cause the loss of percolation by the loss of interaction nodes throughout the gel and result in local concentrated interactions of fibrils in the gel. In the work by Vian et al.[22] it was shown that the presence of hemicellulose did not affect the bundling of fibrils during dehydration of the system yet it prevented the irreversible flocculation of the fibrils. It was also shown that reducing the amount of hemicellulose in the system caused bundling of the fibrils all the more extensively the more hemicellulose was extracted and the flocs grew larger when larger amounts of hemicellulose were removed. This suggests that there might be a similar mechanism of bundling caused by shear forces with and without the removal of hemicellulose, yet the exact structure of the flocs in solution conditions remains unclear. Sonication of samples that were not treated by xylanase led again to increased viscosity, most likely due to/consistent with the opening up of flocculated structures. This finding is consistent with the findings of Vian et al.[22] that fibrils with hemicellulose do not flocculate irreversibly and can be dispersed again. The xylanase treatment of samples that were mixed led to a still larger decrease in modulus. The mechanism that leads to the decrease of modulus in the mixed samples was therefore apparently enhanced by xylanase treatment. This is contradictory to the effect of xylanase without mixing. It could be possible that the increase in interactions brought about by xylanase

treatment is favourable to a certain extent (as when the dispersion is at rest), but that a further increase in interactions during mixing results in such a high level of flocculation that the network structure is hampered.

The elastic-to-viscous transition of the gels as studied by increasing the applied stress supports these conclusions (Fig. 1B, Critical stress). This transition occurs at the lowest stress values for the mixed and xylanase treated samples. The critical stress value then increased in the order, mixed and non-treated, non-mixed and non-treated, with the strongest gels for the xylanase treated and non-mixed. The results follow the logic that mixing induces aggregation of fibrils that leads to weaker gels. Xylan removal enhances this effect, but if samples were not mixed, the xylan removal made the gelling network stronger.

The effect of xylanase treatment for making paper-like films was seen in two ways. Firstly, the thickness of the films was reduced as expected by the loss of mass due to hydrolysis. However also mixing reduced the thickness apparently by allowing a denser packing of the fibrils. In line with this it has previously been shown with pulp materials that the density is increased and that the pore size is decreased when xylan is enzymatically removed indicating that the packing of the fibres is more efficient.[30] There was also a clear effect on the mechanical properties of the films by the treatment with xylanase. When NFC samples were not mixed during the enzymatic reaction, the films became stiffer and stronger as a result of the treatment. This is in line with the rheology data where gel-stiffening occurred by the same treatment. However, continuous mixing of NFC also resulted in stronger and stiffer films without enzymatic treatment. Since the mixed/non-mixed samples without enzymatic treatment were chemically identical there must be other factors leading to increased properties. As can be seen from the measured thicknesses, also the thickness of the mixed samples was lower, which indicates better packaging of fibrils in the films and thus increased interactions between fibrils. The denser packaging allowed by the aggregation of the fibrils then seems to lead to better properties. On the other hand, as the further weakening of the gel properties in the rheological experiments indicated, the enzymatic treatment further weakened interactions between fibrils in mixed samples and thus led to weaker films. Thus the effect of xylanase treatment was in the same way opposite in both film formation and for gel formation depending on how the fibrils were mechanically treated. However, in all cases the values for strain-to-failure of the samples were lower for xylanase treated NFC. This shows that the stiffness and strain values are not necessarily directly dependent and that xylan plays a role in the extension of fibril networks on the region of the plastic deformation. Interactions between fibrils that are mediated by xylan then can allow more creep and extension, while the interactions in fibrils where xylan was removed were stiffer but less flexible. It appears that softening of the interface between NFC fibrils due to the xylan layer is beneficial and allows movement of the fibrils under tensile stress. Although it is difficult to distinguish between the fine effects of dispersion quality and the strength of the interaction between the fibrils, the film properties show consistent results and reveal different aspects of the fibril

properties. It has also been shown previously for pulp materials that the tensile strength is decreased and that the fibre stiffness is increased when hemicelluloses are removed.[30]

The formation of interacting nodes in percolating networks has been seen as a major explanation of the properties of NFC. In this work we addressed the question of how hemicellulose (in our case xylan), a major component of typical NFC preparations, affects its properties. The results support a major role of fibril networks in NFC properties, but show that xylan as an additional component clearly affects fibril interactions and therefore the details of how NFC performs. Investigating the role of interactions within NFC networks is greatly affected by the history of the preparation and in which form the fibrils are present, *i.e.* if they are open or aggregated. Microscopy imaging did not reveal such differences and they were only seen by detailed rheological measurements. The results show that xylan in this way plays a key role in fibril stability in aqueous surroundings preventing for example fibril coalescence during mechanical mixing. In some cases the mechanical properties can be enhanced by xylan removal, but as stability may be decreased a better control of processing conditions may be required when xylan is present.

Conclusions

Only some 35% of the xylan present in the NFC network can be removed by or is accessible to xylanase. The presence of xylan affects the NFC network properties clearly but effects are not unambiguous and the comparison of the effects to gel properties and film properties is somewhat difficult to correlate. The biggest effect of xylan still seems to be on the association behaviour of the NFC fibrils. The xylan that is easily removed by enzyme hydrolysis and affects the stability of NFC seems to be on the surface of the fibrils and the rest of the xylan not affecting the association of the fibrils is within the fibril structure. Despite the presence of xylan NFC is very sensitive to processing history. Mixing for example induces changes in the hydrogel structure that affect the mechanical properties.

Acknowledgements

References

1 D. Klemm, F. Kramer, S. Moritz, T. Lindström, M. Ankerfors, D. Gray and A. Dorris, *Angew. Chem., Int. Ed.*, 2011, **50**, 5438–5466.

2 D. Fengel and G. Wegener, in *Wood: Chemistry, Ultrastructure, Reactions*, Walter de Gruyter, Berlin, New York, 1984 pp. 6–25.

3 D. Klemm, B. Heublein, H.-P. Fink and A. Bohn, *Angew. Chem., Int. Ed.*, 2005, **44**, 3358–3393.

4 M. Pääkkö, M. Ankerfors, H. Kosonen, A. Nykänen, S. Ahola, M. Österberg, J. Ruokolainen, J. Laine, P. T. Larsson, O. Ikkala and T. Lindström, *Biomacromolecules*, 2007, **8**, 1934–1941.

5 S. Eichhorn, A. Dufresne, M. Aranguren, N. Marcovich, J. Capadona, S. Rowan, C. Weder, W. Thielemans, M. Roman, S. Renneckar, W. Gindl, S. Veigel, J. Keckes, H. Yano, K. Abe, M. Nogi, A. Nakagaito, A. Mangalam, J. Simonsen, A. Benight, A. Bismarck, L. Berglund and T. Peijs, *J. Mater. Sci.*, 2010, **45**, 1–33.

6 A. Isogai, T. Saito and H. Fukuzumi, *Nanoscale*, 2011, **3**, 71–85.

7 I. Sakurada, Y. Nukushina and T. Ito, *J. Polym. Sci.*, 1962, **57**, 651–660.

8 A. Šturcová, G. R. Davies and S. J. Eichhorn, *Biomacromolecules*, 2005, **6**, 1055–1061.

9 M. Paakko, J. Vapaavuori, R. Silvennoinen, H. Kosonen, M. Ankerfors, T. Lindstrom, L. A. Berglund and O. Ikkala, *Soft Matter*, 2008, **4**, 2492–2499.

10 A. N. Nakagaito and H. Yano, *Appl. Phys. A: Mater. Sci. Process.*, 2005, **80**, 155–159.

11 H. Sehaqui, Q. Zhou and L. A. Berglund, *Soft Matter*, 2011, **7**, 7342–7350.

12 A. J. Svagan, M. A. S. A. Samir and L. A. Berglund, *Adv. Mater.*, 2008, **20**, 1263–1269.

13 J.-M. Malho, P. Laaksonen, A. Walther, O. Ikkala and M. B. Linder, *Biomacromolecules*, 2012, **13**, 1093–1099.

14 H. Ougiya, K. Watanabe, Y. Morinaga and F. Yoshinaga, *Biosci., Biotechnol., Biochem.*, 1997, **61**, 1541–1545.

15 S. Varjonen, P. Laaksonen, A. Paananen, H. Valo, H. Hahl, T. Laaksonen and M. B. Linder, *Soft Matter*, 2011, **7**, 2402–2411.

16 S. Arola, T. Tammelin, H. Setälä, A. Tullila and M. B. Linder, *Biomacromolecules*, 2012, **13**, 594–603.

17 J. T. Korhonen, M. Kettunen, R. H. A. Ras and O. Ikkala, *ACS Appl. Mater. Interfaces*, 2011, **3**, 1813–1816.

18 J. R. Capadona, K. Shanmuganathan, D. J. Tyler, S. J. Rowan and C. Weder, *Science*, 2008, **319**, 1370–1374.

19 E. Sjöström, *Wood Chemistry Fundamentals and Applications*, Academic Press,Inc., New York, 2nd edn, 1981, pp. 62–66.

20 S. Bjarnestad and O. Dahlman, *Anal. Chem.*, 2002, **74**, 5851–5858.

21 S. Iwamoto, K. Abe and H. Yano, *Biomacromolecules*, 2008, **9**, 1022–1026.

22 B. Vian, D. Reis, D. Darzens and J. C. Roland, *Protoplasma*, 1994, **180**, 70–81.

23 M. Suchy, E. Kontturi and T. Vuorinen, *Biomacromolecules*, 2010, **11**, 2161–2168.

24 E. L. Hult, P. T. Larsson and T. Iversen, *Polymer*, 2001, **42**, 3309–3314.

25 L.-S. Johansson, T. Tammelin, J. M. Campbell, H. Setala and M. Osterberg, *Soft Matter*, 2011, **7**, 10917–10924.

26 L. D. Gomez, C. G. Steele-King and S. J. McQueen-Mason, *New Phytol.*, 2008, **178**, 473–485.

27 C. Somerville, S. Bauer, G. Brininstool, M. Facette, T. Hamann, J. Milne, E. Osborne, A. Paredez, S. Persson, T. Raab, S. Vorwerk and H. Youngs, *Science*, 2004, **306**, 2206–2211.

28 A. Várnai, L. Huikko, J. Pere, M. Siika-aho and L. Viikari, *Bioresour. Technol.*, 2011, **102**, 9096–9104.

29 G. Antranikian, *Crit. Rev. Biotechnol.*, 1997, **17**, 39–67.

30 T. Oksanen, J. Buchert and L. Viikari, *Holzforschung*, 1997, **51**, 355–360.

31 M. A. Kabel, H. van den Borne, J.-P. Vincken, A. G. J. Voragen and H. A. Schols, *Carbohydr. Polym.*, 2007, **69**, 94–105.

32 J. P. Vincken, A. de Keizer, G. Beldman and A. Voragen, *Plant Physiol.*, 1995, **108**, 1579–1585.

33 T. J. Bootten, P. J. Harris, L. D. Melton and R. H. Newman, *Biomacromolecules*, 2009, **10**, 2961–2967.

34 M. Tenkanen, J. Puls and K. Poutanen, *Enzyme Microb. Technol.*, 1992, **14**, 566–574.

35 M. Tenkanen, G. Gellerstedt, T. Vuorinen, A. Teleman, M. Perttula, J. Li and J. Buchert, *J. Pulp Pap. Sci.*, 1999, **25**, 306–311.

36 S. Ahola, J. Salmi, L. S. Johansson, J. Laine and M. Österberg, *Biomacromolecules*, 2008, **9**, 1273–1282.

37 S. Ahola, X. Turon, M. Österberg, J. Laine and O. J. Rojas, *Langmuir*, 2008, **24**, 11592–11599.

38 M. Andresen, L.-S. Johansson, B. S. Tanem and P. Stenius, *Cellulose*, 2006, **13**, 665–677.

39 L. A. Berglund and T. Peijs, *MRS Bull.*, 2010, **35**, 201–207.

40 I. Díez, P. Eronen, M. Österberg, M. B. Linder, O. Ikkala and R. H. A. Ras, *Macromol. Biosci.*, 2011, **11**, 1185–1191.

41 P. Eronen, K. Junka, J. Laine and M. Österberg, *BioResources*, 2011, **6**, 4200–4217.

42 P. Eronen, M. Österberg, S. Heikkinen, M. Tenkanen and J. Laine, *Carbohydr. Polym.*, 2011, **86**, 1281–1290.

43 M. Henriksson, L. A. Berglund, P. Isaksson, T. Lindström and T. Nishino, *Biomacromolecules*, 2008, **9**, 1579–1585.

44 H. Jin, M. Kettunen, A. Laiho, H. Pynnönen, J. Paltakari, A. Marmur, O. Ikkala and R. H. A. Ras, *Langmuir*, 2011, **27**, 1930–1934.

45 K. Larsson, L. A. Berglund, M. Ankerfors and T. Lindström, *J. Appl. Polym. Sci.*, 2012, **125**, 2460–2466.

46 A. Liu and L. A. Berglund, *Carbohydr. Polym.*, 2012, **87**, 53–60.

47 A. Liu, A. Walther, O. Ikkala, L. Belova and L. A. Berglund, *Biomacromolecules*, 2011, **12**, 633–641.

48 H. Mertaniemi, A. Laukkanen, J. E. Teirfolk, O. Ikkala and R. H. A. Ras, *RSC Adv.*, 2012, **2**, 2882–2886.

49 T. Nypelö, H. Pynnönen, M. Österberg, J. Paltakari and J. Laine, *Cellulose*, 2012, **19**, 779–792.

50 R. T. Olsson, M. A. S. Azizi Samir, G. Salazar Alvarez, L. Belova, V. Strom, L. A. Berglund, O. Ikkala, J. Nogues and U. W. Gedde, *Nat. Nanotechnol.*, 2010, **5**, 584–588.

51 H. Sehaqui, Q. Zhou and L. A. Berglund, *Compos. Sci. Technol.*, 2011, **71**, 1593–1599.

52 H. Sehaqui, Q. Zhou, O. Ikkala and L. A. Berglund, *Biomacromolecules*, 2011, **12**, 3638–3644.

53 J. S. Stevanic, E. M. Bergström, P. Gatenholm, L. Berglund and L. Salmén, *J. Mater. Sci.*, 2012, 1–9.

54 A. J. Svagan, L. A. Berglund and P. Jensen, *ACS Appl. Mater. Interfaces*, 2011, **3**, 1411–1417.

55 A. Mihranyan, A. P. Llagostera, R. Karmhag, M. Stromme and R. Ek, *Int. J. Pharm.*, 2004, **269**, 433–442.

56 E. Saarikoski, T. Saarinen, J. Salmela and J. Seppälä, *Cellulose*, 2012, **19**, 647–659.

Publication IV

Binding properties of single and double cellulose binding modules reveal differences between cellulose substrate. Suvi Arola and Markus B. Linder. Submitted to *Nature Chemical Biology.*

Binding properties of single and double cellulose binding modules reveal differences between cellulose substrate

Suvi Arola[1], and Markus B. Linder[2*]

[1]School of Science, Aalto University, P. O. Box 11100, FI-00076, Aalto, [2] School of Chemical Technology, Aalto University, P .O. Box 16100, FI-00076, Aalto

[*]To whom correspondence should be addressed: Markus B. Linder (Aalto University) markus.linder@aalto.fi, aalto.hyber.fi

Abstract

Here we report for the first time that the binding of *Trichoderma reesei* major cellulase Cel6A and Cel7A cellulose binding modules (CBM) have a very different way of binding to the substrates originating from wood compared to microbial cellulose. Our findings indicate that the CBM proteins see the two substrates, nanofibrillated cellulose and bacterial microcrystalline cellulose, as very different from one another. We show that the substrate has a large impact on the exchange rate of the two CBM, and moreover, that CBM-Cel7A seems to have an extra mode of binding on NFC but not on BMCC. This mode is not translated to the double CBM comprising of CBM-Cel7A and CBM-Cel6A. These results have impact on the cellulase research mostly done with non-wood cellulose substrates and offer new understanding on how these industrially relevant enzymes act.

Introduction

Carbohydrate binding modules (CBMs) are found in a large variety of proteins that are active in one way or another on plant cell walls. These are mainly cellulases but also for example xylanases and mannanases[1–4]. There are several examples of convergent evolution leading to

1

several different protein families with similar function[5]. Especially in bacterial these families are very diverse[6]. Analogously the CBMs can show affinity for chitin and are also found as parts of chitin active proteins[7]. In this work we focus on the type of CBM that is found in fungi and are classified as belonging to Family 1[2,8,9]. These have been the subject of much investigation because of the efficiency and importance of fungal enzyme systems for degrading cellulosic material both as a part of the ecosystem and also increasingly for technical applications[10,11]. These fungal CBMs have a compact structure comprising of only about 35 amino acids[12]. The structure has a stable fold that is referred to as a cysteine knot and which is also found in other small adhesion proteins such as conotoxins[13]. As the name indicates, cysteine knots are stabilized by disulfide bonds and in the case of family 1 CBMs, two or three of them are found. On one face of the folded Family 1 CBM proteins there is a distinctive arrangement of three aromatic residues that has been shown to play a key role in cellulose adhesion. The interaction between aromatics and pyranose rings is widely observed also elsewhere, and it has also been shown that by changing the character of the aromatic residues also the binding characteristics can be changes[14]. In addition to these pi-electron interactions, also hydrogen bonding is involved in forming affinity and specificity between protein and cellulose[12]. The binding is highly specific and shows even selectivity for the different crystalline faces of cellulose[15,16].

The CBMs have proved to play an essential role for how enzymes function. There are effects on both substrate recognition and catalytic activities.[17] The most straightforward explanation of their function is to guide the enzyme towards the substrate and enhance local concentrations on surfaces, but in many cases the role have been found to be more subtle[2]. Another reason for an interest in these CBMs is that they provide a way to modify cellulose through a self-assembly mechanism[18,19]. This can be utilized for protein immobilization[20]. However more recently there

has been a large interest in cellulose as a nanoscale material[21]. By either acid hydrolysis or by mainly mechanical disintegration cellulose fibrils and crystallites are released [22–27]. Because cellulose as a polymer has very attractive mechanical and physical properties many types of advanced materials have been made, including photonic materials and high performance composites[28,29]. Interestingly for example the strength of cellulose surpasses steel on a weight-to-weight comparison.

In this work we set out to gain understanding of both cellulose as a structure and how macromolecular architectures can be designed for adhesion to it by a protein engineering approach using family 1 CBMs. It was already known that linking two CBMs together does affect the overall interaction to a very large extent and that this two-domain interaction can to some extent explain the architecture of cellulose degrading enzymes in general[7]. The thermodynamic principles behind such cooperativity are well known [30] and depend on geometric constraints and the general architecture of the complexes that are formed. We hypothesized that making a series of different linkers between two CBMs could reveal how binding sites are located on the cellulose surface and how the linking of binding modules changes the dynamics of interactions. Using a set of differently designed molecules, different sources of cellulose, and accurate measurement techniques enabling the study of binding kinetics allowed a new set of tools to investigate cellulose for use as a material or for the enzymatic breakdown of it.

Results

Analysis of proteins

DCBM-12, -24, and 48 were produced as HFBI-DCBM fusions to aid the purification. Different DCBM proteins were gained by trypsin cleavage of the corresponding HFBI-DCBM.

The CDB-Cel7A and CBM-Cel6A were gained by papain cleavage of HFBI-DCBM-12. Amino acid analysis (AAA) of the fractions from RP-HPLC run after papain cleavages showed the identity of the two fractions; i.e. which of them CBM-Cel7A was and which CBM-Cel6A.

Matrix-assisted laser desorption/ionization mass spectrometry (MALDI-TOF MS) was used to verify the amount of linker region present in the proteins and the extent of glycosylation of the proteins. According to MALDI-TOF DCBM-24 contained14-25 glycan groups and DCBM-48 34-50. Both of the proteins contained multiple O-glycosylation sites on the linker (T, S, see figure S1 for sequences), DCBM-48 double the amount of DCBM-24. The glycosylation patterns were heterogenic and showed a broad peak at m/z ~12730-14500 (DCBM-24) and m/z ~18400-20730 (DCBM-48). DCBM-12 and the single CBMs were not glycosylated. There were no broad peaks on their MALDI-TOF spectra nor do the peaks on the spectra contain differences by m/z 162 (hexose) or m/z 203 (GlcNAc). The multiple peaks on their spectra come from a varying lengths of linker attached on them. Especially the CBM-Cel6A protein that was cleaved by papain showed variation in the linker length on both sides, the main peak was at m/z 5414. CBM-Cel7A main peak was at m/z 3850 (CBM-Cel7A + serine from linker) and minor peaks referring to CBM-Cel7A only (m/z 3763) and CBM-Cel7A + one to four threonine residues. DCBM-12 has a major peak at m/z 9039 and minor peaks showing that trypsin has cleaved on both sides of the arginine in the linker sequence between HFBI and DCBM-12.

Binding isotherms

Figure 1 shows the binding isotherms of CBMs and DCBMs on A: BMCC, and B: on NFC. On BMCC an increase in affinity was seen for DCBM-12 and DCBM-24 constructs compared to single CBMs. Linker length affects the binding of the double constructs; DCBM-48 construct

shows lower affinity compared to DCBM-12 and DCBM-24 and CBM-Cel7A. DCBM-24 shows the highest affinity.

On NFC for the DCBMs the linker length affected the binding in the same way as on BMCC; DCBM-24 and DCBM-12 having a higher affinity than DCBM-48 and CBM-Cel6A having the lowest affinity. On NFC there was no advantage of linking CBM-Cel7A and CBM-Cel6A together because CBM-Cel7A had the highest affinity on its own. Table 1 summarizes the partitioning coefficients, K_r, obtained from the data in the beginning of the isotherm. The corresponding affinities, k_d, and maximum binding capacities, B_{max}, are presented in supplementary table 1. Table 2 shows that the correlation of K_r-values of the five proteins between two substrates. This correlation is consistent for all other proteins being 1.5 except for CBM-Cel7A being much higher 3.6. This indicates clearly that CBM-Cel7A behaves differently on the two substrates compared to the other proteins.

The Gibbs free energy of binding, ΔG

For the calculation of Gibb's free energy for binding the binding capacity, B_{max}, is needs. Binding isotherms with larger protein concentrations (up to 50 µM free protein concentration) are presented for all proteins on both substrates in semi-logarithmic plots in figure 2A-D. The maximum binding capacities obtained from this data are presented in table 3. The linear forms of the binding isotherm graphs are presented in supplementary figure 2. The data with higher protein concentrations shows that CBM-Cel7A binds with a greater capacity than any of the other proteins on both substrates. The data also shows that the single CBMs are far from their actual maximum binding capacities, although substantial amount of protein was used in the experiments. On the other hand, it can be seen that the maximum binding capacity of DCBM-48

has been reached on both substrates, and that DCBM-12 and -24 are not far from their maximum capacities. These values for DCBM-48 can be used to calculate accurate Gibb's free energies, ΔG, for the binding event using equation (4) presented in Online methods. To calculate an estimated range of the ΔG-value for the other proteins on both substrates, we used the K_r-values obtained from the initial slope of the data and varied the B_{max}-value in equation (4). We used three B_{max}-values; B_{max}, low, which was obtained from data in figure 2 and which is lower than the actual B_{max} for all other proteins than DCBM-48, a double that of the low value (B_{max}, intermediate), and a triple that of the low value (B_{max}, high). A schematic illustration of the three B_{max} –value levels are presented in supplementary figure 3 with the binding isotherm for CBM-Cel7A on NFC to illustrate the range of B_{max}-values.

Table 4 summarizes ΔG-values for the different binding events. From table 4 it is evident that the free energies of binding are lower for DCBM-proteins than for CBM-proteins. Thus the binding of DCBMs is more favorable than CBMs. The differences for the ΔG-values are not very large between different DCBMs. We can also see that ΔG-values for CBM-CeI7A on NFC and BMCC are very close to each other and also to the ones obtained for CBM-Cel6A. The ΔG-values for DCBMs are also very close to each other for both substrates indicating that the binding is energetically similar for the double constructs on both substrates. Since the peculiar binding of CDB-Cel7A cannot be explained by energetic differences of the binding events, it seems to a matter of geometry or the substrate or both.

Xylanase assay for CBM-Cel7A

There is roughly 27 % xylan in the NFC material that we use. Of this, 30 % can be specifically hydrolyzed by pI9 xylanase from *T. reesei*, which corresponds to about 10 % loss of

the total mass. To test how the xylan on NFC affects the CBM-Cel7A binding we used xylanase pI9 enzyme to hydrolyze xylan from NFC and tested the binding of CBM-Cel7A on this xylanase treated NFC compared to non-treated NFC. The binding of CBM-Cel7A increased about 20% on the xylanase treated NFC compared to the control. These results suggest that the xylan hydrolysis opens up substantial amount of binding sites on NFC for CBM-Cel7A rather than the CBM-Cel7A binding to xylan.

Nanoscale effect of the NFC substrate

Since NFC has not been widely used as a substrate for CBMs in binding studies it could be that the nanoscale structure somehow induces a boost in CBM-Cel7A affinity. To test this we performed binding studies on the pulp material that the NFC was prepared from. The binding isotherm is shown in supporting information figure S4. The order of binding is the same for the proteins CBM-Cel7A having greater affinity and capacity and thus partitioning coefficient than the DCBMs and CBM-Cel6A. The K_r-values are very close to those obtained for NFC and thus the binding is the same regardless of the nanoscale structure.

Exchange rates of CBM and DCBM on NFC and BMCC

Next, to investigate the kinetics of the bindings, we performed a series of experiments to measure the extent of exchange of proteins from the substrate surface. At equilibrium exactly the same amount of non-labelled protein initially used for the equilibrium reaction at concentration equal to free protein concentration was added to reaction mixture. The amount of ^{3}H-protein in solution was monitored during time and compared to the original amount of ^{3}H-protein at equilibrium state. The results presented in figure 5 shows that the only combination of protein

and substrate that fully exchange to 50% from the original amount of ^{3}H-protein bound are CBM-Cel7A and CDB-Cel6A on BMCC. The exchange of these two proteins on BMCC is fast and fully reversible. On the other hand, none of the DCBMs on BMCC exchanged fully during the time course of the experiment (3600 s). DCBM-12 and DCBM-24 exchange roughly to 10% and DCBM-48 exchanges roughly to 30%. The coupling of the CBMs together clearly hinders the exchange rate. On NFC none of the proteins fully exchange to 50% during the time course of the experiment. The CBMs exchange roughly to 20% showing that the exchange rate is a lot slower for these proteins on NFC compared to BMCC. The DCBMs exchange even slower on NFC than the CBMs showing again that the coupling of the individual pieces together affects the exchange rate by slowing it down. The DCBM-24 seems not to exchange at all from NFC during the time course of the experiment and DCBM-12 and -48 exchanges roughly to 5-10%.

Discussion

By studying the binding initially on BMCC we observed that there was a significant effect of the linker length to the binding properties of the DCBM proteins. The data at low protein concentrations was highly reproducible between experiments due to the excellent accuracy of analytical technique based on scintillation counting (Figure 1). As a measure of affinity we calculated partitioning coefficients ($K_r = B_{max}/k_d$). This coefficient was obtained by fitting the equation for a one-site Langmuir isotherm (equation (1)) to the data and using the values for k_d and B_{max} that were obtained. We note that the uncertainty of the B_{max} (and hence the k_d) is large when only using initial parts of the isotherms for fitting, as will be discussed below. However, the ratio K_r can be reliably estimated since it is mathematically equal to the limit of the derivative of the one-site Langmuir equation as the concentration of free protein approaches zero.

Since this part of the curve is accurate we obtain a reliable value for this ratio. The ratio can also be thought of as the partitioning of free and bound protein at low concentrations when competition for binding sites is negligible. As presented in Table 1 the DCBM-24 shows the highest K_r, closely followed by DCBM-12. Interestingly the CBM-Cel7A showed an affinity that was higher than the DCBM-48, and the CBM-Cel6A showed the lowest K_r. When the experiments were repeated with birch wood NFC a surprising difference was noticed. For NFC the clearly highest partitioning was found for CBM-Cel7A. The rest of the constructs showed the same relative order of affinity although the affinities were higher overall. To investigate the difference between BMCC and NFC more closely we calculated the ratio of K_r-values for each protein at the two different substrates (Table 2). The ratios for the partitioning coefficients were about 1.5 for all proteins except CBM-Cel7A. This indicates that the substrates are seen by these proteins in a very similar way, except that the NFC as expected has 1.5 times more surface area per weight than the BMCC. The CBM-Cel7A on the other hand has a very high partitioning coefficient on NFC, but also the ratio as calculated in Table 2 is over twice that of the other constructs. We can deduce that the CBM-Cel7A can find some binding mode or site on NFC that is not found on BMCC, and which is not found by CBM-Cel6A. Some feature in NFC is available for CBM-Cel7A that does not exist in BMCC, but all other constructs behave identically in relation to each other on the two substrates. It is especially notable that the synergies between modules seen for the DCBM-12 and DCBM-24 constructs are not able to incorporate this extra mode of binding for CBM-Cel7A.

Next we evaluated if full isotherms, allowing the calculation of binding energies would be feasible. Data points were collected at very high protein concentrations. These data points are showed in semi-log plots in Figure 2. The highest protein concentrations were around 50 µM. At

these concentrations only about 1-10 % (DCBM) or 20 % (CBM) of the total protein are bound to cellulose. Due to the high overall protein concentrations and low percentage of total protein bound to cellulose it was not feasible to acquire data points at even higher concentrations. We note that for the DCBM constructs the capacity levels off to a value that can be reliably determined but in the case of the free modules the estimated capacities may be too low. Because these values are likely to be too low it can lead to an error in the estimation of change in ΔG.

The change in free energy was calculated using standard equations (equation (4) in methods). We then used upper and lower estimates of B_{max} (see Supplementary Fig. 3) to evaluate the value of ΔG (Table 4). This allowed us to estimate the degree of synergy in the DCBM constructs. The ΔG values show clearly that in all DCBM constructs there is a synergy that comes from the linkage. It is thus energetically favorable for the proteins to be linked together.

We next considered how differences between the two substrates could explain the observations. The most obvious difference between NFC and BMCC is their polysaccharide composition: BMCC is pure cellulose whereas NFC has, in addition to cellulose, roughly 27% xylan[31]. To try and understand the difference in binding sites available for CBM-Cel7A on NFC but not on BMCC, we thus investigated how the hydrolysis of xylan affected the binding. This was done by using xylanase to hydrolyse xylan from NFC and to study the binding of CBM-Cel7A on this substrate. The results showed that the binding of CBM-Cel7A was increased about 20% by the xylanase treatment. This indicates that the xylan hydrolysis opens up substantial amounts of binding sites on NFC for CBM-Cel7A. From this it seems not plausible that the greater binding affinity of CBM-Cel7A on NFC would be caused by an affinity towards xylan. However, it could be that CBM-Cel7A binds to xylan but when xylan is released it binds to cellulose with a much larger affinity. In this case we could expect to see small differences in the

binding behavior of CBM-Cel7A to hydrolyzed and non-hydrolyzed NFCs since surface area of the fibrils is not changed drastically by hydrolysis of xylan from the fibril surface[31], and it is not expected that these proteins bind elsewhere in the fibril than on the surface[16,17]. On the other hand, it seems still more logical that xylan inhibits the binding of CBM by masking the cellulose surface. This has been shown with cellulases, that xylanase are needed in order for the cellulases to fully hydrolyze NFC[32]. We show that the binding of CBM-Cel7A is greatly affected by xylan hydrolysis and this also suggests that at least partly the xylan available for the xylanase is located on the surface of the fibril at the CBM binding sites.

As the peculiar binding of CBM-Cel7A could not be explained by the xylan content, we sought answers from another difference between the substrates: the nanoscale architecture. NFC from wood source has not been widely used for CBM binding studies; usually substrates include BMCC, Avicel, tunicin and Valonia cellulose. The mechanical processing of pulp to NFC and the nanoscale structure could potentially have affected the substrate in adding features, which are not present in BMCC. To investigate this, we performed similar binding studies on the pulp material from which the NFC is prepared. The results showed that pulp has much less surface are for the proteins to bind but it is seen as the same material as NFC by the proteins since the partitioning coefficients of the proteins on pulp were very close to those obtained for NFC and the order of the binding was the same; namely CBM-Cel7A having the greatest affinity. The results show that cellulose substrate from wood source, no matter how fine or coarse the structures, is seen in a different way by CBM-Cel7A than BMCC. The source of the material seems to count for the protein.

A third difference between the two substrates is their crystalline structure; wood cellulose crystalline regions composing mainly of cellulose I_β and BMCC of cellulose I_α. Also wood

cellulose amorphous to crystalline ratio is different than that of BMCC; BMCC being more crystalline.[26,33,34] This could be of great significance for the two proteins having a difference of one amino acid residue in their binding faces[7,12,35]. We next studied the exchange rate of the different constructs on the two substrates in order to evaluate if they show differences. This was done by equilibrium exchange experiments where the extent of exchange of ^{3}H-labelled protein is determined by competition with unlabeled protein. From the results presented in Figure 3 it was evident that the coupling of the individual CBM together greatly reduced the extent of exchange. On BMCC both CBM alone fully exchange to 50% of the original within the time scale of the experiment (<600 s) and thus the binding can be considered truly reversible and fast (Figure 3 B). The linking slowed the exchange rate and the extent of exchange to only 10-30% for the DCBM constructs (Figure 3 D). On NFC, the exchange of the individual CBM did not reach 50% from the original amount of bound ^{3}H-protein (Figure 3 A) and the exchange was thus markedly slower than for BMCC. This more slow exchange from NFC for the CBM-Cel7A and CBM-Cel6A both could be due to the different structure of NFC compared to BMCC. The exchange of DCBM constructs was even slower from NFC than those of CBM (Figure 3 C) and thus consistent with results on BMCC: linking the two CBM together slows down the exchange rate. These results suggest that CBM-Cel7A and CBM-Cel6A both experience NFC as a different substrate compared to BMCC, yet is doesn't provide a good explanation on why the CBM-Cel7A has a boost in affinity on NFC and why the DCBM proteins do not exhibit this property.

One way would be to experiment whether the two proteins compete on binding sites on the two substrates fully, partially or not at all and if there would be differences between the competitions on different substrates, i.e. to see if the binding of the one is affected by the

presence of the other. This was examined by competing labelled CBM with unlabeled CBM of the same kind and of different and comparing the results (experimental and data in supplementary materials, supplementary Fig 6.). The results showed that both proteins are affected by the presence of the other in a same way as they are affected by the presence of the unlabeled protein of the same kind. This suggests full competition of the CBM-Cel7A and CBM-Cel6A on both substrates and it does not provide straight forward answers to the deviant binding behavior of CBM-Cel7A on NFC.

In conclusion, we were able to show that the linker length plays a critical role in protein constructs with two binding units, in our case the CBM proteins. We showed that the linking provides an increase in affinity at certain lengths for DCBM constructs and it increases the affinity when the proteins binding to BMCC. On the other hand, we were able to show that CBM-Cel7A binding to NFC substrate behaved in a very different way than was expected. The CBM-Cel7A had an increased affinity compared to the DCBM and to the CBM-Cel6A, and the linking of the individual CBM proteins was not favorable affinity or capacity vise. However, the linking of the CBM proteins together was shown to be energetically more favorable, and is beneficial in this regard.

The increased affinity of CBM-Cel7A was shown not to be induced by the nanoscale structure of NFC nor the xylan content. However, we were able to show that the exchange rate of the proteins is greatly dependent on the substrate, since individual CBD proteins exchange reversibly from BMCC but not from NFC. Moreover, the extent of exchange was dependent on the linking; the DCBM constructs exchanged much slower than the CBM proteins on both substrates.

Our findings indicate that the CBM-Cel7A sees the two substrates, NFC and BMCC, as very different from one another. It seems to have another binding mode on NFC rather than another binding site, since we saw no evidence on non-competitive binding of the two CBM on NFC. The other mode of binding of Cel7A-CBM is not translated to the DCBM constructs, since the affinity of DCBM constructs on NFC is lower than that of CBM-Cel7A. It seems that the linking of CBM-Cel7A together with CBM-Cel6A inhibits the other binding mode of CBM-Cel7A, and causes the DCBM construct to behave more like a double CBM-Cel6A. We show for the first time that for the binding of CBM onto substrate the substrate origin matters greatly and results gained from experiments on one substrate are not comparable to results gained with another substrate, or at least the comparison should be done by caution.

Our results can offer new consideration for cellulase studies, especially to the energetics of the cellulase binding. It is clearly more favorable for the enzyme to bind to a substrate together with the CBM than without it[36,37]. The gain seems to be also in the energetics of the binding because the DCBM binding, regardless of the linker length, is more favorable than the binding of an individual CBM. Our results also raise a question whether it is somehow evolutionary that the CBM-Cel7A recognizes wood cellulose with a higher affinity than other cellulose materials because wood is the primary source of energy for the organism is originates from?

Acknowledgements

Authors Contribution

S.A. planned and carried out all experimental work, except for protein production that was conducted by Michael Bayley, and protein cleavage and subsequent protein purificaton which was done by Riitta Suihkonen. S.A. prepared all figures. S.A. and M.B.L. wrote the manuscript together. M.B.L. supervised the research.

Figure Legends

Figure 1. **(A)** The beginning of the binding isotherms of Ce-7A, Cel6A, DCBM-12, DCBM-24, and DCBM-48 on BMCC. **(b)** The beginning of the binding isotherms of Ce-7A, Cel6A, DCBM-12, DCBM-24, and DCBM-48 on NFC. (+) CBM-CeI7A, (x) CBM-Cel6A, (□) DCBM-12, (○) DCBM-24, (Δ) DCBM-48.

Figure 2. **(A)** Semi-logarithmic plots of the binding isotherms of CBM-Cel7A and CBM-Cel-6A on NFC. **(B)** Semi-logarithmic plots of the binding isotherms of CBM-Cel7A and CBM-Cel-6A on BMCC. **(C)** Semi-logarithmic plots of the binding isotherms of DCBM-12, DCBM-24, and DCBM-48 on NFC. **(D)** Semi-logarithmic plots of the binding isotherms of DCBM-12, DCBM-24, and DCBM-48 on BMCC. (+) CBM-Cel7A, (x) CBM-Cel6A, (□) DCBM-12, (○) DCBM-24, (Δ) DCBM-48.

Figure 3. (A) Exchange of ^{3}H-labelled CBM-Cel7A and CBM-Cel6A from NFC. **(B)** Exchange of ^{3}H-labelled CBM-Cel7A and CBM-Cel6A from BMCC. **(C)** Exchange of ^{3}H-labelled DCBM-12, DCBM-24, and DCBM-48 from NFC. **(D)** Exchange of ^{3}H-labelled DCBM-12, DCBM-24, and DCBM-48 from BMCC. (+) CBM-CBHI, (x) CBM-CBHII, (□) DCBM-12, (○) DCBM-24, (Δ) DCBM-48

Tables

Table 1. The partitioning coefficients ($K_r = B_{max}/K_d$) for single and double CBM obtained from the Langmuir isotherm fitted to the data on Figure 1 A and B

	CBM-Cel7A	CBM-Cel6A	DCBM-12	DCBM-24	DCBM-48
BMCC	1,4	0,61	2,47	2,82	1,07
NFC	4,98	1,05	3,87	4,18	1,67

Table 2. The correlations of partitioning coefficients, K_r, for single and double CBM between NFC and BMCC calculated from K_r-values in table 1

	CBM-Cel7A	CBM-Cel6A	DCBM-12	DCBM-24	DCBM-48
K_r^{NFC}/K_r^{BMCC}	3,57	1,72	1,56	1,49	1,56

Table 3. Binding capacities, B_{max}, for single and double CBM on NFC and BMCC obtained from the data shown in figure 2[*]

	CBM-Cel7A	CBM-Cel6A	DCBM-12	DCBM-24	DCBM-48
BMCC	8,20	5,78	4,01	4,09	1,07
NFC	18,24	10,74	9,21	8,61	4,05

[*]The unit of B_{max} is µmol/g

Table 4. Gibb's free energy difference for the binding, ΔG, for CBM-Cel7A, CBM-Cel6A, DCBM-12, DCBM-24, and DCBM-48 on NFC and BMCC.

substrate	B_{max}*	CBM-Cel7A	CBM-Cel6A	DCBM-12	DCBM-24	DCBM-48
NFC	low	-30,7	-28,2	-31,8	-32,1	
	inter	-29,0	-26,5	-30,1	-30,4	-31,7
	high	-28,0	-25,5	-29,1	-29,4	
BMCC	low	-29,6	-28,4	-32,7	-33,0	
	inter	-27,9	-26,7	-31,0	-31,3	-33,9
	high	-26,9	-25,7	-30,0	-30,3	

* B_{max}-value for DCBM-48 from data in figure 2 is an accurate value, thus it can be used to calculate the exact binding energy associated with the binding event. The ΔG-values for CBM-Cel7A, CBM-Cel6A, DCBM-12 and DCBM-24 are estimates (see supplementary information for the estimation, supplementary Fig. 3). B_{max}, low is the value gained from data on figure 2, inter is 2x (B_{max}, low), and high is 3x(B_{max}, low). The unit of ΔG is kJ/mol.

Methods

Protein production and purification

The DCBMs were produced as HFBI-DCBM fusions in *T. reesei* (sequences shown in supplementary information, figure S1) and the following transformants were used: VTT-D-133335 (HFBI-DCBM-12), VTT-D-133336 (HFBI-DCBM-24), and VTT-D-133337 (HFBI-DCBM-48). The strains were then cultivated in 7 L bioreactors on media containing 50 vol-% spent grain extract, 60 g/L lactose, 1 g/L yeast extract, 4 g/L KH2PO4, 2.8 g/L (NH4)2SO4, 0.6 g/L MgSO4 · 7H2O, 0.8 g/L CaCl2 · 2H2O, 2 ml/L trace solution. The pH was let to drop from 5

to about 3 during cultivation. At 24 h intervals 48 mg pepstatin A and 28 mg soy bean trypsin inhibitors (both from Sigma-Aldrich) were added to the cultures to minimize protein degradation. The culture supernatants were separated from the biomass by filtration through GF/A filters (Whatman). Protein expression levels were analyzed by RP-UPLC and were 0.2 g/L, 0.4 g/L, and 3.0 g/L for HFBI-DCBM-12, -24, and -48, respectively. The proteins were purified using aqueous two phase extraction and reverse-phase high-performance liquid chromatography (RP-HPLC) as described earlier29 followed by lyophilization.

Protein preparation

The fusion proteins were cleaved with sequencing grade modified trypsin (Promega) in 25mM Tris-HCl – 150mM NaCl buffer for 2 hours in room temperature to yield DCBMs. The trypsin digestion reaction was followed by RP-UPLC using a 2.1 x 100 mm, 1.7 µm, C4 Acquity BEH300 prST column and an Acquity I-Class system with a photodiode array detector (Waters, MA, USA). The proteins were eluted in a linear mobile phase gradient from 20 – 60% B using water (A) and acetonitrile (B), both containing 0.1% trifluoroacetic acid. Concentrations of the analysed proteins were determined using standard samples with protein concentrations determined by amino acid analysis (Amino Acid Analysis Lab, Uppsala University, Sweden).

In a similar fashion, the HFBI-DCBM-12 was cleaved using papain (Sigma), in 0.1 mM Sodium Phosphate buffer pH 7 for o/n in room temperature to yield CBM-Cel7A and CBM-Cel6A. The papain cleavage was followed and the proteins were purified as described above for the trypsin cleavage. The identity of the individual CBMs were verified by amino acid analysis (Amino Acid Analysis Lab, Uppsala University, Sweden) and matrix-assisted laser desorption/ionization – time of flight mass spectrometry (MALDI-TOF MS, Brucer Autoflex II

MALDI-TOF). MALDI-TOF was also used to analyze the extent of glycosylation of the DCBMs and CBMs.

Protein labelling

All five proteins were labelled with tritium for interaction studies by reductive methylation as reported previously[7,18,38]. 1.9 mg of lyophilized protein was dissolved in 1.9 mL of 0.2 M borate buffer, pH 8.96 and cooled on an ice bath. 13.2 µL of 0.37 % formaldehyde and 100 mCi of 3H enriched NaBH4 (10 Cimmol-1, NET023H100MC, PerkinElmer) in 150 µL of 0.01 M NaOH were added and reacted for 30 minutes, gently mixing every now and then. The reaction was terminated by RP-HPLC. The specific activities were 0.52 Cimmol-1 for DCBM-12, 0.69 Cimmol-1 for DCBM-24 and 1.25 Cimmol-1 for DCBM-48.

Binding isotherms

Binding studies were done essentially in the same way as reported previously[18,38–40]. Shortly, a 100 µM stock solution of DCBM and CBM containing 10 % 3H–labelled proteins in 100 mM sodium acetate buffer (pH 5.0) with 100 mM NaCl and 0.1% BSA was prepared. Solutions with different fusion protein concentrations were made from the stock solution by diluting with the same buffer. The BSA was used to minimize nonspecific binding of the proteins to test tube walls and filters. 100-200 µL of each protein solution was mixed with an equal volume of 1-2 g L-1 NFC in MilliQ–water (or 1.28 g L-1 BMCC) and stirred in ambient temperature with 250 rpm for 1 h. After equilibration, the suspensions were filtered through disposable filters (Millipore, Millex®–GV filter unit, PVDF, hydrophilic, 0.22 µm, 13 mm, non–sterile) and the

amount of free protein was determined by liquid scintillation counter (PerkinElmer, Tri-Carb 2810TR) from the filtrate.

Xylanase assay

The pI9 xylanase of *T. reesei* was used to hydrolyze xylan from NFC[41]. The enzyme specifically hydrolyses xylan from NFC as described by previous reports[31]. The hydrolysis of NFC was carried out for 24h in 45 °C and a control NFC was treated exactly the same but without xylanase. The hydrolysed and non-hydrolysed NFC was used to study the effect of xylan hydrolysis with CBM-Cel7A using a 2.5 µM stock solution of the CBM containing 10% 3H-labelled protein. 100 µL of either the NFC were let to reach equilibrium with 100 µL of the protein solution. The reactions were ended by filtrating and the amount of free protein was measured by liquid scintillation counter.

Exchange rate assay

The exchange rate experiments were done according to previous reports[35,42]. Shortly, to determine the equilibrium exchange rates for CBM and DCBM on both BMCC and NFC, 3H-labelled proteins were allowed to react with the same unbound protein. A 100 µL aliquot of BMCC (1.28 g L-1) or NFC (2 g L-1) was allowed to react with 100 µL of the 3H-labelled protein. When equilibrium was reached the same amount of unlabeled protein was added. The reaction was stopped by filtering the sample after a certain time (11-3600s) from dilution. The concentration of the added protein was equal to the concentration of the free protein in the equilibrium reaction. By this way the equilibrium was not affected, but only the amount of labelled protein in the solution was diluted. The experiments were carried out by taking multiple

time points from a set of parallel samples and comparing to the original equilibrium concentration of the protein.

Calculations used for Gibb's free energy difference

Langmuir one-site binding model is written in equation (1).

$$B = \frac{[B_{max}] \times [Free]}{k_d \times [Free]} \tag{1},$$

where B_{max} is the maximum binding capacity, k_d is the binding affinity, and [Free] is the concentration of the free protein. When the free protein concentration approaches zero the initial slope for Langmuir isotherm is written as follows in equation (2):

$$B'_{[Free] \to 0} = \frac{[B_{max}]}{k_d} = K_r \tag{2}$$

where K_r is the partitioning coefficient and describes the relation of adsorption and desorption at very low protein concentrations. Gibb's free energy is written as follows,

$$\Delta G = RTln(K_d) \tag{3},$$

where K_d is the dissociation constant, which is comparable to the binding affinity k_d, and thus the equation can be written in terms of the B_{max} and K_r, using equation 2, as shown in equation 4,

$$\Delta G = RT(ln(B_{max}) - ln(K_r)) \tag{4},$$

where R is the universal gas constant and T is temperature.

References

1. Henrissat, B. Cellulases and their interaction with cellulose. *Cellulose* **1,** 169–196 (1994).

2. Várnai, A. *et al.* Carbohydrate-Binding Modules of Fungal Cellulases. Occurrence in Nature, Function, and Relevance in Industrial Biomass Conversion. *Adv. Appl. Microbiol.* **88,** 103–165 (2014).

3. Hägglund, P. *et al.* A cellulose-binding module of the Trichoderma reesei β-mannanase Man5A increases the mannan-hydrolysis of complex substrates. *J. Biotechnol.* **101,** 37–48 (2003).

4. Raghothama, S. *et al.* Solution structure of the CBM10 cellulose binding module from pseudomonas xylanase A. *Biochemistry* **39,** 978–984 (2000).

5. Stern, D. L. The genetic causes of convergent evolution. *Nat. Rev. Genet.* **14,** 751–64 (2013).

6. Conant, G. C. & Wagner, A. Convergent evolution of gene circuits. *Nat. Genet.* **34,** 264–266 (2003).

7. Linder, M., Salovuori, I., Ruohonen, L. & Teeri, T. T. Characterization of a Double Cellulose-binding Domain. *J. Biol. Chem.* **271,** 21268–21272 (1996).

8. Linder, M. & Teeri, T. T. The roles and function of cellulose-binding domains. *Journal of Biotechnology* **57,** 15–28 (1997).

9. Tomme, P. & Warren, R. *Cellulose-binding domains: classification and properties. ACS Symposium Series, American Chemical Society* (1995). doi:10.1021/bk-1995-0618

10. Viikari, L., Vehmaanperä, J. & Koivula, A. Lignocellulosic ethanol: From science to industry. *Biomass and Bioenergy* **46,** 13–24 (2012).

11. Wilson, D. B. Cellulases and biofuels. *Current Opinion in Biotechnology* **20,** 295–299 (2009).

12. Linder, M. *et al.* Identification of functionally important amino acids in the cellulose-binding domain of Trichoderma reesei cellobiohydrolase I. *Protein Sci.* **4,** 1056–1064 (1995).

13. Daly, N. L. & Craik, D. J. Structural studies of conotoxins. *IUBMB Life* **61,** 144–150 (2009).

14. Linder, M., Lindeberg, G., Reinikainen, T., Teeri, T. T. & Pettersson, G. The difference in affinity between two fungal cellulose-binding domains is dominated by a single amino acid substitution. *FEBS Lett.* **372,** 96–98 (1995).

15.   Lehtiö, J. *et al.* The binding specificity and affinity determinants of family 1 and family 3 cellulose binding modules. *Proc. Natl. Acad. Sci. U. S. A.* **100,** 484–489 (2003).

16.   Igarashi, K. *et al.* Traffic jams reduce hydrolytic efficiency of cellulase on cellulose surface. *Science* **333,** 1279–1282 (2011).

17.   Igarashi, K. *et al.* High speed atomic force microscopy visualizes processive movement of Trichoderma reesei cellobiohydrolase I on crystalline cellulose. *J. Biol. Chem.* **284,** 36186–36190 (2009).

18.   Varjonen, S. *et al.* Self-assembly of cellulose nanofibrils by genetically engineered fusion proteins. *Soft Matter* **7,** 2402 (2011).

19.   Laaksonen, P. *et al.* Genetic engineering of biomimetic nanocomposites: Diblock proteins, graphene, and nanofibrillated cellulose. *Angew. Chemie - Int. Ed.* **50,** 8688–8691 (2011).

20.   Levy, I. & Shoseyov, O. Expression, refolding and indirect immobilization of horseradish peroxidase (HRP) to cellulose via a phage-selected peptide and cellulose-binding domain (CBD). *J. Pept. Sci.* **7,** 50–57 (2001).

21.   Klemm, D. *et al.* Nanocelluloses: A new family of nature-based materials. *Angewandte Chemie - International Edition* **50,** 5438–5466 (2011).

22.   Fleming, K., Gray, D. G. & Matthews, S. Cellulose crystallites. *Chem. - A Eur. J.* **7,** 1831–1835 (2001).

23.   De Souza Lima, M. M. & Borsali, R. Rodlike cellulose microcrystals: Structure, properties, and applications. *Macromol. Rapid Commun.* **25,** 771–787 (2004).

24.   Beck-Candanedo, S., Roman, M. & Gray, D. G. Effect of reaction conditions on the properties and behavior of wood cellulose nanocrystal suspensions. *Biomacromolecules* **6,** 1048–1054 (2005).

25.   Henriksson, M., Henriksson, G., Berglund, L. a. & Lindström, T. An environmentally friendly method for enzyme-assisted preparation of microfibrillated cellulose (MFC) nanofibers. *Eur. Polym. J.* **43,** 3434–3441 (2007).

26.   Pääkko, M. *et al.* Enzymatic hydrolysis combined with mechanical shearing and high-pressure homogenization for nanoscale cellulose fibrils and strong gels. *Biomacromolecules* **8,** 1934–1941 (2007).

27.   Nakagaito, A. N. & Yano, H. The effect of morphological changes from pulp fiber towards nano-scale fibrillated cellulose on the mechanical properties of high-strength plant fiber based composites. *Appl. Phys. A Mater. Sci. Process.* **78,** 547–552 (2004).

28. Aulin, C., Salazar-Alvarez, G. & Lindström, T. High strength, flexible and transparent nanofibrillated cellulose–nanoclay biohybrid films with tunable oxygen and water vapor permeability. *Nanoscale* **4,** 6622 (2012).

29. Purandare, S., Gomez, E. F. & Steckl, A. J. High brightness phosphorescent organic light emitting diodes on transparent and flexible cellulose films. *Nanotechnology* **25,** 094012 (2014).

30. Mammen, M., Choi, S.-K. & Whitesides, G. M. Polyvalent Interactions in Biological Systems: Implications for Design and Use of Multivalent Ligands and Inhibitors. *Angew. Chemie Int. Ed.* **37,** 2754–2794 (1998).

31. Arola, S., Malho, J., Laaksonen, P., Lille, M. & Linder, M. B. The role of hemicellulose in nanofibrillated cellulose networks. *Soft Matter* **9,** 1319 (2013).

32. Várnai, A., Huikko, L., Pere, J., Siika-aho, M. & Viikari, L. Synergistic action of xylanase and mannanase improves the total hydrolysis of softwood. *Bioresour. Technol.* **102,** 9096–9104 (2011).

33. Wada, M., Sugiyama, J. & Okano, T. Native celluloses on the basis of two crystalline phase (Iα/Iβ) system. *J. Appl. Polym. Sci.* **49,** 1491–1496 (1993).

34. Czaja, W., Romanovicz, D. & Brown, R. malcol. Structural investigations of microbial cellulose produced in stationary and agitated culture. *Cellulose* **11,** 403–411 (2004).

35. Carrard, G. & Linder, M. Widely different off rates of two closely related cellulose-binding domains from Trichoderma reesei. *Eur. J. Biochem.* **262,** 637–643 (1999).

36. Kim, D. W., Jang, Y. H. & Jeong, Y. K. Adsorption behaviors of two cellobiohydrolases and their core proteins from Trichoderma reesei on Avicel PH 101. *Biotechnol. Lett.* **19,** 893–897 (1997).

37. Ståhlberg, J., Johansson, G. & Pettersson, G. A New Model For Enzymatic Hydrolysis of Cellulose Based on the Two-Domain Structure of Cellobiohydrolase I. *Bio/Technology* **9,** 286–290 (1991).

38. Carrard, G. & Linder, M. Widely different off rates of two closely related cellulose-binding domains from Trichoderma reesei. *Eur. J. Biochem.* **262,** 637–643 (1999).

39. Linder, M. & Teeri, T. T. The cellulose-binding domain of the major cellobiohydrolase of Trichoderma reesei exhibits true reversibility and a high exchange rate on crystalline cellulose. *Proc. Natl. Acad. Sci. U. S. A.* **93,** 12251–12255 (1996).

40. Palonen, H., Tenkanen, M. & Linder, M. Dynamic interaction of Trichoderma reesei cellobiohydrolases Cel6A and Cel7A and cellulose at equilibrium and during hydrolysis. *Appl. Environ. Microbiol.* **65,** 5229–5233 (1999).

41.   Tenkanen, M., Puls, J. & Poutanen, K. Two major xylanases of Trichoderma reesei. *Enzyme Microb. Technol.* **14,** 566–574 (1992).

42.   Linder, M. & Teeri, T. T. The cellulose-binding domain of the major cellobiohydrolase of Trichoderma reesei exhibits true reversibility and a high exchange rate on crystalline cellulose. *Proc. Natl. Acad. Sci. U. S. A.* **93,** 12251–12255 (1996).

Supplementary Information

Sequences of the HFBI-DCBM proteins

HFBI-DCBM-12
SNGNGNVCPPGLFSNPQCCATQVLGLIGLDCKVPSQNVYDGTDFRNVCAKTGAQPLCCVAPVAGQALLCQTAVGA
ENLYFQGPGASTSTGRGPGGQACSSVWGQCGGQNWSGPTCCASGSTCVYSNDYYSQCLPGANPPGTTTTSTQSH
YGQCGGIGYSGPTVCASGTTCQVLNPYYSQCL

HFBI-DCBM-24
SNGNGNVCPPGLFSNPQCCATQVLGLIGLDCKVPSQNVYDGTDFRNVCAKTGAQPLCCVAPVAGQALLCQTAVGA
ENLYFQGPGASTSTGRGPGGQACSSVWGQCGGQNWSGPTCCASGSTCVYSNDYYSQCLPGANPPGTTTTSQPAT
TTGSSPGPTQSHYGQCGGIGYSGPTVCASGTTCQVLNPYYSQCL

HFBI-DCBM-48
SNGNGNVCPPGLFSNPQCCATQVLGLIGLDCKVPSQNVYDGTDFRNVCAKTGAQPLCCVAPVAGQALLCQTAVGA
ENLYFQGPGASTSTGRGPGGQACSSVWGQCGGQNWSGPTCCASGSTCVYSNDYYSQCLPGANPPGTTTTSQPAT
TTGSSPGPPGANPPGTTTTSQPATTTGSSPGPTQSHYGQCGGIGYSGPTVCASGTTCQVLNPYYSQCL

Supplementary figure 1. Amino acid sequences of the three different HFBI-fusion proteins that were used to gain the DCBM-12, -24, and -48 by trypsin cleavage. DCBM-12 was used to gain CBM-Cel7A and CBM-Cel6A by papain cleavage. Linker regions are in black (the arginine where trypsin cleaves is shown in pink), HFBI sequence is shown in blue, CBM-CEL7A sequence is shown in red, and CBM-CEL6A sequence is shown in green.

Binding affinities and capacities of CBM and DCBM on BMCC and NFC

Table 1. Binding affinities (k_d) and capacities (B_{max}) for single and double CBM gained from Langmuir one-site binding fit on data in figure 1 of the main text

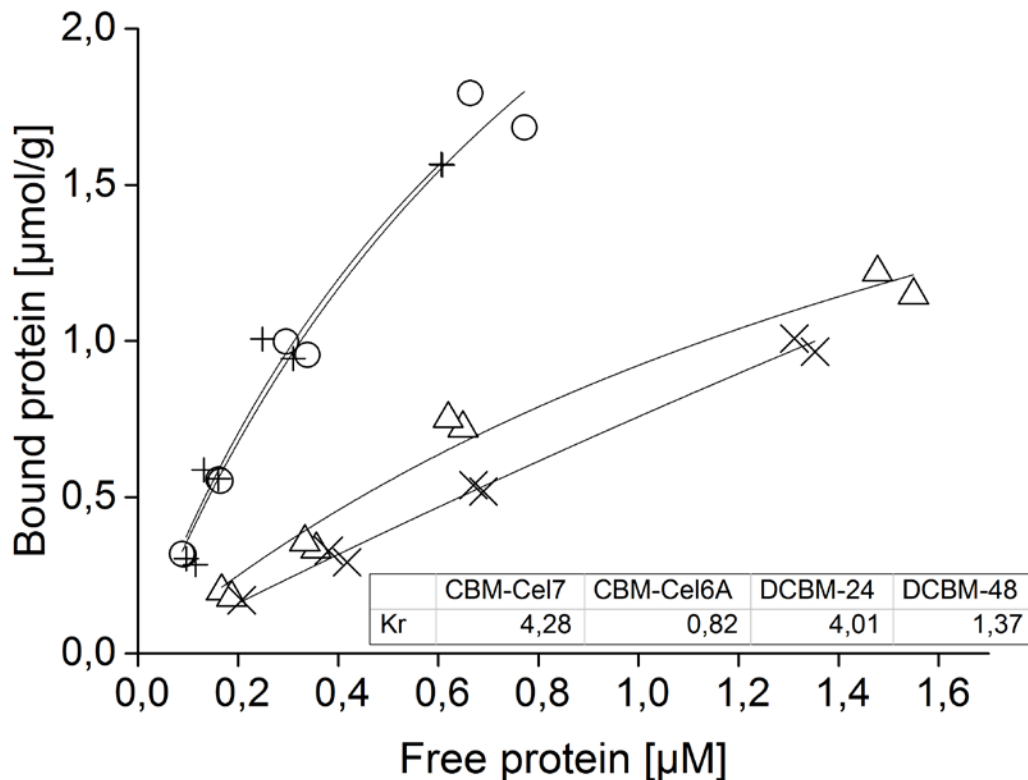|		CBM-CeI7A	CBM-Cel6A	DCBM-12	DCBM-24	DCBM-48
BMCC	B_{max} ($\mu molg^{-1}$)	4,26	5,15	7,48	7,07	3,19
	k_d (μM)	3,03	8,38	3,03	2,51	2,97
NFC	B_{max} ($\mu molg^{-1}$)	28,96	18,45	26,22	29,36	13,8
	k_d (μM)	5,81	17,58	6,77	7,02	8,31
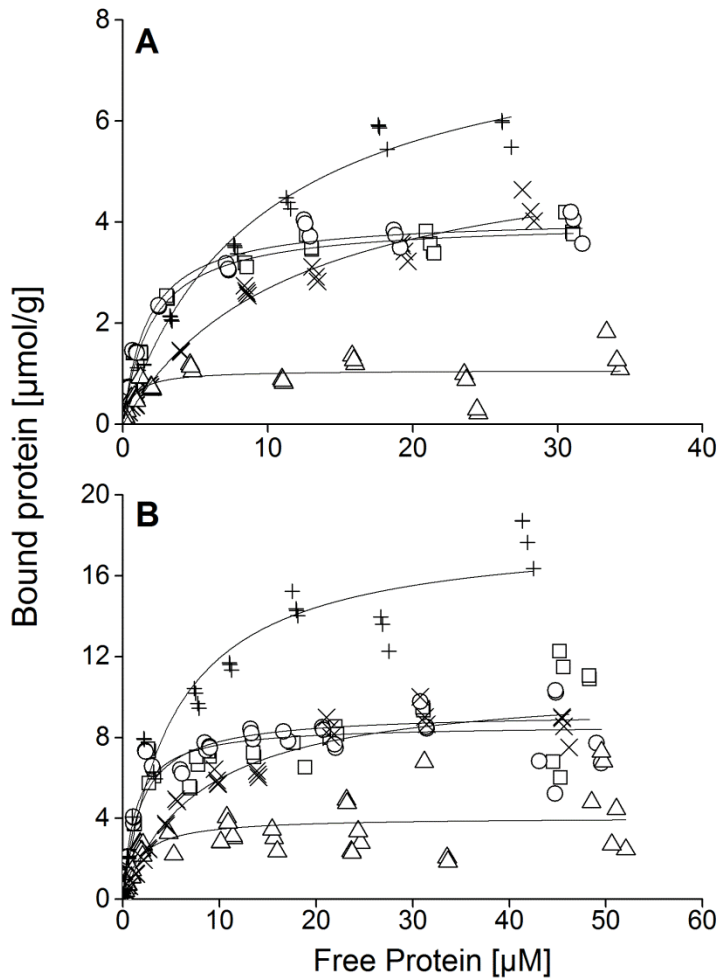
Supplementary figure 2. (A) Linear representation of the binding isotherms of CBM-Cel7A, CBM-Cel6A, DCBM-12, DCBM-24, and DCBM-48 on BMCC. (B) Linear representation of the binding isotherms of CBM-Cel7A, CBM-Cel6A, DCBM-12, DCBM-24, and DCBM-48 on NFC. (+) CBM-CBHI, (x) CBM-CBHII, (□) DCBM-12, (○) DCBM-24, (Δ) DCBM-48.
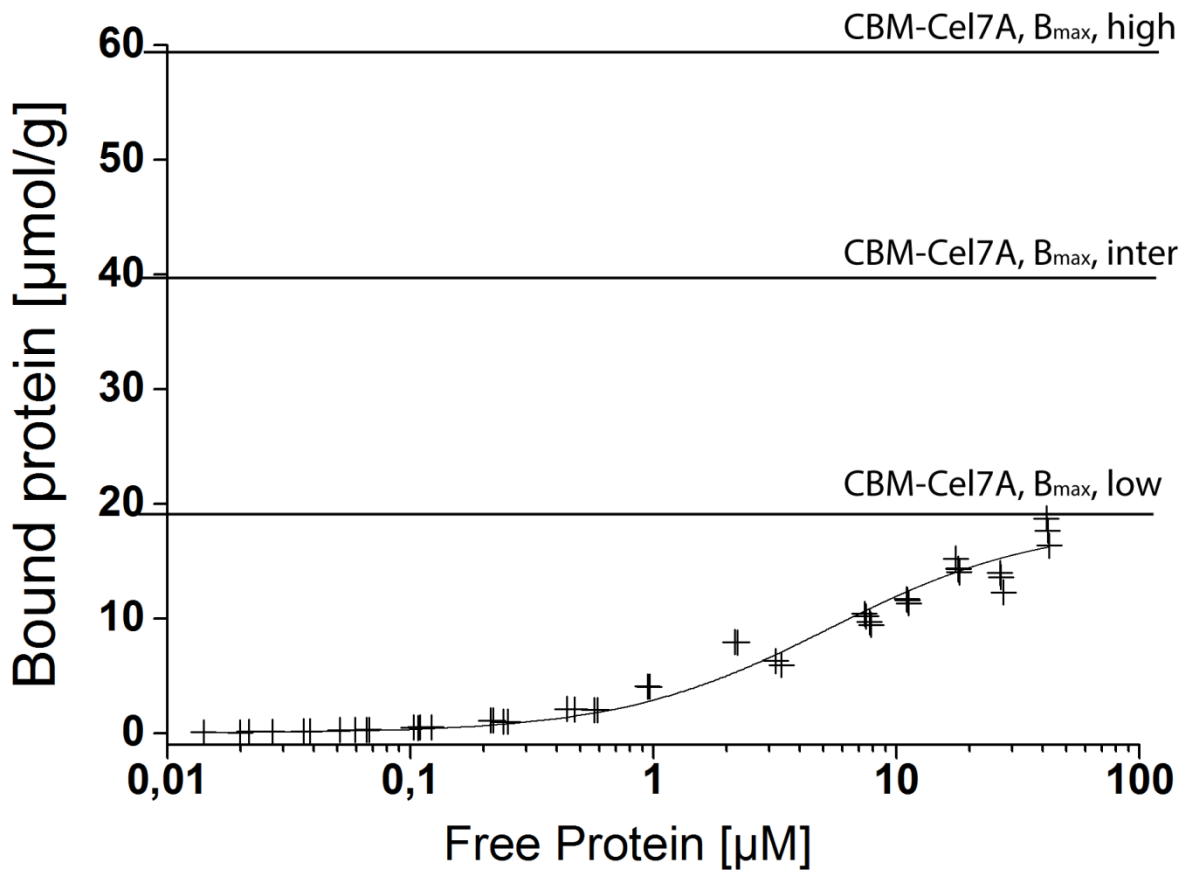
Supplementary figure 3. Schematic illustration of the levels of variation of B_{max}-values shown on semi-log plot of CBM-Cel7A binding isotherm on NFC. The values were used to calculate the variation of free energies of binding for CBM-Cel7A, CBM-Cel6A, DCBM-12, and DCBM-24. B_{max}, low presents the highest value of the maximum capacity that was obtained experimentaly. This value is not an actual maximum and thus represents a minimum which is always exeeded when the cellulose surface is fully covered. B_{max}, intermediate (B_{max}, inter) is double that of B_{max}, low and B_{max}, high is thriple that of B_{max}, low.

Binding isotherms of CBM and DCBM on pulp used to prepare NFC

Supplementary figure 4. Binding isotherms of CBM-Cel7A, CBM-Cel6A, DCBM-24, and DCBM-48 on pulp. The partitioning coefficients, K_r, for the proteins are shown in the table within the figure. (+) CBM-CBHI, (x) CBM-CBHII, (○) DCBM-24, (Δ) DCBM-48

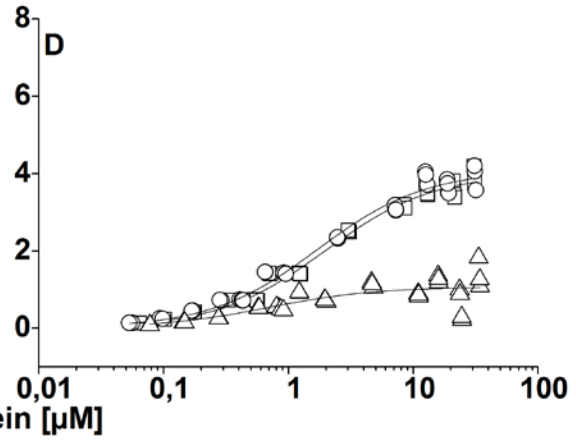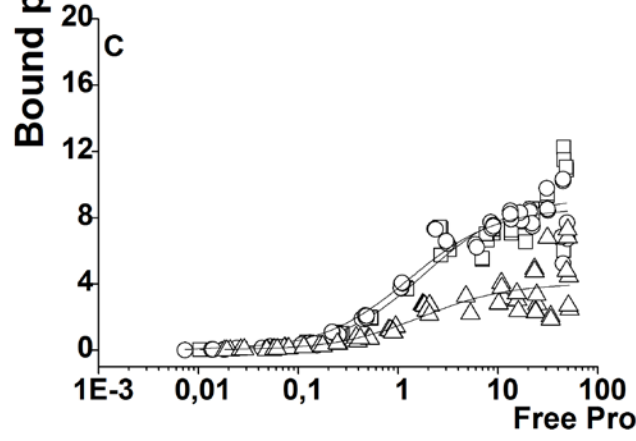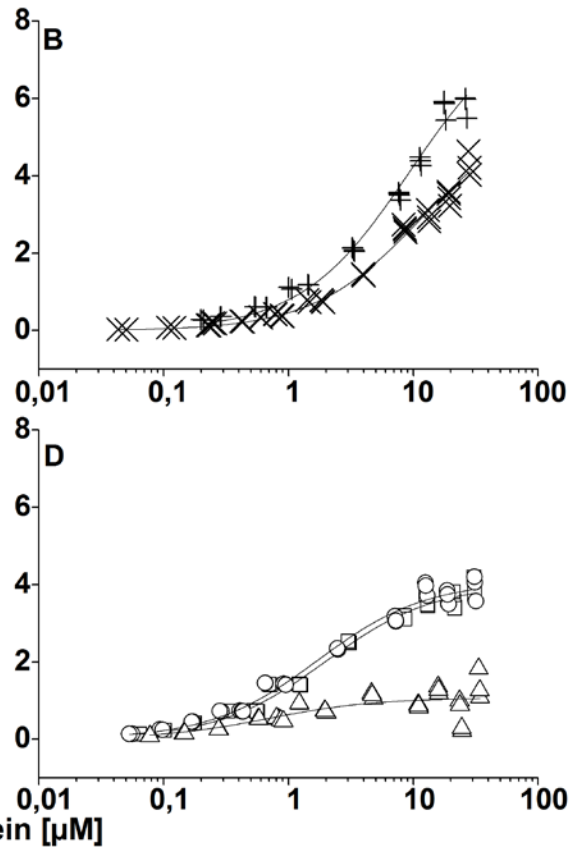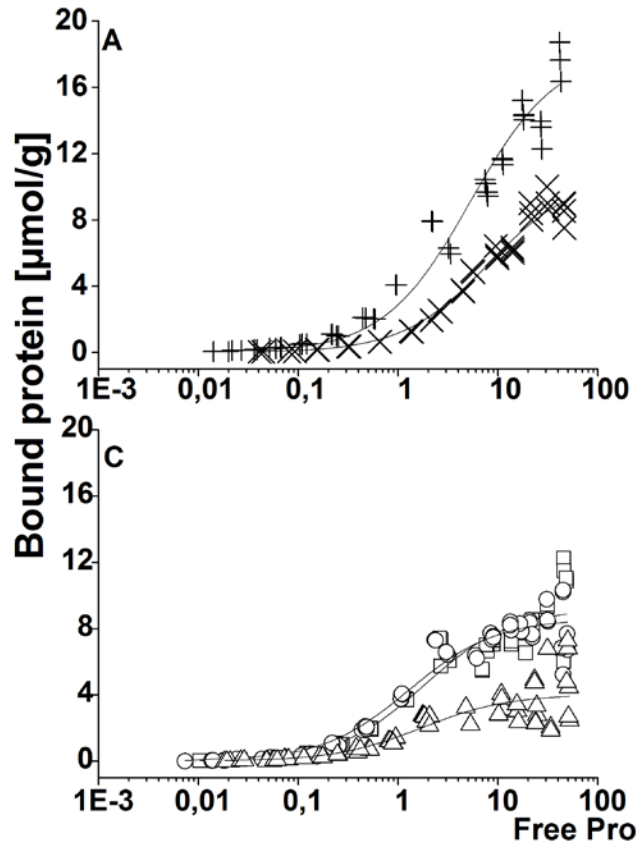## Competition of CBM-Cel7A and CBM-Cel6A on NFC and BMCC

To examine the possible competition of the CBMs on binding sites on BMCC and NFC, we compared how the binding of ^{3}H-labelled CBM-Cel7A was affected by non-labelled CBM-Cel6A and vice versa. A control experiment with buffer only showed the behavior of the protein when the free protein concentration is diluted with no CBM in the solution. This was done in order to see if the added non-labelled CBM affects the binding at all. From the results it was evident that the added non-labelled CBMs affect the binding and they compete with the labelled counterpart in the solution because the results are different form the buffer dilution control. There seems not to be a difference on either substrate whether the competing counterpart is the same or the other CBM because the experiments give very similar results regardless of the components of the experiments. These results suggest that the CBM-Cel7A and CBM-Cel6A fully compete on binding sites on both substrates. This is in agreement with the Gibb's free energies associated with the bindings, also very similar for both proteins on both substrates.
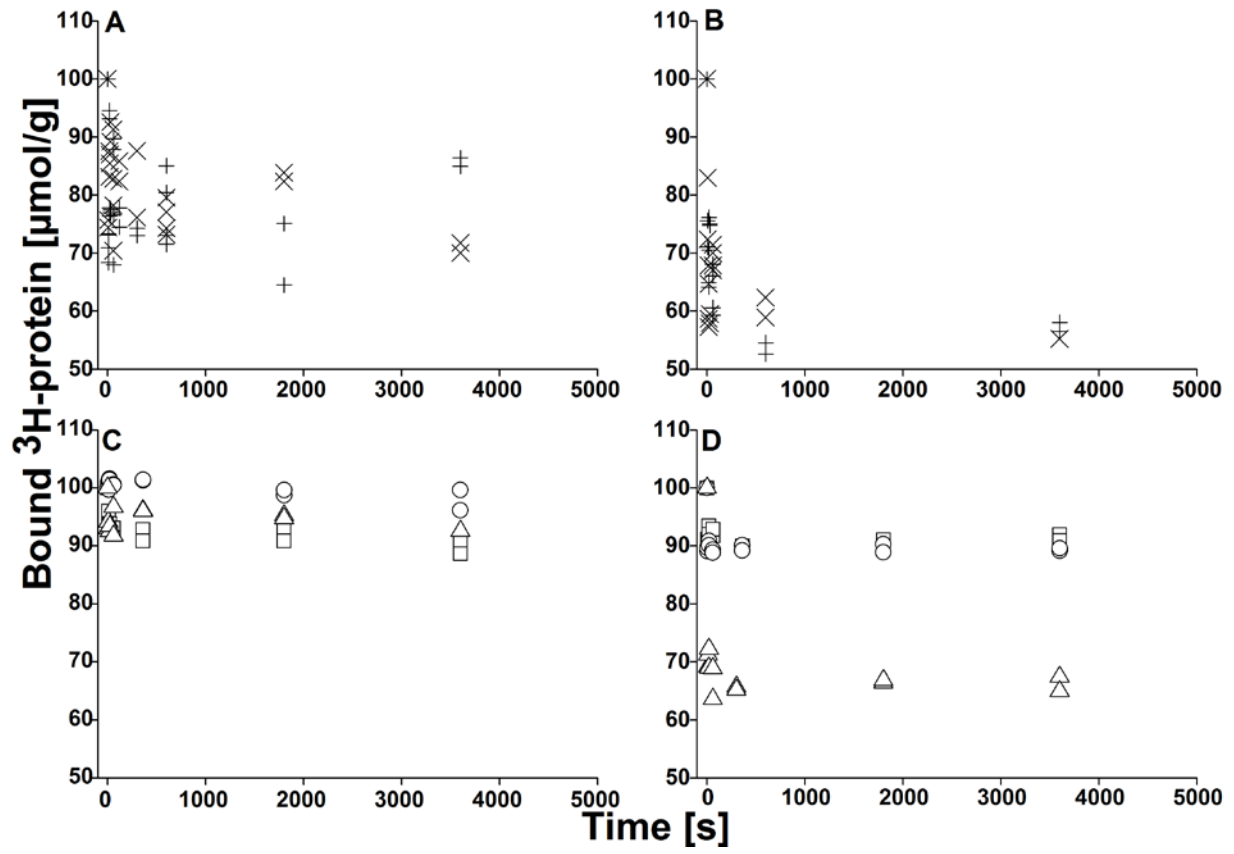
A 25µM solution of CBM containing 10% ^{3}H-protein was diluted 1:1 with a 25 µM solution of the same or the other unlabeled CBM. 100µL of these mixture solutions were let to react with 100 µL of NFC (2 g L-1) and BMCC (1.28 gL-1). As controls the original 25µM solutions with 10% labelled protein and 12.5µM solution with 10% labelled protein (prepared by dilution of 1:1 of the 25µM solution) were used.
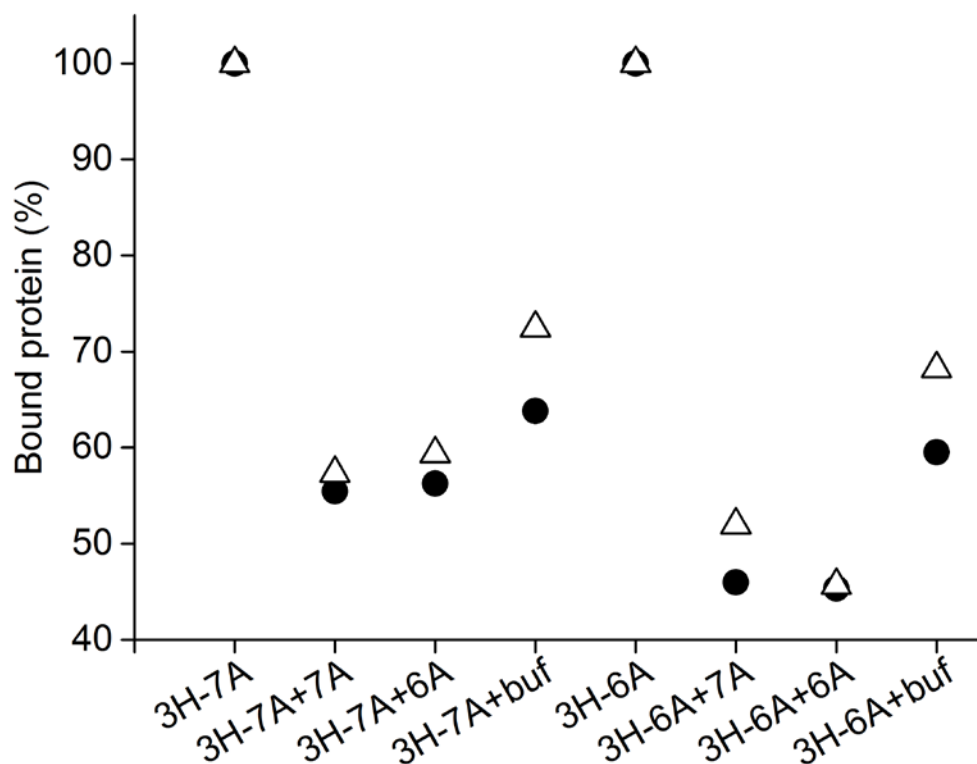
Supplementary figure 6. Competition of ^{3}H-labelled CBM-Cel7A and CBM-Cel6A with non-labelled CBM- Cel7A (3H-7A+7A and 3H6A+7A) and CBM-Cel6A (3H7A+6A and 3H7A+6A) on both substrates, NFC and BMCC. Control experiment with ^{3}H- Cel7A and CBM-Cel6A without dilution (3H-7A and 3H-6A), and with buffer dilution (3H-7A+buf and 3H-6A+buf) were made. Δ BMCC, ● NFC.

Title	**Biochemical modification and functionalization of nanocellulose surface**
Author(s)	Suvi Arola
Abstract	Cellulose is an abundant biopolymer found in many different organisms ranging from microbes to plants and animals. The homopolymer, composed of repeating glucose units, forms mechanically strong nanosized fibrils and rods. In plants cellulose forms macroscopic fibers, which are incorporated in the cell walls. Recently, it has been shown that cellulose fibers can be disintegrated into the fibrils and rods by different chemical treatments. These materials are called nanocellulose. Nanocellulose is a promising material to replace fossil based materials because it is renewable, biodegradable and abundant. It holds great potential in many applications due to its superior mechanical properties and large surface area. For most applications modification of nanocellulose surface is needed due to its tendency to aggregate by hydrogen bonding to adjacent cellulose surfaces. In this thesis we took a biochemical approach on nanocellulose surface modification to achieve modified and functional materials. The advantages of this approach are that the reactions are done in mild aqueous ambient conditions and the amount of functionalities of biomolecules is broad. Four different approaches were chosen. First, genetically engineered cellulose binding proteins, were used to introduce amphiphilic nature to nanocellulose in order to create surface self-assembled nanocellulose films and to stabilize emulsions. This method was shown to be a good method for bringing new function to nanocellulose. (Publication I) Second, covalent coupling of enzymes directly onto modified nanocellulose surfaces provided a route for protein immobilization in bulk. Nanocellulose derivatives were shown to be well suited platforms for easy preparation of bioactive films. More over the film properties could be tuned depending on the properties of the derivative. (Publication II) Third, by modifying the nanocellulose surface with specific enzymes we could study the role of hemicellulose in nanocellulose fibril surface interactions. We showed that hemicellulose has an important role in nanofibrillated cellulose networks, yet its effects were different in aqueous and dry matrixes. (Publication III) Fourth, by modifying the specific function of cellulose binding protein via genetic engineering we showed how the binding properties can be altered and thus the functionalization properties can be tuned, and that the cellulose binding protein properties are substrate dependent. We also showed that nanocellulose as a model substrate in binding studies is a valuable tool for gaining new insight in protein binding behavior. (Publication IV) In conclusion, we showed that biochemical methods are feasible in nanocellulose modification and functionalization to study intrinsic properties of nanocellulose and cellulose binding proteins but also for creating new functional materials.
ISBN, ISSN	
Date	July 2015
Language	English, Finnish abstract
Pages	95 p. + app. 93 p.
Name of the project	
Commissioned by	
Keywords	Nanocellulose, biochemical modification, functionalization of nanocellulose, self-assembly, cellulose binding module, role of hemicellulose, bioactive films
Publisher	

Nimeke	**Nanoselluloosapinnan biokemiallinen muokkaus ja funktionalisointi**
Tekijä(t)	Suvi Arola
Tiivistelmä	Selluloosa on laajalti luonnossa esiintyvä biopolymeeri, jota tuottavat kasvien ja mikrobien lisäksi jotkin eläinkunnan jäsenet. Tämä homopolymeeri, joka muodostuu toistuvista glukoosiyksiköistä, muodostaa mekaanisesti vahvoja nanokokoluokan fibrillejä ja tikkuja. Kasveissa selluloosa muodostaa mikro- ja makrokokoluokan kuituja, jotka ovat osana soluseinärakennetta. Hiljattain on pystytty näyttämään, että selluloosakuidut voidaan hajottaa fibrilleiksi ja tikuiksi erilaisin kemian menetelmin. Näitä materiaaleja kutsutaan nanoselluloosaksi. Nanoselluloosa on lupaava materiaali korvaamaan öljypohjaisia materiaaleja, koska se on uusiutuva, biohajoava ja helposti saatavilla oleva. Nanoselluloosa on myös potentiaalinen materiaali monilla eri teknologioiden aloilla suuren pinta-alansa ja ylivertaisten mekaanisten ominaisuuksiensa takia. Suurin osa sovelluksista vaatii nanoselluloosapinnan ominaisuuksien muokkaamista, koska nanoselluloosakuidut liittyvät helposti yhteen vetysidosten välityksellä.
	Tässä väitöskirjassa on tutkittu biokemiallisten menetelmien soveltuvuutta nanoselluloosapintojen muokkaamisessa ja funktionalisoimisessa. Näiden menetelmien etuja ovat, että reaktiot tapahtuvat miedossa vedellisessä ympäristössä ja että biomolekyylien toiminnollisuuksien joukko on erittäin laaja. Valitsimme neljä erilaista lähestymistapaa. Ensinnä käytimme geneettisesti muokattuja selluloosaan sitoutuvia proteiineja tuomaan amfifiilisyyttä nanoselluloosan pinnalle. Näitä rakenteita käytettiin muodostamaan itsestään järjestäytyneitä pintoja nanoselluloosasta sekä stabiloimaan emulsioita. Tämän menetelmän näytettiin toimivan nanoselluloosan funktionalisoinnissa. (Osajulkaisu I) Toiseksi näytimme, että nanoselluloosan johdannaiset toimivat hyvin matriisina proteiinien suoralle kovalenttiselle kiinnittämiselle bulkissa. Nämä johdannaiset sopivat hyvin bioaktiivisten filmien valmistukseen. Lisäksi filmien ominaisuuksia voitiin muuttaa ja muokata nanoselluloosajohdannaisen ominaisuuksista riippuen. (Osajulkaisu II) Kolmanneksi tutkimme hemiselluloosan roolia nanoselluloosamatriisissa muokkaamalla nanoselluloosan pintaa spesifisillä entsyymeillä. Pystyimme näyttämään, että hemiselluloosalla on tärkeä rooli näissä verkostoissa, joskin se on erilainen kuivissa ja kosteissa systeemeissä. (Osajulkaisu III) Neljänneksi, muokkaamalla geneettisesti selluloosaan sitoutuvan proteiinin spesifiä toimintoa, näytimme, että pystymme vaikuttamaan sen sitoutumisominaisuuksiin ja näin mahdollisesti myös nanoselluloosamateriaalien toiminnollisuuteen. Näytimme myös, että selluloosaan sitoutuvan proteiinin toiminta on riippuvaista sen substraatista ja että nanoselluloosa on hyvä mallisubstraatti sitoutumiskokeissa, sillä se tuo uutta tietoa näiden proteiinien toiminnasta. (Osajulkaisu IV)
	Yhteenvetona voi todeta, että erilaiset biokemialliset menetelmät soveltuvat nanoselluloosapinnan muokkaukseen ja funktionalisointiin, nanoselluloosan ja siihen sitoutuvien proteiinien luontaisten ominaisuuksien tutkimisessa, mutta myös uusien toiminnallisten materiaalien luomiseen.
ISBN, ISSN	ISBN 978-951-38-8330-0 (nid.) ISBN 978-951-38-8331-7 (URL: http://www.vtt.fi/julkaisut) ISSN-L 2242-119X ISSN 2242-119X (Painettu) ISSN 2242-1203 (Verkkojulkaisu)
Julkaisuaika	Heinäkuu 2015
Kieli	Englanti, suomenkielinen tiivistelmä
Sivumäärä	95 s. + liitt. 93 s.
Projektin nimi	
Rahoittajat	
Avainsanat	Nanoselluloosa, biokemiallinen muokkaus, nanoselluloosan funktionalisointi, itsestään järjestäytyminen, selluloosaan sitoutuva moduli, hemiselluloosan rooli, bioaktiiviset filmit
Julkaisija	Teknologian tutkimuskeskus VTT Oy PL 1000, 02044 VTT, puh. 020 722 111

Biochemical modification and functionalization of nanocellulose surface

Cellulose is an abundant biopolymer found in many different organisms ranging from microbes to plants and animals. The homopolymer, composed of repeating glucose units, forms mechanically strong nanosized fibrils and rods. In plants cellulose forms macroscopic fibers, which are incorporated in the cell walls. Recently, it has been shown that cellulose fibers can be disintegrated into the fibrils and rods by different chemical treatments. These materials are called nanocellulose. Nanocellulose is a promising material to replace fossil based materials because it is renewable, biodegradable and abundant. It holds great potential in many applications due to its superior mechanical properties and large surface area. For most applications modification of nanocellulose surface is needed due to its tendency to aggregate by hydrogen bonding to adjacent cellulose surfaces.

In this thesis we took a biochemical approach on nanocellulose surface modification to achieve modified and functional materials.